

**Enrichment and Identification of HLA-Associated Phosphopeptides for the
Development of Novel Cancer Immunotherapeutics**

Paisley Trantham Myers
Irmo, South Carolina

B.S. Forensic Chemistry, Winthrop University, 2012

A Dissertation presented to the Graduate Faculty
of the University of Virginia in Candidacy for the Degree of
Doctor of Philosophy

Department of Chemistry

University of Virginia
August 2016

This dissertation is dedicated to Pop

Acknowledgements

First and foremost, I would like to thank my amazing advisor, Dr. Donald Hunt. I am so honored to have been a part of your lab and for my wonderful graduate school experience. You have helped me to become a better scientist and for that I am eternally grateful. Thank you for providing me with insight and encouragement and for pushing me to do “one more experiment.” Your passion for research and desire to answer scientific questions is truly inspiring. I have learned so much more than I thought possible during these four years and yet I am sure I have not even scratched the surface of your wisdom. I cannot thank you enough for the amazing opportunities that you have provided me with and of course, for the quarters.

Next, I need to thank Dr. Jeffrey Shabanowitz for the huge role he played during my time at the University of Virginia. Not only did you teach me a great deal about mass spectrometry, you taught me valuable life lessons which I will not soon forget. I have so much respect for you and everything that you have accomplished throughout your career. Thank you for helping me through the difficult times when I couldn't get anything in lab to work and for the encouragement to continue on. Thank you for continuing to give me advice even when I didn't want to listen and for never saying “I told you so,” when I realized you were right. And of course, thank you for sitting through my countless stories/pictures/videos of Riley. You have been there for me through both exciting and difficult times and I hope that you know how much I genuinely appreciate that.

I need to thank my collaborators who essentially made all of this work possible – Dr. Mark Cobbold and his students Dr. Sarah Penny, Lora Steadman, and Dr. Nico Büttner. I

am lucky to have had the opportunity to work with such wonderful collaborators and I owe so much of my success to the four of you. Sarah and Lora, thank you for supplying me with the samples I needed for the optimization of STAGE tip technology. Without this, the improvements to the sample desalting procedure could not have been made. Nico, thank you for the endless supply of liver tissue samples to analyze. When you told me you had thirty samples sitting in your freezer, I thought you were exaggerating. I was wrong. Thank you for being so passionate about this work, for always being eager to perform the next experiment, and for your insight into the significance of our findings.

I also need to thank my committee members, Drs. Linda Columbus, David Cafiso, Jill Venton, and MD Kenneth Tung. Thank you so much for taking the time to read my dissertation and to participate in this process. Thank you to Drs. Columbus, Cafiso, and Venton for being a part of my candidacy exam and for showing me how much I did not know. Dr. Columbus, thank you for allowing me to be one of your teaching assistants during my first year of graduate school; it was an experience that I truly enjoyed. Dr. Venton, thank you for all of your help with the LEAD organization. So much of what we accomplished would not have been possible without your support and leadership.

None of my research would have been possible if it weren't for the support and guidance of the many Hunt lab members that I had the pleasure of working with during my time in graduate school. First, I want to thank the former Hunt lab members who helped me get to where I am today. Dr. Jennifer Abelin, thank you for spending so much time training me and for teaching me everything I could ever want to know about IMAC. I am lucky to have had a chance to learn from you and I truly appreciate the role you

played throughout my graduate school career. I would also like to thank Dr. Michelle English for helping me with basically everything else and for always staying positive during the “well, I’ve never seen that before” moments. Of course I owe a huge thank you to Dr. Amanda Wriston for keeping me sane throughout this crazy journey. The walks to calm down (and to get shortbread cookies) helped during the most challenging of times. Thank you for the countless laughs and for listening to all of my ridiculous stories. Your friendship made my time in graduate school so much more enjoyable. I would also like to thank the other former lab members for their support during my time at UVa: Dr. Lissa Anderson, Dr. Aaron Bailey, Dr. Joe Strukl, Dr. Weihan Wang, Dr. Lichao Zhang, and Dr. Andrew Dawdy.

Of course I have to thank the current Hunt lab members who have made the graduate school experience so amazing: Dr. Dina Bai, Dr. Stacy Malaker, Scott Ugrin, Ben Barnhill, Stephanie Miller-Lehman, Garrett Tanner, Ellen Speers, Elizabeth Duselis, Josh Hinkle, Eric Hunt, Rob D’Ippolito, and Mohammad Azizzanjani. Stacy, I might not be a part of the “two best friends that anyone could have,” but I am still so thankful for your friendship and support throughout these past few years. I don’t know how I would make it through the day if it weren’t for the constant gchats about anything and everything. Thank you for listening to me vent, for giving me advice in every situation, and for utilizing my extensive WebMD diagnostic abilities. Scott, thank you for being so supportive through the many stressful and exciting times. You may not be great at fantasy sports, but you are an awesome classmate and even better friend. Dina, thank you for everything you have done for me over the past four years. You have helped to talk me

down through so many stressful situations and I cannot thank you enough for that. Thank you for always being there to listen, for editing my dissertation (at a ridiculous speed!), and for the endless supply of Starbursts. I feel so lucky to have had the chance to go through graduate school with such an amazing group of people.

Before I came to UVa, I spent four amazing years at Winthrop University. During my time there I met so many people who shaped me into the person I am today. I want to thank Dr. Patrick Owens for getting me hooked on chemistry in my first General Chemistry course. You're notes of encouragement on pop quizzes meant so much to me and served as a reminder to keep going when times were tough. I want to thank Dr. Nicholas Grosseohme for being an amazing undergraduate research advisor. I truly enjoyed working for you and am so thankful to have had that opportunity. Thank you for showing me what it meant to be a scientist and for sparking my interest in research. I know that I would not be where I am today if it were not for your mentorship. Additionally, I want to thank Dr. Jason Hurlbert, Dr. Christian Grattan, and Dr. Cliff Calloway for supporting me throughout my undergraduate years and for helping me to make the decision to come to graduate school. I also need to thank all of my "study room friends," for helping me through those stressful times. Your support helped me to accomplish things I never thought were possible. I am so lucky to have been a part of such an amazing group of friends. To Amber Wallace and Katie Bolling, I'm pretty sure I wouldn't have made it through some of those classes if I hadn't had you two to go through them with me! Amber, you have always been such a great friend to me and I am

so appreciate of the years we got to spend together. Katie, you are such a hard worker and an amazing person and I am so proud of everything you have accomplished.

Next I need to thank two of my very best friends, Maricel McGlaulin and Brian Pidgeon. Maricel, where do I even begin? Having known you since second grade, I can't even remember a time when we weren't attached at the hip. Making fake TV commercials and talk shows, fishing in streams with no fish, countless sleepovers (it has to be in the hundreds!), and coordinating outfits every morning, the list goes on and on. Plus all of the crazy memories that probably shouldn't be put in writing! You were such a huge part of my life and I am so thankful for that. You are a wonderful person and an even better friend. Brian, I am so lucky to have met you during that 8th grade French class! You quickly became one of my best friends and I truly cherish the times I spent with you. Our infamous beach trip was literally one of the best times of my life, despite getting my car stuck in a sand pit, finding the washed-up beach monster, and almost being eaten by a shark (or turtle?). I still can't believe those ladies didn't tell us it was right beside us. I love you so very much and can't thank you enough for your friendship. There's so much more that I could say to you but I'll leave you with this - welcome to Snake Island, it's great to be here!

Of course I also need to thank my amazing husband, Jeffery Myers. Oh my gosh, I can say husband now! I don't think I can even come close to explaining how much you mean to me. You are an amazing person and as cliché as it sounds, I honestly can't imagine my life without you in it. Thank you for your support and friendship during our time at Winthrop. You made the countless hours of studying so much more enjoyable,

even if just by making me stare at trees. Thank you for continuing to ask me out on dates and never taking “no” for an answer! I think you knew we were meant to be together all along. I am beyond thankful that we were able to go through the graduate school experience together. Just knowing that you were upstairs going through the same things made a huge difference. Thank you for letting me share the many happy times with you and for letting me scream/cry/etc. during the not so happy times. I look forward to what our future together holds and the many years we get to spend with each other.

I owe a huge thank you to all of my family members who have been so loving and supportive throughout my many endeavors. I would not have made it this far if it weren't for all of you. To Daddy and Mrs. Kim, thank you for always being there for me and for being so excited about even the smallest of accomplishments. Your support means more to me than you know. Micah, thank you for putting up with 13 year old me who I know was quite a handful. I am so appreciative of everything you have done for me and am lucky to have you in my life. Mimi, you are an awesome grandma and I hope I am as cool as you one day! Thank you for the weekly phone calls and for the never-ending encouragement. Lisa and John, thank you for the continued support and interest in my research. Having both of you at my defense means so much to me and I truly appreciate it!

Finally, I need to thank my mom for being a constant source of love, support, and encouragement. Words cannot express how grateful I am to call you not only my mom, but my best friend. Moving away from you to go to graduate school was one of the hardest things I've ever had to do and I thank you so much for being supportive of my

decision. Thank you for every card, text, email, and phone call, all of which meant the world to me. Thank you for showing me the importance of a glass of wine and a good nail salon. Thank you for listening to me complain about work or life in general and for reminding me that everything will work out fine. Of course, you were always right. You are an amazing person and I love you so much!

Table of Contents

Acknowledgements	I
Table of Contents	VIII
List of Figures and Tables.....	XIII
Abbreviations	XVI
Abstract.....	XXVII

Chapter 1

1 Introduction to the Dissertation

1.1 Cancer and the Immune System.....	1
1.2 Introduction to Methods.....	15
1.2.1 HLA-Associated Peptide Isolation.....	15
1.2.2 STAGE Tip Sample Cleanup.....	16
1.2.3 Phosphopeptide Enrichment.....	17
1.2.4 HPLC-ESI-MS/MS	18
1.2.5 Data Processing	26
1.2.6 Biological Testing.....	28
1.3 References	33

Chapter 2

2 Implementation of STop And Go Extraction (STAGE) Tips for Improved Desalting of HLA-Associated Peptide Samples for Mass Spectrometric Analysis

2.1 Introduction.....	37
2.1.1 Sample Preparation for Mass Spectrometric Analyses.....	37
2.1.2 Sample Desalting via STAGE Tip Technology	40
2.1.3 Project Aim.....	42

2.2 Materials	43
2.2.1 Reagents	43
2.2.2 Equipment and Instrumentation	45
2.3 Methods.....	47
2.3.1 Peptide Synthesis.....	47
2.3.2 Cell Line and Tissue Culture	47
2.3.3 Immortalization of Human B Cells with Epstein-Barr Virus.....	47
2.3.4 HLA-Associated Peptide Isolation.....	48
2.3.5 STAGE Tip Fabrication	49
2.3.6 Sample Desalting via STAGE Tips.....	50
2.3.6.1 Synthetic Phosphopeptide Samples	50
2.3.6.2 Off-Bead Cell Line Samples.....	51
2.3.6.3 On-Bead Cell Line and Tissue Samples	51
2.3.7 Sample Desalting via C18 Microcapillary Cleanup Columns	53
2.3.8 Peptide Content Determination by HPLC-ESI-MS/MS	54
2.4 Results	57
2.4.1 STAGE Tip Optimization of Synthetic Phosphopeptide Samples	57
2.4.2 STAGE Tip Optimization of an Off-Bead Cell Line Sample.....	61
2.4.3 STAGE Tip Optimization of On-Bead Cell Line Samples.....	63
2.4.4 STAGE Tip Optimization of On-Bead Tissue Samples.....	68
2.5 Discussion.....	72
2.6 References	81

Chapter 3**3 Complementary IMAC Enrichment for the Identification of HLA-Associated Phosphopeptides**

3.1 Introduction.....	82
3.1.1 Protein Phosphorylation.....	82
3.1.2 Phosphopeptide Enrichment.....	88
3.1.3 Project Aim.....	91
3.2 Materials	92
3.2.1 Reagents	92
3.2.2 Equipment and Instrumentation	93
3.3 Methods.....	95
3.3.1 Tissue Culture	95
3.3.2 HLA-Associated Peptide Isolation.....	95
3.3.3 Peptide Content Determination by HPLC-ESI-MS/MS	96
3.3.4 Sample Desalting via C18 Microcapillary Cleanup Columns	98
3.3.5 Fischer Esterification of Samples	99
3.3.6 Phosphopeptide Enrichment via IMAC.....	99
3.3.6.1 Fe-IDA IMAC Enrichment	99
3.3.6.2 Fe-NTA IMAC Enrichment.....	100
3.3.7 Analysis of Phosphopeptides by HPLC-ESI-MS/MS	102
3.4 Results	105
3.4.1 Identification of Phosphopeptides via Complementary IMAC.....	105
3.4.2 Sequence Analysis of Identified Phosphopeptides	116
3.5 Discussion.....	118
3.6 References	124

Chapter 4**4 Enrichment and Identification of HLA-Associated Phosphopeptides in Hepatocellular Carcinoma for the Development of Novel Cancer Immunotherapeutics**

4.1 Introduction.....	126
4.1.1 Incidence of Hepatocellular Carcinoma	126
4.1.2 Disease Progression.....	127
4.1.3 Current Treatment Options.....	130
4.1.4 Potential for Immunotherapy	132
4.1.5 Project Aim.....	134
4.2 Materials	135
4.2.1 Reagents	135
4.2.2 Equipment and Instrumentation	137
4.3 Methods.....	139
4.3.1 Cell Line and Tissue Culture	139
4.3.2 HLA-Associated Peptide Isolation.....	140
4.3.3 Sample Desalting.....	141
4.3.3.1 C18 Microcapillary Column Cleanup.....	141
4.3.3.2 STop And Go Extraction (STAGE) Tip Cleanup	141
4.3.4 Peptide Content Determination by HPLC-ESI-MS/MS	143
4.3.5 Fischer Esterification of Samples	145
4.3.6 Phosphopeptide Enrichment via IMAC.....	146
4.3.6.1 Fe-IDA IMAC Enrichment	146
4.3.6.2 Fe-NTA IMAC Enrichment	147
4.3.7 Analysis of Phosphopeptides by HPLC-ESI-MS/MS	149
4.3.8 Peptide Synthesis and Validation	151
4.3.9 Isolation of Peripheral Blood Mononucleated Cells	151

4.3.10 Intracellular Cytokine Staining (ISC) Assays	152
4.4 Results	153
4.4.1 Identification of HLA-Associated Phosphopeptides	153
4.4.2 Analysis of Identified HLA-Associated Phosphopeptides	175
4.4.3 Immunological Significance of Identified Phosphopeptides	178
4.4.4 Expansion of TIL Cultures for use in ACT Therapies	183
4.5 Discussion	187
4.6 References	197

Chapter 5

5 Conclusions and Future Applications	200
5.1 References	212

List of Figures and Tables

Chapter 1

Figure 1.1 MHC class I processing pathway	2
Figure 1.2 Structure of HLA class I molecule	4
Figure 1.3 Common HLA class I binding motifs	5
Figure 1.4 Process of positive and negative selection of T cells	6
Figure 1.5 The theory of Immunoediting.....	10
Figure 1.6 The hallmarks of cancer	12
Figure 1.7 The cycle of protein phosphorylation.....	13
Figure 1.8 Mechanism of collision activated dissociation (CAD) fragmentation	21
Figure 1.9 CAD spectrum of a phosphorylated peptide	22
Figure 1.10 Mechanism of electron transfer dissociation (ETD) fragmentation	24
Figure 1.11 Schematic diagram of Orbitrap Fusion Tribrid mass spectrometer.....	25
Figure 1.12 Enzyme-linked immunospot (ELISpot) assay.....	30
Figure 1.13 Intracellular cytokine staining (ICS) assay.....	31

Chapter 2

Figure 2.1 Schematic of microcapillary cleanup column setup.....	39
Figure 2.2 Schematic of STop And Go Extraction (STAGE) Tip.....	40
Figure 2.3 Schematic of STAGE tip fabrication.....	49
Table 2.1 Summary of STAGE tip cleanup of synthetic phosphopeptide mixtures.....	57
Figure 2.4 Chromatograms and base peaks of pre- and post-STAGE tip cleanup screens of JY-A2.....	61
Table 2.2 Percent recovery of identified peptides pre- and post-STAGE tip cleanup of JY-A2.....	62
Table 2.3 Conditions of AML sample preparation for STAGE tip cleanup.....	64

Table 2.4 Comparison of peptides identified in AML patient sample using various preparatory conditions	65
Table 2.5 Comparison of peptides identified in an AML patient sample pre- and post-STAGE tip cleanup	67
Table 2.6 Conditions of sample preparation for STAGE tip cleanup for on-bead tissue samples.....	69

Chapter 3

Figure 3.1 The origin of proteome complexity	82
Figure 3.2 Mechanism of phosphorylation	83
Figure 3.3 Active site of c-AMP dependent protein kinase A (PKA)	85
Figure 3.4 Phosphorylation-mediated signaling cascade.....	86
Figure 3.5 Workflow of Fe-IDA IMAC enrichment	90
Table 3.1 Phosphopeptides identified from HCC tumor tissue sample (LL4857T) using Fe-IDA and Fe-NTA IMAC enrichment techniques	106
Figure 3.6 Chromatograms and base peaks of Fe-IDA and Fe-NTA IMAC enrichments of HCC tumor tissue sample LL4857T	114
Figure 3.7 Phosphopeptides identified using complementary IMAC enrichment methodology	115
Figure 3.8 HLA-type binding specificities of identified phosphopeptides.....	116
Figure 3.9 Distribution of basic amino acid residues in identified phosphopeptides	117
Figure 3.10 Metal coordination of complementary IMAC resins.....	119

Chapter 4

Figure 4.1 Progression of hepatocellular carcinoma.....	128
Table 4.1 Summary of analyzed liver samples	153
Table 4.2 Summary of identified HLA-associated phosphopeptides	155
Figure 4.2 Distribution of phosphorylation sites on identified HLA class I-associated phosphopeptides.....	175

Figure 4.3 Overlap of phosphopeptides identified in various cancer types	176
Figure 4.4 Analysis of dysregulated biological processes	177
Figure 4.5 Example of intracellular cytokine staining data	180
Figure 4.6 Summary of reactive CD8+ T cell populations to HLA-A*02-specific phosphopeptides.....	181
Figure 4.7 Phosphate-dependence of observed immunological responses	182
Figure 4.8 Effect of antigen-specific expansion on TIL cultures	184
Figure 4.9 Immune responses to phosphopeptide antigens throughout the course of disease progression	186

Chapter 5

Figure 5.1 Process of adoptive cell transfer (ACT)	205
Figure 5.2 Genetically-engineered TCRs and TCR-like biomolecules	206
Figure 5.3 ImmTAC generation and mechanism of action.....	209

Abbreviations

°C	degrees Celsius
•	radical species
α	alpha
Å	angstrom
A	solvent A, 0.1M acetic acid in water
AC	analytical column
ACN	acetonitrile
AcOH	acetic acid
ACT	adoptive cell transfer therapy
ADP	adenosine diphosphate
AFP	α-fetoprotein
AGC	automatic gain control
AIRE	autoimmune regulator
Ala, A	alanine
ALL	acute lymphoblastic lymphoma
AML	acute myeloid leukemia
APC	antigen presenting cell, anti-CD3 antibody
APC-Cy7	fixable viability dye
Arg, R	arginine
Asn, N	asparagine
Asp, D	aspartic acid
ATP	adenosine triphosphate

β	beta
β 2m	beta-2-microglobulin
B	solvent B, 0.1M acetic acid in 70% acetonitrile
bar	100,000 Pascals; 14.5038 pounds per square inch
BB7.2	anti-human HLA-A*02 antibody
BCLC	Barcelona clinic liver cancer staging system
BLAST	basic local alignment search tool
B-Raf	proto-oncogene serine/threonine kinase
BSA	bovine serum albumin
C. Eq.	cell equivalents
C18	C18 bonded silica stationary phase
CAD	collision activated dissociation
cAMP	cyclic adenosine monophosphate
CAR	chimeric antigen receptor
CD107a	marker of degranulation
CD19	cluster of differentiation 19
CD3	cluster of differentiation 3
CD4 ⁺	cluster of differentiation 4; T-cell presenting surface glycoprotein CD4
CD8 ⁺	cluster of differentiation 8; T-cell presenting surface glycoprotein CD8
CDR	complementary determining region
CHAPS	3-[(3-cholamidopropyl)dimethylammonio-]-1-propane sulfonate
CLL	chronic lymphocytic leukemia
cm	centimeter

Co	cobalt
CO ₂	carbon dioxide
CRM	charged residue model
Csk	C-Src kinase
C-term	C-terminus of peptide
CTL	cytotoxic T lymphocyte
CTLA-4	cytotoxic T lymphocyte associated protein 4
Cu	copper
Cys, C	cysteine
Δ	delta
Da	dalton
DC	dendritic cell
DMEM	Dulbecco's modified eagle medium
DMSO	dimethylsulfoxide
DNA	deoxyribonucleic acid
Do	deceased donor
EBV	Epstein-Barr virus
EDTA	ethylenediaminetetraacetic acid
ELISpot	enzyme-linked immunospot assay
ER	endoplasmic reticulum
ERAAP1	ER aminopeptidase associated with antigen processing 1
ERAAP2	ER aminopeptidase associated with antigen processing 2
ERAD	endoplasmic reticulum-associated protein degradation
ERp57	endoplasmic reticulum protein 57

ESI	electrospray ionization
ETD	electron transfer dissociation
eV	electron volt, 1.602×10^{-19} J
FBS	fetal bovine serum
Fe ²⁺	iron (II) cation
Fe ³⁺	iron (III) cation
FeCl ₃	iron (III) chloride
FETD	front-end electron transfer dissociation
Fmoc	fluorenylmethyloxycarbonyl chloride
fmol	femtomole, 1×10^{-15} moles
FTICR	Fourier transform ion cyclotron resonance
FTMS	Fourier transform mass spectrometry
g	gram
Gln, Q	glutamine
Glu, E	glutamic acid
Gly, G	glycine
gp100	glycoprotein 100
GPC-3	glypican-3
HBC	hepatitis C
HBV	hepatitis B
HBx	protein of unknown function encoded by HBV
HCC	hepatocellular carcinoma
HCl	hydrochloric acid
HD	healthy donor

HepG2	immortalized hepatoblastoma cell line
HH	hereditary hemochromatosis
His, H	histidine
HIV	human immunodeficiency virus
HLA	human leukocyte antigen
HPLC	high performance liquid chromatography
Hz	Hertz
ICS	intracellular cytokine staining
i.d.	inner diameter
ID	identification
IDA	iminodiacetic acid
IFN- γ	interferon gamma
IGF	insulin-like growth factor
IHL	intrahepatic lymphocyte
IL-2	interleukin 2
Ile, I	isoleucine
IMAC	immobilized metal affinity chromatography
ImmTACs	immune mobilizing monoclonal T cell receptors against cancer
in	inch
IRS	insulin receptor substrate
IRS1	insulin receptor substrate 1
IRS2	insulin receptor substrate 2
ITMS	ion trap mass spectrometer
IU	international unit

JY	Epstein-Barr virus immortalized B cell line
Kasil	potassium silicate solution
kDa	kiloDalton (1×10^3 Da)
KRT18	keratin-18
KRT8	keratin-8
kV	kilovolt (1×10^3 V)
L	liter
LC	liquid chromatography
Leu, L	leucine
LTQ	linear ion trap quadrupole
Lys, K	lysine
m/z	mass-to-charge ratio
MACS	magnetic cell sorting
MAGE-A	melanoma antigen gene-A
MALDI	matrix-assisted laser desorption/ionization
MAPK	mitogen-activated protein kinase
MAPK1	mitogen-activated protein kinase 1
MAP3K3	mitogen-activated protein kinase kinase kinase 3
MAP3K11	mitogen-activated protein kinase kinase kinase 11
MCA	methylcholanthrene
Mg ²⁺	magnesium (II) cation
Met, M	methionine
MHC	major histocompatibility complex
min	minute

mg	milligram (1×10^{-3} g)
μ g	microgram (1×10^{-6} g)
mL	milliliter (1×10^{-3} L)
μ L	microliter (1×10^{-6} L)
mm	millimeter (1×10^{-3} m)
μ m	micrometer (1×10^{-6} m)
mM	millimolar (1×10^{-3} M)
Mn^{2+}	manganese (II) cation
M	molar (moles/liter)
mol	mole, 6.022×10^{23} molecules
mRNA	messenger ribonucleic acid
ms	millisecond (1×10^{-3} seconds)
MS	mass spectrometry
MS1	full mass spectrum
MS2	tandem mass spectrum
mTEC	medullary thymic epithelial cell
MWCO	molecular weight cutoff
N	normal
NA	non-applicable
NaCl	sodium chloride
ND	not detected
NHL	non-Hodgkin lymphoma
NHS	N-hydroxysuccinimide
Ni	nickel

NK	natural killer cell
NKT	natural killer T cell
nL	nanoliter (1×10^{-9} L)
NTA	nitrilotriacetic acid
N-term	amino-terminus of peptide
NY-ESO-1	cancer-testis antigen
o.d.	outer diameter
OMSSA	Open Mass Spectrometry Search Algorithm
p53	tumor suppressor protein 53
Pacific Blue	anti-IL-2 antibody
PANTHER	Protein Analysis THrough Evolutionary Relationships
PBMC	peripheral blood mononucleated cells
PBS	phosphate buffered saline
PC	precolumn
PD1	programmed cell death protein 1
PDGF- β	platelet-derived growth factor receptor-beta
PE	anti-IFN- γ antibody
PE-Cy5.5	anti-TNF α antibody
PEEK	polyetheretherketone
PEI	percutaneous ethanol injection
PerCP	anti-CD8 antibody
pH	potential hydrogen
PHA	phytohaemagglutinin
Phe, F	phenylalanine

PKA	protein kinase A
PLC	peptide-loading complex
pmol, pM	picomole (1×10^{-12} moles)
PMSF	phenylmethylsulfonyl fluoride
ppm	parts per million
Pro, P	proline
psi	pounds per square inch
PTM	post-translational modification
PVDF	polyvinylidene fluoride
Raf-1	proto-oncogene serine/threonine kinase 1
RAG-1	recombination activating gene 1
RAG-2	recombination activating gene 2
REP	rapid expansion protocol
RF	radio frequency
RFA	radiofrequency ablation
RP	reverse phase
rpm	revolutions per minute
RPMI	Roswell Park Memorial Institute
s, sP	phosphorylated serine
s, sT	phosphorylated threonine
s, sY	phosphorylated tyrosine
scFv	single chain variable fragment
SCX	strong cation exchange
SDS	sodium dodecyl sulfate

Ser, S	serine
SH2	Src homology 2
SPE	solid-phase extraction
Src	proto-oncogene tyrosine kinase
SSX-2	protein SSX-2
STAGE	STop And Go Extraction
T	tumor
TAA	tumor-associated antigen
TACE	transarterial chemoembolization
TAP	transporter associated with antigen processing
TCR	T cell receptor
TERT	telomerase reverse transcriptase
Thr, T	threonine
TIC	total ion current
TIL	tumor infiltrating lymphocyte
TNF α	tumor necrosis factor alpha
Tris	tris(hydroxymethyl)aminomethane HCl
Trp, W	tryptophan
Tyr, Y	tyrosine
V	volt
Val, V	valine
VEGF	vascular endothelial growth factor
Vol/vol	volume to volume
W6/32	human HLA class I-specific antibody

X	any amino acid
z	charge
Zn	zinc

Abstract

Despite extensive research efforts, cancer remains the second leading cause of death in the United States. Current treatment options are often ineffective and result in severe side effects due to their inability to distinguish between healthy and cancerous cells. Alternatively, immunotherapy represents an ideal treatment option given the natural ability of the immune system to specifically recognize and clear malignant cells from the body. This is a result of the HLA class I processing pathway, a mechanism employed by the immune system to assess cellular health. This pathway involves the degradation of cytoplasmic proteins by the proteasome into peptides which are subsequently loaded onto HLA class I molecules. HLA:peptide complexes migrate to the cell surface for display to circulating cytotoxic T cells (CTLs) which can trigger the specific killing of cells presenting antigenic peptides. In cancer, cell signaling becomes largely dysregulated, leading to markedly increased, aberrant phosphorylation. Phosphopeptides arising from aberrantly phosphorylated proteins enter into the HLA class I processing pathway where circulating CTLs can recognize them as antigenic and mount a significant immune response against the malignant cells. Therefore, we aim to identify tumor-specific, HLA-associated phosphopeptides, specifically from hepatocellular carcinoma, for the development of novel immunotherapeutics which harness an individual's own immune system to target and eliminate cancer.

In this dissertation, we first implement the use of STop And Go Extraction (STAGE) tips as an improved methodology for HLA-associated peptide sample desalting. Implementation of this robust and sensitive methodology allows for decreased sample

losses, increased peptide recoveries, and the possibility of sample multiplexing. We then evaluate the effectiveness of alternative resins for use in immobilized metal affinity chromatography (IMAC) enrichment of phosphopeptides. By applying complementary IMAC enrichment techniques to a single hepatocellular carcinoma tumor tissue sample, we identify the largest number of phosphopeptides from a single sample in our laboratory to date. Additionally, we show that both enrichment techniques can be used to provide a more complete representation of the HLA-associated phosphopeptides present within tissue samples. We then apply our improved sample desalting methodology and complementary IMAC enrichment techniques to numerous healthy and cancerous liver tissues leading to the identification of a total of 459 HLA-associated phosphopeptides, many of which are tumor-specific. Finally, we show that these phosphopeptides are capable of eliciting an immune response in healthy donors and patients with chronic liver disease, suggesting that they are targets of cancer immune surveillance and therefore represent ideal candidates for use in the development of novel cancer immunotherapeutics.

Chapter 1: Introduction to the Dissertation

1.1 Cancer and the Immune System

Cancer is broadly defined as a collection of diseases resulting from the uncontrolled division of abnormal cells. In a normal cell cycle, cells undergo growth, DNA replication, and division to form new cells only as required by the body. This process is very tightly regulated by a complex series of signaling pathways in addition to mechanisms which function to correct any errors. If this cycle goes awry in any way, damaged cells are killed via apoptosis. In cancer, however, this routine process malfunctions. Through the accumulation of mutational and epigenetic changes, damaged cells are able to escape the restraints that usually keep them in check, ultimately leading to their survival and proliferation.¹

The American Cancer Society estimates that cancer occurrences are expected to exceed 1.6 million in 2016 alone, with over 595,000 Americans predicted to die from the disease. This translates to roughly 1,630 people per day that are fatally affected by cancer. Although cancer is one of the most extensively researched fields, it remains the second leading cause of fatality in the US, accounting for nearly one out of every four deaths.² This discrepancy indicates that while much effort has been put towards treating the disease and measureable progress has been made, the current forms of treatment are frequently ineffective. This is largely due to the non-specific nature of the two most common treatment options, chemotherapy and radiation therapy.³ The inability of these treatments to distinguish between healthy and cancerous cells often results in harsh side

effects and leaves much to be desired in terms of acceptable treatment options. Our efforts focus on the development of novel cancer immunotherapeutics which harness an individual's own immune system to specifically target and eliminate cancer.

In order to understand the vast potential immunotherapy holds as a cancer treatment option, it is necessary to examine the role of the immune system both in healthy

individuals and as it relates to the development of cancer. The immune system employs a mechanism to assess cellular health termed the Major Histocompatibility Complex (MHC) class I processing pathway (Figure 1.1). MHC class I molecules are expressed in all nucleated cells and function to present peptides derived from intracellular proteins to CD8⁺ cytotoxic T cells (CTLs) at the cell surface. To begin, worn-out proteins within the cytosol are tagged with varying numbers of ubiquitin molecules, directing them to the 26S proteasome. The 26S proteasome de-ubiquitinylates and

unfolds the proteins prior to degradation into peptides and is responsible for defining the carboxy termini of the resulting peptides. These 8-16 amino acid residue peptides are

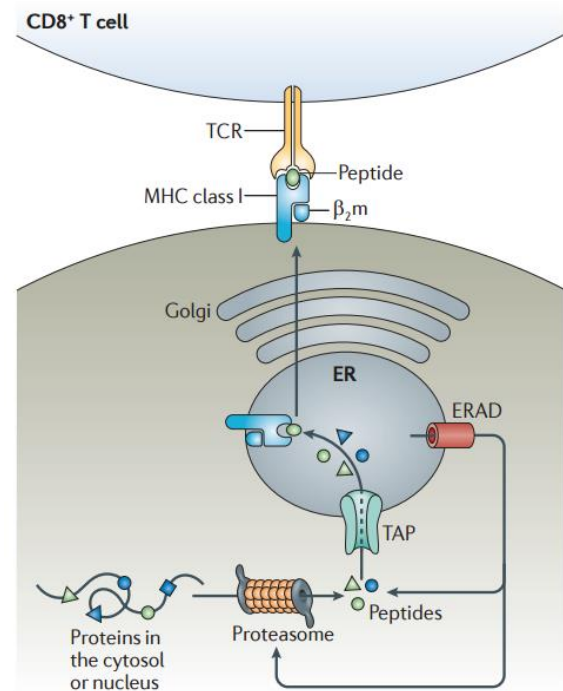


Figure 1.1 MHC class I processing pathway.⁴

Cytosolic proteins are tagged with ubiquitin and degraded by the proteasome into peptides which are transported into the ER via TAP. Peptides are further trimmed and loaded onto MHC class I molecules. Stable MHC:peptide complexes are shuttled to the cell surface where peptides are displayed to circulating CD8⁺ T cells.

unfolds the proteins prior to degradation into peptides and is responsible for defining the carboxy termini of the resulting peptides. These 8-16 amino acid residue peptides are

then translocated into the endoplasmic reticulum (ER) lumen by the transporter associated with antigen presentation (TAP).^{4,5}

Within the ER, newly-synthesized MHC class I molecules are stabilized by two chaperone proteins – calreticulin and ERp57 – which keep the molecules in a partially folded state. This complex binds to one or more molecules of tapasin which are in turn bound to TAP, forming a platform for the complete folding of MHC class I molecules. The resulting complex of TAP, tapasin, ERp57, calreticulin, and the MHC class I molecule is known as the peptide-loading complex (PLC) and helps to ensure sufficient loading of peptides onto MHC class I molecules. The amino termini of the peptides entering the ER via TAP are trimmed to 8-10 amino acids by ER aminopeptidases associated with antigen processing 1 and 2 (ERAAP1/ERAAP2). Peptides with sufficient binding affinities to MHC class I molecules bind in the peptide binding pocket, thus forming stable MHC:peptide complexes and triggering the release from chaperone molecules. The MHC:peptide complexes then exit the ER and travel through the Golgi apparatus to the cell surface where the bound peptides are presented to CTLs. Circulating CTLs sample the displayed peptides and, if the peptide is recognized as antigenic, trigger the specific killing of the infected cell.^{4,5,6}

The MHC is located on chromosome 6, extends over at least 4 million base pairs, and contains more than 200 genes. In humans, these are referred to as human leukocyte antigen (HLA) genes and are the most polymorphic genes known to date. There are three classical HLA class I genes – HLA-A, HLA-B, and HLA-C – all of which are heterodimers comprised of a heavy α -chain and a smaller β 2-microglobulin chain (Figure 1.2). The α -chain consists of three domains, α 1, α 2, and α 3. The α 1 and α 2 domains are

responsible for forming the peptide-binding pocket, made up of a β -sheet floor and two α -helical walls. The $\alpha 3$ domain is noncovalently bound to the $\beta 2$ -microglobulin subunit and contains a short transmembrane region which functions to ensure that each HLA molecule remains associated with the cell that is presenting it.⁷

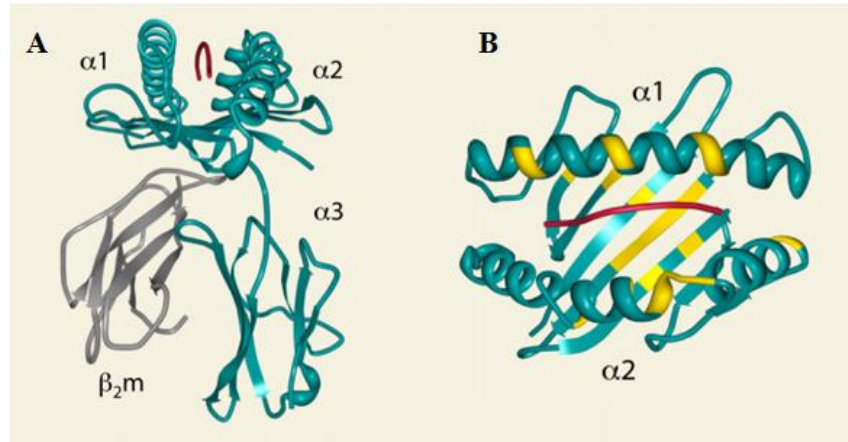


Figure 1.2 Structure of HLA class I molecule.⁶ A) The heterodimeric structure of HLA class I molecules is comprised of a heavy chain consisting of three subunits – $\alpha 1$, $\alpha 2$, $\alpha 3$ – bound to a smaller $\beta 2$ -microglobulin chain. B) The peptide (red) binds in the peptide-binding pocket, which is formed by the $\alpha 1$ and $\alpha 2$ subunits. Polymorphic residues within the binding pocket are highlighted in yellow.

The high degree of variability between HLA class I alleles is a result of the differences in amino acid residues located within the peptide-binding pockets. Subsets of peptides that bind to specific HLA alleles often have the same amino acids in particular positions within the peptide sequence. The amino acid side chains located at these positions insert into pockets within the peptide-binding groove and stabilize the interaction between the peptide and the HLA molecule. These amino acids typically occur at positions two and nine in the peptide sequence and are referred to as anchor residues. The anchor residues of the most common HLA alleles are depicted in Figure 1.3. Despite these binding restrictions, it is estimated that each HLA allele can bind up to

10,000 different peptides. Additionally, each individual has the potential to express up to six different HLA alleles, as one set of HLA-A, -B, and -C are inherited from each parent. The differential expression of HLA alleles combined with the inherent variability of binding specificities drastically increases the number of peptides that can be presented and provides the immune system with an in-depth view of what is occurring within each cell.^{7,8}

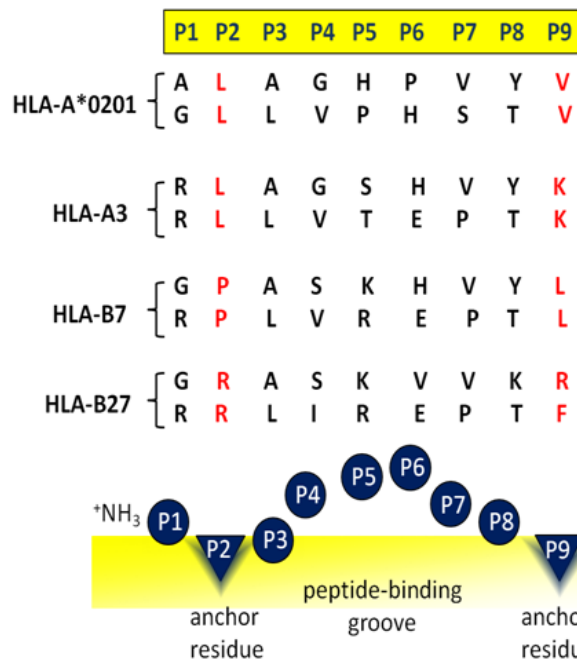


Figure 1.3 Common HLA class I binding motifs. The binding motifs of HLA alleles A*02, A*03, B*07, and B*27 are shown. Amino acids in positions 2 and 9 (red) are called anchor residues and serve to stabilize peptides in the binding pocket of HLA molecules. Amino acids in positions 3 through 8 are solvent exposed and can interact with T cell receptors on circulating CD8⁺ T cells. Figure adapted from JGA.

The ability of the immune system to recognize changes within the cell relies on the interaction between CTLs and HLA:peptide complexes at the cell surface. CTLs sample the peptides presented by HLA class I molecules and are able to distinguish between self and nonself peptides due to a rigorous education process within the thymus. This process begins with the migration of lymphoid progenitor cells from the bone marrow to the thymus where they are referred to as thymocytes. Notch signaling instructs these cells to

commit to a T cell lineage and they undergo a series of maturation steps involving T cell receptor (TCR) gene rearrangement. Successful gene rearrangement results in thymocytes expressing TCRs with differing specificities that are capable of recognizing up to 10^8 unique antigens. These thymocytes now express both CD4 and CD8 coreceptors and are referred to as double-positive. Double-positive thymocytes then undergo two phases of thymic education – positive and negative selection.^{7,9,10}

Positive selection is the process of eliminating thymocytes that are incapable of recognizing self-HLA (Figure 1.4). First, double positive thymocytes are presented with antigens in the context of HLA molecules. Thymocytes that successfully bind to HLA class I molecules downregulate expression of the CD4 coreceptor and become CD8⁺ thymocytes, while those that recognize HLA class II molecules become CD4⁺ thymocytes. Approximately 95% of thymocytes are eliminated by positive selection alone. The remaining 5% undergo negative selection which eliminates single-positive thymocytes that bind too tightly to self-HLA, preventing the development of self-reactive T cells. Thymocytes that survive both processes migrate further through the thymus to the medulla and continue the process of negative selection.⁹

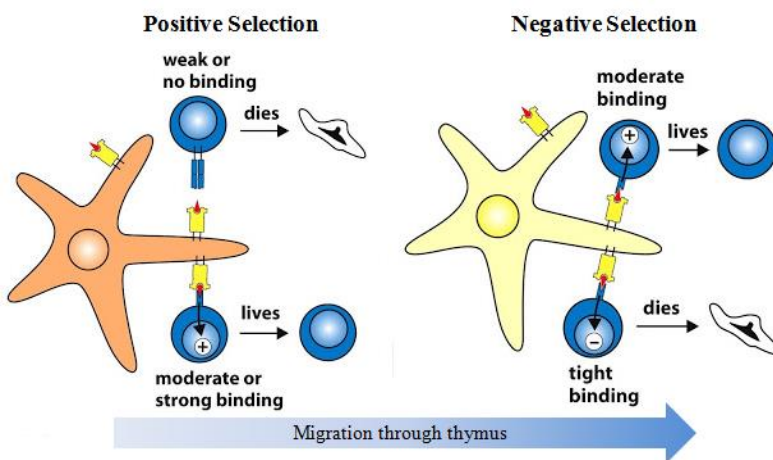


Figure 1.4 Process of positive and negative selection of T cells. Positive selection eliminates thymocytes that do not recognize antigens in the context of self-HLA molecules. Negative selection eliminates thymocytes that bind too strongly to self-HLA molecules. Only 1-3% of progenitor cells survive both processes. Figure adapted from reference 11.

In the medulla, thymocytes are subjected to antigen presenting cells (APCs), such as dendritic cells (DCs) and macrophages.^{7,9} Additionally, thymocytes interact with medullary thymic epithelial cells (mTECs) expressing the autoimmune regulator, AIRE. AIRE expression is upregulated in mTECs, allowing these cells to present tissue-specific self antigens to thymocytes. The process of priming of thymocytes by APCs is called central tolerance and is what ultimately enables them to differentiate between self and nonself peptides. Cells that survive this process then exit the thymus and travel to secondary lymphoid organs as naïve T cells.^{9,10,12} Here, CTLs sample the peptides being presented by HLA class I molecules and become activated if they encounter a foreign peptide, such as those originating from bacteria, viruses, or aberrant proteins associated with cancer. Upon activation, CTLs release the contents of their cytotoxic granules, namely perforin, granzymes, and granulysin, which function together to induce apoptosis of the infected cell. Additionally, CTLs release cytokines, such as interferon gamma (IFN- γ), which recruit additional immune cells to the infection site, ultimately boosting the immune response.^{7,13} While it is evident that immune responses can be mounted towards cells presenting HLA class I molecules displaying foreign antigens, the question remains as to how this process goes awry in the case of cancer. To address this phenomenon, one must turn to the answers provided by the immunoediting theory.

The notion that the immune system could recognize and eliminate malignant cells was first proposed by Paul Erlich in 1909. However, it wasn't until almost 50 years later that this idea was developed into the immunosurveillance hypothesis by Burnet and Thomas.^{14,15} This hypothesis was widely disputed until the mid-1990s when several major developments demonstrating its credibility were made. First, it was shown that

endogenously-produced IFN- γ could protect against transplanted, chemically-induced, and spontaneous tumors. Briefly, Dighe *et al.* found that fibrosarcomas grew faster and more efficiently in mice that had been treated with neutralizing, monoclonal antibodies for IFN- γ .^{16,17} Secondly, it was independently shown that mice lacking perforin, a key component in cytotoxic granules of CTLs, developed significantly more tumors upon treatment with carcinogenic methylcholanthrene (MCA) than their wild-type counterparts.^{16,18,19} The existence of immunosurveillance was further supported upon the generation of mice lacking recombination activating genes 1 and 2 (RAG-1/RAG-2). The deletion of either of these genes results in mice that are unable to successfully rearrange lymphocyte antigen receptors and therefore completely lack natural killer T cells (NKTs), T cells, and B cells.²⁰ Shankaran *et al.* treated these mice with MCA and demonstrated that they developed sarcomas and subsequent epithelial tumors much more rapidly and frequently than mice expressing RAG-1 and/or RAG-2. This demonstrated that not only do lymphocytes protect against the formation of chemically-induced primary sarcomas, they also prevent development of spontaneous epithelial tumors, providing definitive proof of the immunosurveillance theory.^{16,21}

Additional evidence of immunosurveillance in humans is supported by the fact that immunocompromised individuals are more susceptible to tumors of viral and non-viral origins. For example, patients infected with HIV are much more likely to develop certain types of cancer, including Kaposi sarcoma, non-Hodgkin lymphoma (NHL), and cervical cancer, compared to uninfected individuals.²² Furthermore, multiple studies have shown that organ transplant patients receiving immunosuppressant drugs have a greater incidence of cancer. Of 608 patients who received cardiac transplants between 1980 and

1993, the incidence of lung tumors was 25 times greater than that of the general population.²³ The evaluation of 5,692 patients who received renal transplants in Nordic countries between 1964-1982 had increased incidence ratios for colon, lung, bladder, and kidney cancers, in addition to malignant melanoma.²⁴ Finally, 0.3-0.4% of melanomas typically occur in the general pediatric population, yet this increases to 4% when specifically evaluating pediatric transplant patients.²⁵

In addition to the vast amount of evidence supporting the theory of immunosurveillance, several studies also suggested that the immune system is capable of selecting tumor variants that are better equipped to survive in an immunological environment.^{21,26} The idea that tumors are shaped by the immunological environment in which they are formed is referred to as tumor-sculpting. Taken together, this data led Robert Schreiber to hypothesize that the term “immunosurveillance” is no longer suitable. Instead, he proposed the “immunoediting theory” which attempts to describe the complex relationship between the immune system and cancer (Figure 1.5). The immunoediting theory takes into account both the host-protecting nature of the immune system and its tumor-sculpting capabilities and is comprised of three unique phases – elimination, equilibrium, and escape. The elimination phase is what was previously thought of as immunosurveillance. Here, the innate and adaptive immune system work to detect and destroy cancer cells, prior to the development of a medically detectable tumor. If the many immune molecules involved in the elimination phase successfully destroy cancerous cells, then the editing process is complete. However, if the immune system is unsuccessful in the complete eradication of the abnormal cells, then progression to the equilibrium phase occurs.^{16,27}

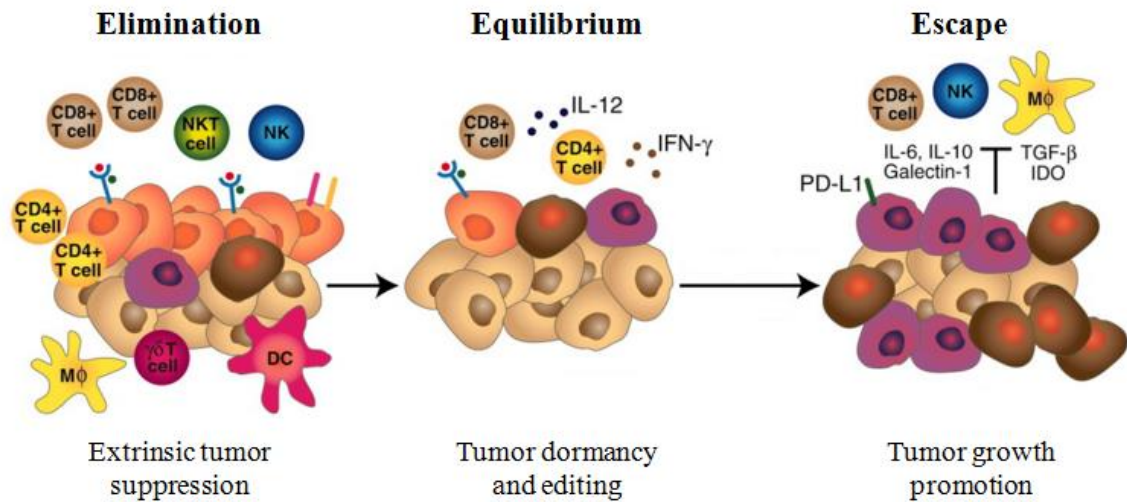


Figure 1.5 The theory of immunoeediting.²⁶ The immunoeediting theory details the relationship between the immune system and the development of cancer and is comprised of three phases. Elimination: the innate and adaptive immune systems work in concert to eliminate abnormal cells prior to growth into a tumor. Equilibrium: immune cells exert selective pressure onto abnormal cells that were not destroyed during elimination, keeping them in a dormant state without complete eradication. Escape: tumor cells that have accumulated genetic and epigenetic changes become insensitive to immune detection and/or elimination, resulting in the development of medically detectable tumors.

Equilibrium is suspected to be the longest phase in the process and can last for the entire lifetime of the host. In this phase, cancer cell variants that were not destroyed during elimination engage in a constant back-and-forth battle with the immune system. Immune cells exert selective pressure on cancer cells, ultimately keeping them in a dormant state but not completely clearing them from the body.^{16,27,28} The most obvious evidence of equilibrium is demonstrated by patients who relapse after decades of remission, suggesting that cancer cells remain in the body even after treatment.²⁹ Additionally, the development of tumors in organ transplant recipients with no outwardly apparent cancer in the donor demonstrates the effectiveness of the equilibrium phase. For

example, a melanoma patient in remission for 16 years donated both kidneys post-mortem to two individuals, both of whom later developed melanoma. This suggests that while the donor's immune system was functioning to keep the cancer in a dormant state, the depleted immune systems of the recipients allowed for progression to full-blown cancer.³⁰ Further evidence of the equilibrium phase was demonstrated when Koebel *et al.* treated mice with MCA and observed that mice with small, stable masses at the site of injection developed tumors when varying immune system components were disabled.^{29,31}

Eventually the immune system is no longer able to effectively keep cancer cells in a functionally dormant state. This failure by the immune system leads to the transition into the escape phase of immunoediting. Prior to this phase, extreme selective pressure is exerted on inherently unstable tumor cells. This results in an accumulation of genetic and epigenetic changes, resulting in poorly immunologic tumor cell variants which have become insensitive to immune detection and/or elimination. At this point, the immunologically-sculpted tumor cells are free to grow and expand in an uncontrolled manner, leading to the formation of tumors that are clinically detectable in size.²⁷

It is evident that an intimate and complex relationship exists between the immune system and the development of cancer. In order to take advantage of this, the focus must be placed arguably on the most important phase of the immunoediting process, equilibrium. By understanding how the immune system recognizes tumor cells, one can begin to envision ways to tip the scales in favor of the immune system, ultimately providing it with the knowledge and capability needed to eliminate transformed cells. The ways in which tumor cells differ from normal cells are referred to as the hallmarks of cancer (Figure 1.6). The first six of these hallmarks were outlined by Hanahan and

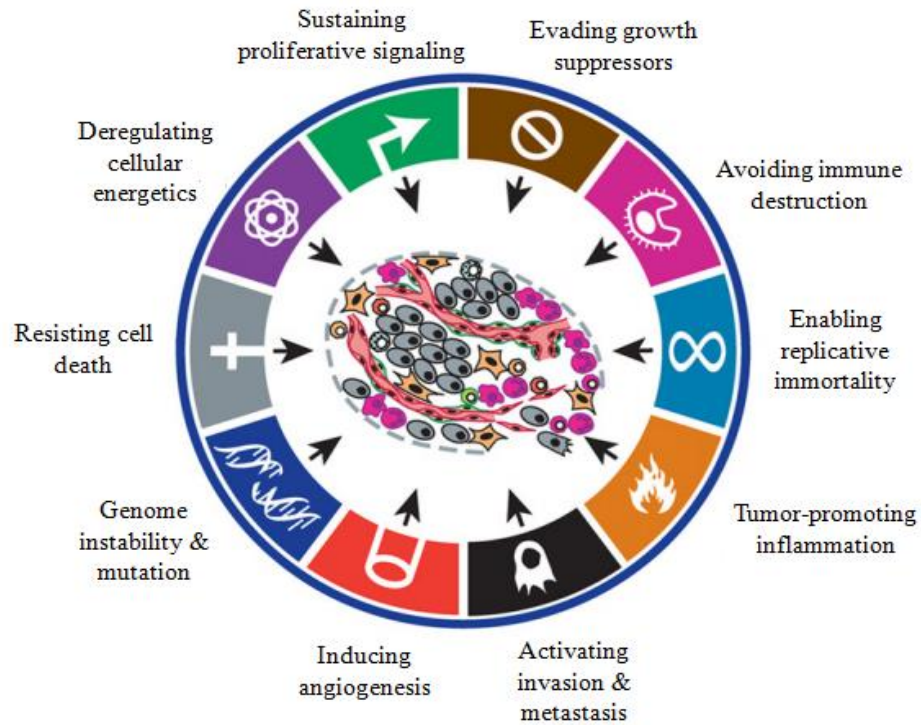


Figure 1.6 The hallmarks of cancer.³² The hallmarks of cancer represent capabilities acquired during the transition of cells from a normal to a cancerous state. These include sustaining proliferative signaling, evading growth suppressors, activating invasion and metastasis, enabling replicative immortality, inducing angiogenesis, and resisting cell death. Recently, four emerging hallmarks and enabling characteristics were added: deregulating cellular energetics, avoiding immune destruction, tumor-promoting inflammation, and genome instability and mutation. The central theme of this transition is the alteration of the intracellular environment.

Weinberg in 2000 and include sustaining proliferative signaling, evading growth suppressors, resisting cell death, enabling replicative immunity, sustained angiogenesis, and tissue invasion and metastasis.³² In 2011, Hanahan and Weinberg expanded on this by adding four emerging hallmarks: genome instability and mutation, tumor-promoting inflammation, reprogramming energy metabolism, and evading immune destruction.³³ While all of the hallmarks of cancer involve unique and complex processes, an underlying theme is the dysregulation of cellular signaling, resulting in the transformation of the intracellular environment.^{32,33}

A central theme in cellular signaling is the post-translational modification (PTM) of proteins, specifically protein phosphorylation which will be extensively discussed in chapter 3. Briefly, protein phosphorylation involves the addition of a phosphate group to

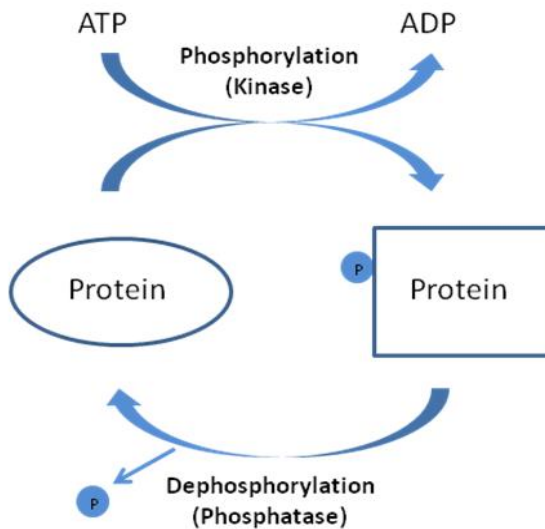


Figure 1.7 The cycle of protein phosphorylation. Kinase enzymes catalyze the transfer of a phosphate group from ATP to a protein at serine, threonine, or tyrosine residues. This process can be reversed by phosphatase enzymes which catalyze the hydrolysis of phosphate groups.

an amino acid side chain, namely serine, threonine, or tyrosine, by a kinase enzyme (Figure 1.7). This process is reversible as the phosphate group can be easily removed by phosphatase enzymes. Protein phosphorylation is the most commonly occurring PTM; over one-third of all proteins are expected to be phosphorylated

at some point during their lifetime.³⁴ In addition, it is responsible for guiding many complex cellular processes such as cell growth, division, and migration. For instance, the Hippo signaling pathway

involves a kinase cascade which results in the control of organ size by regulating cell proliferation and apoptosis.³⁵ One of the most widely studied signaling pathways is the mitogen-activated protein kinase (MAPK) pathway which is involved in cell growth, proliferation, differentiation, migration, and apoptosis.³⁶ Both of these pathways are shown to be dysregulated in cancer, playing a critical role in the development of tumors.^{36,37}

The dysregulation of cell signaling pathways in cancer, resulting from the accumulation of genetic and epigenetic changes, leads to markedly increased, aberrant phosphorylation. These aberrantly phosphorylated proteins are degraded by the proteasome in the same manner as their unmodified counterparts, resulting in a subset of tumor-specific phosphopeptides. These phosphopeptides then enter into the HLA class I processing pathway for presentation where circulating CTLs can recognize them as antigenic and mount a significant immune response towards the malignant cells presenting them.⁸

The goal of this work is to identify tumor-specific phosphopeptides, specifically in human hepatocellular carcinoma (HCC) tumor tissue, using a combination of improved sample preparation techniques, complementary immobilized metal affinity chromatography (IMAC) enrichments, and high resolution mass spectrometry. The tumor-specific phosphopeptides we identify result from dysregulated cell signaling pathways and have likely not been subjected to central tolerance by the immune system. Therefore, their presentation by HLA class I molecules to CTLs should elicit a significant immune response, making them ideal candidates for the development of novel cancer immunotherapeutics.

1.2 Introduction to Methods

1.2.1 HLA-Associated Peptide Isolation (Performed by NB, University of Birmingham)

The process of identifying HLA-associated phosphopeptides involves first isolating all bound peptides from cancer tissues or immortalized cell lines. Tumor and adjacent normal tissue samples are obtained from patients in varying stages of liver disease from the Queen Elizabeth Hospital and Center for Liver Research at the University of Birmingham. Additionally, immortalized cancerous cell lines, such as HepG2, are used for analysis. To begin, 10^8 - 10^{10} cells from either sample origin are lysed using 3-[(3-cholamidopropyl) dimethylammonio]-1-propane sulfonate (CHAPS) buffer and undergo centrifugation to separate the intracellular contents from cell membrane debris. The supernatant is then incubated overnight with NHS-sepharose beads conjugated to HLA class I specific antibodies (W6/32). The beads are rinsed and transferred to a 5 kDa molecular weight cut off (MWCO) filter. Finally, 10% acetic acid is used to elute the peptides from the HLA molecules by disrupting the noncovalent interactions within the peptide binding groove. Samples are then centrifuged allowing for the eluted peptides to pass through the MWCO filter.^{8,38} The resulting peptide mixture is then sent to our laboratory for analysis. Alternatively, beads still bound to HLA:peptide complexes can be sent to our laboratory allowing for in-house peptide elution.

1.2.2 STAGE Tip Sample Cleanup

In order to effectively analyze HLA-associated peptide samples, any salts present which could interfere with the analysis must first be removed. This desalting step has been routinely performed using the peptide mixture sent to our laboratory after the 10% acetic acid elution step. This mixture is passed through a cleanup column (360 μm o.d. x 150 μm i.d.) packed with irregular C18 (5-20 μm diameter) packing material. The sample is then rinsed to remove salts and the peptides are eluted into a tube using a gradient of 100% solvent A (0.1M acetic acid in water) and 0% solvent B (70% acetonitrile and 0.1M acetic acid) to 80% solvent B in 70 minutes. Alternatively, STop And Go Extraction (STAGE) tips are used. In this methodology, peptides are eluted from HLA molecules bound to beads using 10% acetic acid directly onto a pipette tip containing a punch-out of C18 resin. The sample is rinsed to remove salts and peptides are eluted from the resin using a gradient step elution of increasing organic solvent concentrations (20%, 40%, 60%, 80% acetonitrile) and collected for further analysis.³⁹ After either desalting procedure, an aliquot corresponding to $1e7$ cell equivalents (C. Eq.) is subjected to high pressure liquid chromatography-electrospray ionization-tandem mass spectrometry (HPLC-ESI-MS/MS) to determine the total peptide content of the sample as well as the amount of sample needed for subsequent phosphopeptide enrichment. The implementation of STAGE tips for improved sample desalting will be discussed in further detail in chapter 2.

1.2.3 Phosphopeptide Enrichment

The task of identifying phosphopeptides presented by HLA class I molecules at the cell surface is challenging for a number of reasons. First, protein phosphorylation is a transient post-translational modification. Kinase and phosphatase enzymes work together to incorporate and remove phosphate groups throughout the course of cell signaling processes. The fast on-off rate at which this occurs limits the time that phosphate groups remain on specific sites of a given protein.³⁴ Secondly, each cell is capable of presenting up to 250,000 HLA class I molecules on its surface. Finally, each individual can express up to six different HLA alleles, all of which can present 10,000 unique peptides. Taken together, these elements result in phosphopeptides accounting for only 1% of all peptides presented by HLA class I molecules at the cell surface. In order to detect and sequence these low-level phosphopeptides, enrichment techniques must be employed.⁴⁰

Here, we use immobilized metal affinity chromatography (IMAC) techniques to separate low-level phosphopeptides from their unmodified counterparts in complex tissue samples and immortalized cell lines. This methodology takes advantage of the affinity of negatively-charged phosphate groups for positively-charged metal ions, specifically iron(III) cations. Briefly, complex mixtures of HLA-associated peptides are exposed to a resin chelated with Fe^{3+} metal ions. Phosphorylated peptides bind via electrostatic interactions while unmodified peptides are washed away. Bound phosphopeptides are then eluted using ascorbic acid which reduces Fe^{3+} to Fe^{2+} , lowering the affinity for phosphate groups. These phosphopeptides are then analyzed via HPLC-ESI-MS/MS and

detected at sub-stoichiometric levels. We utilize two IMAC techniques – iron(III)-iminodiacetic acid (Fe-IDA) IMAC and iron(III)-nitrilotriacetic acid (Fe-NTA) IMAC – to enrich for unique subsets of phosphopeptides from various samples.⁴¹ The incorporation of these complementary enrichment techniques will be extensively discussed in chapter 3.

1.2.4 HPLC-ESI-MS/MS

The enriched phosphopeptide elution is loaded onto a precolumn, or PC, (360 μm o.d. x 75 μm i.d.) packed with irregular C18 (5-20 μm diameter) packing material. The PC is thoroughly rinsed with 0.1% acetic acid before connecting it to an analytical column, or AC, (360 μm o.d. x 50 μm i.d.) packed with regular C18 (5 μm diameter) packing material and equipped with a laser-pulled, electrospray emitter tip (2 μm diameter). Known concentrations of two internal peptide standards (angiotensin and vasoactive intestinal peptide) are loaded onto the column for quantitation purposes. Enriched phosphopeptides are separated on column by reverse-phase HPLC using a gradient of 100% solvent A and 0% solvent B to 60% solvent B in 60 minutes at a flow rate of 60 nL/min. Peptides bind to the C18 stationary phase through hydrophobic interactions. By increasing the organic solvent concentration, the hydrophobicity of the mobile phase increases, causing peptides to elute from the C18 resin in order of increasing hydrophobicity.⁴¹

Upon elution from the column, peptide ions are generated through electrospray ionization (ESI), an extremely sensitive technique commonly used for biological samples

due to their nonvolatile nature.⁴² During this process, a +2 kV voltage is applied to the waste line of the HPLC, which in turn provides a significant positive potential at the emitter tip of the analytical column. As the liquid leaves the column the solution in the droplet polarizes, causing a buildup of positively-charged ions that migrate toward the grounded counter electrode at the inlet of the mass spectrometer. This process eventually causes the formation of a Taylor cone, in which a fine mist of charged droplets is ejected. As the droplets move toward the inlet, they undergo solvent evaporation. Eventually, the electrostatic repulsions within the droplet overcome the surface tension holding the droplet together. At this point, the Rayleigh limit is reached and the droplets undergo Coulombic fission, resulting in a population of progeny droplets. According to the Charged Residue Model (CRM), this cycle of evaporation followed by Coulombic fission continues until the remaining droplet contains only one solute molecule. This molecule is then desorbed into the gas phase and retains the positive charge imparted onto it from the solvent.⁴³ Multiply protonated peptide ions generated by ESI are focused by RF-only quadrupoles into a high resolution mass analyzer.

A tandem MS experiment involves two stages of mass analysis in which MS1 and MS2 spectra are acquired. The first stage of mass analysis is acquisition of a full-scan, high resolution mass spectrum which identifies every precursor mass eluting at any point during a chromatographic elution. MS1 spectra are obtained using either Fourier transform ion cyclotron resonance (FT-ICR) or an Orbitrap mass analyzer. FT-ICR mass analysis involves trapping ions in a purely magnetic field, in which their trajectories are inherently curved. Ions will travel in a circular path with a frequency of orbit specific to each mass-to-charge (m/z) ratio. In order to detect a signal from these ions, a spatially

coherent packet must be formed which oscillates with a large radius. To accomplish this, a uniform, electric field oscillating at the frequency of a given ion is applied, causing all ions with that particular m/z ratio to be accelerated to the same radius. As the trajectory of the packet of ions passes a pair of electrodes, an image current is induced which is then Fourier transformed into a mass spectrum.^{44,45}

In Orbitrap mass analysis, peptide ions are focused into the C-trap, an RF-only bent quadrupole, where they are stored prior to injection into the Orbitrap mass analyzer. Storage of ions in the C-trap fulfills the main requirement of injection which is that the entering packet of ions must have narrow spatial and temporal distributions to ensure their stability and coherency. Ion packets are radially ejected from the C-trap into the Orbitrap where they become trapped in a purely electrostatic field around a central electrode. The ions begin to orbit in the axial directions and distribute into oscillating rings, each with a frequency that is characteristic of their m/z ratio. This movement induces an image current between the ions and the two outer electrodes that can be measured and fast Fourier transformed into a mass spectrum.⁴⁶

After acquisition of an MS1 spectrum, the most abundant precursor masses are selected for fragmentation in the linear ion trap (LTQ) of the instrument. Two fragmentation techniques are used – collision activated dissociation (CAD)⁴⁷ and electron transfer dissociation (ETD)⁴⁸ – to generate fragment ions which are then radially ejected from the ion trap and detected by electron multipliers.⁴⁶ In CAD, peptide ions that have been randomly protonated along the peptide backbone as a result of the ESI process are kinetically excited and undergo hundreds of low-energy collisions with inert helium gas molecules. During each collision, a portion of translational energy is converted into

vibrational energy, which is then distributed throughout the covalent bonds within the molecule. The internal energy increases upon each collision, eventually exceeding the activation barrier for a particular bond cleavage. At this point the molecule fragments, resulting in the formation of complementary b- and y-ions which contain the N- and C-termini, respectively (Figure 1.8). By examining the mass differences between adjacent members of the b- or y-ion series, the sequence of the peptide can be elicited. CAD fragmentation is ideal for short peptides (<15 amino acid residues) with low charge states ($z \leq +3$).⁴⁷

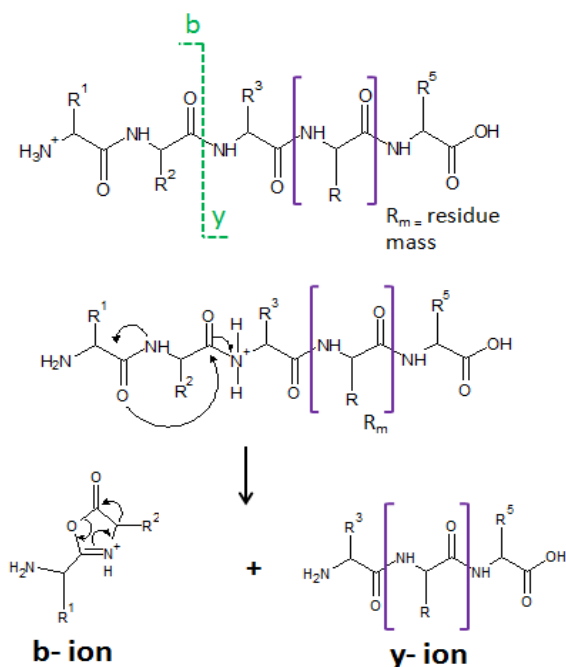


Figure 1.8 Mechanism of collision activated dissociation (CAD) fragmentation. Peptide ions are randomly protonated along the peptide backbone as a result of ESI. Ions are kinetically excited and undergo hundreds of low-energy collisions with inert helium gas molecules. On collisions, a portion of translational energy is converted into vibrational energy and is distributed throughout the covalent bonds within the molecule. Eventually the internal energy exceeds the activation barrier for a particular bond cleavage, causing the molecule to fragment into complementary b- and y-ion pairs, containing the N- and C-termini, respectively. Purple brackets indicate a single amino acid residue.

While CAD can provide adequate sequence information for unmodified peptides, there are drawbacks associated with using this fragmentation technique to sequence phosphorylated peptides. When a peptide ion builds up enough internal energy to

fragment, it tends to do so through the lowest energy pathway possible.⁴⁷ In the case of phosphorylation, this occurs through a β -elimination of phosphoric acid ($\Delta 98$ Da), which requires less energy than cleavage of an amide linkage. This phenomenon results in an MS2 dominated by the mass of the parent ion after the loss of phosphoric acid (Figure 1.9). As a result, it can be difficult to obtain full sequence coverage of phosphorylated peptides using only CAD fragmentation.⁴⁸

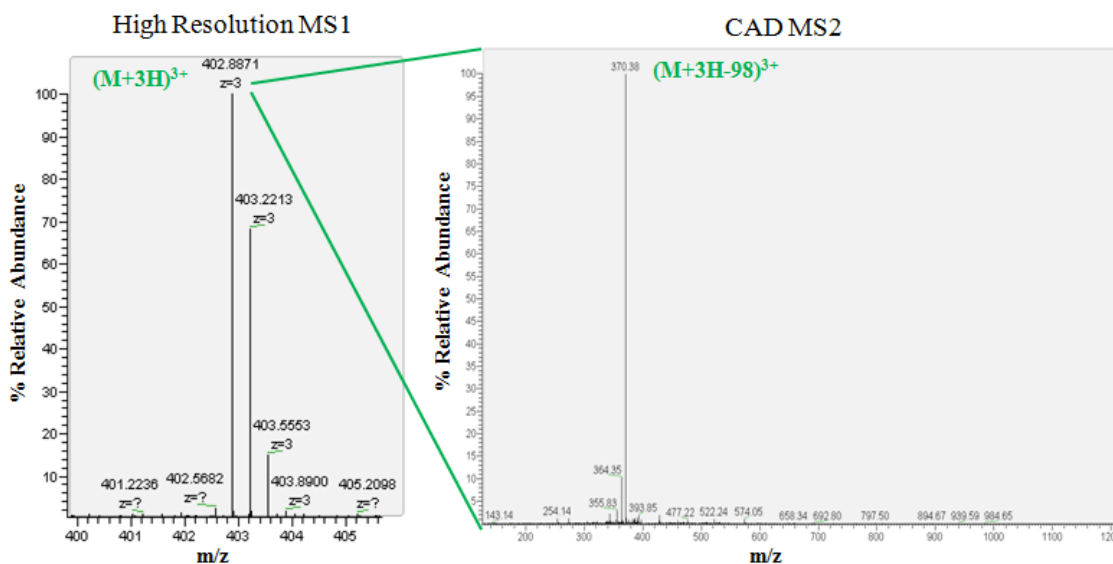


Figure 1.9 CAD spectrum of a phosphorylated peptide. A full MS1 spectrum is acquired showing an $(M+3H)^{3+}$ peptide precursor isolated using a 3 m/z window. CAD fragmentation results in an MS2 containing a predominant peak associated with the neutral loss of phosphoric acid ($\Delta 98$ Da) from the precursor ion. The lack of sequence information provided by CAD fragmentation of phosphorylated peptides makes spectral interpretation difficult, demonstrating the need for additional fragmentation methods. Figure adapted from reference 41.

To combat this issue, ETD fragmentation is used in addition to CAD fragmentation. Electron transfer dissociation was developed in the Hunt laboratory in 2004 and is capable of preserving labile PTMs, such as phosphorylation. In ETD, a radical anion is used as a vehicle for delivering thermal electrons (<0.2 eV) to multiply charged peptide ions formed by ESI. A subsequent reaction occurs in which an electron is transferred to an amide bond along the peptide backbone, generating a carbonyl radical anion. This anion can then abstract a proton from a nearby positively-charged nitrogen atom, inducing cleavage of the amide bond. This cleavage results in formation of complementary c- and z[•]-ions containing the N- and C-termini, respectively (Figure 1.10). Similarly to CAD, mass differences between c- and z[•]-ions in series can be used for sequence determination.⁴⁸ The mechanism of ETD inherently results in more backbone cleavages than CAD, providing greater sequence coverage of longer, highly charged peptides.⁴⁹ However, since HLA-associated phosphopeptides are typically 8-12 amino acids in length with a predominant charge state of +2, ETD rarely provides full sequence coverage. Thus, a combination of CAD and ETD fragmentation is used to provide adequate sequence coverage for phosphopeptide identification.

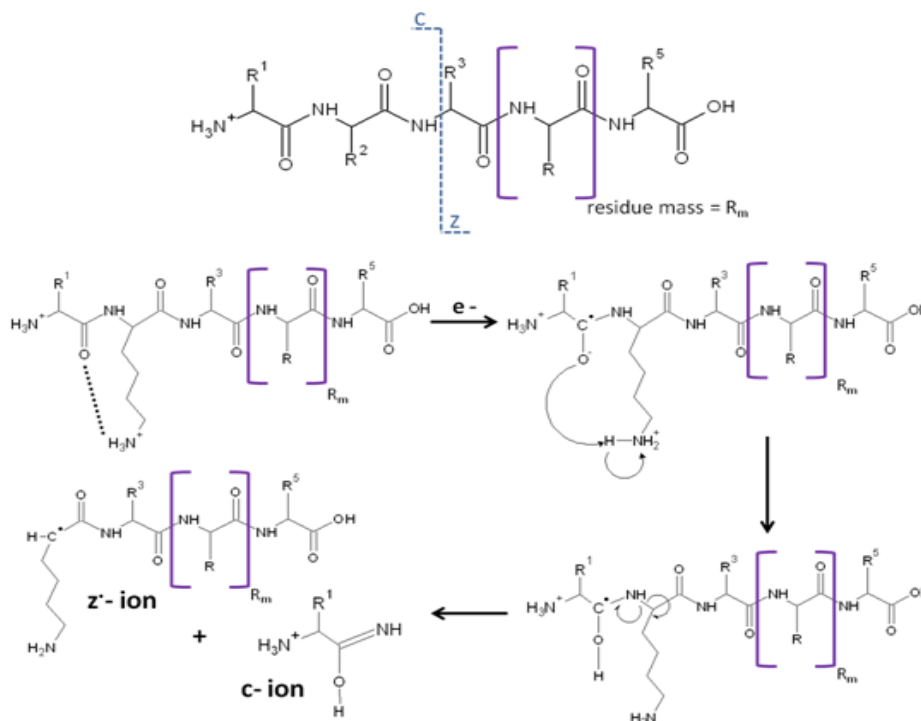


Figure 1.10 Mechanism of electron transfer dissociation (ETD) fragmentation. Radical anions are used as vehicles for delivering electrons to multiply charged peptide ions. An electron is transferred to an amide bond along the peptide backbone, generating a carbonyl radical anion. This anion abstracts a proton from a nearby positively-charged nitrogen atom, inducing cleavage of the amide bond and forming complementary c - and z' -ions, containing the N- and C-termini, respectively.

In addition to the combination of fragmentation techniques for improved phosphopeptide sequencing, we have incorporated a new Orbitrap Fusion Tribid mass spectrometer for enhanced sample analysis. The novel architecture of this instrument includes a T-configuration comprised of three separate mass separation devices – a mass filter quadrupole, a dual-pressure linear ion trap, and an ultra-high-field Orbitrap mass analyzer (Figure 1.11).⁵⁰ This unique structure allows for parallelization which is not possible with previous instrumentation in which the Orbitrap is located in the rear of the instrument. With the Orbitrap Fusion instrument, precursor selection can be performed in

the quadrupole mass filter and ions sent to either the Orbitrap mass analyzer or the linear ion trap. In this way, MS1 spectra are obtained in the Orbitrap while MS2 spectra are simultaneously obtained upon fragmentation in the linear ion trap, allowing for acquisition of a greater amount of data in the same time frame.⁵⁰

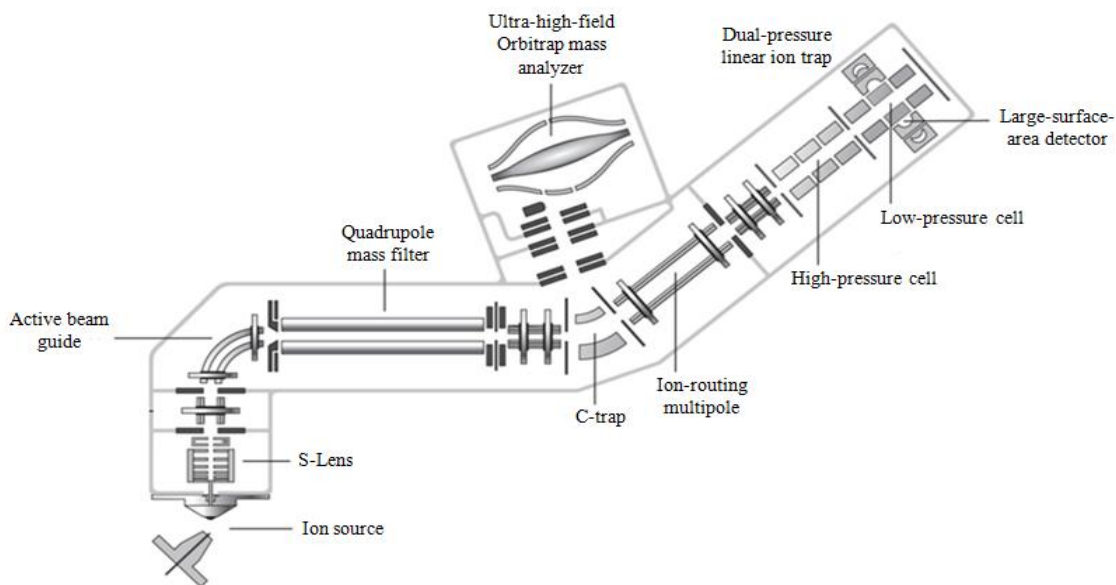


Figure 1.11 Schematic diagram of Orbitrap Fusion Tribrid mass spectrometer. T-configuration comprised of a quadrupole mass filter, a dual-pressure linear ion trap, and an ultra-high-field mass spectrometer increases efficiency of ion transmission and allows for parallelization of MS1 and MS2 acquisition. Figure adapted from Planet Orbitrap.

Additionally, the improved Orbitrap Fusion software allows for deeper sample analysis for several reasons. First, precursor ions can be selected in a top-speed fashion as opposed to selecting a set number of precursors to undergo fragmentation. Previous instrumentation allowed for a data-dependent toggle run in which the top 5-10 precursor ions were selected for CAD fragmentation followed by ETD fragmentation. However, incorporation of a top-speed acquisition option allows the user to define a specific time

window during which the instrument will select and fragment as many precursor ions as possible. Second, availability of a triggered instrument method allows for more selective fragmentation and results in increased numbers of useful MS2 spectra during sample runs. Here, ETD scans are only acquired if a neutral loss characteristic of the loss of a phosphate group is present in the previous CAD spectrum. The improved speed of data acquisition coupled with the ability to selectively perform ETD on potentially phosphorylated peptides results in a drastic increase in the number of phosphopeptide identifications in each sample. Using this methodology, we are able to 1) regularly detect phosphopeptides present at attomole levels in tumor and normal tissue samples as well as immortalized cell lines, 2) accurately assign sequences to detected phosphopeptides and 3) confidently site-localize modifications of these extremely low-level phosphopeptides.

1.2.5 Data Processing

The enhanced speed and sensitivity of the Orbitrap Fusion Tribrid mass spectrometer allows for the acquisition of a greater number of MS2 spectra during a sample run. The interpretation of this data relies heavily on the use of several data processing tools. Once a data file is acquired, the MS2 spectra are searched against human protein databases, such as RefSeq or Uniprot, as well a phosphopeptide library containing previously identified phosphopeptides from various tumor and normal tissue samples in our laboratory. These searches are performed using two search algorithms – Open Mass Spectrometry Search Algorithm (OMSSA)⁵¹ and Byonic.⁵²

OMSSA is a probability-based matching algorithm that filters noise peaks and extracts m/z values from experimentally obtained MS2 spectra. These values are then compared to m/z values of peptides resulting from an *in silico* digestion of a protein sequence library. The resulting search hits are statistically scored, where a low score indicates a low probability that the search hit occurred by random chance.⁵¹ Alternatively, Byonic is a search algorithm that combines *de novo* sequencing with database searching. Using *de novo* analysis, this algorithm looks for m/z values that are likely to be b- and y-ion or c- and z•-ion pairs. It then uses these pairs to extract candidate peptides from the protein database. The predicted fragmentation of the candidate peptides is then compared to the observed peaks in the experimentally acquired MS2 spectra. Matching peptides are statistically evaluated where a high score indicates that the peptide is more likely to be an accurate match to the spectrum.⁵² Both search algorithms allow for user-defined mass tolerance windows as well as the selection of variable and static chemical modifications to the peptides. By using a combination of the OMSSA and Byonic search algorithms, we can search for HLA-associated peptides that are phosphorylated. Search hits that have the highest probability of being correct are manually validated using accurate precursor mass (± 5 ppm) and analysis of fragmentation patterns in CAD and ETD spectra.

Although OMSSA and Byonic provide a list of many possible phosphopeptides present within a sample, there are occasionally spectra that do not match to any peptides in the protein database. In this case, we utilize an in-house neutral loss program to generate a list of potential phosphopeptides for further evaluation. This program scans every CAD spectrum in a data file and looks for signature ions indicative of a loss of phosphoric acid ($\Delta 98$ Da). When a peak corresponding to this loss is present, the program

checks that 1) the intensity of the peak is greater than 50% relative abundance or 2) the peak is in the top five most abundant peaks within the spectrum. If one or both of these criteria are met, the spectrum is reported as a potential phosphopeptide. We then use a combination of *de novo* sequencing and bioinformatic tools, such as Mascot (matrixsciences.com), to assign sequences to the unknown spectra. Mascot allows the user to input a precursor mass and assigned fragment ions which are then searched against peptides in a protein database. Potential hits are reported where higher scores indicate a low probability of a random match and manual validation is then used to confirm the peptide sequence. By combining these data processing tools, we are able to ensure that the sequences of the HLA-associated phosphopeptides we identify are correct.

1.2.6 Biological Testing (Performed by NB, University of Birmingham)

Once HLA-associated phosphopeptides are identified, the sequences are synthesized using Fmoc chemistry and purified via HPLC to >95% purity. The sequences of the synthetic phosphopeptides are confirmed using mass spectrometry prior to biological testing. During the course of chronic liver disease many mutations and epigenetic changes accumulate in liver cells, leading to increased amounts of aberrantly phosphorylated peptides on the surface of altered hepatocytes. Based on the immunoediting theory, we believe that transformation events are common occurrences and that the immune system is able to detect and clear malignant cells during the transition from healthy to diseased liver prior to the formation of full-blown HCC.^{27,28} Thus, we hypothesize that these patients should have memory T cell responses to tumor-

specific phosphopeptides. To confirm this hypothesis, we test the ability of our phosphopeptide antigens to stimulate immune responses in healthy donors (HD) and patients with chronic liver disease for comparison to those of patients with HCC. Using two screening techniques – enzyme-linked immunospot (ELISpot)^{38,53} and intracellular cytokine staining (ICS)⁵⁴ – to evaluate elicited immune responses, we are able to identify the best candidates for development of cancer immunotherapeutics.

Enzyme-linked immunospot assays are a highly-sensitive screening technique which allow for the evaluation of immunological activity at the single-cell level. Additionally, this tool is extremely reliable in that correlation between immunological responses in ELISpot assays have been linked to clinical benefits in recent cancer immunotherapeutic trials. The basic principle of ELISpot involves incubating peripheral blood mononuclear cells (PBMCs) from donors with antigens of interest and measuring the number of cells which release cytokines in response to a specific antigen (Figure 1.12).⁵³ The results are displayed as a number of spot-forming units per 10^6 PBMCs. Responses of the individual peptide antigens are compared to those of the positive control and viral peptides to which most individuals will respond due to previous exposure. Peptides capable of eliciting responses similar in magnitude to positive controls and viral peptides are considered strong candidates for immunotherapeutics.³⁸

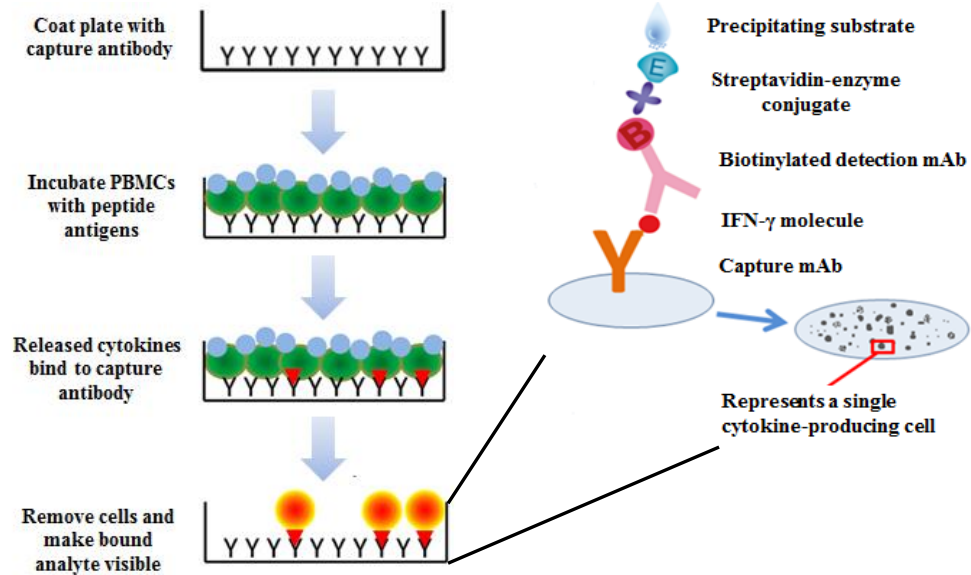


Figure 1.12 Enzyme-linked immunospot (ELISpot) assay. IFN- γ -specific antibodies are immobilized on a polyvinylidene fluoride (PVDF)-backed membrane. Isolated PBMCs are incubated in wells with peptide antigens. CTLs with TCRs specific to that peptide antigen produce and secrete cytokines which bind to the capture antibody. Addition of a biotinylated detection antibody in combination with a streptavidin enzyme conjugate results in the formation of visible spots. Each spot is indicative of a single cytokine-producing cell allowing for evaluation of immunological response to specific antigens at a single cell level. Figure adapted from reference 53 and Bioconnect Diagnostics Protocols.

While we have used ELISpot assays routinely in the past in our laboratory as a sensitive, high throughput method for analyzing the ability of phosphopeptide antigens to elicit an immune response, it is not possible to be certain where that response originates. This is because PBMCs include any blood cell with a round nucleus, i.e. lymphocytes (T cells, B cells, NK cells), monocytes, and macrophages. Thus, while it is likely that the immune responses against the antigens tested do come as a result of CTL activation, it cannot be definitively stated. Therefore, we have implemented the use of intracellular cytokine staining assays to combat this issue. In ICS, cells are exposed to specific stimuli and any cytokines produced are trapped within the cell using Golgi inhibitors.

Fluorescently-labeled antibodies specific to various cytokines are then used to visualize which cytokines are present and at what levels (Figure 1.13). In this work, donors are tested against various phosphorylated peptide antigens and the production of three cytokine molecules is measured.⁵⁴ These cytokines include IFN- γ , responsible for recruitment and activation of the innate immune system, tumor necrosis factor α (TNF α), a central regulator of inflammation, and interleukin-2 (IL-2), responsible for activation and proliferation of T cells. Additionally, we monitor the presence of CD107a, a cell surface protein that is upregulated following degranulation and loss of perforin and is thus indicative of CTL-mediated killing.⁵⁵

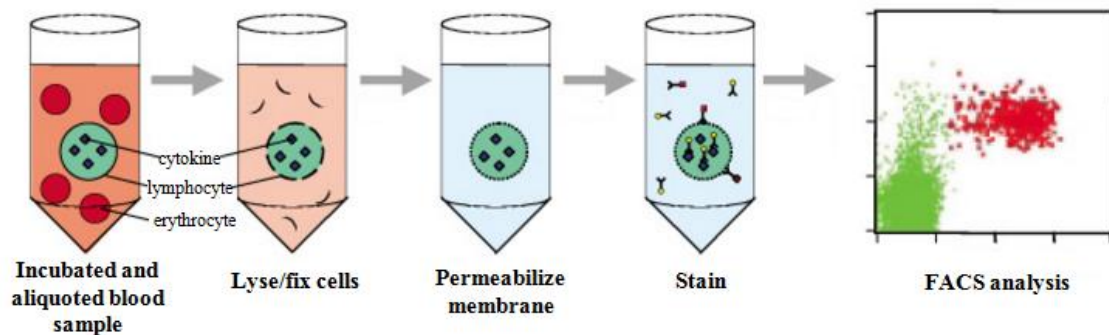


Figure 1.13 Intracellular cytokine staining (ICS) assay. Cytokine production in response to specific stimuli is measured using ICS. PBMCs are isolated, exposed to phosphorylated peptides and expanded for seven days. Golgi inhibitors are used to prevent cytokine release from the cells. Upon fixation and permeabilization, cytokine-specific antibodies are allowed access to intracellular compartments where they bind to trapped antibodies. Flow cytometry is then used to visualize the stains and measure the levels of cytokines produced. Figure adapted from BD Biosciences protocol.

PBMCs are isolated from donors and resuspended in AIM-V medium with 10% human AB serum. Cells are stimulated with synthetic phosphopeptide antigens (10 $\mu\text{g/mL}$) and expanded for 7 days. Unstimulated cells are used as a negative control while phytohaemagglutinin (PHA) is used as a positive control (1 $\mu\text{g/mL}$). On day 6 of expansion, cells are restimulated with peptide antigens and incubated overnight. Cells are

then harvested, washed with phosphate-buffered saline (PBS), and stained with a fixable viability dye (APC-Cy7) and surface antibodies – anti-CD3 (APC) and anti-CD8 (PerCP). The cells are then washed, fixed using 2% paraformaldehyde, permeabilized using 0.5% saponin, and stained with anti-IFN- γ (PE), anti-IL-2 (Pacific blue), and anti-TNF α (PE-Cy5.5) for 30 minutes at room temperature. Finally, cells are washed and analyzed for cytokine production using flow cytometry.

Using ICS data, we are able to obtain reliable results demonstrating the ability of the tumor-specific phosphopeptides we identify to elicit immune responses in a variety of patients. Additionally, we are able to show that the resulting immune responses do reside in the central memory compartment, suggesting that these phosphopeptides may be targets of cancer immune surveillance.⁵⁶ Taken together, this data provides strong evidence pointing to the importance of tumor-specific phosphopeptides in the development of novel cancer immunotherapeutics.

1.3 References

1. Smyth MJ, Dunn GP, Schreiber RD. Cancer immunosurveillance and immunoediting: the roles of immunity in suppressing tumor development and shaping tumor immunogenicity. *Adv Immunol.* 2006; 90: 1-50.
2. American Cancer Society. *Cancer Facts & Figures 2015*. Atlanta: American Cancer Society; 2015.
3. Schuster M, Nechansky A, Loibner H, Kircheis R. Cancer Immunotherapy. *Biotechnol.* 2006; 1:138-147.
4. Neefjes J, Jongsma ML, Paul P, Bakke O. Towards a systems understanding of MHC class I and MHC class II antigen presentation. *Nat Rev Immunol.* 2011; 11(12):823-836.
5. Sijts EJ, Kloetzel PM. The role of the proteasome in the generation of MHC class I ligands and immune response. *Cell Mol Life Sci.* 2011; 68(9):1491-1502.
6. Blum JS, Wearsch PA, Cresswell P. Pathways of antigen processing. *Annu Rev Immunol.* 2013; 31:443-473.
7. Murphy K. (2012) *Janeway's Immunobiology*, 8th edition. New York, NY: Garland Science.
8. Zarling AL, Ficarro SB, White FM, Shabanowitz J, Hunt DF, Engelhard VH. Phosphorylated peptides are naturally processed and presented by major histocompatibility complex class I molecules in vivo. *J Exp Med.* 2000; 192(12):1755-1762.
9. Starr TK, Jameson SC, Hogquist KA. Positive and negative selection of T cells. *Annu Rev Immunol.* 2003; 21:139-176.
10. Godfrey DI, Kennedy J, Mombaerts P, Tonegawa S, Zlotnik A. Onset of TCR-beta gene rearrangement and role of TCR-beta expression during CD3-CD4-CD8 thymocyte differentiation. *J Immunol.* 1994; 152(10):4783-4792.
11. Parham P. (2009) *The Immune System*, 3rd edition. New York, NY: Garland Science.
12. Anderson MS, Su MA. Aire and T cell development. *Curr Opin Immunol.* 2011; 23(2):198-206.
13. Berke G. The CTL's kiss of death. *Cell.* 1995; 81(1):9-12.
14. Burnet M. Cancer – a biological approach. *Br Med J.* 1957; 1(5023):841-847.
15. Thomas, L. 1959. Discussion. In *Cellular and Humoral Aspects of the Hypersensitive States*, H. S. Lawrence (ed.), Hoeber-Harper, New York, pp. 529–533.
16. Dunn GP, Bruce AT, Ikeda H, Old LJ, Schreiber RD. Cancer immunoediting: from immunosurveillance to tumor escape. *Nat Immunol.* 2002; 3(11):991-998.
17. Dighe AS, Richards E, Old LJ, Schreiber RD. Enhanced in vivo growth and resistance to rejection of tumor cells expressing dominant negative IFN γ receptors. *Immunity.* 1994; 1:447-456.
18. Kaplan DH, Shankaran V, Dighe AS, Stockert E, Aquet M, Old LJ, Schreiber RD. Demonstration of an interferon gamma-dependent tumor surveillance system in immunocompetent mice. *Proc Natl Acad Sci.* 1998; 95(13):7556-7661.

19. Van den Broek ME, Kagi D, Ossendorp F, Toes R, Vamvakas S, Lutz WK, Melief CJ, Zinkernagel RM, Hengartner H. Decreased tumor surveillance in perforin-deficient mice. *J Exp Med*. 1996; 184(5):1781-1790.
20. Shinkai Y, Rathbun G, Lam KP, Oltz EM, Stewart V, Mendelsohn M, Charron J, Datta M, Young F, Stall AM, Alt FW. RAG-2-deficient mice lack mature lymphocytes owing to inability to initiate V(D)J rearrangement. *Cell*. 1992; 68(5):855-867.
21. Shankaran V, Ikeda H, Bruce AT, White M, Swanson PE, Old LJ, Schreiber RD. IFN γ and lymphocytes prevent primary tumor development and shape tumor immunogenicity. *Nature*. 2001; 410:1107-1111.
22. Grulich AE, van Leeuwen MT, Falster MO, Vajdic CM. Incidence of cancers in people with HIV/AIDS compared with immunosuppressed transplant recipients: a meta-analysis. *Lancet*. 2007; 370(9581):59-67.
23. Pham SM, Kormos RL, Landreneau RJ, Kawai A, Gonzalez-Cancel I, Hardesty RL, Hattler BG, Griffith BP. Solid tumors after heart transplantation: lethality of lung cancer. *Ann Thorac Surg*. 1995; 60(6):1623-1626.
24. Birkeland SA, Storm HH, Lamm LU, Barlow L, Blohme I, Forsberg B, Eklund B, Fjeldborg O, Friedberg M, Frodin L. Cancer risk after renal transplantation in the Nordic countries. *Int J Cancer*. 1995; 60(2):183-189.
25. Penn I. Malignant melanoma in organ allograft recipients. *Transplantation*. 1996; 61(2):274-278.
26. Street SE, Trapani JA, MacGregor D, Smyth MJ. Suppression of lymphoma and epithelial malignancies effected by interferon gamma. *J Exp Med*. 2002; 196(1):129-134.
27. Schreiber RD, Old LJ, Smyth MJ. Cancer immunoediting; integrating immunity's roles in cancer suppression and promotion. *Science*. 2011; 331(6024):1565-1570.
28. Bhatia A, Kumar Y. Cancer-immune equilibrium: questions unanswered. *Cancer Microenviron*. 2011; 4(2):209-217.
29. Teng MW, Swann JB, Koebel CM, Schreiber RD, Smyth MJ. Immune-mediated dormancy: an equilibrium with cancer. *J Leukoc Biol*. 2008; 84(4):988-993.
30. MacKie RM, Reid R, Junor B. Fatal melanoma transferred in a donated kidney 16 years after melanoma surgery. *N Engl J Med*. 2003; 348(6):567-568.
31. Koebel CM, Vermi W, Swann JB, Zerafa N, Rodig SJ, Old LJ, Smyth MJ, Schreiber RD. Adaptive immunity maintains occult cancer in an equilibrium state. *Nature*. 2007; 450:903-907.
32. Hanahan D, Weinberg RA. The hallmarks of cancer. *Cell*. 2000; 100(1):57-70.
33. Hanahan D, Weinberg RA. Hallmarks of cancer: the next generation. *Cell*. 2011; 144(5):646-674.
34. Sefton, B. M. 2001. Overview of Protein Phosphorylation. *Curr Protoc in Cell Biol*. 00:14.1:14.1.1–14.1.3.
35. Yu F, Zhang Y, Park HW, Jewell JL, Chen O, Deng Y, Pan D, Taylor SS, Lai Z, Gaun K. Protein kinase A activates the hippo pathway to modulate cell proliferation and differentiation. *Genes Dev*. 2013; 27(11):1223-1232.
36. Dhillon AS, Hagan S, Rath O, Kolch W. MAP kinase signaling pathways in cancer. *Oncogene*. 2007; 26:3279-3290.

37. Harvey KF, Zhang X, Thomas DM. The hippo pathway and human cancer. *Nat Rev Can.* 2013; 13:246-257.
38. Zarling AL, Polefrone JM, Evans AM, Mikesch LM, Shabanowitz J, Lewis ST, Engelhard VH, Hunt DF. Identification of class I MHC-associated phosphopeptides as targets for cancer immunotherapy. *PNAS.* 2006; 103(40):14889-14894.
39. Rappsilber J, Mann M, Ishihama Y. Protocol for micro-purification, enrichment, pre-fractionation and storage of peptides for proteomics using StageTips. *Nat Protoc.* 2007; 2(8):1896-1906.
40. Weidanz JA, Hawkins O, Verma B, Hildebrand WH. TCR-like biomolecules target peptide/MHC class I complexes on the surface of infected and cancerous cells. *Int Rev Immunol.* 2011; 30(5-6):328-340.
41. Abelin JG, Trantham PD, Penny SA, Patterson AM, Ward ST, Hildebrand WH, Cobbold M, Bai DL, Shabanowitz J, Hunt DF. Complementary IMAC enrichment methods for HLA-associated phosphopeptide identification by mass spectrometry. *Nat Protoc.* 2015; 10:1308-1318.
42. Gaskell S. Electrospray: principles and practice. *J Mass Spectrom.* 1997; 32:677-688.
43. Wilm M. Principles of electrospray ionization. *Mol Cell Proteomics.* 2011; 10:1-14.
44. Heeren RM, Kleinnijenhuis AJ, McDonnell LA, Mize TH. A mini-review of mass spectrometry using high-performance FTICR-MS methods. *Anal Bioanal Chem.* 2004; 378(4): 1048-1058.
45. Marshall AG, Hendrickson CL, Jackson GS. Fourier transform ion cyclotron resonance mass spectrometry: a primer. *Mass Spectrom Rev.* 1998; 17(1): 1-35.
46. Perry R, Cooks G, Noll R. Orbitrap mass spectrometry: instrumentation, ion motion, and applications. *Mass Spectrom Rev.* 2008; 27:661-699.
47. Tang X, Thibault P, Boyd R. Fragmentations of multiply-protonated peptides and implications for sequencing by tandem mass spectrometry with low-energy collision-induced dissociation. *Anal Chem.* 1993; 5: 2824-2834.
48. Syka J, Coon J, Schroeder M, Shabanowitz J, Hunt DF. Peptide and protein sequence analysis by electron transfer dissociation mass spectrometry. *PNAS.* 2004; 101: 9528-9533.
49. Coon J, Ueberheid B, Syka J, Dryhurst D, Ausio J, Shabanowitz J, Hunt DF. Protein identification using sequential ion/ion reactions and tandem mass spectrometry. *PNAS.* 2005; 102: 9463-9468.
50. Senko MW, Remes PM, Canterbury JD, Mathur R, Song Q, Eliuk SM, Mullen C, Earley L, Hardman M, Blethrow JD, Bui H, Specht A, Lange O, Denisov E, Makarov A, Horning S, Zabrouskov V. Novel parallelized quadrupole/linear ion trap/Orbitrap Tribrid mass spectrometer improving proteome coverage and peptide identification rates. *Anal Chem.* 2013; 85:11710-11714.
51. Geer LY, Markey SP, Kowalak JA, Wagner L, Xu M, Maynard DM, Yang X, Shi W, Bryant SH. Open mass spectrometry search algorithm. *J Proteome Res.* 2004; 3(5): 958-964.
52. Bern M, Kil YJ, Becker C. Byonic: advanced peptide and protein identification software. *Curr Protoc Bioinformatics.* 2012; 13: Unit 13.20.
53. Janetzki S, Price L, Schroeder H, Britten CM, Welters MJ, Hoos A. Guidelines for the automated evaluation of Elispot assays. *Nat Protoc.* 2015; 10(7): 1098-1115.

-
54. Letsch A, Scheibenbogen C. Quantification and characterization of specific T-cells by antigen-specific cytokine production using ELISPOT assay or intracellular cytokine staining. *Methods*. 2003; 31(2): 143-149.
 55. Betts MR, Brenchley JM, Price DA, De Rosa SC, Douek DC, Roederer M, Koup RA. Sensitive and viable identification of antigen-specific CD8⁺ T cells by a flow cytometric assay for degranulation. *J Immunol Methods*. 2003; 281: 65-78.
 56. Cobbold M, De La Pena H, Norris A, Polefrone J, Qian J, English MA, Cummings K, Penny S, Turner JE, Cottine J, Abelin JG, Malaker SA, Zarlind AL, Huang H, Goodyear O, Freeman S, Shabanowitz J, Pratt G, Craddock, C, Williams ME, Hunt DF, Engelhard VH. MHC class-I associated phosphopeptides are the targets of memory-like immunity in leukemia. *Sci Transl Med*. 2013; 5(203): 1-10.

Chapter 2: Implementation of STop And Go Extraction Tips for Improved Desalting of HLA-Associated Peptide Samples for Mass Spectrometric Analysis

2.1 Introduction

2.1.1 Sample Preparation for Mass Spectrometric Analyses

Mass spectrometry is undeniably the most reliable, sensitive, and indispensable tool available for proteomics research to date. Vast improvements over the past three decades have allowed for the in-depth characterization of biological samples and the ultimate translation of large data sets into a comprehensive understanding of complex biological processes.¹⁻⁴ However, the highly sensitive nature of this methodology lends itself to issues involving the required purity of samples which are to be analyzed. Thus, in order to obtain the desired quality and sensitivity of sample analyses, it is crucial to ensure that sample preparatory techniques are compatible with mass spectrometric methodology.⁴

A major issue regarding sample purity arises from the use of detergents and buffers during sample preparation, both of which cannot be easily coupled to highly-sensitive mass spectrometric analysis.⁵ The basic principle of mass spectrometry involves the measurement of charged species. Thus, the presence of salt-containing buffers can have a drastic negative impact on the performance of the mass spectrometer because the system will be overwhelmed with charged salt ions. This effect is further enhanced by the fact that salts are usually present in a much greater excess within a sample compared to the peptides or proteins of interest. Additionally, salt ions can form analyte-salt adducts, which further complicate the interpretation of spectra. The presence of detergents, such as

sodium dodecyl sulfate (SDS) or Triton-X, is equally crippling in that these can interfere with peptide ionization, lead to signal suppression, and increase the overall background of the obtained mass spectra. To avoid these issues, it is necessary to implement a strategy of removal of contaminants or impurities from samples prior to analysis by mass spectrometry.⁶

Sample cleanup, or desalting, can be performed using many on-line or off-line methodologies.⁶ One of the most common on-line methods of sample cleanup is through the use of trap columns which allow for the concentration or purification of samples. Trap columns consists of a small cartridge packed with a binding material which allows for the separation of the desired analyte from salts or impurities present within the sample. By passing the entire sample to be analyzed through the trap column, peptides or proteins can be retained via their strong affinity to the binding material while the rest of the sample matrix flows through the column as waste. The resulting desalted sample can then be eluted from the trap column and injected into the mass spectrometer for subsequent analysis. While trap columns are often an efficient method for the removal of impurities from samples, they are ideal for large, dilute sample volumes and therefore are impractical for applications in which sample volume or material is limited.^{6,7}

An alternative to methods of on-line sample cleanup or desalting is off-line methodologies which can be quite useful for effective sample cleanup prior to mass spectrometric analysis. While there are many commercially available methods for off-line sample cleanup, the most common involve the use of reversed-phase chromatographic resin packed into a pipette tip, spin column, or syringe column system. These methodologies allow for binding of peptides to C18 resin, washing to aid in removal of

salts or impurities, and elution of bound peptides using organic solvent. The resulting cleaned up sample can then undergo further sample preparation techniques, such as enrichment, prior to analysis. However, limitations of commercially available off-line cleanup systems do exist, including incomplete elution of desalted samples, introduction of contaminants, and difficulty in coupling reagents to subsequent mass spectrometric analyses.⁶

In contrast to commercially available off-line cleanup methodologies, our laboratory has routinely performed desalting of HLA-associated peptide samples using fused silica microcapillary columns packed with C18 reversed phase resin (Figure 2.1). Using this methodology, aliquots of samples are pressure loaded onto the microcapillary cleanup columns allowing for peptides to bind to the C18 resin. Rinse steps are then performed to remove any salts present within the sample. The peptides are then eluted using an HPLC gradient of increasing organic solvent concentrations and collected into a tube for subsequent sample preparation steps and ultimately

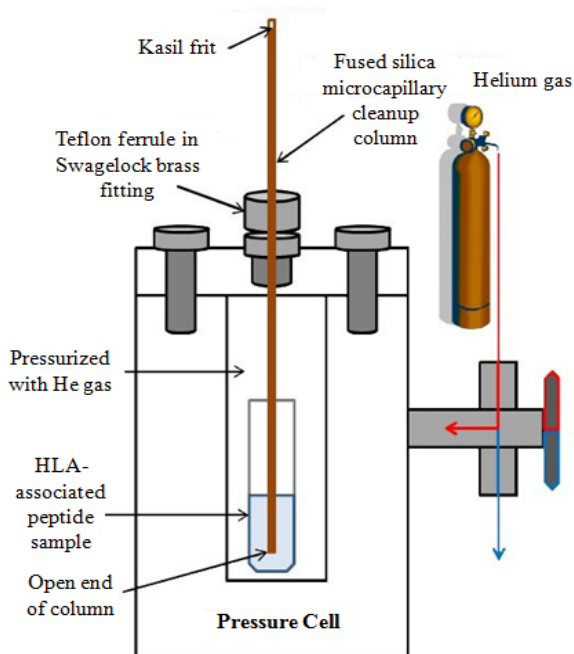


Figure 2.1 Schematic of microcapillary cleanup column setup. A pressure cell is connected to a helium gas tank through a 3-way valve. The HLA-associated peptide sample is pressure loaded onto the microcapillary column equipped with a Kasil frit. The cleanup column is then transferred to an HPLC where it is rinsed to remove salts or impurities and the peptides are eluted into a tube using an acetonitrile gradient. Figure adapted from reference 8.

analysis via mass spectrometry.⁸ Although this step has been shown to effectively remove interfering salts from samples, it is often very time consuming. It can take several days to fashion an effective cleanup column in addition to four to five hours to perform the actual desalting step. Additionally, this methodology can result in severe sample losses as indicated by internal standards spiked into the sample prior to cleanup.

2.1.2 Sample Desalting via STAGE Tip Technology

To address the issues associated with the use of microcapillary cleanup columns, we turned to an alternative approach using STop And Go Extraction (STAGE) tip technology, first introduced by Mann *et al.* in 2003. STAGE tips are comprised of a pipette tip packed with a small Empore disk consisting of chromatographic material immobilized in a Teflon meshwork (Figure 2.2). Empore extraction disks of different functionalities are available, including reversed phase C18, strong cation exchange (SCX), and metal-chelating resins, giving rise to the overall versatility of STAGE tips in a variety of sample preparation applications.

Additionally, the use of Empore material is advantageous compared to loose beads which are typically used in other off-line sample cleanup methodologies. The immobilization of the beads in the Teflon meshwork ensures that the sample is equally distributed among the resin. This prevents the formation of

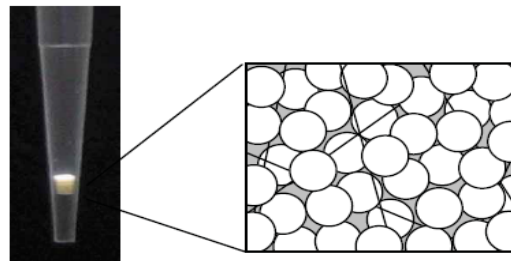


Figure 2.2 Schematic of STop And Go Extraction Tip.⁴ STAGE tips are comprised of a pipette tip packed with a small disk of Empore material. Empore material can contain a variety of chromatographic resins of different functionalities which are immobilized in a Teflon meshwork. Immobilization of resin allows for equal distribution of the sample, resulting increased sample recovery.

primary-flow channels, a common source of decreased sample recovery, while simultaneously allowing for peptides to be retained by the resin and eluted with higher efficiency.^{4,5}

Another advantage of STAGE tip technology is the ease by which individual tips can be constructed in a laboratory setting. Briefly, a blunt syringe is used to punch out a small disk of Empore resin which is then inserted into a pipette tip using a piece of PEEK tubing. Varying sizes of pipette tips can be used as the extraction disk is held in place by the tapering of the pipette tip itself. Multiple STAGE tips can be constructed in under one minute, adding <0.1 cent in material costs to the price of each tip.^{4,5} Additional disks can be added to each tip to allow for increased binding capacity. Furthermore, disks of different functionalities can be combined to create multi-functional STAGE tips. For instance, Jensen *et al.* used multifunctional STAGE tips consisting of three disks combined in a C18-SCX-C18 fashion for desalting and fractionation of serum protein samples prior to matrix-assisted laser desorption/ionization (MALDI) mass spectrometric analysis.⁹

A typical reversed phase C18 STAGE tip experiment involves four main steps: 1) equilibration of the tip to the solvents of choice, binding of the sample to the resin, washing of the tip to remove salts or any other impurities within the sample, and 4) elution of the peptides using a stepwise gradient of organic solvent. These steps can be performed either by pressure devices, such as syringes, or by centrifugation. This robust STAGE tip methodology has been applied routinely to various sample preparation applications, allowing for minimal material costs, increased peptide recoveries, and decreased sample losses.¹⁰⁻¹²

2.1.3 Project Aim

In this chapter, we seek to develop a robust, sensitive off-line method for HLA-associated peptide sample cleanup and desalting which achieves quantitative yields of internal standards and results in decreased sample losses. To allow for the most effective use of STAGE tip technology in regards to our HLA-associated peptide samples, we plan to first alter the typical sample preparation steps performed by our collaborators at the University of Birmingham. Next, we plan to optimize the conditions in which we desalt HLA-associated peptide samples using STAGE tips to allow for the cleanup of entire samples at once over a period of less than two hours, including the preparation of the STAGE tip itself. Finally, we plan to show that our STAGE tip methodology drastically improves sample cleanup compared to the previous approach of fused silica microcapillary C18 cleanup columns.

2.2 Materials

2.2.1 Reagents

Amersham Pharmacia Biotech (Amersham, UK)

NHS-activated sepharose beads

Applied Biosystems (Carlsbad, CA)

POROS ® MC 20 metal chelating packing material, 20 µm diameter

Atlantic Peptides LLC (Lewisburg, PA)

Phosphopeptide standards, RVKsPLFQF, RTHsLLLLG, ≥95% purity

Grace Davison Discovery Science (Deerfield, IL)

Acetyl chloride, anhydrous

D₀ methanol, anhydrous

Honeywell (Morristown, NJ)

Acetonitrile, HPLC grade, ≥99.8% purity

IDEX Health & Science LLC (Middleboro, MA)

PEEK natural tubing

J.T. Baker (Phillipsburg, NJ)

Glacial acetic acid, ≥99.9% purity

Pierce (Rockford, IL)

LC-MS grade water

PQ Corporation (Valley Forge, PA)

Kasil ® 1624 potassium silicate solution

Sigma Aldrich (Saint Louis, MO)

Angiotensin I acetate salt hydrate, $\geq 90\%$ purity

Angiotensin II phosphate (DRVYIHPHF)

Aprotinin

CHAPS buffer

Corning Costar low-binding microcentrifuge tubes

Empore C18 SPE disks

Ethylenediaminetetraacetic acid (EDTA), analytical grade

Formamide

Iron (III) chloride

L-ascorbic acid

Leupeptin

Pepstatin A

Phenylmethylsulfonyl fluoride (PMSF)

Roswell Park Memorial Institute (RPMI) medium

Sodium azide

Sodium Chloride

Tris-HCl

Vasoactive intestinal peptide fragment 1-12, $\geq 90\%$ purity

VWR (Atlanta, GA)

Pipetting needles with 90° blunt ends, 16 gauge

YMC Company, LTD (Kyoto, Japan)

ODS-AQ, C18 5 μm spherical silica particles, 120 \AA pore size

2.2.2 Equipment and Instrumentation

Agilent Technologies (Palo Alto, CA)

1100 Agilent high performance liquid chromatograph

Branson (Danbury, CT)

Branson 1200 Ultrasonic bath

Beckman Coulter (Pasadena, CA)

Optima LE-8K ultracentrifuge (Ti70 rotor)

Fisher Scientific (Waltham, MA)

Fetal bovine serum (FBS)

Model 50 sonic dismembrator system, 117V, 50/60 Hz

Model 50 probe, 5/64 in

Labonco Corp. (Kansas City, MO)

Centrivap centrifugal vacuum concentrator

Millipore (Billerica, MA)

Amicon ultra, 10 kDa regenerated cellulose spin filter

PolyMicro Technologies, Inc. (Phoenix, AZ)

360 μm o.d. x 50 μm i.d. polyimide coated fused silica capillary

360 μm o.d. x 75 μm i.d. polyimide coated fused silica capillary

360 μm o.d. x 150 μm i.d. polyimide coated fused silica capillary

Sutter Instrument Co. (Novato, CA)

P-2000 microcapillary laser puller with fused silica adapter

Thermo-Fisher Scientific (San Jose, CA/Bremen, Germany)

LTQ mass spectrometer (back-end ETD)

LTQ FTICR hybrid mass spectrometer (custom modified with front-end ETD)

LTQ Orbitrap mass spectrometer (custom modified with front-end ETD)

LTQ Orbitrap Fusion Tribrid mass spectrometer (front-end ETD)

Zeus Industrial Products, Inc. (Orangeburg, SC)

Teflon tubing, 0.012 inch i.d. x 0.060 inch o.d.

2.3. Methods

2.3.1 Peptide Synthesis

Phosphorylated peptides were synthesized using Fmoc chemistry, purified via HPLC to >95% purity, and the sequences confirmed by mass spectrometry. Three synthetic phosphopeptides, DRVyIHPF, RVKsPLFQF, and RTHsLLLLG, were utilized as internal standards for STAGE tip optimization.

2.3.2 Cell Line and Tissue Culture (Performed by NB, University of Birmingham)

Acute myeloid leukemia (AML) cell lines were cultured from patient samples in which leukapheresis was performed to isolate white blood cells from whole blood. Hepatocellular carcinoma tissue samples (normal/tumor) were obtained one-hour post-removal from patients at the Queen Elizabeth Hospital and Center for Liver Research at the University of Birmingham. Tissue samples were cut into smaller pieces and stored at -80°C until further use. The entire sample was prepared for HLA-associated peptide isolation, assuming that 1 gram is equivalent to 1e9 cell equivalents (C. Eq.).

2.3.3 Immortalization of Human B Cells with Epstein-Barr Virus (EBV)

(Performed by KC, University of Virginia)

EBV stocks were prepared by growing B95-8 cells at a concentration of 10⁶ cells/mL in RPMI 10% fetal bovine serum (FBS) medium. The virus-containing supernatant was

filtered through a 0.45 μm filter and stored in aliquots at -80°C until further use. Ten million PBMCs were infected with 2.5 mL of EBV stock prior to incubation for 2 hours at 37°C . RPMI 10% FBS medium containing cyclosporin A, an immunosuppressant drug used to kill any EBV-specific cytotoxic T lymphocytes, was added to the mixture to give a final concentration of 0.5 $\mu\text{g}/\text{mL}$ of cyclosporin A. The cells were plated into 4 wells of a 24-well plate. One third of the medium volume was exchanged each week for 3 weeks total. At this point, the transformed B cells were transferred to culture flasks and rapidly expanded in RPMI 10% FBS medium.

2.3.4 HLA-Associated Peptide Isolation (Performed by KC, University of Virginia and NB, University of Birmingham)

For cell line samples, cells were first lysed in 10 mL of lysis buffer (20 mM Tris-HCl pH 8, 150 mM NaCl, 1% 3-[(3-cholamidopropyl) dimethylammonio]-1-propane sulfonate (CHAPS)). For tissue samples, frozen pieces of tissue were first resuspended in lysis buffer and homogenized using a tissue ruptor (Qiagen). Next, protease inhibitors (1 mM PMSF, 5 $\mu\text{g}/\text{mL}$ aprotinin, 10 $\mu\text{g}/\text{mL}$ pepstatin A, and 10 $\mu\text{g}/\text{mL}$ leupeptin) were added to prevent degradation of HLA molecules. Phosphatase inhibitor cocktails II and III were added in 1:100 dilutions to prevent dephosphorylation of isolated peptides. Lysates were centrifuged at 100,000 \times g for 1 hour at 4°C . Supernatants were incubated with an HLA class I-specific antibody (W6/32, 5 mg/1e9 cells) or an HLA-A*02-specific antibody (BB7.2, 5mg/1e9 cells) bound to NHS-Sepharose beads and rotated at 4°C for 16 hours. Beads were pelleted via centrifugation at 2000 rpm for 2 minutes and the supernatant was removed. Beads then underwent a series of four wash steps including:

lysis buffer, 20 mM Tris-HCl and 150 mM NaCl, 20 mM Tris-HCl and 1 M NaCl, and finally 20 mM Tris-HCl before being transferred to a 5 kDa molecular weight cutoff (MWCO) filter. At this point peptides were either eluted from HLA class I molecules using 10% acetic acid (for C18 microcapillary column cleanup) or left untouched (for STAGE tip cleanup). The isolated peptide mixtures or the dried beads on MWCO filters were stored at -80°C and shipped to the University of Virginia for analysis.

2.3.5 STAGE Tip Fabrication

STAGE tips were fabricated as depicted in Figure 2.3. A 16-gauge pipetting needle with a 90° blunt end was used to punch out the required number of Empore C18 solid phase extraction (SPE) disks, assuming that binding capacity is $\sim 8 \mu\text{g}$ of material per disk. A piece of natural PEEK tubing (1/32 inch o.d. x $25 \mu\text{m}$ i.d.) was used to push the Empore disk out of the blunt needle and into the bottom of a 200 μL pipette tip. Constructed STAGE tips were placed into STAGE tips adapters connected to 1.5 mL Eppendorf tubes for collection of equilibration, sample load, rinse, and elution flow through fractions.

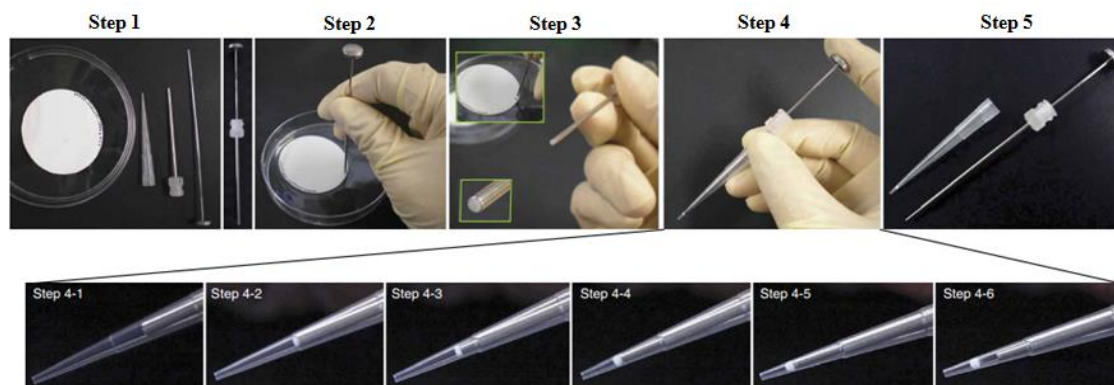


Figure 2.3 Schematic of STAGE tip fabrication.⁴ STAGE tips are fabricated using a pipetting needle to punch out small disks of Empore C18 resin. PEEK tubing is then used to push the resin out of the needle and into a pipette tip. Ease of fabrication allows for the construction of many STAGE tips at a time which can be saved for future use.

2.3.6 Sample Desalting via STAGE Tips

2.3.6.1 Synthetic Phosphopeptide Samples

Prior to use on precious samples, STAGE tip cleanup was first optimized using synthetic phosphopeptides for proof of concept based on a previously published protocol.⁴ Loading of the following steps onto STAGE tips was accomplished using centrifugation. Times and speeds varied throughout the optimization process and will be discussed in the results section of this chapter. Fabricated STAGE tips were equilibrated using the following wash steps: two washes of 100 μL of methanol, one wash of 50 μL of 80% acetonitrile/0.01% acetic acid, and two washes of 100 μL of 1% acetic acid. Synthetic mixtures of three phosphopeptide standards, DRVyIHPF, RVKsPLFQF, and RTHsLLLLG, at equal concentrations were prepared in 50 μL of 0.1% acetic acid, dried to completion in a Centrivap, and stored at -80°C until further use.

Synthetic mixtures were reconstituted in 100 μL of 3% acetonitrile/5% acetic acid and loaded onto STAGE tips. Following sample loading, 100 μL of 3% acetonitrile/5% acetic acid were added to the sample tube and loaded onto the STAGE tip twice to ensure complete sample loading. STAGE tips were washed using four rounds of 100 μL of 1% acetic acid. Synthetic peptides were eluted from the C18 resin in the STAGE tips using the following stepwise gradient of increasing acetonitrile concentrations: 10 μL of 20% acetonitrile/0.1% acetic acid, 10 μL of 40% acetonitrile/0.1% acetic acid, 10 μL of 60% acetonitrile/0.1% acetic acid, and 10 μL of 80% acetonitrile/0.1% acetic acid. Equilibration, sample load, wash, and elution flow through fractions were dried to completion using a Centrivap and stored at -80°C until further use.

2.3.6.2 Off-Bead Cell Line Samples

Post optimization of STAGE tip cleanup methodology of synthetic phosphopeptide samples, an EBV-immortalized B cell lymphoblastoid line (JY-A2) was used to mimic a patient cell line or tissue sample. Fabricated STAGE tips were equilibrated using the following wash steps: two 2-minute washes of 100 μ L of methanol at 1500 x g, one 1-minute wash of 50 μ L of 80% acetonitrile/0.01% acetic acid at 1500 x g, and two 2-minute washes of 100 μ L of 1% acetic acid at 1500 x g. Phosphopeptide standards were spiked into an aliquot of 5e8 C. Eq. of JY-A2 at 200 fmol each. The sample was then reconstituted in 100 μ L of 3% acetonitrile/5% acetic acid and loaded onto STAGE tips for 5 minutes at 300 x g. Following sample loading, 100 μ L of 3% acetonitrile/5% acetic acid were added to the sample tube and loaded onto the STAGE tip twice for 3 minutes at 300 x g to ensure complete sample loading. STAGE tips were washed using four rounds of 100 μ L of 1% acetic acid. Peptides were eluted from the C18 resin in the STAGE tips using the following stepwise gradient of increasing acetonitrile concentrations: 20 μ L of 20% acetonitrile/0.1% acetic acid, 20 μ L of 40% acetonitrile/0.1% acetic acid, 20 μ L of 60% acetonitrile/0.1% acetic acid, and 20 μ L of 80% acetonitrile/0.1% acetic acid. Equilibration, sample load, wash, and elution flow through fractions were dried to completion using a Centrivap and stored at -80°C until further use.

2.3.6.3 On-Bead Cell Line and Tissue Samples

Post optimization of STAGE tip cleanup methodology for synthetic phosphopeptide samples and an off-bead cell line sample, STAGE tip cleanup was applied to an AML patient cell line sample. This sample was sent with dry beads still bound to HLA:peptide

complexes on a MWCO filter. Fabricated STAGE tips were equilibrated using the following wash steps: two 2-minute washes of 100 μ L of methanol at 1500 x g, one 1-minute wash of 50 μ L of 80% acetonitrile/0.01% acetic acid at 1500 x g, and two 2-minute washes of 100 μ L of 1% acetic acid at 1500 x g. Dried beads were transferred from the filter to a separate low-protein binding tube using subsequent water rinses to ensure complete transfer. Beads were spun down at 300 x g for 1 minute and the supernatant was loaded onto the STAGE tip in 150 μ L aliquots for 2 minutes at 2000 x g. Two washes of the beads using 100 μ L of 3% acetonitrile/5% acetic acid followed by 50 μ L of 1% acetic acid were performed and loaded onto STAGE tips for 2 minutes each at 2000 x g to ensure loading of any peptides which had become dissociated from HLA molecules.

For the elution of peptides from HLA molecules bound to beads, 150 μ L of 10% acetic acid was added to the tube which was then shaken for 5 minutes at room temperature. The beads were spun down at 300 x g for 1 minute and the supernatant transferred to a low-binding tube. This process was repeated to ensure complete elution of peptides from HLA molecules and the supernatant added to the low-binding tube. Phosphopeptide standards were spiked into the 10% acetic acid elution supernatant at 200 fmol each. The combined supernatants were loaded onto the STAGE tip in 150 μ L aliquots at 2000 x g until the entire volume had passed through. STAGE tips were washed using four rounds of 100 μ L of 1% acetic acid. Peptides were eluted from the C18 resin in the STAGE tips using the following stepwise gradient of increasing acetonitrile concentrations: 20 μ L of 20% acetonitrile/0.1% acetic acid, 20 μ L of 40% acetonitrile/0.1% acetic acid, and 20 μ L of 60% acetonitrile/0.1% acetic acid. A

subsequent elution of 20 μ L of 80% acetonitrile/0.1% acetic acid was performed and collected in a separate tube. Equilibration, sample load, wash, and C18 elution flow through fractions were dried to completion using a Centrivap and stored at -80°C until further use.

Upon application of STAGE tip cleanup methodology to AML patient cell line samples, severe clogging of tips was observed during the loading of the 10% acetic acid elution step. This was attributed to “sticky” DNA which we hypothesized was bound non-specifically to beads and was then eluted during this step. To combat this issue, a sonication step was incorporated to break up large DNA molecules when applying STAGE tip technology to HCC tissue samples. STAGE tip cleanup of these samples was performed as outlined with AML patient cell line samples with one exception - the combined supernatants of the 10% acetic acid elution steps were first sonicated using a Model 50 sonic dismembrator system at 50 Hz for 5 seconds prior to loading onto the STAGE tips. Equilibration, sample load, wash, and elution flow through fractions were dried to completion using a Centrivap and stored at -80°C until further use.

2.3.7 Sample Desalting via C18 Microcapillary Cleanup Columns

Peptides isolated from $1\text{e}8\text{-}1\text{e}9$ C. Eq. in 0.1% acetic acid were combined with additional 0.1% acetic acid for a total sample volume of 50 μ L. For estimation of sample losses, 200 fmol of two internal phosphopeptide standards – angiotensin II phosphate (DRVyIHPF) and RVKsPLFQF – were spiked into the sample. The sample was pressure loaded onto a fused silica microcapillary cleanup column (360 μm o.d. x 150 μm i.d.) equipped with a 2 mm Kasil $\text{\textcircled{R}}$ 1624 frit and packed with 5 cm of irregular C18 reversed

phase resin at a flow rate of 0.5 $\mu\text{L}/\text{min}$. The column was rinsed by loading 25 μL of 0.1% acetic acid at a flow rate of 0.5 $\mu\text{L}/\text{min}$. The flow through and column rinse volumes were collected in an Eppendorf tube and stored at -35°C . The cleanup column was connected to an HPLC and rinsed with solvent A (0.1M acetic acid in water) for 10 minutes at 12-15 bar. At the same backpressure, peptides were eluted from the cleanup column into an Eppendorf tube using a gradient of 0-80% solvent B (70% acetonitrile, 0.1M acetic acid) in 40 minutes followed by a 30 minute hold at 80% solvent B. Finally, 200 fmol of a third internal phosphopeptide standard, RTHsLLLLG, was spiked into the sample and the tube was dried to completion using a Centrivap. The dried, cleaned-up sample was stored at -35°C until further use.

2.3.8 Peptide Content Determination by HPLC-ESI-MS/MS

Isolated peptide mixtures from cleanup via C18 microcapillary columns were reconstituted in 0.1% acetic acid for a final concentration of $1\text{e}7$ C. Eq./ μL . For sample screens, 1 μL ($1\text{e}7$ C. Eq.) of peptide sample was added to 4 μL of 0.1% acetic acid. For samples cleaned up via STAGE tips, dried C18 elution fractions were reconstituted in 0.1% acetic acid for a final concentration of $1\text{e}7$ C. Eq./ μL and 1-10% was removed for screening purposes. Samples were loaded onto a fused silica microcapillary precolumn (PC) (360 μm o.d. x 75 μm i.d.) equipped with a 2 mm Kasil @ 1624 frit and packed with 8-10 cm of irregular C18 reversed phase resin (5-20 μm diameter, 120 \AA pore size) at a flow rate of $<1\mu\text{L}/\text{min}$. The PC was rinsed on an HPLC with solvent A for 20 minutes at 30 bar. The PC was then dried using a pressure bomb and connected to a fused silica microcapillary analytical column (AC) (360 μm o.d. x 50 μm i.d.) packed with 6-8 cm of

regular C18 reversed phase resin (5 μm diameter, 120 \AA pore size) and equipped with a laser-pulled, electrospray emitter tip (2 μm diameter) via a Teflon sleeve. The ACPC was rehydrated by rinsing on an HPLC with solvent A for 10 minutes at 30 bar. Next, 100 fmol of two internal peptide standards (angiotensin and vasoactive intestinal peptide) were loaded onto the ACPC for a quantitation purposes prior to mass spectrometric analysis.

Peptides were eluted using an HPLC gradient of 0-60% solvent B in 40 minutes at a flow rate of 60 nL/min and electrospray ionized directly into an LTQ Orbitrap Classic or FT-ICR mass spectrometer. Full-scan high resolution mass spectra (MS1) were acquired in the Orbitrap or FT-ICR mass analyzers and MS/MS spectra (MS2) were acquired using CAD and ETD fragmentation methods in the linear ion trap of the instrument. A data-dependent top-6 CAD/ETD toggle method was used in which one high resolution MS1 scan (resolving power of 60,000 at 400 m/z) was acquired followed by selection of the top 6 most abundant parent ions for fragmentation by CAD and ETD. Data-dependent parameters included a repeat count of 3, repeat duration of 10 seconds, and exclusion list duration of 10. Additionally, ions with a charge state of +1 were excluded. ETD parameters included a 45 ms reaction time, FTMS automatic gain control (AGC) target of $2\text{e}5$ charges, ITMS AGC target of $1\text{e}4$ charges, and an ETD reagent target of $2\text{e}5$ charges.

Data analysis was performed using Xcalibur software (Thermo Electron Corporation). Raw data files were searched using OMSSA (version 2.1.1) against the Swissprot human protein database with the following parameters: no enzyme specificity, E-value cutoff of 1, variable modifications of oxidation of methionine and phosphorylation of serine, threonine, and tyrosine, ± 0.01 Da precursor mass tolerance, and ± 0.35 Da product ion

mass tolerance. Database hits were used to guide the analysis and peptide sequences were determined by accurate mass measurement and manual interpretation of MS2 spectra.

Relative abundances of peptides were calculated by comparing peptide peak areas to those of two internal peptide standards (angiotensin and vasoactive intestinal peptide) which were present at a fixed concentration of 100 fmol each. Percent recoveries were determined by comparing the relative abundance of the three phosphopeptide standards to expected values.

2.4 Results

2.4.1 STAGE Tip Optimization of Synthetic Phosphopeptide Samples

Prior to use on precious patient samples, of which material may be limited, STAGE tip cleanup methodology was first optimized using synthetic phosphopeptide mixtures. A protocol was developed based on a previous publication⁴ and applied to a total of eight trials using synthetic phosphopeptides. Throughout these trials, various conditions were altered to increase the average recoveries. Average recoveries were calculated by comparing the peak area of the three standards to those in a previous standards run and accounting for the percentage of the elution fraction that was screened. These conditions and resulting recoveries are summarized in Table 2.1.

Table 2.1 Summary of STAGE tip cleanup of synthetic phosphopeptide mixtures. Eight trials were conducted in which varying conditions were changed to optimize recovery of phosphopeptide standards. Conditions listed are changes from the protocol in the previous trial.

Trial	Concentration of Phosphopeptide Standards	Conditions	Average Recovery of Standards
1	100 fmol	-----	6%
2	200 fmol	Doubled concentration of standards, screened 10% of elution fraction as opposed to 1%	5%
3	200 fmol	Loaded 10% screen directly onto PC as opposed to ACPC	14%
4	5 pmol	Increased concentration of standards	21%
5	5 pmol	Increased number of Empore disks, decreased spin speeds and times	38%
6	5 pmol	Used only 1 Empore disk with reduced spin speeds and times	33%
7	5 pmol	Conditioned STAGE tips with angiotensin prior to use	31%
8	5 pmol	Eluted with methanol as opposed to acetonitrile	24%

The first synthetic trial was performed using 100 fmol of each of the three phosphopeptide standards. STAGE tip cleanup consisted of: 1) an equilibration step to hydrate the C18 resin and equilibrate to the solvents of choice, 2) a sample loading step in which the synthetic peptide mixture was passed through the C18 resin allowing for binding of phosphopeptides, 3) a wash step in which any impurities or salts present were removed from the tip, and 4) a gradient elution step in which bound phosphopeptides were eluted from the C18 resin and collected into a tube. To assess recoveries, 1% of the C18 elution fraction was screened on the mass spectrometer. This procedure resulted in average standard recovery of only 6%, an unacceptable value for future application to patient samples.

For the second synthetic trial, the amount of phosphopeptide standards was increased to 200 fmol each, in hopes that higher starting concentrations would yield higher recoveries. Additionally, 10% of the C18 elution fraction was screened as opposed to 1%. Based on this increase, we expected to see 20 fmol of each standard in the post-elution screen as opposed to 1 fmol, an easier and more reliable amount of material to detect. However, this procedure resulted in a similar average recovery of only 5%. Additionally, the sample screen showed poor chromatography, making quantitation of standards difficult and presenting future obstacles for application to patient samples. To address this issue, the procedure was repeated in trial 3, with the exception that the 10% C18 elution fraction was loaded onto the PC only. The PC was then rinsed with solvent A on the HPLC for approximately 10 minutes prior to reconnection to the AC. This resulted in improved chromatography and a slightly higher average recovery of 14%. From this

point forward, all C18 elution fraction screens were loaded directly onto the PC which was then rinsed and reconnected to the AC for mass spectrometric analysis.

Given that STAGE tips are designed to be used on complex samples, the concentrations of phosphopeptide standards were increased to 5 pmol each for trials 4-8 to mimic that of an actual patient sample. This increase immediately resulted in an average recovery of 21%, higher than previously seen although still less than ideal. Although the binding capacity of each Empore disk is stated to be approximately 8 μg of material, we tested the ability of additional disks to yield higher recoveries. For synthetic trial 5, a phosphopeptide mixture containing 5 pmol of each standard was cleaned up using a STAGE tip containing four Empore C18 SPE disks. During the equilibration step, it was observed that the liquid was flowing rapidly through the tip. Thus, centrifugation times and speeds were appropriately adjusted to allow for an adequate amount of interaction time between the phosphopeptides and the C18 resin within the tip. These alterations resulted in an average recovery of 38%, the highest recovery of synthetic phosphopeptides via STAGE tip cleanup technology to date.

While the conditions used in synthetic trial 5 resulted in increased standard recoveries, it was difficult to tell whether this increase was attributable to the use of multiple Empore disks or the decrease in centrifugation speeds and times. To test this, we performed STAGE tip cleanup of a synthetic phosphopeptide mixture using one Empore C18 SPE disk with drastically reduced centrifugation speeds and times in synthetic trial 6. This resulted in an average standard recovery of 33%. Seeing as this value is comparable to that of synthetic trial 5, we concluded that the increase in standard recoveries was in fact due to a decrease in centrifugation speeds and times. Thus,

decreased centrifugation speeds and times were used throughout the remaining synthetic trials to allow for adequate binding of standards to the C18 resin in hopes of increasing average recoveries.

To determine if conditioning STAGE tips allowed for increased peptide binding, we conditioned one STAGE tip with 30 pmol of a standard peptide, angiotensin, for use in synthetic trial 7. We performed two rounds of conditioning in which 10 pmol of angiotensin was loaded onto the STAGE tip and allowed to incubate with the C18 resin for 1-2 hours prior to elution using 80% acetonitrile. A final round was then performed in which 10 pmol of angiotensin was loaded onto the STAGE tip, incubated with the C18 resin overnight, and eluted using 80% acetonitrile. The conditioned STAGE tip was then used to clean up a synthetic phosphopeptide mixture, resulting in an average recovery of 31%. Since this value was not considerably greater than the synthetic trials using unconditioned STAGE tips, we determined that conditioning had no significant impact on phosphopeptide recovery.

For the final synthetic trial, we tested methanol as an alternative solvent for C18 elution of phosphopeptide standards. The STAGE tip cleanup protocol was performed using one Empore C18 SPE disk with reduced centrifugation speeds and times. Methanol was used to elute phosphopeptide standards from the C18 resin in the same stepwise manner as acetonitrile. Methanol elution resulted in a lower average standard recovery of 24%. Thus, we determined that acetonitrile was the preferable solvent for use in peptide elution from C18 resin. Overall, we were able to increase average recoveries for STAGE tip cleanup of synthetic phosphopeptide mixtures from 5% to 38%. However, because mixtures of synthetic phosphopeptides are unrealistic of actual patient samples, as they

are far less complex, we decided at this point to move forward with optimization of STAGE tip cleanup methodology on an immunology sample.

2.4.2 STAGE Tip Optimization of an Off-Bead Cell Line Sample

To mimic conditions more realistic of actual patient samples, an EBV-immortalized B cell lymphoblastoid line (JY-A2) was subjected to cleanup via STAGE tip methodology. To begin with, an aliquot of 1×10^7 C. Eq. of JY-A2 was screened on the mass spectrometer to assess the quality of the sample and determine peptide content. We then added 300 fmol of each phosphopeptide standard into an aliquot of 5×10^8 C. Eq. of JY-A2 and subjected the mixture to STAGE tip cleanup. For this procedure, two Empore C18 SPE disks were used and centrifugation speeds and times were lowered to ensure adequate interaction time between peptides and C18 resin. Post STAGE tip cleanup, 1% of the C18 elution fraction was screened. A comparison of the total ion current and base peak chromatograms pre- and post-cleanup is illustrated in Figure 2.4.

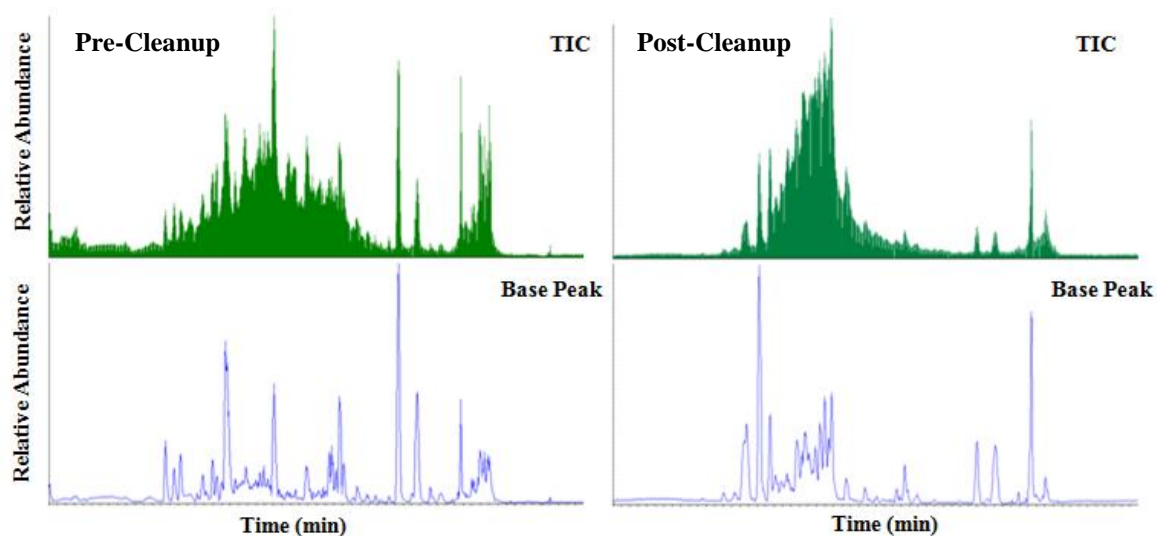


Figure 2.4 Chromatograms and base peaks of pre- and post-STAGE tip cleanup screens of JY-A2. Total ion current (TIC) chromatograms and base peak chromatograms of a 1% screen of JY-A2 are compared to those of a 1% screen post-STAGE tip cleanup.

For comparison purposes, we identified the top 10 most abundant peptides in the 1% screen of JY-A2 and calculated their relative abundances by comparing their peak areas to those of two internal peptide standards (angiotensin and vasoactive intestinal peptide) which were present at fixed concentrations of 100 fmol each. We then identified these 10 peptides in the 1% screen of JY-A2 post-STAGE tip cleanup and calculated their relative abundances in the same manner. The percent recovery for each peptide was calculated by dividing the observed amount of material by that of the theoretical amount assuming a 100% recovery and accounting for the actual amount of material screened – 1×10^7 C. Eq. and 5×10^6 C. Eq. for pre- and post-STAGE tip screens, respectively. Additionally, the average recovery of the internal phosphopeptide standards was calculated as previously described. The identified peptides and corresponding recoveries are listed in Table 2.2.

Table 2.2 Percent recovery of identified peptides pre- and post-STAGE tip cleanup of JY-A2. The relative abundances of the ten most abundant peptides identified in the 1% pre-cleanup screen of JY-A2 were compared to those in the 1% post-STAGE tip cleanup screen. Average recoveries of the identified peptides and the internal phosphopeptide standards were determined to be 60% and 51%, respectively.

Peptide	Amount in 1% Screen (fmol)	Amount in 1% Post STAGE Tip Screen (fmol)	Corrected Percent Recovery
YLLPAIVHI	118.84	32.62	55%
ALLDKLYAL	50.68	12.24	48%
SLLGGDVVSV	19.20	5.35	56%
IMLEALERV	18.55	3.92	42%
GLIEILKKV	11.00	4.27	78%
SLAQYLINV	8.97	1.83	41%
LLGPPVGV	8.20	3.71	90%
ILTDITKGV	7.46	3.39	91%
VLMTEDIKL	5.69	1.40	49%
ALIEKLVEL	5.09	1.27	50%
Average Recovery of Peptides			60%
Average Recovery of Phosphopeptide Standards			51%

Overall, the STAGE tip cleanup procedure of the EBV-immortalized B cell lymphoblastoid line, JY-A2, resulted in an average recovery of 51% for internal phosphopeptide standards. Additionally, the percent recoveries of the 10 most abundant peptides identified in the original screen were found to range from 41% to 91%, with an average recovery of 60%. These values assured us that the STAGE tip cleanup methodology was applicable to actual patient samples, thus we moved forward with the optimization process.

2.4.3. STAGE Tip Optimization of On-Bead Cell Line Samples

The ultimate goal of the implementation of STAGE tip technology for HLA-associated peptide sample cleanup is the ability to elute peptides from HLA molecules bound to NHS-Sepharose beads directly onto STAGE tips. This would eliminate the step performed by our collaborators in which the HLA-associated peptides are eluted using 10% acetic acid and the isolated peptide mixtures shipped to our laboratory for analysis. Given the success of STAGE tip cleanup methodology on the JY-A2 sample, we decided to move forward for use on an actual patient sample. White blood cells from a patient with acute myeloid leukemia (AML) were obtained via leukapheresis and cultured. Cells were split into five aliquots and processed using varying conditions in order to determine the most optimal conditions for STAGE tip cleanup of HLA-associated peptides. Each of the five trials was shipped to our laboratory with peptides bound to HLA molecules which were still attached to NHS-Sepharose beads, allowing for direct elution onto STAGE tips. The conditions and respective purposes of the five trials are outlined in Table 2.3.

Table 2.3 Conditions of AML sample preparation for STAGE tip cleanup. White blood cells obtained from a patient with AML were cultured and prepared using a variety of conditions to determine the optimal conditions for cleanup via STAGE tip methodology.

Trial	Condition	Purpose	
1	Performed entire process as usual	Control	-----
2	Performed process up to drying beads, shipped on wet ice	Filter vs. No Filter	-----
3	Performed process up to drying beads on filter, shipped on wet ice		Frozen vs. Not Frozen
4	Performed process up to drying beads on filter, shipped on dry ice	Prewashed vs. Unwashed Filter	
5	Performed process up to drying beads on a prewashed filter, shipped on dry ice		-----

For the STAGE tip cleanup of on-bead samples (trials 2-5), the protocol was altered to include an additional step in which 10% acetic acid was used to elute peptides from the HLA molecules in order to allow them to bind to the C18 resin within the tips. The STAGE tips were then washed with several rounds of 1% acetic acid to remove salts or other impurities within the sample prior to the C18 gradient elution. Unfortunately, when the 10% acetic acid elution step was loaded onto the STAGE tips, the flow rate slowed severely. Despite increasing the centrifugation speeds and times, the STAGE tip eventually stopped flowing. At this point, samples were loaded onto new STAGE tips and the process was continued; however, clogging of these STAGE tips occurred as well. In an attempt to elute any peptides that were able to bind to the C18 resin, a gradient elution step using increasing concentrations of acetonitrile was performed. Unfortunately, the STAGE tip used in trial 2 completely clogged and thus the sample had to be

abandoned. While we were able to elute approximately 15 μ L from the STAGE tips used in trials 3-5, the severe clogging issue made it impossible to perform a complete C18 elution of retained peptides. Despite the inability to completely elute peptides from the C18 resin of the STAGE tips used in trials 3-5, we screened 10% of the available C18 elution fraction. For comparison purposes, we identified the top 20 most abundant peptides in the 10% screens of each of the trials and calculated their relative abundances using internal peptide standards as previously described. The comparison of the relative abundances of the 20 most abundant peptides is listed in Table 2.4.

Table 2.4 Comparison of peptides identified in AML patient sample using varying preparatory conditions. Trials 3-5 were subjected to STAGE tip cleanup and 10% of the elution fractions were screened. The relative abundances of the top 20 most abundant peptides are compared between the three trials. Peptides that were not detected are indicated by “ND.”

Peptide	Amount in 10% Screen (fmol)		
	Trial 3	Trial 4	Trial 5
DTIEIITDR	149	225	82
NTDSPLRY	98	112	23
KEIFLRELI	73	102	1
DTDHYFLRY	72	82	12
EVILIDPFHK	70	114	13
IVVPKAAIVAR	62	86	7
TIIDILTKR	50	88	1
ITDSAGHILY	31	46	19
DVYSDLNTQR	21	24	1
ETIGEILKK	19	23	ND
LLDIRSEY	19	21	3
DVYPEIIER	18	27	5
QTDKCLKELY	17	15	15
SIFDGRVVAK	14	19	26
KRGDVIYIL	14	15	4
YADPVNAHY	12	15	3
YTDFDGTRVY	12	14	ND
IPVLVVQAQR	11	17	5
GEHGLIIRV	10	16	55
FLDASGAKLDY	9	11	3

It was difficult to make accurate comparisons between the three trials given the clogging issues encountered during the STAGE tip cleanup procedures. However, we attempted to make rough comparisons to determine which of the conditions would be ideal for future experiments. A comparison of dried beads shipped on filters versus in tubes was impossible given the unfortunate clogging of the STAGE tip used in trial 2. When comparing beads shipped on wet ice versus dry ice, it appeared that the frozen sample showed higher abundances of peptides. Additionally, we did not observe any drastic improvement using a filter that was prewashed with a viral peptide prior to the transfer of beads in an effort to reduce irreversible binding. Thus, we decided that the ideal conditions for STAGE tip cleanup of future patient samples would include transferring beads to unwashed filters and shipping them to our laboratory on dry ice for processing and subsequent analysis.

For a direct comparison between untouched samples and samples cleaned up via STAGE tips, we screened 10% of the isolated peptide mixture from trial one which was not subjected to any cleanup procedure. We then compared the values of the top 20 most abundant peptides present in the 10% screens of the STAGE tip elution fractions from trials 3-5 to the abundances in the screen of the untouched sample. The comparison of relative abundances of an untouched sample compared to those of the sample cleaned up via STAGE tips is listed in Table 2.5. For the majority of the peptides listed, greater relative abundances were observed in the samples cleaned up using STAGE tips, presumably due to the removal of salts present within the sample and thus illustrating the promise of STAGE tip methodology for cleanup of samples prior to mass spectrometric analysis.

Table 2.5 Comparison of peptides identified in an AML patient sample pre- and post-STAGE tip cleanup. Trials 3-5 were subjected to STAGE tip cleanup and 10% of the elution fractions were screened. The relative abundances of the top 20 most abundant peptides were compared to a 10% screen of the sample prior to STAGE tip cleanup. Peptides that were not detected are indicated by “ND.”

Peptide	Amount in 10% Screen (fmol)			
	Trial 1	Trial 3	Trial 4	Trial 5
DTIEIITDR	169	149	225	82
NTDSPLRY	222	98	112	23
KEIFLRELI	36	73	102	1
DTDHYFLRY	44	72	82	12
EVILIDPFHK	47	70	114	13
IVVPKAAIVAR	48	62	86	7
TIIDILTKR	54	50	88	1
ITDSAGHILY	21	31	46	19
DVYSDLNTQR	18	21	24	1
ETIGEILKK	20	19	23	ND
LLDIRSEY	8	19	21	3
DVYPEIHER	11	18	27	5
QTDKLELY	24	17	15	15
SIFDGRVAK	12	14	19	26
KRGDVIIYL	9	14	15	4
YADPVNAHY	9	12	15	3
YTDFDGTRVY	8	12	14	ND
IPVLVVQAQR	8	11	17	5
GEHGLIRV	9	10	16	55
FLDASGAKLDY	7	9	11	3

2.4.4 STAGE Tip Optimization of On-Bead Tissue Samples

We attributed the clogging issues observed in the STAGE tip cleanup of the on-bead AML samples to DNA which we believed was binding nonspecifically to the beads, eluting during the 10% acetic acid elution step, and clogging the C18 resin within the tips. Once this initial clogging occurred, it was no longer possible to pass the remaining sample through the STAGE tip, thus drastically impacting sample recovery. In an attempt to alleviate this issue, we implemented a sonication step which would serve to break up any DNA molecules present into smaller fragments that were less likely to clog the STAGE tips. We cleaned up six matched set (normal/tumor tissue) hepatocellular carcinoma (HCC) samples, LL4908, LL5437, and LLX, with an adapted STAGE tip protocol incorporating brief sonication. In this protocol, the 10% acetic acid elution steps were performed as usual and the supernatants combined in a low-binding tube. The combined supernatants were then subjected to sonication for 5-10 seconds prior to loading onto the STAGE tips.

While the sonication step appeared beneficial to some extent, a certain level of clogging was still observed when subjecting each of the HCC samples to cleanup via STAGE tips. Given these results, we designed an experiment to test whether the clogging issues were sample-specific (i.e. nonspecifically-bound “sticky” DNA) or simply bead-related. To do this, our collaborators performed the immunopurification process on four samples. Samples one and two contained only beads which had never been exposed to any cell line or tissue samples, accordingly serving as “blank” controls. These samples contained older beads which had been used for the previous STAGE tip optimization

steps and fresh beads which were prepared immediately prior to immunopurification.

Samples three and four contained beads bound to HLA:peptide complexes which were immunopurified from a sample of healthy liver tissue, LL5238. Again, these samples were obtained using either the old aliquot of beads or the freshly-prepared batch. The results from the STAGE tip cleanup of each of the four samples are outlined in Table 2.6.

Table 2.6 Conditions of sample preparation for STAGE tip cleanup for on-bead tissue samples.

An old aliquot of beads and an aliquot of a freshly-prepared batch were used to determine the origin of clogging issues previously observed using STAGE tip cleanup methodology. Samples one and two served as “blank” controls and contained beads which had never been exposed to cell line or tissue samples. Samples three and four contained HLA:peptide complexes immunopurified from a sample of healthy liver tissue (LL5238) using both old and new aliquots of beads. The total amount listed corresponds to the amount of beads needed for immunopurification of 2 grams of tissue or the actual amount of tissue processed for the “blank” and tissue samples, respectively. The conditions by which each of the samples were processed using STAGE tips are listed as well as the results in terms of observed clogging for each cleanup procedure.

	Sample	Total Amount	Aliquot	Conditions	Results
1	Old Beads "Blank"	2 grams equivalent	1a	Split into 3 aliquots and loaded onto separate STAGE tips	No clogging observed
			1b	Loaded entire aliquot onto STAGE tip	No clogging observed
2	New Beads "Blank"	2 grams equivalent	2a	Split into 3 aliquots and loaded onto separate STAGE tips	No clogging observed
			2b	Loaded entire aliquot onto STAGE tip	No clogging observed
3	Old Beads "LL5238"	2 grams tissue	3a	Split into 3 aliquots and loaded onto separate STAGE tips	No clogging observed
			3b	Split into 3 aliquots and loaded onto separate STAGE tips	No clogging observed
4	New Beads "LL5238"	2 grams tissue	4a	Split into 3 aliquots and loaded onto separate STAGE tips	No clogging observed
			4b	Loaded entire aliquot onto STAGE tip	Drastic clogging observed

Each of the four samples was subjected to STAGE tip cleanup using a variety of conditions to assess the origin of the previously observed clogging issue. Sample one, containing old beads equivalent to the amount needed to process two grams of tissue, was split into two aliquots (1a and 1b) and shipped to our laboratory. Aliquot 1a was further split into three aliquots, each containing roughly 3.33×10^8 equivalent beads, to allow for three attempts at optimizing the STAGE tip protocol. The first aliquot from sample 1a was processed using the original STAGE tip protocol as if an actual sample were present on the beads. We observed no clogging of the STAGE tip during any steps of this procedure. We then repeated the protocol using the remaining aliquots of sample 1a on separate STAGE tips and again observed no clogging. To determine whether the reduction in clogging was due to splitting the beads into separate aliquots, containing roughly one-third of the original material, we loaded the entire remaining aliquot of sample one (1b) onto a single STAGE tip and again observed no clogging. We repeated this entire process using the second sample, processed using the freshly-prepared beads, and observed no clogging for either of the loading conditions.

Given the results of STAGE tip cleanup of the “blank” controls, we confirmed that the previously observed clogging issues were not bead-related, but instead were sample-related. To address this issue, we moved on to use of STAGE tips on samples three and four, which contained immunopurified HLA:peptide complexes, in hopes of determining a method of eliminating the occurrence of clogging. Sample three was split into two aliquots (3a and 3b) and shipped to our laboratory. Aliquot 3a was further split into three aliquots, each containing roughly 3.33×10^8 C. Eq., to allow for three attempts at optimizing the STAGE tip protocol. The first aliquot from sample 3a was processed using the

original STAGE tip protocol including the sonication step. Interestingly, we observed no clogging of the STAGE tip during any steps of this procedure. To confirm these results, we repeated the protocol using the remaining aliquots of sample 3a on separate STAGE tips and again observed no clogging.

For the final sample, we tested whether the reduction in clogging was in fact due to splitting the beads into separate aliquots when sample material was present. Sample four was split into two aliquots (4a and 4b) and shipped to our laboratory for analysis. Aliquot 4a was further split into three aliquots, each containing roughly 3.33×10^8 C. Eq., and processed on separate STAGE tips using the same protocol implemented for sample three. As expected, we observed no clogging of the STAGE tips. We then loaded the entire remaining aliquot of sample four (4b) onto a single STAGE tip. This resulted in drastic clogging of the STAGE tip making it impossible for any material to flow through, suggesting that an inherent loading capacity of less than 4×10^8 C. Eq. exists for processing HLA-associated peptides from on-bead tissue samples.

2.5 Discussion

The goal of this chapter was to utilize STop And Go Extraction tips as a robust, sensitive, off-line methodology for the cleanup of HLA-associated peptide samples, ultimately resulting in decreased sample preparation times and increased sample recoveries. STAGE tips have several advantages compared to C18 microcapillary cleanup columns, which were the previously used methodology of choice in our laboratory for routine cleanup of samples. STAGE tips are reproducible, easily fabricated at minimal cost, lead to higher efficiency of peptide elution as a result of the immobilization of chromatographic resin in a Teflon meshwork, and have the potential to serve multifunctional purposes.⁹⁻¹²

However, the greatest advantage associated with the implementation of STAGE tip technology for cleanup of HLA-associated peptide samples lies in the potential for drastically decreased sample losses. Through our collaboration with the University of Birmingham, we are given access to hepatocellular carcinoma tissue samples post-surgical resection. However, our greatest obstacle in this process is that we are often limited in the amount of material which we receive. Thus, it is crucial that we minimize losses of starting material during all of the steps we perform on the sample to prepare it for subsequent mass spectrometric analysis. This requirement is of an even greater concern when considering that the material we cleanup will ultimately be used for phosphopeptide enrichment, given the already low levels of phosphopeptides present within tissue samples.⁸ Therefore, the development of a method for sample cleanup that

routinely results in decreased sample losses is of undeniable importance for this application.

In order to avoid wasting precious patient samples, we first optimized STAGE tip cleanup methodology using a series of synthetic phosphopeptide mixtures. By doing this, we hoped to assess the capabilities of STAGE tips and determine the ideal conditions for the future application to patient samples. During the use of STAGE tips for the synthetic phosphopeptide mixtures, we altered various steps within a previously published protocol.⁴ Our protocol involved the equilibration of the STAGE tip to acetic acid, the binding of phosphopeptides to the C18 resin, the removal of salts or impurities using a series of wash steps, and the elution of retained phosphopeptides using a gradient of increasing organic solvent concentrations. Optimization of the protocol included: altering the starting concentrations of phosphopeptide standards, using a variable number of Empore C18 SPE disks, adjusting centrifugation speeds and times, conditioning the resin with a commonly used internal standard, using alternative solvents for peptide elution, and changing the conditions of loading elution fractions onto microcapillary columns for subsequent screening purposes.

Throughout the course of the optimization of STAGE tips using synthetic phosphopeptide mixtures, we increased the average recovery of the three phosphopeptide standards from 5% to 38% (Table 2.1). We determined that the conditions resulting in the greatest recovery of standards included the use of one Empore C18 SPE disk, decreased centrifugation speeds and times, and peptide elution using a stepwise gradient of acetonitrile. Additionally, we found that loading a portion of the elution fraction onto a PC only, as opposed to an ACPC combination, resulted in improved chromatography and

more reliable quantitation of phosphopeptide standards during post-STAGE tip cleanup screens. The optimization of STAGE tip technology using synthetic phosphopeptides provided us with vast insight as to how to improve this cleanup methodology. However, given that these mixtures are far from complex, and therefore very unrealistic of actual patient samples, we decided to move forward with the optimization process and focus our efforts on an actual immunology sample.

To do this, we turned to an EBV-immortalized B cell lymphoblastoid line – JY-A2 – which has been routinely characterized in our laboratory. An aliquot of JY-A2 containing internal phosphopeptide standards was subjected to cleanup via STAGE tip methodology. By comparing a pre-cleanup screen with a post-STAGE tip cleanup screen, we were able to visualize the capabilities of this methodology for cleanup of immunology samples. As illustrated in Figure 2.4, a comparison of the total ion current and base peak chromatograms from the pre- and post-cleanup screens shows a significantly reduced background level upon cleanup with STAGE tips. This is likely due to the significant reduction in salts and other impurities within the sample, resulting in the most abundant peaks within the base peak chromatogram being attributable to peptidic species. Additionally, a comparison of the relative abundances of the top 10 most abundant peptides between the pre- and post-cleanup screens demonstrated an average peptide recovery of 60%. We also calculated the average recovery of the internal phosphopeptide standards, which were spiked into the sample pre-cleanup, to be 51% (Table 2.2).

We attributed the improvement in average standard recovery compared to recoveries seen when using synthetic phosphopeptide mixtures to the increased complexity of the sample. STAGE tips are routinely used to remove excess amounts of salts from complex

peptidic samples, thus it is not surprising that a sample with a large amount of peptidic material would lend itself to improved cleanup using STAGE tip technology.⁵ However, the observed recoveries were still less than ideal in terms of applying this methodology to precious patient samples. This can potentially be explained by the fact that the JY-A2 sample was an “off-bead” sample in which peptides were eluted from HLA molecules prior to loading onto STAGE tips for sample cleanup. Additionally, the isolated peptide mixture was several years old and had undergone multiple freeze-thaw cycles which could have potentially resulted in sample degradation. Therefore, these values led us to believe that STAGE tip cleanup methodology was in fact applicable to actual patient samples and led us to expect to see higher recoveries for cleanup of “on-bead” samples.

Therefore, the next step in the optimization process for STAGE tip cleanup of HLA-associated peptide samples was application of this methodology to an on-bead sample. For previously processed samples, peptides were eluted from HLA molecules bound to beads using 10% acetic acid and separated from degraded HLA molecular subunits via a MWCO filter. This isolated peptide mixture was shipped to our laboratory for cleanup using microcapillary C18 cleanup columns. For the application of STAGE tip cleanup to on-bead samples, we altered the protocol to eliminate the 10% elution step and isolation of peptides prior to shipment. Instead, samples were shipped to our laboratory containing NHS-Sepharose beads with HLA:peptide complexes still attached, allowing for the direct elution of peptides onto STAGE tips.

We first incorporated this change using a sample in which white blood cells were obtained from a patient with acute myeloid leukemia (AML) via leukapheresis and cultured. The large cell sample was split into five aliquots (trials 1-5) and processed using

a variety of conditions prior to shipment to our laboratory for cleanup via STAGE tip methodology. Trial 1 was processed in the same manner as previously described for off-bead samples and accordingly served as a positive control. In contrast to this, we tested several conditions for the remaining on-bead samples including: the transfer and drying of beads on a filter prior to shipment versus leaving in tube, freezing beads versus leaving unfrozen, and the use of a filter that was prewashed prior to transfer versus an unwashed filter (Table 2.3). Using these variations, we sought to determine ideal conditions for sample preparation of immunopurified HLA:peptide complexes for STAGE tip cleanup methodology.

The AML samples were subjected to STAGE tip cleanup using the previously optimized protocol with the addition of a 10% acetic acid elution step to elute peptides from HLA molecules prior to loading onto STAGE tips. Additionally, we incorporated decreased centrifugation speeds and times to allow for adequate binding of peptides to the C18 resin. The major obstacle we encountered when using STAGE tips for the cleanup of on-bead samples was the drastic clogging of tips. Unfortunately, when loading the 10% acetic acid elution step onto the STAGE tips for all four sample conditions (trials 2-5), we observed significantly reduced flow of the samples through the tips. The centrifugation speeds and times for the sample loading step were increased considerably, yet we were unable to overcome the issue, ultimately resulting in the abandonment of the sample from trial 2. Despite this, we attempted to elute any peptides that were able to bind to the C18 resin from trials 3-5 using a gradient of increasing acetonitrile concentrations, successfully eluting approximately 15 μ L worth of volume from each STAGE tip. For a comparison of sample conditions, we screened 10% of the C18 elution

fraction from each trial and compared the relative abundances of the top 20 most abundant peptides (Table 2.4). Though difficult to make accurate comparisons due to clogging issues, it appeared that the sample in which beads were transferred onto an unwashed filter and shipped to our laboratory on dry ice resulted in the maximum abundance of observed peptides, making these the ideal sample preparation conditions for cleanup via STAGE tip technology.

A final experiment using the on-bead AML samples included evaluating the quality of samples post-cleanup via STAGE tips compared to their untouched counterpart. Here, we calculated the relative abundances of the previously mentioned top 20 most abundant peptides in a 10% screen of the untouched sample from trial 1 for a direct comparison to the abundances observed in the post-cleanup screens in samples from trials 3-5. This comparison clearly indicated an increased relative abundance of almost every peptide post-cleanup via STAGE tips (Table 2.5). We attributed this to the enhanced ability of STAGE tips to eliminate salts and impurities within the sample, thus reducing the suppression of peptides and resulting in increased observed amounts.

Given the clogging issues observed in the STAGE tip cleanup of the on-bead AML samples, we sought to both determine the origin and eliminate the issue upon application of STAGE tips to on-bead tissue samples. We believed that the clogging issue could be attributed to “sticky” DNA which was binding nonspecifically to the NHS-Sepharose beads. This issue was not observed with samples processed using the old methodology in which peptides were eluted and isolated prior to shipment, presumably because the non-specifically bound DNA remained on top of the MWCO filter. However, alteration of the protocol resulted in elimination of this step, thus allowing for the presence of non-

specifically bound DNA within our samples. We hypothesized that subjection of beads to 10% acetic acid for the elution of peptides from HLA molecules also led to the elution of DNA, ultimately resulting in clogging of the STAGE tips.

To address this issue, we incorporated an additional step in which the 10% acetic acid elution supernatants were subjected to sonication for 5-10 seconds prior to loading onto STAGE tips. We believed that sonication could be used to fragment large molecules of DNA into smaller pieces which would no longer clog the STAGE tips. To test this, we subjected three matched sets of hepatocellular carcinoma tissue samples to cleanup via STAGE tip methodology using a protocol revised to include the sonication step. Ultimately we observed that while sonication did reduce clogging to some extent, presumably by fragmenting the non-specifically bound DNA, it was unable to eliminate the issue completely. Thus we designed an experiment to test whether the clogging issue was a result of the beads themselves or was sample-related (Table 2.6).

By testing two “blank” samples which contained only beads that were never exposed to cell line or tissue samples, we determined that the clogging issue was not inherent to the actual NHS-Sepharose beads. Additionally, we determined that up to the equivalency of beads needed to process two grams of tissue could be processed and the elution loaded onto STAGE tips without any clogging issues when no sample material was present. This data suggested that the observation of clogged STAGE tips was in fact due to the presence of a species within the sample which is binding nonspecifically to the beads and eluting during the 10% acetic acid elution step.

To confirm this, we analyzed two samples containing immunopurified HLA:peptide complexes from healthy liver tissue attached to beads. We split these samples into

multiple aliquots to allow for numerous attempts at optimizing the protocol to eliminate the clogging issue. Originally, we believed that by implementing additional wash steps to the beads prior to sample loading onto STAGE tips, we could potentially remove any substances which may be bound to the beads that could interfere with the flow through STAGE tips. However, upon splitting the first sample into aliquots containing roughly one-third of the original sample material, we found that we were able to avoid clogging of the STAGE tips entirely. This led us to believe that while the clogging issue was due in part to a non-specifically bound substance being retained by the beads and eluting during the 10% acetic acid elution step, we could potentially overcome this phenomenon by processing less material per STAGE tip. To test this, we repeated the protocol using the final sample in which we loaded approximately 1×10^9 C. Eq. onto one STAGE tip, ultimately resulting in severe clogging of the tip and confirming our hypothesis.

Taken together, the data obtained for the implementation of STAGE tip cleanup of on-bead tissue samples suggests that 1) clogging of STAGE tips is sample-specific and not simply an artifact of the use of NHS-Sepharose beads, 2) sonication reduces clogging, presumably by breaking up large DNA molecules into smaller fragments, but does not completely eliminate the issue, and 3) the amount of material loaded onto one STAGE tip should not exceed 4×10^8 C. Eq. for optimal sample cleanup. Using these stipulations, we applied STAGE tip cleanup methodology to multiple HCC tissue samples and routinely obtained average internal standard recoveries ranging from 70-95%. Additionally, we significantly reduced the time needed to cleanup HLA-associated peptide samples from several days when using C18 microcapillary columns to under two hours when using

STAGE tip technology. Therefore, we believe that the STAGE tip methodology that we implemented is an ideal process for sample cleanup prior to mass spectrometric analysis.

Future directions of this work will involve further optimization of STAGE tip methodology for additional processing steps of HLA-associated peptide samples. For instance, phosphopeptide enrichment using immobilized metal affinity chromatography (IMAC) could be adapted for use on STAGE tips. This would involve the use of metal chelating Empore disks for specific chelation of iron cations for subsequent phosphopeptide enrichment. Adaptation of this methodology has the potential to significantly reduce sample preparation times from a full day using on-column IMAC to less than two hours. Additionally, the use of STAGE tips for IMAC would allow for sample multiplexing in which several enrichments could be performed at once, a task that is currently not possible when using on-column IMAC. Furthermore, multifunctional STAGE tips could be created in which Empore disks are combined for cleanup and IMAC of samples on a single tip. While this would be the ultimate goal for application of STAGE tips for processing of HLA-associated peptide samples, the issue of esterification of samples prior to phosphopeptide enrichment would need to be addressed.

2.6 References

1. Cravatt BF, Simon GM, Yates JR 3rd. The biological impact of mass-spectrometry-based proteomics. *Nature*. 2007; 450(7172): 991-1000.
2. Aebersold R, Mann M. Mass spectrometry-based proteomics. *Nature*. 2003; 422(6928): 198-207.
3. Han X, Aslanian A, Yates JR 3rd. Mass spectrometry for proteomics. *Curr Opin Chem Biol*. 2008; 12(5): 483-490.
4. Rappsilber J, Mann M, Ishihama Y. Protocol for micro-purification, enrichment, pre-fractionation and storage of peptides for proteomics using StageTips. *Nat Protoc*. 2007; 2(8): 1896-1906.
5. Rappsilber J, Ishihama Y, Mann M. Stop and go extraction tips for matrix-assisted laser desorption/ionization, nanoelectrospray, and LC/MS sample pretreatment in proteomics. *Anal Chem*. 2003; 75(3): 663-670.
6. Gundry RL, White MY, Murray CI, Kane LA, Fu Q, Stanley BA, Vay Eyk JE. Preparation of proteins and peptides for mass spectrometry analysis in a bottom-up proteomics workflow. *Curr Protoc Mol Biol*. 2009; Unit 10.05: 1-29.
7. Optimize Technologies. LC Trapping: a practical guide to techniques and products. 2015.
8. Abelin JG, Trantham PD, Penny SA, Patterson AM, Ward ST, Hildebrand WH, Cobbold M, Bai DL, Shabanowitz J, Hunt DF. Complementary IMAC enrichment methods for HLA-associated phosphopeptide identification by mass spectrometry. *Nat Protoc*. 2015; 10: 1308-1318.
9. Callesen AK, Mohammed S, Bunkenborg J, Kruse TA, Cold S, Mogensen O, Christensen RD, Vach W, Jorgensen PE, Jensen ON. Serum protein profiling by miniaturized solid-phase extraction and matrix-assisted laser desorption/ionization mass spectrometry. *Rapid Commun Mass Spectrom*. 2005; 19(12): 1578-1586.
10. Wisniewski, JR, Zougman A, Mann M. Combination of FASP and StageTip-based fractionation allows in-depth analysis of the hippocampal membrane proteome. *J Proteome Res*. 2009; 8(12): 5674-5678.
11. Kokubu M, Ishihama Y, Sato T, Nagasu T, Oda Y. Specificity of immobilized metal affinity-based IMAC/C18 tip enrichment of phosphopeptides for protein phosphorylation analysis. *Anal Chem*. 2005; 77(16): 5144-5154.
12. Ishihama Y, Rappsilber J, Mann M. Modular stop and go extraction tips with stacked disks for parallel and multidimensional peptide fractional in proteomics. *J Proteome Res*. 2006; 5(4): 988-994.

Chapter 3: Complementary IMAC Enrichment for the Identification of HLA-Associated Phosphopeptides

3.1 Introduction

3.1.1 Protein Phosphorylation

It is estimated that the human genome contains approximately 20,000-25,000 protein-coding genes, yet the human proteome is comprised of greater than 1 million proteins (Figure 3.1).^{1,2} The increase in complexity of the human proteome is partially due to the ability of single genes to encode for multiple proteins. This is accomplished through genomic recombination, differential transcription promoters, and alternative splicing, all of which allow for the generation of varying mRNA transcripts from single genes. While these elements do increase

the diversity of the human proteome to some extent, they do not fully account for the discrepancy in number between gene and protein expression.³ The remaining variability can be explained, however, by the extensive presence of post-

translational modifications (PTMs). Post-translational modifications are enzyme-

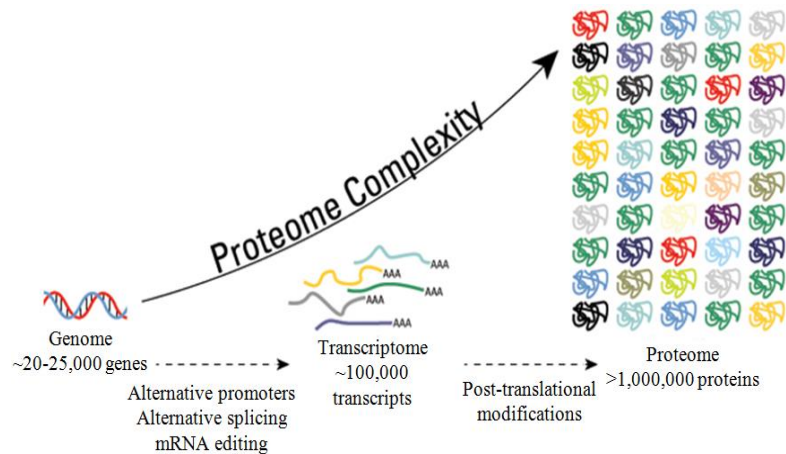


Figure 3.1 The origin of proteome complexity. The human genome, comprised of 20,000-25,000 genes, gives rise to a human proteome of greater than one million proteins due to alternative promoters, alternative splicing, mRNA editing, and most importantly, post-translational modifications. Figure adapted from Thermo Scientific.

mediated, chemical alterations to proteins that occur after translation which can affect protein structure and ultimately function. The existence of over 300 known PTMs, all of which are capable of altering varying forms of proteins, gives rise to the overall variability seen within the protein population.⁴

The most commonly occurring post-translational modification is protein phosphorylation. Protein phosphorylation is the most important mechanism associated with regulating protein function and signal transmission. Accordingly, it guides virtually every biological process in the cell including growth, division, proliferation, and migration.⁵ Protein phosphorylation is believed to effect over one-third of all proteins in the human proteome and occurs at serine, threonine, and tyrosine residues with a ratio of 1800:200:1.^{6,7} The mechanism of protein phosphorylation involves the nucleophilic attack of a terminal phosphate group on an ATP molecule by the negatively-charged hydroxyl group of serine, threonine, or tyrosine. The transfer of the phosphate group is facilitated by magnesium, which lowers the energy threshold for phosphoryl transfer (Figure 3.2). Protein phosphorylation is a reversible modification, in that phosphate groups can be easily removed via hydrolysis.⁸

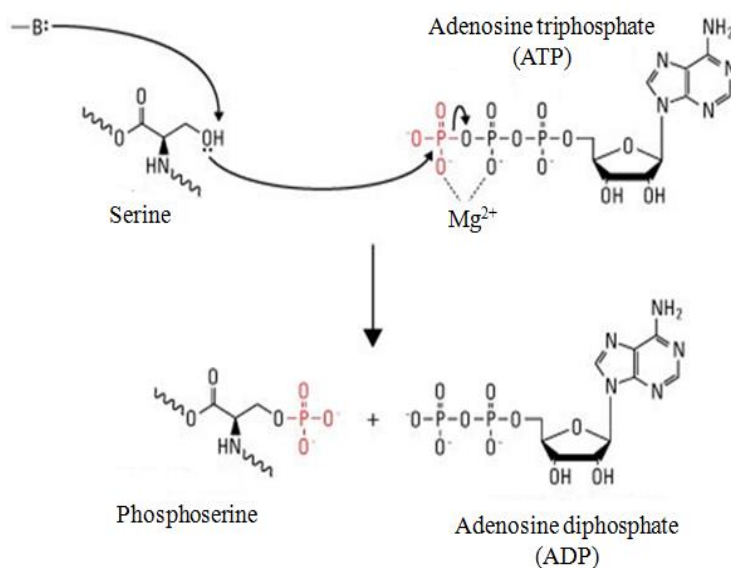


Figure 3.2 Mechanism of phosphorylation. The hydroxyl group of a serine, threonine, or tyrosine residue first imitates nucleophilic attack on a terminal phosphate group of ATP. Transfer of the phosphate group to the amino acid side chain is facilitated by coordination of magnesium to the γ - and β -phosphate groups, which lowers the energy threshold for phosphoryl transfer. Figure adapted from Thermo Scientific.

The transfer and removal of phosphate groups to and from proteins within the cell is facilitated by kinase and phosphatase enzymes, respectively. The kinase family represents one of the largest families of eukaryotic genes, accounting for over 2% of the entire human genome. This translates to a human kinome comprised of over 500 unique kinase enzymes.^{8,9} Classical protein kinases are structurally similar, with the majority containing a catalytic domain of approximately 250 amino acid residues. The substrate binding cleft is comprised of a small N-terminal region of β -sheets and a large C-terminal region of α -helices in which ATP resides to provide the origin for phosphoryl transfer. Although classical kinases share a common structure in regards to their catalytic domains, discrete changes in the charge and hydrophobicity of various surface residues within the active site result in kinase specificity for certain protein substrates.⁸

The relative size of the active site of a kinase plays a role in determining its specificity. For instance, a kinase with a relatively small active site is able to accommodate the side chains of serine and threonine residues easily and thus, is serine/threonine-specific. Serine/threonine kinases account for roughly 80% of all protein kinases. The remaining 20% of kinases have a much larger active site, allowing them to accommodate tyrosine residues specifically. Specificity of kinases is also generated through their ability to recognize consensus sequences in protein substrates. Typically, the four amino acids located N- and C-terminal to the residue to be phosphorylated contribute significantly to kinase-substrate recognition. Residues within the kinase active site recognize and bind residues in the consensus sequence through charge, hydrogen bonding, or hydrophobic interactions. For example, the active site of cAMP-dependent protein kinase A (PKA) contains two negatively-charged glutamic acid residues which

favor binding of positively-charged residues in the protein substrate in positions P-3 and P-2. Additionally, a hydrophobic pocket in the kinase favors a hydrophobic residue in position P+1. These requirements result in a consensus sequence for PKA of R-R-X-S/T-Z, where X is any amino acid and Z is any hydrophobic amino acid (Figure 3.3).^{8,10}

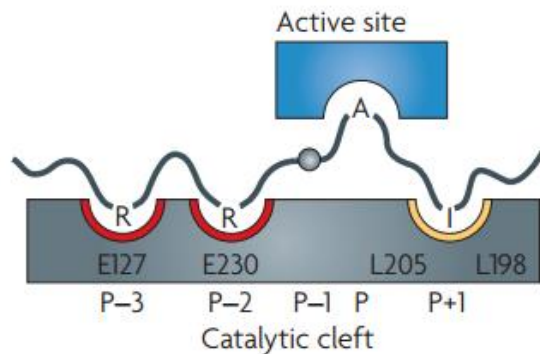


Figure 3.3 Active site of c-AMP dependent protein kinase A (PKA).⁸ Two negatively-charged glutamic acid residues in the catalytic cleft of PKA provide favorability for positively-charged arginine residues in positions P-3 and P-2. An additional hydrophobic pocket favors binding of a hydrophobic residue in position P+1. This gives rise to a consensus sequence for PKA of R-R-X-S/T-Z.

When a kinase enzyme recognizes and binds a consensus sequence, resulting in the transfer of a phosphate group, it induces a conformational change in the phosphorylated protein. This conformational change affects the protein by 1) regulating the catalytic activity of the protein by converting it into an active state and 2) inducing the protein to recruit neighboring proteins with domains that bind to specific phospho-motifs. The combination of these factors provides kinase enzymes with the power to drastically direct signal transduction. In a typical signal transduction cascade, one protein may become phosphorylated which can in turn phosphorylate and activate proteins downstream. Some of these downstream targets may also be kinases which can continue to phosphorylate and activate further downstream substrates until a desired response occurs (Figure 3.4).¹¹

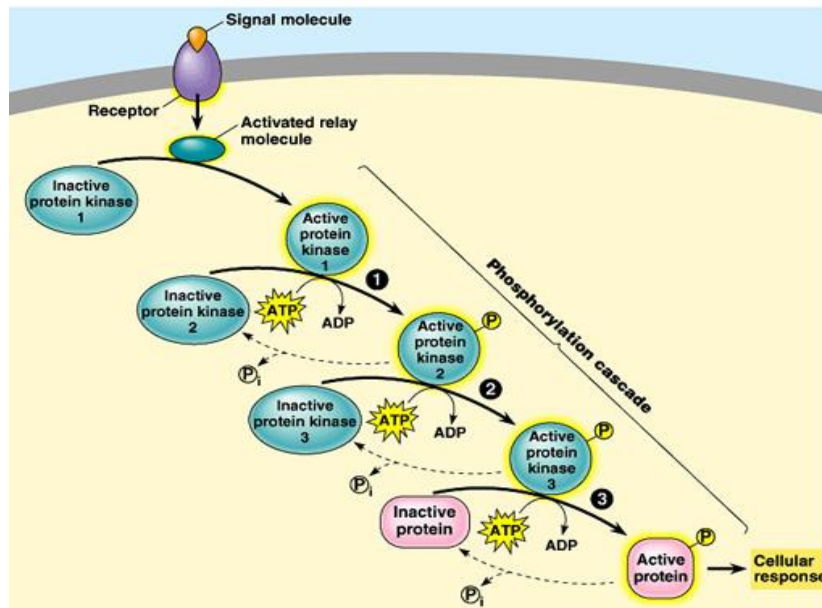


Figure 3.4 Phosphorylation-mediated signaling cascade. In a typical phosphorylation signaling cascade, a protein kinase is activated via a signaling molecule. This active protein kinase can then activate additional downstream proteins via phosphorylation. These downstream targets may be protein kinases which can in turn phosphorylate and activate further downstream substrates until the desired response is achieved, resulting in an amplification of the original signal. Figure adapted from Pearson Education.

The duration of phosphorylation-induced signaling cascade is further regulated by phosphatase enzymes. Phosphatase enzymes are less abundant than kinases, with only an estimated 255 encoded by the human genome. However, recent evidence suggests that they play a key role in maintaining levels of phosphorylation in cells, thus complementing kinase activity and further directing many biological processes.¹² Similarly to kinase enzymes, phosphatases show phosphoserine/threonine-¹³ or phosphotyrosine-specificity¹⁴ which is achieved through various combinatorial interactions between catalytic and regulatory subunits. While both phosphatase families serve to remove phosphate groups from specific residues in proteins, they do so by different mechanisms. Serine/threonine-specific phosphatases contain two metal ions (commonly Mn^{2+} and Fe^{2+}) which bind and

activate water molecules, resulting in nucleophilic attack on phosphorous atoms.¹³

Conversely, tyrosine-specific phosphatases utilize the formation of an enzyme-thiophosphoryl intermediate. Here, a cysteine residue within the enzyme active site initiates nucleophilic attack on the phosphorous atom of the protein substrate. During cleavage of the ester bond, a nearby acidic residue donates a proton to the leaving group oxygen atom. A water molecule then hydrolyzes the phosphoenzyme intermediate, resulting in a restored phosphatase enzyme and inorganic phosphate.¹⁴

The necessity of kinase and phosphatase enzymes to work in concert is nicely illustrated by the tyrosine-kinase Src, which plays a key role in various physiological processes such as cell differentiation, motility, and survival. The ability of Src to control these processes relies on phosphorylation and dephosphorylation of specific residues within the protein. Specifically, Src is activated via autophosphorylation of Tyr416 and deactivated by phosphorylation of Tyr527 by the tyrosine-protein kinase, Csk. Dephosphorylation of either of these sites results in a decrease or increase in Src activity, respectively. In normal cells, Src remains in an inactive state until it is needed; however, dysregulation in phosphorylation or dephosphorylation dynamics results in drastic changes in Src activity which have been linked to multiple cancers including colon and breast cancer.¹⁵ As discussed in chapter 1, proteins which are aberrantly phosphorylated enter into the HLA class I processing pathway, resulting in a pool of tumor-specific phosphopeptides. These phosphopeptides are then presented to circulating cytotoxic T cells and have the potential to stimulate a tumor-specific immune response.¹⁶ Thus, the goal of this work is to identify tumor-specific phosphopeptides derived from dysregulated

cellular signaling events which are likely due to alterations in kinase and phosphatase activity.

3.1.2 Phosphopeptide Enrichment

As discussed in chapter 1, the task of identifying phosphopeptides presented by HLA class I molecules as a result of dysregulated cell signaling events is quite challenging. These challenges arise from 1) the transient nature of protein phosphorylation, 2) the ability of each HLA allele to present up to 10,000 unique peptides, and 3) the possibility for each individual to express up to six different HLA alleles.⁶ Thus, in order to detect and sequence this subset of phosphopeptides, which accounts for only 1% of all peptides presented by HLA class I molecules at the cell surface, it is necessary to use extremely sensitive enrichment techniques prior to analysis by mass spectrometry.¹⁷

The most commonly used method for enrichment of phosphorylated species from complex samples is immobilized metal affinity chromatography (IMAC), which was first introduced by Porath *et al.* in 1975. This separation technique utilizes a solid chromatographic support covalently bound to a chelating resin to entrap metal ions. Trapped metal ions can then serve as affinity ligands for phosphorylated amino acid residues.¹⁸ The basic principle of IMAC, in regards to phosphopeptide enrichment, involves selective binding of phosphate groups to metal ions bound to a chelating resin, a rinse step to remove any impurities, and an elution step to yield a concentrated solution of phosphopeptides.¹⁹ The most frequently used resin is iminodiacetic acid (IDA) which is chelated to positively charged transition metal ions, usually Cu(II), Ni(II), Zn(II), Co(II), or Fe(III). These metal cations act as Lewis acids which can accept electron pairs from

phosphate groups. Coordination of the resin to the metal cation can be bi-, tri-, or tetradentate depending on the number of occupied coordination sites.¹⁸ For instance, IDA is a tridentate ligand because it binds to Fe(III) through three coordination sites, with the remaining sites occupied by water. Alternative resins, such as nitrilotriacetic acid (NTA), can be used which provide stronger binding of metal cations based on the tetradentate nature of the ligand.²⁰

The overall workflow for IMAC enrichment is illustrated in Figure 3.5. In this method, activated iron is first immobilized onto IDA resin packed into a fused silica microcapillary column. This activated Fe-IDA resin is now capable of binding any negatively charged species within the peptide sample. However, this leads to a major issue associated with phosphopeptide enrichment via IMAC – nonspecific binding of negatively-charged carboxy termini and acidic residues to Fe^{3+} cations. To block this interaction, we perform a Fischer esterification which utilizes acetyl chloride in excess methanol to convert carboxyl groups of amino acids into their corresponding methyl esters.²¹ Following esterification, aliquots of isolated HLA-associated peptides are pressure-loaded onto the IMAC column, allowing for the electrostatic interaction between the positively-charged metal ions and any negatively-charged phosphate groups present. Any unmodified peptides are washed off of the column, leaving behind only phosphorylated peptides bound to the resin.

Elution of phosphopeptides is achieved using ascorbic acid, which reduces Fe^{3+} to Fe^{2+} . The reduction of the hard acid, Fe^{3+} , lowers the affinity for the oxygen atoms of the phosphate group via transition to an intermediate acid, Fe^{2+} . Phosphopeptides are then released from the IMAC column and directly eluted onto a reversed phase C18

precolumn. This precolumn is then attached to a reversed phase C18 analytical column equipped with a laser-pulled electrospray emitter tip. Finally, phosphopeptides are eluted into a high resolution mass spectrometer for analysis. This methodology allows for the reliable enrichment and detection of tumor-specific phosphopeptides at the sub-femtomole level.

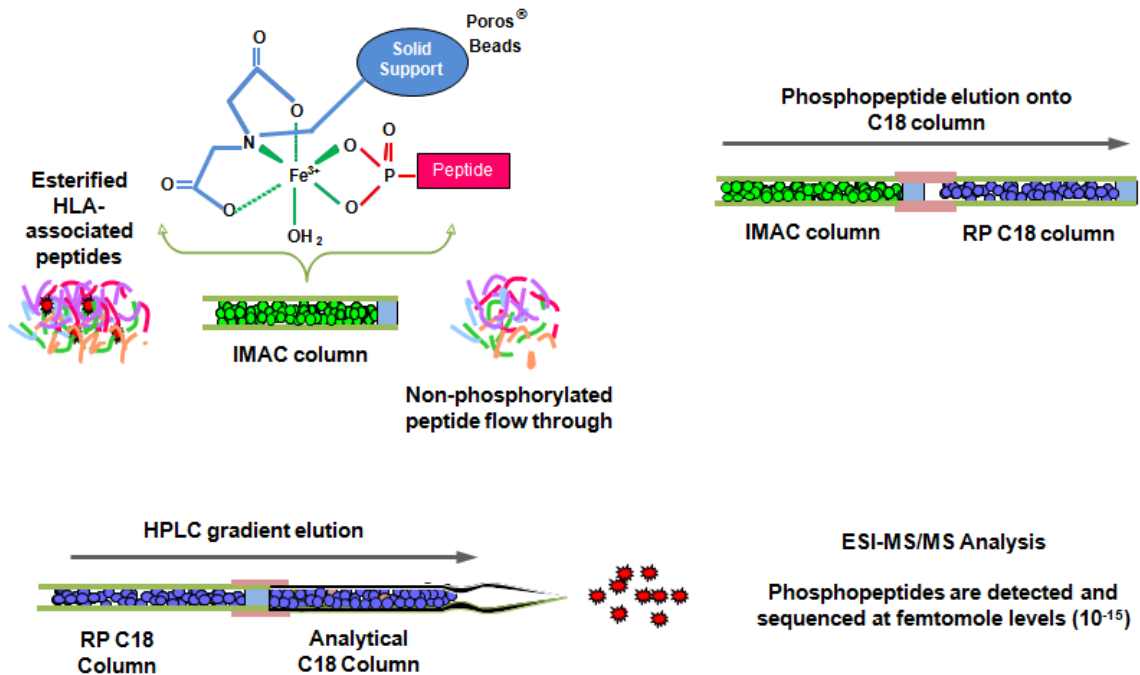


Figure 3.5 Workflow of Fe-IDA IMAC enrichment. HLA-associated peptides are isolated from tissue samples and esterified to block carboxyl groups of amino acid residues. Esterified aliquots are pressure-loaded onto an IMAC column packed with Fe-IDA resin. Phosphopeptides bind to the resin via electrostatic interactions while unmodified peptides flow through. Ascorbic acid is used to elute phosphopeptides directly onto a reversed phase C18 precolumn. Attachment of the precolumn to a reversed phase C18 analytical column allows for subsequent elution of phosphopeptides into a high resolution mass spectrometer for detection.

3.1.3 Project Aim

In this chapter, we will utilize complementary IMAC enrichment techniques – Fe-IDA and Fe-NTA – to enrich for phosphopeptides presented at the cell surface by HLA class I molecules in a human hepatocellular carcinoma tumor tissue sample. Given the tetradentate nature of NTA, we believe that metal ions will be retained on the IMAC column with greater efficiency, leading to decreased nonspecific binding of unmodified peptides. Additionally, we hypothesize that both IMAC resins can be used on a single sample to enrich for unique subsets of phosphopeptides, providing a more complete phosphopeptide profile of analyzed samples.

3.2 Materials

3.2.1 Reagents

Amersham Pharmacia Biotech (Amersham, UK)

NHS-activated sepharose beads

Applied Biosystems (Carlsbad, CA)

POROS ® MC 20 metal chelating packing material, 20 µm diameter

Atlantic Peptides LLC (Lewisburg, PA)

Phosphopeptide standards, RVKsPLFQF, RTHsLLLLG, ≥95% purity

Grace Davison Discovery Science (Deerfield, IL)

Acetyl chloride, anhydrous

D₀ methanol, anhydrous

Honeywell (Morristown, NJ)

Acetonitrile, HPLC grade, ≥99.8% purity

J.T. Baker (Phillipsburg, NJ)

Glacial acetic acid, ≥99.9% purity

Pierce (Rockford, IL)

LC-MS grade water

PQ Corporation (Valley Forge, PA)

Kasil ® 1624 potassium silicate solution

Sigma Aldrich (Saint Louis, MO)

Angiotensin I acetate salt hydrate, ≥90% purity

Angiotensin II phosphate

Aprotinin

CHAPS buffer

Ethylenediaminetetraacetic acid (EDTA), analytical grade

Formamide

Iron (III) chloride

L-ascorbic acid

Leupeptin

Pepstatin A

Phenylmethylsulfonyl fluoride (PMSF)

Sodium azide

Sodium Chloride

Tris-HCl

Vasoactive intestinal peptide fragment 1-12, \geq % purity

YMC Company, LTD (Kyoto, Japan)

ODS-AQ, C18 5 μ m spherical silica particles, 120 Å pore size

ODS-AQ, C18 5-20 μ m spherical silica particles, 120 Å pore size

3.2.2 Equipment and Instrumentation

Agilent Technologies (Palo Alto, CA)

1100 Agilent high performance liquid chromatograph

Branson (Danbury, CT)

Branson 1200 Ultrasonic bath

Beckman Coulter (Pasadena, CA)

Optima LE-8K ultracentrifuge (Ti70 rotor)

Labonco Corp. (Kansas City, MO)

Centrivap centrifugal vacuum concentrator

Millipore (Billerica, MA)

Amicon ultra, 10 kDa regenerated cellulose spin filter

PolyMicro Technologies, Inc. (Phoenix, AZ)

360 μm o.d. x 50 μm i.d. polyimide coated fused silica capillary

360 μm o.d. x 75 μm i.d. polyimide coated fused silica capillary

360 μm o.d. x 150 μm i.d. polyimide coated fused silica capillary

Qiagen (Valencia, CA)

Ni-NTA spin column

Sutter Instrument Co. (Novato, CA)

P-2000 microcapillary laser puller with fused silica adapter

Thermo-Fisher Scientific (San Jose, CA/Bremen, Germany)

LTQ mass spectrometer (back-end ETD)

LTQ FTICR hybrid mass spectrometer (custom modified with front-end ETD)

LTQ Orbitrap mass spectrometer (custom modified with front-end ETD)

LTQ Orbitrap Fusion Tribrid mass spectrometer (front-end ETD)

Zeus Industrial Products, Inc. (Orangeburg, SC)

Teflon tubing, 0.012 inch i.d. x 0.060 inch o.d.

3.3 Methods

3.3.1 Tissue Culture (Performed by NB, University of Birmingham)

A hepatocellular carcinoma tumor tissue sample (LL4857T) weighing 2.2 grams was obtained one-hour post-removal from a 77 year old female patient with no underlying chronic liver disease at the Queen Elizabeth Hospital and Center for Liver Research at the University of Birmingham. The tissue sample was first cut into smaller pieces and stored at -80°C until further use. The entire sample was prepared for HLA-associated peptide isolation, assuming that 1 gram is equivalent to $1\text{e}9$ cell equivalents (C. Eq.).

3.3.2 HLA-Associated Peptide Isolation (Performed by NB, University of Birmingham)

Frozen pieces of tumor tissue were resuspended in lysis buffer (20 mM Tris-HCl pH 8, 150 mM NaCl, 1% 3-[(3-cholamidopropyl) dimethylammonio]-1-propane sulfonate (CHAPS)) and homogenized using a tissue ruptor (Qiagen). Protease inhibitors (1 mM PMSF, 5 $\mu\text{g}/\text{mL}$ aprotinin, 10 $\mu\text{g}/\text{mL}$ pepstatin A, and 10 $\mu\text{g}/\text{mL}$ leupeptin) were added to prevent degradation of HLA molecules. Phosphatase inhibitor cocktails II and III were added in 1:100 dilutions to prevent dephosphorylation of isolated peptides. Lysates were centrifuged at $100,000 \times g$ for 1 hour at 4°C . Supernatants were incubated with an HLA class I-specific antibody (W6/32, 5 $\text{mg}/1\text{e}9$ cells) bound to NHS-Sepharose beads and rotated at 4°C for 16 hours. Beads were pelleted via centrifugation at 2000 rpm for 2 minutes and the supernatant removed. Beads then underwent a series of four wash steps

including: lysis buffer, 20 mM Tris-HCl and 150 mM NaCl, 20 mM Tris-HCl and 1 M NaCl, and finally 20 mM Tris-HCl. Beads were then transferred to a 5 kDa molecular weight cutoff (MWCO) filter and peptides eluted from HLA class I molecules using 10% acetic acid. Isolated peptides were stored at -80°C prior to shipment to the University of Virginia for analysis.

3.3.3 Peptide Content Determination by HPLC-ESI-MS/MS

Isolated peptide mixtures were dried to completion in a Centrivap and reconstituted in 0.1% acetic acid for a final concentration of 1×10^7 C. Eq./ μL . For sample screens, 1 μL (1×10^7 C. Eq.) of peptide sample was added to 4 μL of 0.1% acetic acid. This mixture was pressure loaded onto a fused silica microcapillary precolumn (PC) (360 μm o.d. x 75 μm i.d.) equipped with a 2 mm Kasil[®] 1624 frit and packed with 8-10 cm of irregular C18 reversed phase resin (5-20 μm diameter, 120 \AA pore size) at a flow rate of $<1 \mu\text{L}/\text{min}$. The PC was rinsed on an HPLC with solvent A (0.1M acetic acid in water) for 20 minutes at 30 bar. The PC was then dried using a pressure bomb and connected to a fused silica microcapillary analytical column (AC) (360 μm o.d. x 50 μm i.d.) packed with 6-8 cm of regular C18 reversed phase resin (5 μm diameter, 120 \AA pore size) and equipped with a laser-pulled, electrospray emitter tip (2 μm diameter) via a Teflon sleeve. The ACPC was rehydrated by rinsing on an HPLC with solvent A for 10 minutes at 30 bar. Next, 100 fmol of two internal peptide standards (angiotensin and vasoactive intestinal peptide) were loaded onto the ACPC for a quantitation purposes prior to mass spectrometric analysis.

Peptides were eluted using an HPLC gradient of 0-60% solvent B (70% acetonitrile, 0.1M acetic acid) in 40 minutes at a flow rate of 60 nL/min and electrospray ionized directly into an LTQ Orbitrap Classic or FT-ICR mass spectrometer. Full-scan high resolution mass spectra (MS1) were acquired in the Orbitrap or FT-ICR mass analyzers and MS/MS spectra (MS2) were acquired using CAD and ETD fragmentation methods in the linear ion trap of the instrument. A data-dependent top-6 CAD/ETD toggle method was used in which one high resolution MS1 scan (resolving power of 60,000 at 400 m/z) was acquired followed by selection of the top 6 most abundant parent ions for fragmentation by CAD and ETD. Data-dependent parameters included a repeat count of 3, repeat duration of 10 seconds, and exclusion list duration of 10. Additionally, ions with a charge state of +1 were excluded. ETD parameters included a 45 ms reaction time, FTMS automatic gain control (AGC) target of 2e5 charges, ITMS AGC target of 1e4 charges, and an ETD reagent target of 2e5 charges.

Data analysis was performed using Xcalibur software (Thermo Electron Corporation). Raw data files were searched using OMSSA (version 2.1.1) against the Swissprot human protein database with the following parameters: no enzyme specificity, E-value cutoff of 1, variable modifications of oxidation of methionine and phosphorylation of serine, threonine, and tyrosine, ± 0.01 Da precursor mass tolerance, and ± 0.35 Da product ion mass tolerance. Database hits were used to guide the analysis and peptide sequences were determined by accurate mass measurement and manual interpretation of MS2 spectra.

Relative abundances of peptides were calculated by comparing peptide peak areas to those of two internal peptide standards (angiotensin and vasoactive intestinal peptide) which were present at a fixed concentration of 100 fmol each. The total peptide content

of the sample was summed and compared to that of a well-characterized sample which was previously analyzed by IMAC. This comparison allowed for the determination of the amount of material needed to perform enrichment on the current sample.

3.3.4 Sample Desalting via C18 Microcapillary Cleanup Columns

Peptides isolated from $1e8-1e9$ C. Eq. in 0.1% acetic acid were combined with additional 0.1% acetic acid for a total sample volume of 50 μ L. For estimation of sample losses, 100 fmol of two internal phosphopeptide standards – angiotensin II phosphate (DRVyIHPPF) and RVKsPLFQF – were spiked into the sample. The sample was pressure loaded onto a fused silica microcapillary cleanup column (360 μ m o.d. x 150 μ m i.d.) equipped with a 2 mm Kasil® 1624 frit and packed with 5 cm of irregular C18 reversed phase resin at a flow rate of 0.5 μ L/min. The column was rinsed by loading 25 μ L of 0.1% acetic acid at a flow rate of 0.5 μ L/minute. The flow through and column rinse volumes were collected in an Eppendorf tube and stored at -35°C . The cleanup column was connected to an HPLC and rinsed with solvent A for 10 minutes at 12-15 bar. At the same backpressure, peptides were eluted from the cleanup column into an Eppendorf tube using a gradient of 0-80% solvent B in 40 minutes followed by a 30 minute hold at 80% solvent B. Finally, 100 fmol of a third internal phosphopeptide standard, RTHsLLLLG, was spiked into the sample and the tube was dried to completion using a Centrivap. The dried, cleaned-up sample was stored at -35°C until further use.

3.3.5 Fischer Esterification of Samples

Samples were subjected to a Fischer esterification to block C-termini and acidic side chains of amino acid residues. Desalted peptide samples were dried in triplicate using 50 μL of anhydrous methanol. Esterification reagents were prepared by adding 160 μL of anhydrous acetyl chloride drop-wise to 1 mL of anhydrous methanol, forming methanolic HCl. Next, 80 μL of the cooled reaction mixture was added to the dried peptide samples and allowed to react at room temperature for 1 hour. The samples were dried to completion, rinsed with 50 μL of anhydrous methanol, and dried again. This process was repeated using fresh reagents to ensure completeness of the reaction. Esterified samples were stored at -35°C until further use.

3.3.6 Phosphopeptide Enrichment via IMAC

3.3.6.1 Fe-IDA IMAC Enrichment

A fused silica microcapillary column (360 μm o.d. x 75 μm i.d.) equipped with a 2 mm Kasil $\text{\textcircled{R}}$ 1624 frit was packed with 5 cm of POROS $\text{\textcircled{R}}$ MC 20 iminodiacetate resin. The IMAC column was pressure rinsed at a flow rate of 20 $\mu\text{L}/\text{min}$ with the following steps: a 20 minute water rinse, a 10 minute 50 mM EDTA rinse, and a 10 minute water rinse. The column was activated using filtered 100 mM FeCl_3 for 5 minutes at a flow rate of 20 $\mu\text{L}/\text{min}$ followed by a 3 minute incubation period in which the iron was allowed to sit on the column to ensure diffusion into resin particles. This process was repeated three times to ensure complete activation. The activated column was equilibrated with 25 μL of

0.01% acetic acid at a flow rate of 0.5 $\mu\text{L}/\text{min}$. The dried, esterified peptide sample was reconstituted in 50 μL of 1:1:1 (methanol:acetonitrile:0.01% acetic acid (vol/vol)) and pressure loaded onto the activated IMAC column at a flow rate of 0.5 $\mu\text{L}/\text{min}$. Following sample loading, 25 μL of 1:1:1 was added to the sample tube and loaded onto the IMAC column at a flow rate of 0.5 $\mu\text{L}/\text{min}$. A final rinse with 15 μL of 0.01% acetic acid at a flow rate of 0.5 $\mu\text{L}/\text{min}$ was completed. The sample flow through, 1:1:1 rinse, and 0.01% acetic acid rinse were collected in an Eppendorf tube and stored at -35°C .

At this point, a PC was rinsed on a HPLC with solvent A at 30 bar for 10 minutes. The PC was butt-connected to the end of the IMAC column with a Teflon sleeve and the IMAC-PC column was rinsed with 0.01% acetic acid for 10 minutes at a flow rate of 0.5 $\mu\text{L}/\text{min}$ to ensure that no leaks were present. Phosphopeptides were eluted directly onto the PC by pressure loading freshly-prepared 250 mM L-ascorbic acid in water (pH 2) at a flow rate of 0.5-1 $\mu\text{L}/\text{min}$ for 25 minutes. A final rinse of 0.01% acetic acid at the same flow rate was completed prior to disconnection of the PC from the IMAC column. The PC was rinsed on an HPLC with solvent A at for 25 minutes at 30 bar. The PC was dried and connected to a C18 AC using a Teflon sleeve. The ACPC was rehydrated by rinsing on an HPLC with solvent A at a flow rate of 60 nL/min for 10 minutes. Next, 100 fmol of two internal peptide standards (angiotensin and vasoactive intestinal peptide) were loaded onto the ACPC for a quantitation purposes prior to mass spectrometric analysis.

3.3.6.2 Fe-NTA IMAC Enrichment

For the preparation of Fe-NTA resin using a 10 kDa molecular weight cutoff filter, all forward spins were performed at 14,000 \times g for 5 minutes at room temperature and all reverse spins at 1,000 \times g for 1 minute at room temperature. A 10 kDa spin filter was

rinsed twice with 500 μL of 0.01% acetic using one forward and one reverse spin during each round. Ni-NTA resin was removed from a Qiagen Ni-NTA spin column, reconstituted in water (1 mg/mL), and added to the spin filter in three aliquots, each followed by a forward spin. When adding solutions to the spin filter, the mixture was aspirated to remove any resin that had accumulated on the rim of the filter. The resin was rinsed using the following steps: two rinses with 450 μL of water using two forward spins, two rinses with 450 μL of 50 mM EDTA using two forward spins, and two rinses with 450 μL of water using two forward spins. The resin was activated by three rounds of 450 μL of filtered 100 mM FeCl_3 using three forward spins. The activated resin was washed using the following steps: one rinse with 450 μL of 0.01% acetic acid using one forward spin, two rinses of 450 μL of 15% acetonitrile in 0.01% acetic acid using two forward spins, and one rinse with 450 μL of 0.01% acetic acid using one forward spin. The prepared Fe-NTA resin was stored in 0.01% acetic acid at 4°C for up to 1 month.

A fused silica microcapillary column (360 μm o.d. x 150 μm i.d.) equipped with a 2 mm Kasil® 1624 frit was packed with 2.5 cm of previously prepared Fe-NTA resin. The column was re-activated by pressure loading filtered 100 mM FeCl_3 for 10 minutes at a flow rate of 20 $\mu\text{L}/\text{min}$ followed by a 3 minute incubation period in which the iron was allowed to sit on the column to ensure diffusion into resin particles. This process was repeated two times to ensure complete activation. The activated column was equilibrated with 25 μL of 0.01% acetic acid at a flow rate of 0.5 $\mu\text{L}/\text{min}$. The dried, esterified peptide sample was reconstituted in 50 μL of 1:1:1 (methanol:acetonitrile:0.01% acetic acid (vol/vol)) and pressure loaded onto the activated IMAC column at a flow rate of 0.5 $\mu\text{L}/\text{min}$. Following sample loading, 25 μL of 1:1:1 was added to the sample tube and

loaded onto the IMAC column at a flow rate of 0.5 $\mu\text{L}/\text{min}$. A final rinse with 15 μL of 0.1% acetic acid at a flow rate of 0.5 $\mu\text{L}/\text{min}$ was completed. The sample flow through, 1:1:1 rinse, and 0.1% acetic acid rinse were collected in an Eppendorf tube and stored at -35°C .

At this point, a PC was rinsed on a HPLC with solvent A at 30 bar for 10 minutes. The PC was butt-connected to the end of the IMAC column with a Teflon sleeve and the IMAC-PC column was rinsed with 0.01% acetic acid for 10 minutes at a flow rate of 0.5 $\mu\text{L}/\text{min}$ to ensure that no leaks were present. Phosphopeptides were eluted directly onto the PC by pressure loading freshly-prepared 250 mM L-ascorbic acid in water (pH 2) at a flow rate of 0.5-1 $\mu\text{L}/\text{min}$ for 25 minutes. A final rinse of 0.01% acetic acid at the same flow rate was completed prior to disconnection of the PC from the IMAC column. The PC was rinsed on an HPLC with solvent A at for 25 minutes at 30 bar. The PC was dried and connected to a C18 AC using a Teflon sleeve. The ACPC was rehydrated by rinsing on an HPLC with solvent A at a flow rate of 60 nL/min for 10 minutes. Next, 100 fmol of two internal peptide standards (angiotensin and vasoactive intestinal peptide) were loaded onto the ACPC for a quantitation purposes prior to mass spectrometric analysis.

3.3.7 Analysis of Phosphopeptides by HPLC-ESI-MS/MS

Peptides were eluted using an HPLC gradient of 0-60% solvent B in 60 minutes at a flow rate of 60 nL/min and electrospray ionized directly into an Orbitrap Fusion Tribrid mass spectrometer. Full-scan high resolution mass spectra (MS1) were acquired in the Orbitrap mass analyzer and MS/MS spectra (MS2) were acquired using CAD and ETD fragmentation methods in the linear ion trap of the instrument. A top-speed, neutral-loss

triggered method was used in which one high resolution MS1 scan (resolving power of 60,000 at 400 m/z) was first acquired, followed by selection of as many parent ions as possible in a two second timeframe (in order of decreasing abundance) for fragmentation by CAD. If a neutral loss characteristic of the loss of phosphoric acid ($\Delta 98$ Da) was present in the CAD spectrum, an ETD scan of that precursor was then acquired. Data-dependent parameters included a repeat count of 3, repeat duration of 10 seconds, and exclusion list duration of 10. Additionally, ions with a charge state of +1 were excluded. ETD parameters included a 45 ms reaction time, FTMS automatic gain control (AGC) target of 2×10^5 charges, ITMS AGC target of 1×10^4 charges, and an ETD reagent target of 1×10^4 charges.

Data analysis was performed using Xcalibur software (Thermo Electron Corporation). Raw data files were searched using OMSSA (version 2.1.1) against the Swissprot human protein database with the following parameters: no enzyme specificity, E-value cutoff of 1, fixed modifications of methyl esters of aspartic acid, glutamic acid, and C-termini, variable modifications of oxidation of methionine and phosphorylation of serine, threonine, and tyrosine, ± 0.01 Da precursor mass tolerance, and ± 0.35 Da product ion mass tolerance. Additionally, CAD data files were searched using an in-house program, "Neutral Loss Finder," discussed in chapter 1 (section 1.2.5) to identify MS2 spectra exhibiting the neutral loss of phosphoric acid. CAD and ETD spectra were also back-checked against an in-house phosphopeptide database containing all identified phosphopeptides from previous samples. Peptide hits from these three sources were used to guide the analysis and peptide sequences were determined by accurate mass measurement and manual interpretation of MS2 spectra.

Sample recovery for IMAC enrichments was calculated by comparing the peak areas of the three internal phosphopeptide standards, DRVyIHPF, RVKsPLFQF, and RTHsLLLLG, present at fixed concentrations of 100 fmol each in the IMAC run to those of a standards-only run performed on the same day. Calculating the recoveries of the internal phosphopeptide standards spiked in at varying time points throughout the procedure allowed for an assessment of peptide losses from the desalting and esterification steps as well as the actual enrichment. Relative abundances of phosphopeptides identified from the IMAC enrichments were calculated by comparing peptide peak areas to the average peak areas of two internal peptide standards (angiotensin and vasoactive intestinal peptide) present at fixed concentrations of 100 fmol each.

3.4 Results

3.4.1 Identification of HLA-Associated Phosphopeptides from a Hepatocellular Carcinoma Tissue Sample using Complementary IMAC Enrichment Techniques

A large, primary liver cancer tumor was resected from a patient at the Queen Elizabeth Hospital and Center for Liver Research at the University of Birmingham. The HLA-type of the sample was determined to be HLA-A*02/A*03, HLA-B*07/B*44, and HLA-C*05/C*07. A portion of the tumor tissue was homogenized and HLA-associated peptides isolated. Equal aliquots corresponding to 4e8 C. Eq. were enriched for phosphopeptides using both Fe-IDA and Fe-NTA IMAC enrichments. A total of 262 phosphopeptides were identified from the single HCC tumor tissue sample (LL4857T). The following table (Table 3.1) summarizes the phosphopeptides identified using the complementary IMAC enrichment techniques. The source proteins for each identified phosphopeptide were determined using OMSSA, MASCOT (matrixsciences.com), and/or BLAST (blast.ncbi.nlm.nih.gov) and are listed using their corresponding Uniprot gene names (uniprot.org). In some cases, the origin of the phosphopeptide is unknown and therefore a Uniprot gene name is listed as non-applicable (NA). The ability of phosphopeptides to bind to the specific HLA-alleles present was predicted using the “MHC-I binding prediction” algorithm from the immune epitope database (tools.ideb.org/mhci). Relative abundances of the identified phosphopeptides were calculated using two internal standards (angiotensin and vasoactive intestinal peptide) which were present at known levels of 100 fmol each in both IMAC enrichments. If a

phosphopeptide was unable to be detected in either IMAC enrichment, the relative abundance is listed as “ND.”

Table 3.1 Phosphopeptides identified from HCC tumor tissue (LL4357T) using Fe-IDA and Fe-NTA IMAC enrichment techniques. A total of 262 phosphopeptides were identified from the single tumor tissue sample. A lowercase “s,” “t,” or “y” in the peptide sequence indicates a phosphorylated serine, threonine, or tyrosine residue while a lowercase “m” indicates an oxidized methionine residue. Instances where entries are non-applicable or not detected are indicated by “NA” or “ND,” respectively.

#	Phosphopeptide	Protein of Origin	HLA-Type	Relative Abundance in Fe-NTA IMAC (fmol)	Relative Abundance in Fe-IDA IMAC (fmol)
1	RPVtPVSDL	KLF10	B*07	ND	1.16
2	IMDRtPEKL	BCAR3	A*02	ND	0.13
3	VMIGsPKKV	TNS3	A*02	ND	1.85
4	GIMsPLAKK	ARID5A	A*03	ND	1.88
5	KVLSPtAAK	PPP1R10	A*03	ND	0.20
6	SVKsPVTVK	TCF7L1	A*03	ND	1.31
7	VLDsPASKK	C12orf45	A*03	ND	0.31
8	LPAsPRARL	MAP7D1	B*07	ND	2.17
9	RPAsEARAPGL	MAG11	B*07	ND	0.68
10	RPDsPTRPTL	MICAL3	B*07	ND	0.49
11	RPIsPRIGAL	EPN1	B*07	ND	0.47
12	RPVsPGKDI	HIVEP2	B*07	ND	0.22
13	TDKYsKMM	SHQ1	B*07	ND	1.81
14	YPSsPRKAL	SIPA1L1	B*07	ND	0.34
15	KLPDsPALAKK	STIM1	A*03	ND	0.73
16	SVRRsVLMK	PDCL3	A*03	ND	1.50
17	KPRsPPRAL	PEG10	B*07	ND	3.76
18	RPRtPLRSL	NA	B*07	ND	0.90
19	ALGNtPPFL	YTHDF3	A*02	0.56	ND
20	ALMGsPQLV	JUP	A*02	0.91	ND
21	ALMGsPQLVAA	JUP	A*02	0.70	ND
22	AMPGsPVEV	CBFA2T2	A*02	0.15	ND
23	GLIsPVWGA	CEP68	A*02	0.29	ND
24	GLLDsPTSI	ZFP36L1	A*02	0.51	ND
25	IQFsPPFPGA	SBNO2	A*02	0.35	ND
26	LMFsPVTSL	SETD5	A*02	0.04	ND
27	NMDsPGPML	ELF1	A*02	0.17	ND
28	SIMsPEIQL	CIC	A*02	1.45	ND

#	Phosphopeptide	Protein of Origin	HLA-Type	Relative Abundance in Fe-NTA IMAC (fmol)	Relative Abundance in Fe-IDA IMAC (fmol)
29	SIMsPEIQL	CIC	A*02	0.09	ND
30	SISsMEVNV	DBNDD2	A*02	0.10	ND
31	SISStPPAV	GORASP2	A*02	0.18	ND
32	SLFsGDEENA	PDCD4	A*02	0.04	ND
33	SLFsPQNTL	RPRD2	A*02	0.14	ND
34	SLQsLETSV	ATP2B4	A*02	0.35	ND
35	TVFsPTLPAA	ZC3HAV1	A*02	0.05	ND
36	VLFsPPQM	MCM4	A*02	0.03	ND
37	VLIENVAsL	GPX2	A*02	0.17	ND
38	VLLsPVPEL	ANAPC1	A*02	0.27	ND
39	VLYsPQMAL	MGEA5	A*02	0.11	ND
40	SPDsSQSSL	DDIT3	B*07	0.17	ND
41	AAEsPSFL	NCK2	C*05	0.64	ND
42	VVDsPGQEVV	GRF3C2	C*05	0.08	ND
43	AIMRsPQMV	CTNNB1	A*02	0.58	ND
44	GLDsGFHSV	LRCH4	A*02	0.11	ND
45	KIGsIIFQV	PARP14	A*02	0.12	ND
46	KLMsDVEDV	BRWD1	A*02	0.12	ND
47	KVLsSLVTL	ARHGEF7	A*02	0.15	ND
48	KVYsSSEFL	MAST3	A*02	0.11	ND
49	RASsDIVSL	FAM110A	A*02	0.16	ND
50	RASsDIVsL	FAM110A	A*02	0.17	ND
51	RLAsLQSEV	NA	A*02	0.15	ND
52	RLLsPQQPAL	MEF2D	A*02	0.17	ND
53	RLLsTDAEAV	TAF7	A*02	0.08	ND
54	RMYsFDDVL	LMO7	A*02	0.16	ND
55	RQAsLSISV	PRKD2	A*02	0.05	ND
56	RQLsSGVSEI	HSPB1	A*02	0.48	ND
57	RSLsESYEL	IQSEC1	A*02	0.11	ND
58	RSLsQELVGV	ZNF318	A*02	0.08	ND
59	SLHDIQLsL	CCSER2	A*02	0.08	ND
60	SMSsLSREV	SEC16A	A*02	0.13	ND
61	TLMERTVsL	FAM114A1	A*02	0.07	ND
62	ATYtPQAPK	PLEKHO1	A*03	0.32	ND
63	IISsPLTGK	USP36	A*03	0.13	ND
64	RIYQyIQ	DYRK1B	A*03	0.07	ND

#	Phosphopeptide	Protein of Origin	HLA-Type	Relative Abundance in Fe-NTA IMAC (fmol)	Relative Abundance in Fe-IDA IMAC (fmol)
65	SLYDRPAsY	PDGFRA	A*03	0.05	ND
66	APRNGsGVAL	EEPD1	B*07	0.57	ND
67	APSLFHLNtL	DLC1	B*07	0.07	ND
68	GPRSA _s LL	GPSM3	B*07	0.15	ND
69	KLSGL _s F	MARCKSL1	B*07	0.06	ND
70	LPKGLSA _s L	LARP1	B*07	0.12	ND
71	LPRSS _s MAA	BAIAP2	B*07	0.19	ND
72	RPAFF _s PSL	KIAA093-	B*07	0.38	ND
73	RPA _s AGAmL	MEF2D	B*07	0.41	ND
74	RPA _s PSLQL	PPP1R13L	B*07	0.23	ND
75	RPA _s PSLQLL	PPP1R13L	B*07	0.09	ND
76	RPI _s PGLSY	CCDC6	B*07	0.32	ND
77	RP _s NPQL	UNC5B	B*07	0.10	ND
78	RPS _s GFYEL	DACT1	B*07	0.11	ND
79	RPS _s PALYF	TSC22D4	B*07	0.12	ND
80	RPT _s FADEL	FAM21C	B*07	0.11	ND
81	RPT _s PIQIM	FILIP1L	B*07	0.05	ND
82	RPY _s PPFFSL	FAM53C	B*07	0.24	ND
83	RPY _s QVNVL	UTRN	B*07	0.24	ND
84	SPRGEAS _s L	YAF2	B*07	0.17	ND
85	VPKSGRSS _s L	WDR33	B*07	0.14	ND
86	AEQGS _s PRVSY	SPTBN1	B*44	0.07	ND
87	RSE _s PPAEL	TRIP12	C*05	3.00	ND
88	sDDEKMPDLE	PTGES3	C*05	0.09	ND
89	RLLDP _s SPLAL	SLITRK1	C*07	0.07	ND
90	RLD _s YVRSL	TRAPPC1	A*02	0.14	ND
91	RLS _s PLHFV	FAM134A	A*02	0.20	ND
92	RQI _s QDVKL	AMPD2	A*02	0.19	ND
93	RTL _s HISEA	FAM65A	A*02	0.26	ND
94	RMF _s PMEEK	SDC1	A*03	0.08	ND
95	RSY _s RSFSR	RBBP6	A*03	0.39	ND
96	RTN _s PGFQK	RBM26	A*03	0.10	ND
97	RVA _s PTSGVK	IRS2	A*03	0.58	ND
98	RVWEDRPS _s A	NCOR2	A*03	0.53	ND
99	GPPYQRRG _s L	ETV5	B*07	0.49	ND
100	GPR _s PKAPP	ARHGAP4	B*07	0.37	ND

#	Phosphopeptide	Protein of Origin	HLA-Type	Relative Abundance in Fe-NTA IMAC (fmol)	Relative Abundance in Fe-IDA IMAC (fmol)
101	KPSsPRGSL	AJUBA	B*07	0.18	ND
102	KRAsGQAFEL	STMN1	B*07	0.19	ND
103	RPFHGISTVsL	DENND4C	B*07	0.33	ND
104	RPKsNIVLL	MS4A1	B*07	0.08	ND
105	RPRIPsPIGF	EIF4ENIF1	B*07	0.13	ND
106	RPRPAsSPAL	NEURL1B	B*07	0.16	ND
107	RPRPsSVL	DEPP	B*07	0.33	ND
108	RPRPVsPSSLL	SIK1	B*07	0.41	ND
109	RPRsAVEQL	PLEKHA5	B*07	0.51	ND
110	RPRSGsTGSSL	ARFGEF3	B*07	0.50	ND
111	RPRSLsSPTVTL	NEDD4L	B*07	0.74	ND
112	RPRsPPGGP	ZBTB46	B*07	0.33	ND
113	RPRsPTGPSNSFL	RBM17	B*07	0.68	ND
114	RPWsNSRGL	CDC42SE1	B*07	1.06	ND
115	YPGGRRsSL	MRC1	B*07	0.67	ND
116	KRAsYILRL	SMG1	C*07	0.16	ND
117	RRIsDPEVF	FILIP1L	C*07	0.23	ND
118	RRPsIAPVL	KCNT1	C*07	0.10	ND
119	RRPsYTLGM	SIPA1L1	C*07	0.31	ND
120	RRSsFLQVF	SEC23A	C*07	0.54	ND
121	RRSsQSWSL	FAM21C	C*07	1.86	ND
122	KASPKRLsL	MTSS1L	A*02	0.62	ND
123	KLKDRLPsI	LBH	A*02	0.21	ND
124	RLFsKELR	TAF13	A*02	0.12	ND
125	KRAsVFVKL	ST13	A*03	0.27	ND
126	RAKsPISLK	CARD11	A*03	0.39	ND
127	RLSsPISKR	BARD1	A*03	0.25	ND
128	RTYsHGTYR	RSBN1L	A*03	0.07	ND
129	FPRRHsVTL	ZFP36L1	B*07	9.27	ND
130	FRKsMVEHY	RAB33A	B*07	0.09	ND
131	KPPYRSHsL	CEP95	B*07	0.13	ND
132	RPRPHsAPSL	MIIP	B*07	1.80	ND
133	RPRsMVRSF	DOCK1	B*07	0.58	ND
134	RPRsPAARL	ZNF219	B*07	0.17	ND
135	RPRsPWGKL	SEPT4	B*07	0.18	ND
136	RPRsQYNTKL	SRGAP1	B*07	0.36	ND

#	Phosphopeptide	Protein of Origin	HLA-Type	Relative Abundance in Fe-NTA IMAC (fmol)	Relative Abundance in Fe-IDA IMAC (fmol)
137	RPTsRLNRL	NCOA1	B*07	0.51	ND
138	RSRsPRPAL	NA	B*07	0.12	ND
139	SPGLARKRsL	ZNF106	B*07	0.15	ND
140	TPMKKHLsL	FAM126B	B*07	0.20	ND
141	KRKSFTSLY	CEP170	C*07	0.12	ND
142	RVRRsSFLNAK	RAPGEF2	A*03	0.14	ND
143	RPA sYKKK SML	PDGFRA	B*07	0.07	ND
144	RPRDtRRISL	PIEZO1	B*07	1.76	ND
145	GID sPSSSV	FGD3	A*02	1.09	0.17
146	VLSDVIPsI	FAM199X	A*02	1.31	0.16
147	AGDsPGSQF	FOXO1	A*03	0.83	0.01
148	SYPsPVATSY	EGR1	A*03	0.27	0.16
149	KIA sEIAQL	CASKIN2	A*02	0.44	0.5
150	KTM sGTFL L	STAT2	A*02	1.47	0.26
151	RLSDtPPLL	RAB3B	A*02	0.22	0.57
152	RQAsIELPSM	LSP1	A*02	0.51	0.5
153	RTFsPTYGL	SYNM	A*02	4.15	4.32
154	RVAsPTSGV	IRS2	A*02	2.25	0.94
155	SLFGGsVKL	PDC6IP	A*02	0.56	0.6
156	SLQPRSHsV	PLEKHA6	A*02	0.45	0.36
157	KLPDsPALA	STIM1	A*03	0.15	0.08
158	TLLAsPMLK	FLT1	A*03	0.58	0.78
159	APDsPRAFL	NA	B*07	0.36	0.39
160	APSSARAsPLL	DOCK4	B*07	0.25	0.4
161	GPRPGsPSAL	RPUSD1	B*07	0.75	0.55
162	GPRsAsLLSL	GPSM3	B*07	0.69	1.2
163	GPRsAsLLsL	GPSM3	B*07	0.72	0.38
164	KPYsPLASL	NFATC2	B*07	0.35	0.31
165	LPIFSRLsI	ZFP36L2	B*07	0.19	0.15
166	LPRGsSPSVL	TGIF2	B*07	1.64	0.99
167	LPRPAsPAL	MAP1A	B*07	0.14	0.04
168	LPRSSsMAAGL	BAIAP2	B*07	3.29	1.07
169	RPA sAGAML	MEF2D	B*07	8.38	6.47
170	RPA sPEPEL	KIF1A	B*07	0.14	0.25
171	RPA sPGPSL	MICALL2	B*07	0.75	0.81
172	RPNsPSPTAL	TLK1	B*07	0.63	0.79

#	Phosphopeptide	Protein of Origin	HLA-Type	Relative Abundance in Fe-NTA IMAC (fmol)	Relative Abundance in Fe-IDA IMAC (fmol)
173	RPPsPGPVL	SCAP	B*07	0.10	0.23
174	RPSsLPDL	ARID1B	B*07	0.21	0.28
175	RPVsPFQEL	NA	B*07	0.65	0.44
176	RPWsPAVSA	SKI	B*07	2.46	1.16
177	SPAsPKISL	ATXN2L	B*07	0.20	0.62
178	SPRSPsTTYL	CHAF1A	B*07	1.48	1.26
179	TPRsPPLGL	MAP3K11	B*07	3.65	8.45
180	TPRsPPLGLI	MAP3K11	B*07	2.51	4.32
181	AENARSAsF	GAB2	B*44	0.50	0.17
182	AENsPTRQQF	DDX42	B*44	0.68	0.69
183	AENsSSREL	PML	B*44	0.80	0.4
184	AtAGPRLGW	PPFIBP1	B*44	0.51	0.21
185	EELsPTKAF	KLF6	B*44	0.34	0.59
186	KVDsPVIF	DENND4A	C*05	0.37	0.42
187	RSDsYVEL	TP53BP1	C*05	2.01	1.41
188	SIDsPQKL	TP53BP1	C*05	1.29	3.45
189	HTAsPTGMMK	SEC24D	A*02	0.19	0.38
190	KIFsGVFVK	RPL7L1	A*02	0.51	0.3
191	KLIDRTEsL	LSP1	A*02	0.54	0.18
192	RLAsYLDRV	KRT18	A*02	0.57	1.15
193	RTYsGPMNK	POF1B	A*02	3.20	4
194	RTYsGPMNKV	POF1B	A*02	0.71	0.79
195	yLQSRYYRA	HIPK3	A*02	1.66	1.49
196	HVYtPSTTK	ANKRA2	A*03	0.30	2.4
197	KLPDsPALAK	STIM1	A*03	0.09	2.28
198	RIGsPLSPK	LARP1B	A*03	0.17	0.7
199	RILsGVVTK	RPS11	A*03	3.58	1.06
200	RIYQyIQSR	DYRK1B	A*03	0.71	1.23
201	RIYQyIQSRF	DYRK1B	A*03	0.33	1.95
202	RLFVGsIPK	HNRNPR	A*03	0.39	0.06
203	RLSsPVLHR	DBN1	A*03	0.41	0.72
204	RTAsPPPPPK	SRRM1	A*03	0.64	2.34
205	RTSsPLFNK	KIAA1671	A*03	0.30	6.04
206	RVLsPLIIK	RNF169	A*03	0.13	1.75
207	APRKGsFSAL	CUL4A	B*07	2.97	2.03
208	APRRYsSSL	ARHGAP17	B*07	3.19	2.17

#	Phosphopeptide	Protein of Origin	HLA-Type	Relative Abundance in Fe-NTA IMAC (fmol)	Relative Abundance in Fe-IDA IMAC (fmol)
209	KPA _s PKFIVTL	ZC3H14	B*07	0.22	1.01
210	KPRPL _s MDL	KIAA1671	B*07	0.34	0.31
211	KPRPPPL _s P	TRIP10	B*07	1.70	0.58
212	KPR _s PVVEL	ADRBK1	B*07	2.85	17.19
213	MPRQP _s ATRL	MZT2B	B*07	2.26	9.06
214	RPAK _s MDSL	ARHGAP30	B*07	1.04	0.93
215	RPA _s PAAKL	KANSL3	B*07	0.21	1.84
216	RPA _s PQRAQL	NA	B*07	0.87	5.75
217	RPF _s PREAL	LUZP1	B*07	1.58	7.74
218	RPK _s VDFDSL	CD2AP	B*07	0.89	1.26
219	RPKtPPVVI	SYAP1	B*07	0.06	1.18
220	RPQKTQ _s II	SETX	B*07	0.15	0.04
221	RPQRAtSNVF	MYL9	B*07	4.99	2.05
222	RPRAN _s GGVDL	RREB1	B*07	1.77	0.99
223	RPRG _s ESLL	ERBB3	B*07	0.92	0.09
224	RPRG _s QSL	ERBB3	B*07	26.77	11.65
225	RPRPV _s PSSL	SIK1	B*07	1.09	1.23
226	RPR _s AVLL	AKAP13	B*07	1.72	2.89
227	RPR _s ISVEEF	SETX	B*07	0.93	0.75
228	RPR _s MTVSA	MTSS1	B*07	1.08	2.39
229	RPR _s PNMQDL	RASL11A	B*07	0.22	0.2
230	RPRSP _s PIS	GRM5	B*07	0.82	0.41
231	RPR _s PTGPSNSF	RBM17	B*07	1.12	1.5
232	RTR _s PSPTL	PHLDB1	B*07	0.49	0.05
233	SPFKRQL _s L	NUMBL	B*07	9.23	4.32
234	SPFLSKR _s L	CDK12	B*07	0.28	0.05
235	SPK _s PGLKA	RCSD1	B*07	0.07	0.24
236	SPR _s PGRSL	NA	B*07	0.43	2.52
237	VAKRL _s L	BCAR3	B*07	0.39	0.43
238	RAD _s PVHM	MED26	C*05	0.16	9.4
239	RVD _s PSHGL	DAXX	C*05	0.21	1.35
240	KRY _s GNMEY	LATS1	C*07	2.69	0.31
241	RRF _s GTAVY	ZNF518A	C*07	4.97	2.06
242	RRG _s FEVTL	SELH	C*07	2.01	1.18
243	RRIsDPQVF	FILIP1L	C*07	5.22	4.27
244	RRL _s FLVSY	QARS	C*07	0.46	0.39

#	Phosphopeptide	Protein of Origin	HLA-Type	Relative Abundance in Fe-NTA IMAC (fmol)	Relative Abundance in Fe-IDA IMAC (fmol)
245	RTHsLLLLL	RNASE4	C*07	18.45	20.38
246	KLPsPAPARK	MICALL2	A*03	0.05	1.63
247	KLRsPFLQK	DBNL	A*03	0.45	0.25
248	KVQsLRRAL	PRKCDBP	A*03	0.30	0.22
249	RSYsYPRQK	GAREM1	A*03	3.20	1.43
250	RVYsPYNHR	TOPORS	A*03	12.40	9.62
251	HRYsTPHAF	RAF1	B*07	1.54	0.09
252	KPRsPFSKI	RAB11FIP5	B*07	2.22	6.9
253	RPDVAKRLsL	BCAR3	B*07	4.04	1.52
254	RPKsPLSKM	TANC2	B*07	0.57	1.65
255	RPRARsVDAL	LSR	B*07	10.97	9.13
256	RPRPsSVLRTL	DEPP	B*07	0.97	0.52
257	RPRsPRENSI	ATXN2	B*07	0.12	2.49
258	RPRsPRQNSI	ATXN2	B*07	5.22	0.99
259	SPRRsRSISL	SRSF7	B*07	2.49	12.84
260	VPRPERRsSL	TMCO3	B*07	1.40	0.24
261	KPRRFsRsL	RSRC2	B*07	6.93	4.48
262	KPRRFsRSL	RSRC2	B*07	1.06	0.58

Equal aliquots of 4×10^8 C. Eq. of HCC tumor tissue were enriched using Fe-IDA and Fe-NTA IMAC methodology. The corresponding chromatograms, illustrating the total ion current (TIC), and the base peak chromatograms, representing the most abundant species eluting throughout the HPLC-ESI-MS/MS analyses, for each IMAC enrichment are depicted in Figure 3.6. The average recoveries were calculated by comparing the peak areas of three phosphopeptide standards (DRVyIHPF, RVKsPLFQF, and RTHsLLLLG), spiked in during various stages of the enrichment at known levels of 100 fmol each, with those of two internal peptide standards (angiotensin and vasoactive intestinal peptide) added at the same levels prior to HPLC-ESI-MS/MS analysis.

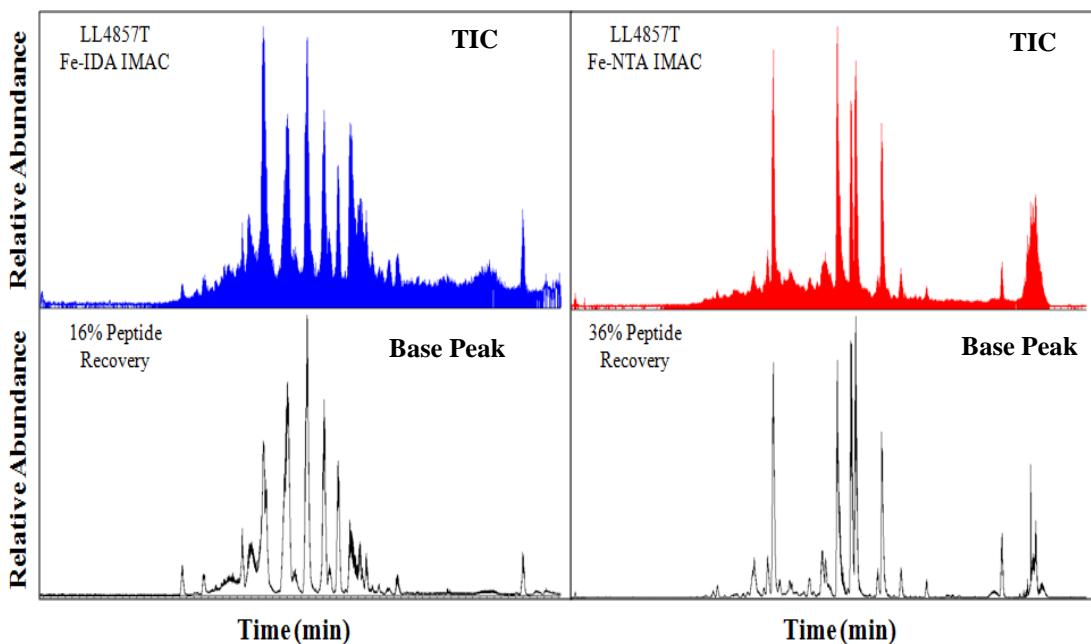


Figure 3.6 Chromatograms and base peaks of Fe-IDA and Fe-NTA IMAC enrichments of HCC tumor tissue. Total ion current (TIC) chromatograms and base peak chromatograms seen in the Fe-IDA IMAC (blue) of LL4857T are compared to those of the Fe-NTA IMAC (red). The average recovery of three phosphopeptide standards is shown for each IMAC enrichment.

A total of 262 phosphopeptides were identified from the single HCC tumor tissue sample using a combination of Fe-IDA and Fe-NTA IMAC enrichment techniques. While many of these phosphopeptides were present in both enrichment elutions, specific subsets were identified that were unique to either Fe-IDA or Fe-NTA enrichments. Of the total 262 phosphopeptides identified, 118 were common to both Fe-IDA and Fe-NTA enrichments. However, an additional 126 phosphopeptides were only identified using Fe-NTA IMAC while 18 additional phosphopeptides were only identified using Fe-IDA IMAC (Figure 3.7).

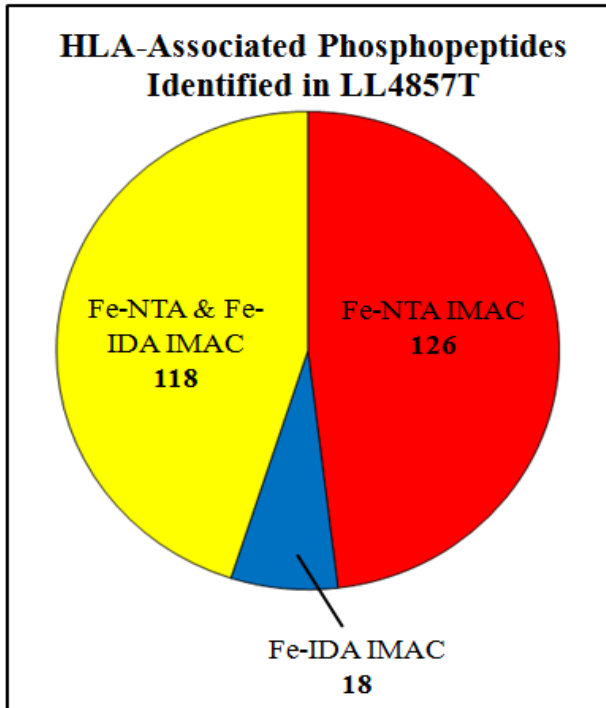


Figure 3.7 Phosphopeptides identified using complementary IMAC enrichment methodology. Pie chart displaying the number of HLA-associated phosphopeptides identified from HCC tumor tissue sample LL4857T using only Fe-IDA (blue) or Fe-NTA (red) IMAC compared to those identified using a both Fe-IDA and Fe-NTA enrichments (yellow). A total of 262 phosphopeptides were identified with 118 present using both Fe-IDA and Fe-NTA IMAC. Additionally, 126 phosphopeptides were only identified in the Fe-NTA IMAC enrichment while 18 phosphopeptides were only identified in the Fe-IDA IMAC enrichment.

3.4.2 Sequence Analysis of Identified Phosphopeptides from Complementary IMAC Enrichment Elutions

The predicted HLA-types of the identified phosphopeptides unique to Fe-IDA IMAC enrichment were compared to those of the identified phosphopeptides unique to Fe-NTA IMAC enrichment. The percentages of peptides expected to bind to HLA-types A*02, A*03, B*07, B*44, C*05, and C*07 are depicted in Figure 3.8. A greater percentage of peptides specific to HLA-A*02, HLA-B*44, HLA-C*05, and HLA-C*07 were evident in the Fe-NTA IMAC enrichment whereas a greater percentage of peptides specific to HLA-A*03 and HLA-B*07 were evident in the Fe-IDA IMAC enrichment. Additionally, the binding motifs of the six represented HLA-types are depicted in Figure 3.8.

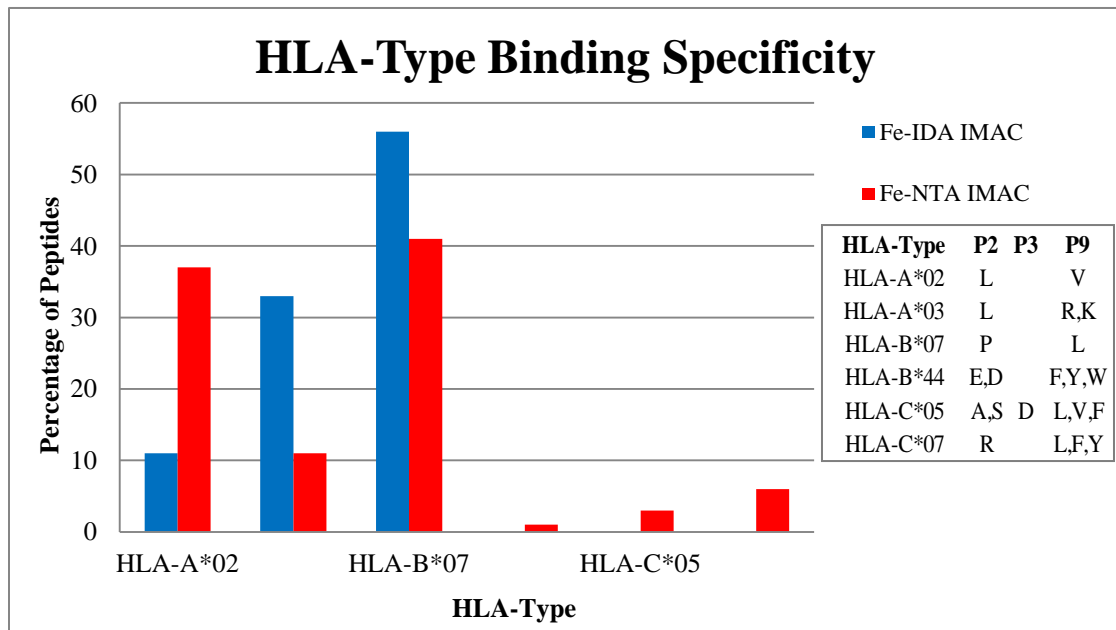


Figure 3.8 HLA-type binding specificities of identified phosphopeptides. The unique subsets of phosphopeptides identified using Fe-NTA (red) or Fe-IDA (blue) IMAC enrichments were analyzed to determine percentages of peptides specific to each of the six represented HLA-types. HLA-A*02-specific peptides were more prevalent in the Fe-NTA IMAC enrichment whereas HLA-A*03 and HLA-B*07 peptides were more prevalent in the Fe-IDA IMAC enrichment. Peptides specific to HLA-B*44, HLA-C*05, and HLA-C*07 were rare and were only observed in the Fe-NTA IMAC enrichment.

In order to determine if basicity of peptide sequences resulted in changes in efficiency of binding to IDA or NTA resin, the percentage of peptides with varying numbers of basic residues (0-4) were determined for phosphopeptides unique to either Fe-IDA or Fe-NTA IMAC enrichments (Figure 3.9). A greater percentage of the sequences of phosphopeptides unique to the Fe-NTA IMAC enrichment contained 0-1 basic amino acid residues. Alternatively, sequences with 2-3 basic amino acid residues were more common in phosphopeptides identified using Fe-IDA IMAC enrichment. A small number of sequences containing four amino acid residues (2%) were seen using Fe-NTA IMAC enrichment.

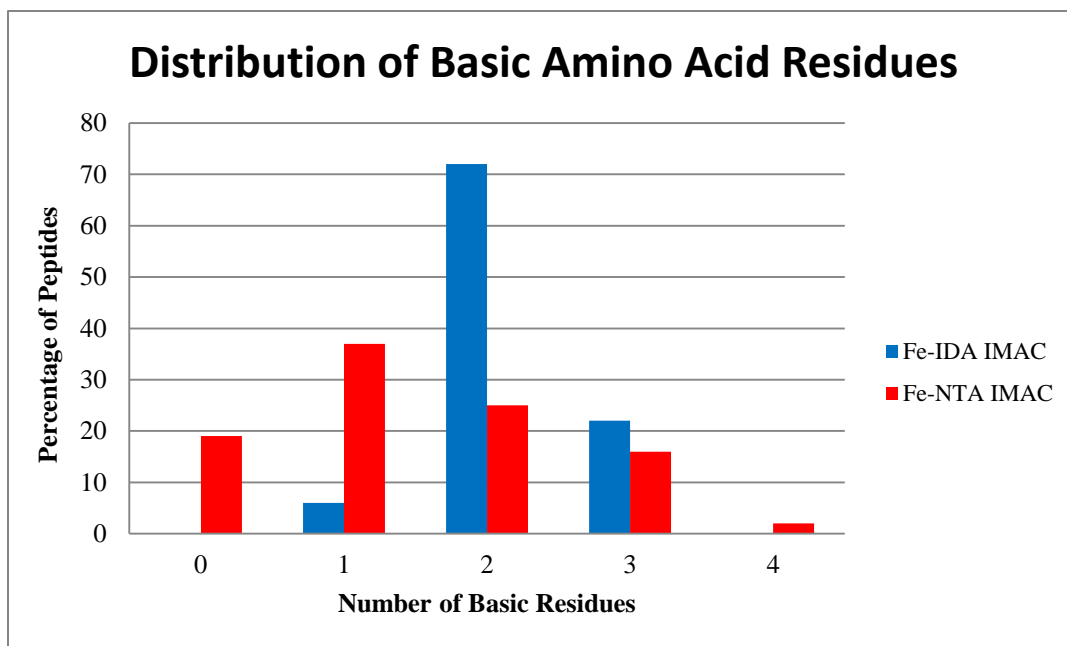


Figure 3.9 Distribution of basic amino acid residues in identified phosphopeptides. The unique subsets of phosphopeptides identified using Fe-NTA (red) or Fe-IDA (blue) IMAC enrichments were analyzed to determine percentages of peptides with varying numbers of basic amino acid residues. Sequences with 0-1 basic amino acid residues were more prevalent in the Fe-NTA IMAC enrichment whereas sequences with 2-3 basic amino acid residues were more prevalent in the Fe-IDA IMAC enrichment.

3.5 Discussion

The goal of this chapter was to examine multiple metal chelating resins for use in immobilized metal affinity chromatography for phosphopeptide enrichment of a human hepatocellular carcinoma tumor tissue sample. Previous efforts in our laboratory involved the use of a porous IMAC resin consisting of an iminodiacetic acid (IDA) group chelated to an iron(III) metal ion for enrichment of phosphopeptides. This method has been optimized over the years to allow for decreased nonspecific binding of non-peptidic species and unmodified peptides as well as increased peptide recoveries. However, inherent qualities of the IDA resin itself do not allow for complete optimization of this methodology. To address these issues, we looked to an alternative IMAC resin functionalized with a nitrilotriacetic acid (NTA) group. This resin is also capable of coordination to iron(III) metal ions and has been suggested to demonstrate virtually no nonspecific binding.^{18,20}

The principle behind IMAC enrichment using IDA or NTA resin is essentially the same, involving the immobilization of metal cations to the resin which allows for binding of phosphorylated species via electrostatic interactions. The major difference between IDA and NTA resin, however, is the strength of chelation by which metal ions are bound. The coordination between IDA and NTA resin and iron(III) cations is depicted in Figure 3.10. IDA is a tridentate ligand, meaning that three of the available six coordination sites of iron participate in the binding interaction. Two of the remaining sites are available for interaction with the negatively charged oxygen atoms of phosphate groups. This interaction leaves one coordination site free, which is typically occupied by water.²⁰

Since the metal cations are not held tightly to the IDA resin, metal leaching often occurs, leaving negatively charged oxygen atoms exposed and providing an opportunity for basic species to bind to the IDA resin. This phenomenon partially converts the IMAC column into an ion-exchange column, thus increasing nonspecific binding.²² In contrast, NTA is a tetradentate ligand, coordinating to the metal cations through four of the six available sites. The remaining two coordination sites are available to participate in the interaction with phosphate groups. This stronger interaction by which NTA binds to the iron(III) cations ensures that metal leaching will not occur and virtually eliminates the presence of nonspecific binding.²⁰

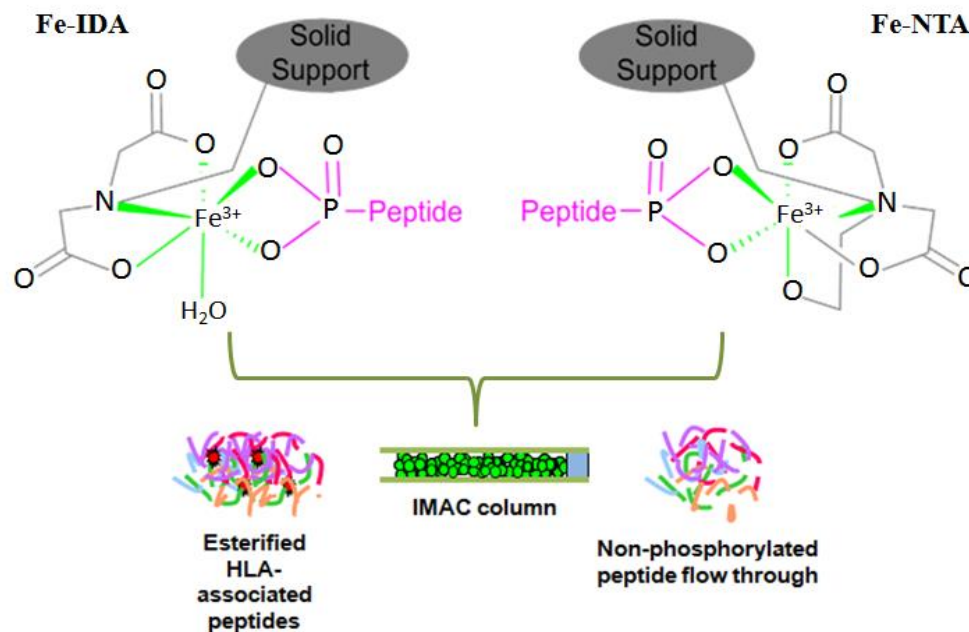


Figure 3.10 Metal coordination of complementary IMAC resins. The tridentate IDA ligand coordinates to iron(III) cations through three of the six available coordination sites, leaving two exposed for coordination to phosphate groups. The remaining free coordination site is typically occupied by water. The tetradentate NTA ligand coordinates to four of the available six coordination sites, with the remaining two available for coordination to phosphate groups. The tetradentate nature of NTA results in a stronger interaction with the metal cations and leads to less metal leaching from the column, ultimately eliminating nonspecific binding of non-peptidic or unmodified peptides.

To test this theory, we subjected a single HCC tumor tissue sample (LL4857T) to phosphopeptide enrichment using both Fe-IDA and Fe-NTA IMAC techniques. As illustrated in Figure 3.6, a comparison of the total ion current chromatograms and the base peak chromatograms from each IMAC enrichment shows a significantly decreased background level in the Fe-NTA IMAC compared to that of the Fe-IDA IMAC. Whereas the majority of abundant peaks in the base peak chromatogram of the Fe-IDA IMAC enrichment correspond to non-peptidic polymer species, the most abundant peaks in the base peak chromatogram of the Fe-NTA IMAC enrichment can all be attributed to internal standards or enriched phosphopeptides. Not only was the presence of polymer species decreased in the Fe-NTA IMAC enrichment, the level of nonspecific binding of unmodified peptides was significantly reduced as well. Additionally, the Fe-NTA IMAC enrichment resulted in a greater average recovery of phosphopeptide standards compared to the Fe-IDA IMAC enrichment (36% vs. 16%). This is likely due to the fact that the tetradentate nature of the NTA ligand retains metal ions with a greater efficiency than the tridentate IDA ligand. This reduces the possibility of nonspecific interactions and leads to an increased number of sites available for preferred binding of phosphorylated species.

A combination of OMSSA, Mascot, and BLAST allowed for the identification of a combined total of 262 phosphopeptides from the HCC tumor tissue sample, the largest number of phosphopeptides identified from a single sample to date (Table 3.1). Interestingly, analysis of the IMAC enrichments revealed unique subsets of phosphopeptides. For instance, 118 phosphopeptides were present in both the Fe-IDA and Fe-NTA IMAC enrichments. However, 18 and 126 phosphopeptides were only present in the Fe-IDA or Fe-NTA IMAC enrichments, respectively. To ensure that these

phosphopeptides were actually unique to a particular resin, all charge states of the specific phosphopeptides were searched for in the enrichment using the alternative resin and were determined to be undetectable. These experiments demonstrate that the use of complementary IMAC enrichment techniques can be applied to a single sample to potentially enrich for a greater number of phosphopeptides.

A question remained as to whether the complementary IMAC resins preferentially enrich for phosphopeptides with specific characteristics. To address this, we analyzed the unique subsets of phosphopeptides identified using Fe-IDA or Fe-NTA IMAC enrichments to determine 1) the representation of phosphopeptides specific to the HLA-types within the sample and 2) the similarities between the phosphopeptide sequences which bind to the various HLA-types. The patient from which the analyzed HCC tumor tissue sample originated was positive for HLA-A*02/A*03, HLA-B*07/B*44, and HLA-C*05/C*07 alleles. Using the immune epitope database, the preferred binding for each phosphopeptide identified using either IMAC resin was determined. The percentages of phosphopeptides expected to bind to the six HLA-types represented within the sample illustrated a clear preference between Fe-IDA and Fe-NTA IMAC resin (Figure 3.8). The Fe-IDA IMAC resin appears to preferentially bind phosphopeptides specific to HLA-A*03 and HLA-B*07 alleles. Conversely, the Fe-NTA IMAC resin appears to preferentially bind phosphopeptides specific to the HLA-A*02 allele. There are phosphopeptides specific to HLA-B*44, HLA-C*05 and HLA-C*07 represented within the subset of phosphopeptides unique to the Fe-NTA IMAC enrichment. However, these phosphopeptides are very low level and could simply be a result of increased phosphopeptide binding and recovery.

As mentioned in chapter 1, each HLA-allele has a distinct binding motif in which certain residues with the second and ninth position of the peptide are preferred. We analyzed the sequences of the phosphopeptides specific to the represented HLA alleles which showed preferential binding to the Fe-IDA or Fe-NTA IMAC resins to determine if basicity was a key factor in the occurrence of unique phosphopeptide subsets. Analysis of the percentage of phosphopeptides specific to each resin which displayed varying numbers of basic amino acid residues suggests that the Fe-IDA resin preferentially enriches for basic phosphopeptides. As depicted in Figure 3.9, a greater percentage of the sequences of phosphopeptides unique to the Fe-NTA IMAC resin contained 0-1 basic amino acid residues whereas the majority of phosphopeptides unique to the Fe-IDA resin contained 2-3 basic amino acid residues. This trend corroborates our hypothesis which suggests that the tridentate nature of metal binding to the IDA ligand leads to increased metal leaching from the IMAC column. This ultimately results in the transformation of the IMAC column into an ion-exchange column which is then capable of binding basic residues within the sequences of phosphopeptides.

Ultimately we have demonstrated that 1) the use of Fe-NTA IMAC enrichment results in decreased nonspecific binding and thus increased phosphopeptide recovery, 2) Fe-IDA IMAC resin preferentially enriches for phosphopeptides with increased numbers of basic amino acid residues within the peptide sequence and 3) Fe-NTA and Fe-IDA IMAC enrichments are complementary techniques which can be used on a single tissue sample to provide a more complete, in-depth analysis of HLA-associated phosphopeptides, ultimately giving rise to an expanded repertoire of potential immunotherapeutic targets.

While the complementary IMAC enrichment approach has been shown to work well for phosphopeptide enrichment, there remains a need for further optimization of this methodology. Future work will entail addressing the current drawback in the use of complementary IMAC enrichment, namely that the processes are independent of one another. Accordingly, a sample must be divided into two aliquots, allowing for the use of both IMAC enrichment techniques. In some cases however, the tissue samples that we receive are from much less than one gram of tissue, thus there is only enough material for one round of enrichment and a choice must be made as to which IMAC resin should be used. It would be greatly beneficial to develop a sequential approach in which a sample is first subjected to Fe-IDA IMAC for phosphopeptide enrichment and the resulting flow through kept for subsequent enrichment using Fe-NTA IMAC methodology. Alternatively, a coupled IMAC enrichment approach could be implemented in which an Fe-NTA IMAC column is butt-connected to an Fe-IDA IMAC column. This would allow for the flow through of the Fe-IDA IMAC enrichment to be directly and immediately enriched using Fe-NTA IMAC methodology. However, working with extremely low-level phosphopeptides makes development of this sequential approach challenging, thus implementation would require a method of reducing excessive sample loss.

3.6 References

1. International Human Genome Sequencing Consortium. Finishing the euchromatic sequence of the human genome. *Nature*. 2004; 431(7011): 931-945.
2. Kim MS *et al.* A draft map of the human proteome. *Nature*. 2014; 509(7502): 575-581.
3. Milanese L, Petrillo M, Spe L, Boccia A, D'Agostino N, Passamano M, Di Nardo S, Tasco G, Casadjo R, Paoletta G. Systemic analysis of human kinase genes: a large number of genes and alternative splicing events result in functional and structural diversity. *BMC Bioinformatics*. 2005; 6: 1-11.
4. Jensen ON. Modification-specific proteomics: characterization of post-translational modifications by mass spectrometry. *Curr Opin Chem Biol*. 2004; 8(1): 33-41.
5. Hanahan D, Weinberg RA. The hallmarks of cancer. *Cell*. 2000; 100(1):57-70.
6. Sefton BM. Overview of protein phosphorylation. *Curr Protoc Cell Biol*. 2001; 14(Unit 14.1): 1-3.
7. Mann M, Ong SE, Gronborg M, Steen H, Jensen ON, Pandey A. Analysis of protein phosphorylation using mass spectrometry: deciphering the phosphoproteome. *Trends Biotechnol*. 2002; 20(6): 261-268.
8. Ubersax JA, Ferrell JE Jr. Mechanisms of specificity in protein phosphorylation. *Nat Rev Mol Cell Biol*. 2007; 8(7): 530-541.
9. Manning G, Whyte DB, Martinez R, Hunter T, Sudarsanam S. The protein kinase complement of the human genome. *Science*. 2002; 298(5600): 1912-1934.
10. Songyang Z, Blechner S, Hoagland N, Hoekstra MF, Piwnicka-Worms H, Cantley LC. Use of an oriented peptide library to determine optimal substrates of protein kinases. *Curr Biol*. 1994; 4(11): 973-982.
11. Robinson MJ, Cobb MH. Mitogen-activated protein kinase pathways. *Curr Opin Cell Biol*. 1997; 9(2): 180-186.
12. Sacco F, Perfetto L, Castagnoli L, Cesareni G. The human phosphatase interactome: An intricate family portrait. *FEBS Lett*. 2012; 586(17): 2732-2739.
13. Shi Y. Serine/threonine phosphatases: Mechanism through structure. *Cell*. 2009; 139(3): 468-484.
14. Kolmodin K, Agvist J. The catalytic mechanism of protein tyrosine phosphatases revisited. *FEBS Lett*. 2001; 498(2-3): 208-213.
15. Roskoski R Jr. Src kinase regulation by phosphorylation and dephosphorylation. *Boichem Biophys Res Commun*. 2005; 331(1): 1-14.
16. Zarling AL, Ficarro SB, White FM, Shabanowitz J, Hunt DF, Engelhard VH. Phosphorylated peptides are naturally processed and presented by major histocompatibility complex class I molecules in vivo. *J Exp Med*. 2000; 192(12):1755-1762.
17. Weidanz JA, Hawkins O, Verma B, Hildebrand WH. TCR-like biomolecules target peptide/MHC class I complexes on the surface of infected and cancerous cells. *Int Rev Immunol*. 2011; 30(5-6):328-340.
18. Gaberc-Porekar V, Menart V. Perspectives of immobilized-metal affinity chromatography. *J Biochem Biophys Methods*. 2001; 49: 335-360.

-
19. Reinders J, Sickmann A. State-of-the-art in phosphoproteomics. *Proteomics*. 2005; 5: 4052-4061.
 20. Dunn JD, Reid GE, Bruening ML. Techniques for phosphopeptide enrichment prior to analysis by mass spectrometry. *Mass Spectrom Rev*. 2010; 29: 29-54.
 21. Ficarro SB, McClelland ML, Stukenberg PT, Burke DJ, Ross MM, Shabanowitz J, Hunt DF, White FM. Phosphoproteome analysis by mass spectrometry and its application to *saccharomyces cerevisiae*. *Nat Biotechnol*. 2002; 20: 301-305.
 22. Block H, Maertens B, Spriestersbach A, Brinker N, Kubicek J, Fabis R, Labahn J, Schafer F. Immobilized-metal affinity chromatography (IMAC): A review. *Methods Enzymol*. 2009; 463: 439-473.

Chapter 4: Enrichment and Identification of HLA-Associated Phosphopeptides in Hepatocellular Carcinoma for the Development of Novel Cancer Immunotherapeutics

4.1 Introduction

4.1.1 Incidence of Hepatocellular Carcinoma

Hepatocellular carcinoma (HCC) is the most common form of liver cancer and the third leading cause of cancer-related deaths worldwide.¹ This disease predominantly affects men, with an incidence rate two to four times higher than that observed in women. Hepatocellular carcinoma is typically diagnosed in older individuals, rarely occurring before the age of 40 with a peak occurrence at approximately 70 years of age. Out of the half a million people diagnosed worldwide each year, approximately 85% of cases occur in developing countries such as Southeast Asia and sub-Saharan Africa. However, over 20,000 cases of HCC are diagnosed every year in the United States alone. Furthermore, the incidence rate of hepatocellular carcinoma in the United States has tripled over the past two decades, yet the 5 year survival rate has remained below 12%.^{2,3}

The key factor in the poor survival rate associated with hepatocellular carcinoma is the stage in which it is commonly diagnosed. Hepatocellular carcinoma is grouped into four stages based on the Barcelona Clinical Liver Cancer (BCLC) staging system: early stage, intermediate stage, advanced stage, and end stage. The BCLC system is the standard means of assessing HCC and classifies the disease in terms of the number and size of tumors present and the extent to which they have mobilized throughout the body.⁴ Expectantly, the prognosis of HCC corresponds with the stage in which the cancer is

diagnosed, with average survival rates of 28%, 7%, and 2% for localized, regional, and distant cancers, respectively.⁵ While early diagnosis of HCC is ideal, these patients usually present with few, if any, specific symptoms. This results in greater than 60% of patients being diagnosed with HCC during later stages of disease in which metastasis has already occurred.^{6,7} The fast-growing nature combined with the poor survival rate of hepatocellular carcinoma demonstrates the clear need for more effective treatment options aimed at eradicating this devastating disease.

4.1.2 Disease Progression

Hepatocellular carcinoma is unique with respect to many common types of cancer given that the ultimate cause is fundamentally known – chronic liver disease.⁸ In fact, approximately 70-90% of patients with hepatocellular carcinoma present with this particular background.⁹ The progression of HCC begins with a healthy liver being subjected to chronic infection, leading to cirrhosis of liver tissue. Cirrhosis of the liver involves a decrease in proliferation of hepatocytes, suggesting the exhaustion of the regenerative ability of the liver. This in turn leads to an increase in the presence of fibrous tissue and the further destruction of hepatocytes, potentially resulting in the formation of cancerous nodules (Figure 4.1).^{9,10}

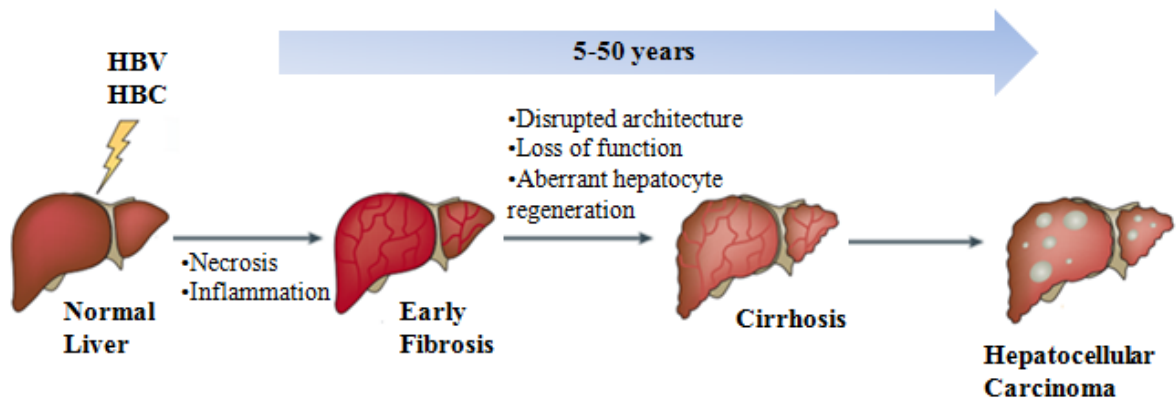


Figure 4.1 Progression of hepatocellular carcinoma. Chronic infection via hepatitis B or C leads to prolonged necrosis, inflammation, and regeneration of hepatocytes. This results in cirrhosis of the liver and ultimately the development of hepatocellular carcinoma. Figure adapted from Reference 10.

While there are several conditions associated with the development of chronic liver disease, the most common origin is viral infections of hepatitis B (HBV) and/or hepatitis C (HCV), both of which result in severe cirrhosis of liver tissue. Hepatitis B is estimated to affect approximately 2 billion individuals worldwide, causing 320,000 deaths annually. Of these HBV-related deaths, 30-50% can be attributed to the development of hepatocellular carcinoma. Similarly, hepatitis C affects 170 million individuals worldwide, with common development of liver cirrhosis (20%) and progression towards hepatocellular carcinoma (2.5%).¹¹ Overall, 50% and 25% of all cases of hepatocellular carcinoma are clearly linked to HBV or HCV, respectively.⁹

The exact relationship between hepatitis B infection and the development of hepatocellular carcinoma is complex, yet there are key aspects that suggest a direct involvement in the transformation process of HBV-infected cells to cancerous cells. When the hepatitis B virus integrates into the genome, certain host DNA sequences are deleted. These microdeletions can affect cancer-relevant genes such as telomerase reverse

transcriptase (TERT) and mitogen activated protein kinase 1 (MAPK1). Additionally, transcriptional activation activity of HBx, a protein of unknown function encoded by HBV, can alter the expression of genes associated with cell growth, such as Src tyrosine kinases. Finally, HBx is capable of binding to the tumor suppressor p53 *in vitro*, rendering it inactive and increasing cellular proliferation and survival despite DNA damage.¹⁰

Infection by HBV elicits a T cell-mediated immune response which leads to hepatocyte necrosis, inflammation, and regeneration, allowing for clearance of the infection. However, approximately 10% of individuals do not experience complete clearance and thus enter into a sustained cycle of necrosis, inflammation, and regeneration. This constant cycle leads to chronic liver disease, increased cirrhosis of liver tissue, and ultimately development of hepatocellular carcinoma.^{11,12} Similarly, interactions between host and viral factors upon infection with hepatitis C are thought to contribute significantly to the development of HCC. Specifically, the continuous cycle of immune-mediated hepatocyte death and subsequent regeneration often results in an accumulation of mutations. However, HCV infection illustrates an increased likelihood of development of chronic infection compared to HBV – 60-80% of HCV cases versus 10% of HBV cases. Additionally, 5-10% of HCV cases result in liver cirrhosis after 10 years of infection, approximately 10-20 times greater than the number of HBV cases which result in a similar fate.^{11,13}

4.1.3 Current Treatment Options

Current treatment options for hepatocellular carcinoma can be categorized into two groups – potentially curative and palliative treatments. Potentially curative treatments include tumor resection, liver transplantation, percutaneous ethanol injection (PEI), and radiofrequency ablation (RFA). While the most ideal forms of treatment for HCC are tumor resection and liver transplantation, these are often not feasible options for the vast majority of individuals with the disease. For instance, the ideal treatment of choice, tumor resection, is most commonly used only in cases where liver tissue is non-cirrhotic and the disease is diagnosed in an early stage; however, this is uncommon in typical diagnoses of HCC. Resection can be performed if cirrhosis is present in some cases, provided that the tumor is small in size. However, tumor resection from cirrhotic liver encompasses a 5-year recurrence rate of 70%, given that cirrhosis itself can ultimately lead to the development of hepatocellular carcinoma. These data combined with the fact that less than 5% of patients in the United States are candidates for tumor resection, make this a less than adequate method of treating hepatocellular carcinoma.^{3,14} Conversely, liver transplantation is the treatment option associated with the lowest risk of tumor recurrence, given that it addresses the issue of cirrhosis directly. Additionally, liver transplantation in cases of HCC results in an average 4-year survival rate of 85% and a recurrence-free survival rate of 92%. Although these statistics are overwhelmingly positive, the actual occurrence of liver transplantation is quite low due to the limitation of available organs. As a result, very strict criteria must be met in order to qualify for liver transplantation.³

When tumor resection or liver transplantation are not viable options, individuals with HCC can potentially undergo percutaneous ethanol injection (PEI) treatment. Direct injection of ethanol into the tumor can lead to the dehydration of tumor cells and the denaturing of cellular proteins. While PEI has the potential to effectively treat HCC, the vast number of requirements which must be met to undergo this treatment make it less than favorable for the majority of affected individuals. For example, PEI works best in cases where there are less than three tumors present, all of which are less than 3 cm in diameter, have well-defined margins, and are not located near the surface of the liver. Additionally, PEI is only applicable in cases where patients retain some liver function and can require multiple sessions before any signs of improvement appear.¹⁵

A final potentially curative approach for hepatocellular carcinoma is the use of radiofrequency ablation (RFA) therapy, specifically in cases of early stage diagnosis in which resection or transplantation are not applicable. This approach involves targeting a tumor with a rapidly alternating current and generating heat from the friction of rapid agitation of cells, ultimately triggering tumor cell destruction.¹⁶ This methodology has been shown superior in comparison to traditional treatment with PEI, resulting in 100% and 98% survival rates 1 or 2 years post-treatment, respectively. However, while RFA treatment shows positive short-term outcomes, the long-term benefits are less than ideal, resulting in a 5-year recurrence rate of over 70%.^{3,15-16}

For cases of hepatocellular carcinoma diagnosed in later stages of disease, palliative treatments are often used. The most common palliative treatment for intermediate-stage HCC is transarterial chemoembolization (TACE). TACE involves the injection of chemotherapeutic drug combinations directly into the hepatic artery, interrupting blood

supply to the tumor and inhibiting growth. Direct injection limits systemic exposure of unaffected tissue to the chemotherapeutic agents. Despite this, TACE is often linked to severe side effects including intense abdominal pain and chronic liver failure. Treatment of hepatocellular carcinoma via TACE typically results in 5-year survival rates ranging from 8-43%.¹⁷

Finally, in cases of advanced hepatocellular carcinoma, affected individuals are often prescribed the multikinase inhibitor sorafenib (Nexavar) for palliative treatment. Sorafenib targets signaling pathways involved in cancer which are related to tumor cell proliferation and tumor angiogenesis. This is accomplished by inhibiting cell surface tyrosine kinase receptors – vascular endothelial growth factor receptors (VEGF) and platelet-derived growth factor receptor-beta (PDGF- β) – and downstream intracellular serine/threonine protein kinases – Raf-1 and B-Raf (Figure 4.3). Sorafenib is often referred to as the “gold standard of treatment” for late-stage HCC given that it is the only drug that has shown any increase in survival rate. However, this increase translates to an extension in survival from 8 months to slightly less than 11 months. Additionally, inhibition of kinases involved in tumor cell signaling by sorafenib does not allow for specificity of treatment to tumor tissue as normal cell function also relies heavily on these pathways.^{18,19}

4.1.4 Potential for Immunotherapy

The overwhelming poor prognosis combined with the lack of largely applicable therapeutic options leaves much to be desired in the realm of treatment for hepatocellular carcinoma. Recent evidence suggests that hepatocellular carcinoma tumors are

immunogenic in that patients with tumor-infiltrating lymphocytes (TILs) were shown to have a reduced risk of tumor recurrence following liver transplantation. Additionally, the infusion of autologous T lymphocytes stimulated with anti-CD3 and IL-2 into patients with HCC demonstrated an increase in post-surgical recurrence-free survival. This data strongly suggests that the development of immunotherapeutics which harness an individual's own immune system to target and eliminate cancer cells could be tremendously beneficial for those affected with hepatocellular carcinoma.^{20,21}

Treatment of hepatocellular carcinoma via immunotherapy relies heavily on the identification of tumor-associated antigens (TAAs). However, only six TAAs for hepatocellular carcinoma have been identified to date: α -fetoprotein (AFP), glypican-3 (GPC3), NY-ESO-1, SSX-2, melanoma antigen gene-A (MAGE-A), and telomerase reverse transcriptase (TERT). Of these, α -fetoprotein is currently the most studied and potentially promising target for treatment of HCC using immunotherapy. AFP is expressed during fetal development and becomes transcriptionally repressed shortly after birth. However, AFP becomes re-expressed in approximately 80% of patients with HCC. Furthermore, studies have shown that CD8⁺ T cell responses can be elicited towards HLA-A2-restricted AFP epitopes in human lymphocyte cultures and HLA-A2 transgenic mice.²⁰

While these findings highlight the potential of immunotherapy-based treatments for hepatocellular carcinoma, they also bring to light the need for identification of additional relevant targets. It is a well-known fact that mutations and epigenetic changes accumulate within hepatocytes throughout the course of chronic liver disease. These alterations can ultimately lead to the dysregulation of signaling pathways which are largely reliant on

complex phosphorylation networks. Thus, we hypothesize that aberrantly phosphorylated peptides are increasingly presented by HLA class I molecules on the cell surface of hepatocytes tracking with the progression of chronic liver disease to full-blown hepatocellular carcinoma. Furthermore, we believe that these phosphopeptides represent a new class of tumor-associated antigens which holds great promise in the battle against hepatocellular carcinoma.

4.1.5 Project Aim

In this chapter, we aim to identify differentially-expressed, aberrantly phosphorylated peptides isolated from the cell surface of hepatocellular carcinoma tumor tissue using STAGE tip cleanup methodology, complementary IMAC enrichment techniques, and high resolution mass spectrometry. Expression of identified phosphopeptides will be evaluated in normal tissue for the identification of truly tumor-specific antigens. We will then test the immunological activity of relevant tumor-specific phosphopeptides to identify strong candidates for the future development of novel cancer immunotherapeutics.

4.2 Materials

4.2.1 Reagents

Amersham Pharmacia Biotech (Amersham, UK)

NHS-activated sepharose beads

Applied Biosystems (Carlsbad, CA)

POROS ® MC 20 metal chelating packing material, 20 µm diameter

Atlantic Peptides LLC (Lewisburg, PA)

Phosphopeptide standards, RVKsPLFQF, RTHsLLLLG, ≥95% purity

Fisher Scientific (Waltham, MA)

Dulbecco's Modified Eagle Medium (DMEM)

Fetal bovine serum (FBS)

Phosphate buffered saline (PBS)

Grace Davison Discovery Science (Deerfield, IL)

Acetyl chloride, anhydrous

D₀ methanol, anhydrous

Honeywell (Morristown, NJ)

Acetonitrile, HPLC grade, ≥99.8% purity

IDEX Health & Science LLC (Middleboro, MA)

PEEK natural tubing

J.T. Baker (Phillipsburg, NJ)

Glacial acetic acid, ≥99.9% purity

Pierce (Rockford, IL)

LC-MS grade water

PQ Corporation (Valley Forge, PA)

Kasil ® 1624 potassium silicate solution

Sigma Aldrich (Saint Louis, MO)

Angiotensin I acetate salt hydrate, $\geq 90\%$ purity

Angiotensin II phosphate (DRVYIHPHF)

Aprotinin

CHAPS buffer

Corning Costar low-binding microcentrifuge tubes

Dimethyl sulfoxide (DMSO)

Empore C18 SPE disks

Ethylenediaminetetraacetic acid (EDTA), analytical grade

Formamide

Iron (III) chloride

L-ascorbic acid

Leupeptin

Pepstatin A

Phenylmethylsulfonyl fluoride (PMSF)

Roswell Park Memorial Institute (RPMI) medium

Sodium azide

Sodium Chloride

Tris-HCl

Vasoactive intestinal peptide fragment 1-12, $\geq 90\%$ purity

VWR (Atlanta, GA)

Pipetting needles with 90° blunt ends, 16 gauge

YMC Company, LTD (Kyoto, Japan)

ODS-AQ, C18 5 μm spherical silica particles, 120 Å pore size

ODS-AQ, C18 5-20 μm spherical silica particles, 120 Å pore size

4.2.2 Equipment and Instrumentation

Agilent Technologies (Palo Alto, CA)

1100 Agilent high performance liquid chromatograph

Branson (Danbury, CT)

Branson 1200 Ultrasonic bath

Beckman Coulter (Pasadena, CA)

Optima LE-8K ultracentrifuge (Ti70 rotor)

Fisher Scientific (Waltham, MA)

Model 50 sonic dismembrator system, 117V, 50/60 Hz

Model 50 probe, 5/64 in

Labonco Corp. (Kansas City, MO)

Centrivap centrifugal vacuum concentrator

Millipore (Billerica, MA)

Amicon ultra, 10 kDa regenerated cellulose spin filter

PolyMicro Technologies, Inc. (Phoenix, AZ)

360 μm o.d. x 50 μm i.d. polyimide coated fused silica capillary

360 μm o.d. x 75 μm i.d. polyimide coated fused silica capillary

360 μm o.d. x 150 μm i.d. polyimide coated fused silica capillary

Qiagen (Valencia, CA)

Ni-NTA spin column

Sutter Instrument Co. (Novato, CA)

P-2000 microcapillary laser puller with fused silica adapter

Thermo-Fisher Scientific (San Jose, CA/Bremen, Germany)

LTQ mass spectrometer (back-end ETD)

LTQ FTICR hybrid mass spectrometer (custom modified with front-end ETD)

LTQ Orbitrap mass spectrometer (custom modified with front-end ETD)

LTQ Orbitrap Fusion Tribrid mass spectrometer (front-end ETD)

Zeus Industrial Products, Inc. (Orangeburg, SC)

Teflon tubing, 0.012 inch i.d. x 0.060 inch o.d.

4.3 Methods

4.3.1 Cell Line and Tissue Culture (Performed by NB, University of Birmingham)

The HepG2 cell line was grown up from a laboratory stock consisting of human liver carcinoma cells derived from the liver tissue of a 15 year-old male with a well-differentiated hepatocellular carcinoma. Cells were managed in sterile conditions in a laminar flow hood and incubated at 37°C in a humidified atmosphere with 5% CO₂. HepG2 cells were cultured in vented tissue culture flasks in Dulbecco's Modified Eagle Medium (DMEM) supplemented with 10% Fetal Bovine Serum (FBS) and 2 mM L-glutamine. Cells were grown until dense and split 1:2 every 2-3 days.

Matched tissue samples (normal/tumor) from patients with hepatocellular carcinoma (LL370N/T, LL981N/T, LL3907T, LL4857N/T, LL3081T, LL5437N/T, and LL5721N/T) were obtained one-hour post-removal at the Queen Elizabeth Hospital and Center for Liver Research at the University of Birmingham. Tissue samples ranged in size from 0.8 to 2.7 grams. Large tissue samples were cut into smaller pieces and stored at -80°C until further use. Entire samples were prepared for HLA-associated peptide isolation, assuming that 1 gram is equivalent to 1e9 cell equivalents (C. Eq.).

4.3.2 HLA-Associated Peptide Isolation (Performed by NB, University of Birmingham)

Frozen pieces of tumor tissue were resuspended in lysis buffer (20 mM Tris-HCl pH 8, 150 mM NaCl, 1% 3-[(3-cholamidopropyl) dimethylammonio]-1-propane sulfonate (CHAPS)) and homogenized using a tissue ruptor (Qiagen). Cells from the HepG2 cell line were resuspended in lysis buffer as well. Protease inhibitors (1 mM PMSF, 5 µg/mL aprotinin, 10 µg/mL pepstatin A, and 10 µg/mL leupeptin) were added to prevent degradation of HLA molecules. Phosphatase inhibitor cocktails II and III were added in 1:100 dilutions to prevent dephosphorylation of isolated peptides. Lysates were centrifuged at 100,000 x g for 1 hour at 4°C. Supernatants were incubated with an HLA class I-specific antibody (W6/32, 5 mg/1e9 cells) bound to NHS sepharose beads and rotated at 4°C for 16 hours. Beads were pelleted via centrifugation at 2000 rpm for 2 minutes and the supernatant was removed. Beads then underwent a series of four wash steps including: lysis buffer, 20 mM Tris-HCl and 150 mM NaCl, 20 mM Tris-HCl and 1 M NaCl, and finally 20 mM Tris-HCl before being transferred to a 5 kDa molecular weight cutoff (MWCO) filter. At this point peptides were either eluted from HLA class I molecules using 10% acetic acid (for C18 microcapillary column cleanup) or left untouched (for STAGE tip cleanup). The isolated peptide mixtures or the dried beads on MWCO filters were stored at -80°C and shipped to the University of Virginia for analysis.

4.3.3 Sample Desalting

4.3.3.1 C18 Microcapillary Column Cleanup

Peptides isolated from $1e8$ - $1e9$ C. Eq. in 0.1% acetic acid were combined with additional 0.1% acetic acid for a total sample volume of 50 μ L. For estimation of sample losses, 100 fmol of two internal phosphopeptide standards – angiotensin II phosphate (DRVyIHPF) and RVKsPLFQF – were spiked into the sample. The sample was pressure loaded onto a fused silica microcapillary cleanup column (360 μ m o.d. x 150 μ m i.d.) equipped with a 2 mm Kasil® 1624 frit and packed with 8 cm of irregular C18 reversed phase resin (5-20 μ m diameter, 120 Å pore size) at a flow rate of 0.5 μ L/min. The column was rinsed by loading 25 μ L of 0.1% acetic acid at a flow rate of 0.5 μ L/min. The flow through and column rinse volumes were collected in an Eppendorf tube and stored at -35°C . The cleanup column was connected to an HPLC and rinsed with solvent A (0.1M acetic acid in water) for 10 minutes at 12-15 bar. At the same backpressure, peptides were eluted from the cleanup column into an Eppendorf tube using a gradient of 0-80% solvent B (70% acetonitrile, 0.1M acetic acid) in 40 minutes followed by a 30 minute hold at 80% solvent B. Finally, 100 fmol of a third internal phosphopeptide standard, RTHsLLLLG, were spiked into the sample and the tube was dried to completion using a Centrivap. The dried, cleaned-up sample was stored at -35°C until further use.

4.3.3.2 Stop And Go Extraction (STAGE) Tip Cleanup

Samples were sent with dry beads still bound to HLA:peptide complexes on a MWCO filter for STAGE tip cleanup methodology. STAGE tips were fabricated using a

16-gauge pipetting needle with a 90° blunt end to punch out the required number of Empore C18 solid phase extraction (SPE) disks. A piece of natural PEEK tubing (1/32 inch o.d. x 25 µm i.d.) was used to push the Empore disk out of the blunt needle and into the bottom of a 200 µL pipette tip. Constructed STAGE tips were placed into STAGE tips adapters connected to 1.5 mL Eppendorf tubes for collection of equilibration, sample load, rinse, and elution flow through fractions. Fabricated STAGE tips were equilibrated using the following wash steps: two 2-minute washes of 100 µL of methanol at 1500 x g, one 1-minute wash of 50 µL of 80% acetonitrile/0.01% acetic acid at 1500 x g, and two 2-minute washes of 100 µL of 1% acetic acid at 1500 x g. Dried beads were transferred from the filter to a separate low-protein binding tube using subsequent water rinses to ensure complete transfer. Beads were centrifuged at 300 x g for 1 minute and the supernatant was loaded onto the STAGE tip in 150 µL aliquots for 2 minutes at 2000 x g. Two washes of the beads using 100 µL of 3% acetonitrile/5% acetic acid followed by 50 µL of 1% acetic acid were performed and loaded onto STAGE tips for 2 minutes each at 2000 x g to ensure loading of any peptides which had become dissociated from HLA molecules.

For the elution of peptides from HLA molecules bound to beads, 150 µL of 10% acetic acid was added to the tube which was then shaken for 5 minutes at room temperature. The beads were centrifuged at 300 x g for 1 minute and the supernatant transferred to a low-binding tube. This process was repeated to ensure complete elution of peptides from HLA molecules and the supernatant added to the low-binding tube. Two phosphopeptide standards, DRVyIHPF and RVKsPLFQF were spiked into the 10% acetic acid elution supernatant at 200 fmol each. The combined supernatants were

sonicated using a Model 50 sonic dismembrator system at 50 Hz for 5-10 seconds. The sonicated elution supernatant was loaded onto the corresponding number of STAGE tips (~4e8 C. Eq./tip) in 150 μ L aliquots at 2000 x g until the entire volume had passed through. STAGE tips were washed using four rounds of 100 μ L of 1% acetic acid. Peptides were eluted from the C18 resin in the STAGE tips using the following stepwise gradient of increasing acetonitrile concentrations: 20 μ L of 20% acetonitrile/0.1% acetic acid, 20 μ L of 40% acetonitrile/0.1% acetic acid, and 20 μ L of 60% acetonitrile/0.1% acetic acid. A subsequent elution of 20 μ L of 80% acetonitrile/0.1% acetic acid was performed and collected in a separate tube. Finally, 200 fmol of a third internal phosphopeptide standard, RTHsLLLLG, were spiked into C18 elution fraction. Equilibration, sample load, wash, and C18 elution flow through fractions were dried to completion using a Centrivap and stored at -80°C until further use.

4.3.4 Peptide Content Determination by HPLC-ESI-MS/MS

Isolated peptide mixtures from cleanup via C18 microcapillary columns were reconstituted in 0.1% acetic acid for a final concentration of 1e7 C. Eq./ μ L. For sample screens, 1 μ L (1e7 C. Eq.) of peptide sample was added to 4 μ L of 0.1% acetic acid. For samples cleaned up via STAGE tips, approximately 1% (~2 μ L) of the C18 elution fractions were removed prior to drying down and added to 4 μ L of 0.1% acetic acid for screening purposes. Sample screen aliquots were loaded onto a fused silica microcapillary precolumn (PC) (360 μ m o.d. x 75 μ m i.d.) equipped with a 2 mm Kasil® 1624 frit and packed with 8-10 cm of irregular C18 reversed phase resin at a flow rate of <1 μ L/min. The PC was rinsed on an HPLC with solvent A for 20 minutes at 30 bar. The

PC was then dried using a pressure bomb and connected to a fused silica microcapillary analytical column (AC) (360 μm o.d. x 50 μm i.d.) packed with 6-8 cm of regular C18 reversed phase resin (5 μm diameter, 120 \AA pore size) and equipped with a laser-pulled, electrospray emitter tip (2 μm diameter) via a Teflon sleeve. The ACPC was rehydrated by rinsing on an HPLC with solvent A for 10 minutes at 30 bar. Next, 100 fmol of two internal peptide standards (angiotensin and vasoactive intestinal peptide) were loaded onto the ACPC for a quantitation purposes prior to mass spectrometric analysis.

Peptides were eluted using an HPLC gradient of 0-60% solvent B in 40 minutes at a flow rate of 60 nL/min and electrospray ionized directly into an LTQ Orbitrap Classic or FT-ICR mass spectrometer. Full-scan high resolution mass spectra (MS1) were acquired in the Orbitrap or FT-ICR mass analyzers and MS/MS spectra (MS2) were acquired using CAD and ETD fragmentation methods in the linear ion trap (LTQ) of the instrument. A data-dependent top-6 CAD/ETD toggle method was used in which one high resolution MS1 scan (resolving power of 60,000 at 400 m/z) was acquired followed by selection of the top 6 most abundant parent ions for fragmentation by CAD and ETD. Data-dependent parameters included a repeat count of 3, repeat duration of 10 seconds, and exclusion list duration of 10. Additionally, ions with a charge state of +1 were excluded. ETD parameters included a 45 ms reaction time, FTMS automatic gain control (AGC) target of $2e5$ charges, ITMS AGC target of $1e4$ charges, and an ETD reagent target of $2e5$ charges.

Data analysis was performed using Xcalibur software (Thermo Electron Corporation). Raw data files were searched using OMSSA (version 2.1.1) against the Swissprot human protein database with the following parameters: no enzyme specificity, E-value cutoff of

1, variable modifications of oxidation of methionine and phosphorylation of serine, threonine, and tyrosine, ± 0.01 Da precursor mass tolerance, and ± 0.35 Da product ion mass tolerance. Database hits were used to guide the analysis and peptide sequences were determined by accurate mass measurement and manual interpretation of MS2 spectra.

Relative abundances of peptides were calculated by comparing peptide peak areas to those of two internal peptide standards (angiotensin and vasoactive intestinal peptide) which were present at a fixed concentration of 100 fmol each. The total peptide content of the sample was summed and compared to that of a well-characterized sample which was previously analyzed by IMAC. This comparison allowed for the determination of the amount of material needed to perform enrichment on the current sample.

4.3.5 Fischer Esterification of Samples

Samples were subjected to a Fischer esterification to block C-termini and acidic side chains of amino acid residues. Desalted peptide samples were dried in triplicate using 50 μL of anhydrous methanol. Esterification reagents were prepared by adding 160 μL of anhydrous acetyl chloride drop-wise to 1 mL of anhydrous methanol, forming methanolic HCl. Next, 80 μL of the cooled reaction mixture was added to the dried peptide samples and allowed to react at room temperature for 1 hour. The samples were dried to completion, rinsed with 50 μL of anhydrous methanol, and dried again. This process was repeated using fresh reagents to ensure completeness of the reaction. Esterified samples were stored at -35°C until further use.

4.3.6 Phosphopeptide Enrichment via IMAC

4.3.6.1 Fe-IDA IMAC Enrichment

A fused silica microcapillary column (360 μm o.d. x 75 μm i.d.) equipped with a 2 mm Kasil $\text{\textcircled{R}}$ 1624 frit was packed with 5 cm of POROS $\text{\textcircled{R}}$ MC 20 iminodiacetate resin. The IMAC column was pressure rinsed at a flow rate of 20 $\mu\text{L}/\text{min}$ with the following steps: a 20 minute water rinse, a 10 minute 50 mM EDTA rinse, and a 10 minute water rinse. The column was activated using filtered 100 mM FeCl_3 for 5 minutes at a flow rate of 20 $\mu\text{L}/\text{min}$ followed by a 3 minute incubation period in which the iron was allowed to sit on the column to ensure diffusion into resin particles. This process was repeated three times to ensure complete activation. The activated column was equilibrated with 25 μL of 0.01% acetic acid at a flow rate of 0.5 $\mu\text{L}/\text{min}$. The dried, esterified peptide sample was reconstituted in 50 μL of 1:1:1 (methanol:acetonitrile:0.01% acetic acid (vol/vol)) and pressure loaded onto the activated IMAC column at a flow rate of 0.5 $\mu\text{L}/\text{min}$. Following sample loading, 25 μL of 1:1:1 was added to the sample tube and loaded onto the IMAC column at a flow rate of 0.5 $\mu\text{L}/\text{min}$. A final rinse with 15 μL of 0.01% acetic acid at a flow rate of 0.5 $\mu\text{L}/\text{min}$ was completed. The sample flow through, 1:1:1 rinse, and 0.01% acetic acid rinse were collected in an Eppendorf tube and stored at -35°C .

At this point, a PC was rinsed on a HPLC with solvent A at 30 bar for 10 minutes. The PC was butt-connected to the end of the IMAC column with a Teflon sleeve and the IMAC-PC column was rinsed with 0.01% acetic acid for 10 minutes at a flow rate of 0.5 $\mu\text{L}/\text{min}$ to ensure that no leaks were present. Phosphopeptides were eluted directly onto the PC by pressure loading freshly-prepared 250 mM L-ascorbic acid in water (pH 2) at a

flow rate of 0.5-1 $\mu\text{L}/\text{min}$ for 25 minutes. A final rinse of 0.01% acetic acid at the same flow rate was completed prior to disconnection of the PC from the IMAC column. The PC was rinsed on an HPLC with solvent A at for 25 minutes at 30 bar. The PC was dried and connected to a C18 AC using a Teflon sleeve. The ACPC was rehydrated by rinsing on an HPLC with solvent A at a flow rate of 60 nL/min for 10 minutes. Next, 100 fmol of two internal peptide standards (angiotensin and vasoactive intestinal peptide) were loaded onto the ACPC for a quantitation purposes prior to mass spectrometric analysis.

4.3.6.2 Fe-NTA IMAC Enrichment

For the preparation of Fe-NTA resin using a 10 kDa molecular weight cutoff filter, all forward spins were performed at 14,000 $\times g$ for 5 minutes at room temperature and all reverse spins at 1,000 $\times g$ for 1 minute at room temperature. A 10 kDa spin filter was rinsed twice with 500 μL of 0.01% acetic using one forward and one reverse spin during each round. Ni-NTA resin was removed from a Qiagen Ni-NTA spin column, reconstituted in water (1 mg/mL), and added to the spin filter in three aliquots, each followed by a forward spin. When adding solutions to the spin filter, the mixture was aspirated to remove any resin that had accumulated on the rim of the filter. The resin was rinsed using the following steps: two rinses with 450 μL of water using two forward spins, two rinses with 450 μL of 50 mM EDTA using two forward spins, and two rinses with 450 μL of water using two forward spins. The resin was activated by three rounds of 450 μL of filtered 100 mM FeCl_3 using three forward spins. The activated resin was washed using the following steps: one rinse with 450 μL of 0.01% acetic acid using one forward spin, two rinses of 450 μL of 15% acetonitrile in 0.01% acetic acid using two

forward spins, and one rinse with 450 μL of 0.01% acetic acid using one forward spin.

The prepared Fe-NTA resin was stored in 0.01% acetic acid at 4°C for up to 1 month.

A fused silica microcapillary column (360 μm o.d. x 150 μm i.d.) equipped with a 2 mm Kasil ® 1624 frit was packed with 2.5 cm of previously prepared Fe-NTA resin. The column was re-activated by pressure loading filtered 100 mM FeCl_3 for 10 minutes at a flow rate of 20 $\mu\text{L}/\text{min}$ followed by a 3 minute incubation period in which the iron was allowed to sit on the column to ensure diffusion into resin particles. This process was repeated two times to ensure complete activation. The activated column was equilibrated with 25 μL of 0.01% acetic acid at a flow rate of 0.5 $\mu\text{L}/\text{min}$. The dried, esterified peptide sample was reconstituted in 50 μL of 1:1:1 (methanol:acetonitrile:0.01% acetic acid (vol/vol)) and pressure loaded onto the activated IMAC column at a flow rate of 0.5 $\mu\text{L}/\text{min}$. Following sample loading, 25 μL of 1:1:1 was added to the sample tube and loaded onto the IMAC column at a flow rate of 0.5 $\mu\text{L}/\text{min}$. A final rinse with 15 μL of 0.1% acetic acid at a flow rate of 0.5 $\mu\text{L}/\text{min}$ was completed. The sample flow through, 1:1:1 rinse, and 0.1% acetic acid rinse were collected in an Eppendorf tube and stored at -35°C.

At this point, a PC was rinsed on a HPLC with solvent A at 30 bar for 10 minutes. The PC was butt-connected to the end of the IMAC column with a Teflon sleeve and the IMAC-PC column was rinsed with 0.01% acetic acid for 10 minutes at a flow rate of 0.5 $\mu\text{L}/\text{min}$ to ensure that no leaks were present. Phosphopeptides were eluted directly onto the PC by pressure loading freshly-prepared 250 mM L-ascorbic acid in water (pH 2) at a flow rate of 0.5-1 $\mu\text{L}/\text{min}$ for 25 minutes. A final rinse of 0.01% acetic acid at the same flow rate was completed prior to disconnection of the PC from the IMAC column. The

PC was rinsed on an HPLC with solvent A at for 25 minutes at 30 bar. The PC was dried and connected to a C18 AC using a Teflon sleeve. The ACPC was rehydrated by rinsing on an HPLC with solvent A at a flow rate of 60 nL/min for 10 minutes. Next, 100 fmol of two internal peptide standards (angiotensin and vasoactive intestinal peptide) were loaded onto the ACPC for a quantitation purposes prior to mass spectrometric analysis.

4.3.7 Analysis of Phosphopeptides by HPLC-ESI-MS/MS

Peptides were eluted using an HPLC gradient of 0-60% solvent B in 60 minutes at a flow rate of 60 nL/min and electrospray ionized directly into an Orbitrap Fusion Tribrid mass spectrometer. Full-scan high resolution mass spectra (MS1) were acquired in the Orbitrap mass analyzer and MS/MS spectra (MS2) were acquired using CAD and ETD fragmentation methods in the linear ion trap of the instrument. A top-speed, neutral-loss triggered method was used in which one high resolution MS1 scan (resolving power of 60,000 at 400 m/z) was first acquired, followed by selection of as many parent ions as possible in a 2 second timeframe (in order of decreasing abundance) for fragmentation by CAD. If a neutral loss characteristic of the loss of phosphoric acid ($\Delta 98$ Da) was present in the CAD spectrum, an ETD scan of that precursor was then acquired. Data-dependent parameters included a repeat count of 3, repeat duration of 10 seconds, and exclusion list duration of 10. Additionally, ions with a charge state of +1 were excluded. ETD parameters included a 45 ms reaction time, FTMS automatic gain control (AGC) target of $2e5$ charges, ITMS AGC target of $1e4$ charges, and an ETD reagent target of $1e4$ charges.

Data analysis was performed using Xcalibur software (Thermo Electron Corporation). Raw data files were searched using OMSSA (version 2.1.1) and/or Byonic (version 2.6)

against the Swissprot human protein database with the following parameters: no enzyme specificity, E-value cutoff of 1, fixed modifications of methyl esters of aspartic acid, glutamic acid, and C-termini, variable modifications of oxidation of methionine and phosphorylation of serine, threonine, and tyrosine, ± 0.01 Da precursor mass tolerance, and ± 0.35 Da product ion mass tolerance. Additionally, CAD data files were searched using an in-house program, “Neutral Loss Finder,” discussed in chapter 1 (section 1.2.5) to identify MS2 spectra exhibiting the neutral loss of phosphoric acid. CAD and ETD spectra were also back-checked against an in-house phosphopeptide database containing all identified phosphopeptides from previous samples analyzed in our laboratory. Peptide hits from these four sources were used to guide the analysis and peptide sequences were determined by accurate mass measurement and manual interpretation of MS2 spectra.

Sample recovery for IMAC enrichments was calculated by comparing the peak areas of the three internal phosphopeptide standards, DRVyIHPF, RVKsPLFQF, and RTHsLLLLG, present at fixed concentrations of 100 fmol each in the IMAC run to those of a standards-only run performed on the same day. Calculating the recoveries of the internal phosphopeptide standards spiked in at varying time points throughout the procedure allows for an assessment of peptide losses from the desalting and esterification steps as well as the actual enrichment. Relative abundances of phosphopeptides identified from the IMAC enrichments were calculated by comparing peptide peak areas to the average peak areas of two internal peptide standards (angiotensin and vasoactive intestinal peptide) present at fixed concentrations of 100 fmol each.

4.3.8 Peptide Synthesis and Validation

Relevant phosphorylated peptides identified in IMAC analyses were synthesized using Fmoc chemistry and purified via HPLC to >95% purity. Stock solutions were prepared in 0.1% acetic acid and 100 fmol of each phosphopeptide run on the mass spectrometer for sequence confirmation. Aliquots of each of the correctly synthesized phosphopeptides were shipped to the University of Birmingham for use in biological assays.

4.3.9 Isolation of Peripheral Blood Mononucleated Cells (PBMCs)

(Performed by NB, University of Birmingham)

For isolation of PBMCs for use in biological assays, 50 mL of blood were obtained from healthy donors, patients with chronic liver disease, and patients with hepatocellular carcinoma using 50 mL syringes with lithium heparin solution (20 IU/mL) added. Centrifugation for 10 minutes at 1200 x g was performed to allow for extraction of plasma from the top layer. Plasma was stored with additional EDTA at a concentration of 2 mg/mL at -20°C until further use. Blood samples were mixed with an equal volume of 10% FBS and layered onto a ficoll paque. Samples were centrifuged for 20 minutes at 500 x g and PBMCs were collected from the interface. Extracted PBMCs were washed twice in RPMI 10% FBS, counted, and resuspended in RPMI 10% FBS for use in biological assays or FBS 10% DMSO at 1e7 cells/mL for storage at -80°C.

4.3.10 Intracellular Cytokine Staining (ICS) Assays (Performed by NB, University of Birmingham)

ICS assays were used to measure the production of cytokines in response to stimulation by phosphopeptides antigens. Expanded tumor-infiltrating lymphocytes (TILs) were plated at 200,000 TILs/well of a 96-well plate in T cell medium (5 $\mu\text{g}/\text{mL}$ Brefeldin A, 5 $\mu\text{g}/\text{mL}$ monensin) and 0.5 μg anti-human CD107a-FITC antibody 75. TILs were then stimulated with 10 $\mu\text{g}/\text{mL}$ of the individual phosphopeptides of interest and expanded for 7 days. Unstimulated TILs served as a negative control while TILs stimulated with 5 $\mu\text{g}/\text{mL}$ of phytohaemagglutinin (PHA) and 400 $\mu\text{g}/\text{mL}$ Ionomycin served as a positive control. On day 6 of expansion, TILs were washed twice in RPMI 10% FBS and resuspended in T cell medium. Wells were then restimulated with 10 $\mu\text{g}/\text{mL}$ of individual phosphopeptide antigens overnight. The following day, TILs were harvested, washed with PBS, and stained with a fixable viability dye (APC-Cy7) and surface antibodies – anti-CD3 (APC) and anti-CD8 (PerCP). The cells were then washed in magnetic cell-sorting (MACS) buffer, fixed using 2% paraformaldehyde, permeabilized using 0.5% saponin, and stained with anti-IFN- γ (PE), anti-IL-2 (Pacific blue), and anti-TNF α (PE-Cy5.5) for 30 minutes at room temperature. Cells were then washed again with MACS buffer lightly fixed prior to analysis via flow cytometry.

4.4 Results

4.4.1 Identification of HLA-Associated Phosphopeptides

Samples of primary hepatocellular carcinoma tumor tissue and adjacent surrounding normal tissue were obtained from patients at the Queen Elizabeth Hospital and Center for Liver Research at the University of Birmingham. Additionally, cells were grown from a laboratory stock of a well-characterized hepatoblastoma cell line, HepG2. HLA class I-associated peptides were isolated and sent to our laboratory for analysis. The sample names, tissue origins, HLA types, and amount of material sent are shown in Table 4.1.

Table 4.1 Summary of analyzed liver samples. Samples from primary tumor tissue and surrounding adjacent tissue were obtained for analysis. The HLA-types and amount of material sent are listed for each sample. Several samples did not contain enough material for complete typing, thus some HLA-A or C loci are unknown.

Sample Name	Tissue Type	HLA-A Locus	HLA-B Locus	HLA-C Locus	Amount Sent (grams)
LL370N	Normal Tissue	A*02	B*08	C*07	0.84
LL370T	Primary HCC		B*18		2.20
LL981N	Normal Tissue	A*01	B*27	C*02	1.40
LL981T	Primary HCC	A*02	B*37	C*06	1.30
LL3907T	Primary HCC	A*02 A*26	B*08 B*49	C*07	0.91
LL4857N	Normal Tissue	A*02	B*07	C*05	2.20
LL4857T	Primary HCC	A*03	B*44	C*07	2.45
LL3081T	Primary HCC	A*03	B*07 B*35	-----	0.80
LL5437N	Normal Tissue	A*02	B*15	C*03	2.70
LL5437T	Primary HCC	A*03	B*40	C*04	1.00
LL5721N	Normal Tissue	-----	B*08	-----	1.50
LL5721T	Primary HCC				1.40
HepG2	Liver Hepatoblastoma	A*02 A*24	B*35 B*51	C*04 C*16	1.00

An aliquot of each sample was desalted, esterified, and subjected to IMAC for phosphopeptide enrichment. In total, 459 phosphopeptides were identified from the liver tissue samples and the HepG2 cell line. The following table (Table 4.2) summarizes the identified phosphopeptides. The source proteins for each identified phosphopeptide were determined using OMSSA, Byonic, MASCOT (matrixsciences.com), and/or BLAST (blast.ncbi.nlm.nih.gov) and are listed using their corresponding Uniprot gene names (uniprot.org). In cases where the source protein from which the phosphopeptide originates is unknown, a Uniprot gene name is listed as non-applicable (NA). The ability of phosphopeptides to bind to specific HLA-alleles was predicted using the “MHC-I binding prediction” algorithm from the immune epitope database (tools.ideb.org/mhci) in combination with the HLA type of each sample when known. Several phosphopeptides did not produce an adequate binding score to a specific allele, thus the HLA-type is left blank. For each phosphopeptide, the liver samples in which it was observed are listed using the sample names outlined in Table 4.1. Additionally, the presence of each identified phosphopeptide in previously analyzed leukemia, colorectal, melanoma, ovarian, breast, and esophageal cancer samples are indicated by gray boxes when applicable.

Table 4.2 Summary of identified HLA-associated phosphopeptides. A total of 459 phosphopeptides were identified from hepatocellular carcinoma tumor tissue, adjacent normal tissue, and a liver hepatoblastoma cell line. The sequence, source protein, and HLA-type of each phosphopeptide are listed. A lowercase “s,” “t,” or “y” in the peptide sequence indicates a phosphorylated serine, threonine, or tyrosine residue. A lowercase “m” indicates an oxidized methionine residue while a lowercase “c” indicates the presence of cysteinylolation. Liver samples in which each phosphopeptide was identified are listed using the names provided in Table 4.1. Additionally, the presence of phosphopeptides in previously analyzed samples including leukemia, colorectal cancer, melanoma, ovarian cancer, breast cancer, and esophageal cancer is indicated by gray boxes. White boxes indicate instances in which the phosphopeptide is unique to liver samples.

#	Sequence	Source Protein	HLA-Type	Liver Samples	Leukemia	Colorectal	Melanoma	Ovarian	Breast	Esophageal
1	AEQGsPRVSY	SPTBN1	A*01	LL4857T						
2	GsPHYFSPFRPY	SRSF9	A*01	LL5721T						
3	ISSsMHSLY	TOB1	A*01	LL5437N						
4	ITQGtPLKY	NCOR2	A*01	LL981T						
5	LLDPSRSYsY	GAREM1	A*01	LL981T						
6	SLDsPSYVLY	FNTA	A*01	LL981T, LL5721N/T						
7	SLYDRPAsY	PDGFRA	A*01	LL4857T						
8	SYPsPVATSY	EGR1	A*01	LL4857T						
9	TMAAsPGKDNy	KPNA6	A*01	LL981T						
10	YFsPFRPY	SRSF9	A*01	LL5721N/T						
11	YPLsPTKISQY	HIPK1	A*01	HepG2						
12	YQRPFsPSAY	SORBS2	A*01	LL5437N						
13	AIMRsPQMV	CTNNB1	A*02	LL4857T						
14	ALDsGASLLHL	RIPK4	A*02	LL981T, LL370T, HepG2						
15	ALGNtPPFL	YTHDF3	A*02	LL4857T						
16	ALMGsPQLV	JUP	A*02	LL4857T						
17	ALMGsPQLVAA	JUP	A*02	LL4857T						

#	Sequence	Source Protein	HLA-Type	Liver Samples	Leukemia	Colorectal	Melanoma	Ovarian	Breast	Esophageal
18	AVVsPPALHNA	BRD4	A*02	LL981T, HepG2						
19	DLKRRsmSI	DOCK7	A*02	LL3907T, LL370T						
20	DLKRRsMSI	DOCK7	A*02	LL3907T, LL370T						
21	ELFSsPPAV	NFAT5	A*02	HepG2						
22	FLDtPIAKV	NKD1	A*02	LL981T, HepG2						
23	GIDsPSSSV	FGD3	A*02	LL4857T						
24	GLDsGFHSV	LRCH4	A*02	LL4857T						
25	GLIsPVWGA	CEP68	A*02	LL370T, LL4857T						
26	GLLDsPTSI	ZFP36L1	A*02	LL4857T						
27	IMDRtPEKL	BCAR3	A*02	LL4857T						
28	IQFsPPFPGA	SBNO2	A*02	LL4857T						
29	KAFsPVR	ID2	A*02	LL981T, HepG2						
30	KAFsPVRSV	ID2	A*02	LL981N/T, HepG2						
31	KIAsEIAQL	CASKIN2	A*02	LL981T, LL370T, LL5437N/T, LL4857T						
32	KIGsIIFQV	PARP14	A*02	LL4857T						
33	KLAsPELERL	JUN	A*02	LL370T, HepG2						
34	KLDsPRVTV	FAM86A	A*02	HepG2						
35	KLFPDtPLAL	ILF3	A*02	LL370T, HepG2						
36	KLIDIVsSQKV	CHEK1	A*02	HepG2						
37	KLIDRTEsL	LSP1	A*02	LL4857T						
38	CLKDRLPsI	LBH	A*02	LL4857T						
39	KLMsDVEDV	BRWD1	A*02	LL4857T, HepG2						
40	KLMsPKADVKL	KIAA1328	A*02	HepG2						
41	KLsGDQPAAR	TCOF1	A*02	HepG2						

#	Sequence	Source Protein	HLA-Type	Liver Samples	Leukemia	Colorectal	Melanoma	Ovarian	Breast	Esophageal
42	KQDsLVINL	SUPT16H	A*02	LL370T						
43	KTMsGTFL	STAT2	A*02	LL5437N/T, LL4857T						
44	KVAsLLHQV	TNIP2	A*02	HepG2						
45	LMFsPVTSL	SETD5	A*02	LL4857T						
46	PmVTLsLNL	LY6G5B	A*02	LL3907T						
47	RASsLSITV	FAM65A	A*02	LL370T						
48	RLAsASRAL	NA	A*02	LL370T						
49	RLAsLQSEV	NA	A*02	LL4857T, HepG2						
50	RLAsYLDKV	KRT19	A*02	HepG2						
51	RLAsYLDRV	KRT18	A*02	LL4857T						
52	RLDsYVR	TRAPPC1	A*02	LL4857T						
53	RLDsYVRSL	TRAPPC1	A*02	LL370T, LL4857T						
54	RLFsKEL	TAF13	A*02	LL370T						
55	RLFsKELR	TAF13	A*02	LL4857T						
56	RLFsKELRC	TAF13	A*02	LL370T						
57	RLlsDLEEL	CCDC28A	A*02	LL5437N						
58	RLlsTDAEAV	TAF7	A*02	LL4857T, HepG2						
59	RLSDtPPLL	RAB3B	A*02	LL4857T						
60	RLSsPLHFV	FAM134A	A*02	LL981T, LL4857T, HepG2						
61	RMYSFDDVL	LMO7	A*02	LL5437T, LL4857T						
62	RQAsIELPSM	LSP1	A*02	LL370T, LL5437N, LL4857T						
63	RQAsIELPSMAV	LSP1	A*02	LL370T						
64	RQAsLSISV	PRKD2	A*02	LL4857T						
65	RQDsTPGKVFL	NR2C1	A*02	LL370T, HepG2						

#	Sequence	Source Protein	HLA-Type	Liver Samples	Leukemia	Colorectal	Melanoma	Ovarian	Breast	Esophageal
66	RQIsQDVKL	AMPD2	A*02	LL4857T, HepG2						
67	RQLsALHRA	RPL15	A*02	HepG2						
68	RQLsSGVSEI	HSPB1	A*02	LL370T, LL4857T						
69	RSLsESYEL	IQSEC1	A*02	LL4857T						
70	RSLsQELVGV	ZNF318	A*02	LL4857T, HepG2						
71	RTFsPTYGL	SYNM	A*02	LL981T, LL370T, LL5437N/T, LL4857T, HepG2						
72	RTLsHISEA	FAM65A	A*02	LL4857T						
73	RTYsGPMNKV	POF1B	A*02	LL4857T						
74	RVAsPTSGV	IRS2	A*02	LL3081T, LL4857N/T, LL4922N/T						
75	SIMsPEIQL	CIC	A*02	LL4857T						
76	SImSPEIQL	CIC	A*02	LL4857T						
77	SISsMEVNV	DBNDD2	A*02	LL4857T						
78	SISStPPAV	GORASP2	A*02	LL4857T						
79	SLFGGsVKL	PDCD6IP	A*02	LL4857T, HepG2						
80	SLFsGDEENA	PDCD4	A*02	LL4857T, HepG2						
81	SLFsPQNTL	RPRD2	A*02	LL4857T						
82	SLFsSEESNL	VTN	A*02	LL370T						
83	SLFsSEESNLGA	TAF13	A*02	LL370T						
84	SLHDIQLsL	CCSER2	A*02	LL4857T						
85	SLQPRSHsV	PLEKHA6	A*02	LL4857T						
86	SLQsLETSV	ATP2B4	A*02	LL4857T						
87	SMSsLSREV	SEC16A	A*02	LL4857T						
88	SMTRsPPRV	SRSF8	A*02	HepG2						
89	SVKPRRTsL	HIVEP1	A*02	LL3907T						

#	Sequence	Source Protein	HLA-Type	Liver Samples	Leukemia	Colorectal	Melanoma	Ovarian	Breast	Esophageal
90	TVFsPTLPAA	ZC3HAV1	A*02	LL4857T						
91	VLFPEsPARA	KMT2D	A*02	HepG2						
92	VLFSsPPQM	MCM4	A*02	LL4857T						
93	VLIENVAsL	GPX2	A*02	LL4857T						
94	VLLsPVPEL	ANAPC1	A*02	LL4857T, HepG2						
95	VLSDVIPsI	FAM199X	A*02	LL4857T						
96	VLVVDTPsI	GIMAP5	A*02	LL370T						
97	VLYsPQMAL	MGEA5	A*02	LL4857T						
98	VMIGsPKKV	TNS3	A*02	LL3907T						
99	yLQSRYYRA	HIPK3	A*02	LL981T, LL4857T						
100	ATYtPQAPK	PLEKHO1	A*03	LL4857T						
101	FLIIRtVLQL	OR51E2	A*03	LL370T						
102	FRYsGKTEY	EPB41L5	A*03	LL981T						
103	GIMsPLAKK	ARID5A	A*03	LL3081T, LL4922N/T						
104	HTAsPTGMMK	SEC24D	A*03	LL3081T, LL4857T						
105	HVYtPSTTK	ANKRA2	A*03	LL4857T						
106	IISsPLTGK	USP36	A*03	LL4857T						
107	ILKPRRsL	UBD	A*03	LL3907T						
108	IYQyIQSRF	DYRK1B	A*03	LL5721T, LL4922N/T						
109	KLPDsPALA	STIM1	A*03	LL4857T						
110	KLPDsPALAK	STIM1	A*03	LL4922N/T, LL4857T						
111	KLPDsPALAKK	STIM1	A*03	LL3081T						
112	KLPsPAPARK	MICALL2	A*03	LL3081T, LL4857N, LL4922N/T						
113	KLRsPFLQK	DBNL	A*03	LL4922N/T, LL4857T						

#	Sequence	Source Protein	HLA-Type	Liver Samples	Leukemia	Colorectal	Melanoma	Ovarian	Breast	Esophageal
114	KMPTtPVKAK	TBC1D22A	A*03	LL3081T, LL4922N/T						
115	KRAsvFVKL	ST13	A*03	LL981T, LL370T, LL3081T, LL4922N/T, LL4857T						
116	KTPTsPLKMK	SMARCA5	A*03	LL4922N/T						
117	KVQsLRRAL	PRKCDBP	A*03	LL4857T						
118	MTRsPPRVSK	SRSF8	A*03	LL3081T						
119	RAKsPISLK	CARD11	A*03	LL3081T, LL4922N/T, LL4857T						
120	RIGsPLSPK	LARP1B	A*03	LL4857T						
121	RILsGVVTK	RPS11	A*03	LL3081T, LL4922N/T, LL4857T						
122	RIYQyIQ	DYRK1B	A*03	LL4857T						
123	RIYQyIQSR	DYRK1B	A*03	LL3081T, LL4857N/T, LL4922N/T						
124	RIYQyIQSRF	DYRK1B	A*03	LL5437N/T, LL4922N, LL4857T						
125	RLFVGSIPK	HNRNPR	A*03	LL4857T						
126	RLLDRSPsRSAK	CDKL5	A*03	LL4922N/T						
127	RLSsPISKR	BARD1	A*03	LL4857T						
128	RLSsPVLHR	DBN1	A*03	LL4857T						
129	RMFsPMEEK	AFF4	A*03	LL4857T						
130	RSLsVEIVY	TOPORS	A*03	LL5721N/T						
131	RSYsRSFSR	RBBP6	A*03	LL4857T						
132	RSYsYPRQK	GAREM1	A*03	LL3081T, LL4922N/T, LL4857T						
133	RTAsFAVRK	SAMM50	A*03	LL4922N/T						
134	RTAsPPPPPK	SRRM1	A*03	LL3081T, LL4922N/T, LL4857T						
135	RTNsPGFQK	RBM26	A*03	LL4857T						
136	RTRsLSSLREK	FRYL	A*03	LL3081T, LL4922N/T						
137	RTSsPLFNK	KIAA1671	A*03	LL3081T, LL4857N/T, LL4922N/T						

#	Sequence	Source Protein	HLA-Type	Liver Samples	Leukemia	Colorectal	Melanoma	Ovarian	Breast	Esophageal
138	RTYsHGTYR	RSBN1L	A*03	LL4857T						
139	RVA sPTSGVK	IRS2	A*03	LL3081T, LL4857N/T, LL4922N/T						
140	RVKtPTSQSYR	ZNF281	A*03	LL4922N/T						
141	RVLsPLIIK	RNF169	A*03	LL3081T, LL4857N/T, LL4922N/T						
142	RVRQsPLATR	PEX14	A*03	LL4922T						
143	RVYsPYNHR	TOPORS	A*03	LI3081T, LL4857N/T, LL4922N/T						
144	SVKsPVTVK	TCF7L1	A*03	LL4922N/T						
145	SVRRsVLMK	PDCL3	A*03	LL3081T, LL4922N/T						
146	TLLAsPMLK	FLT1	A*03	LL4857T						
147	yIQSRF	DYRK1B	A*03	LL4922T						
148	PYDPALGsPSR	SP5	A*24	HepG2						
149	RYQtQPVTL	SVIL	A*24	LL4922N/T, HepG2						
150	VYTyIQSRF	DYRK4	A*24	HepG2						
151	FTKsPYQEF	RPS2	A*26	LL3907T						
152	RTSsFTFQN	ARNT	A*31	LL4922N/T						
153	APDsPRAFL	NA	B*07	LL3081T, LL4922N/T, LL4857T						
154	APRKGsFSAL	CUL4A	B*07	LL3081T, LL4922N/T, LL4857T						
155	APRNGsGVAL	EEPD1	B*07	LL4857T						
156	APRRYsSSL	ARHGAP17	B*07	LL3081T, LL4922N/T, LL4857T						
157	APRsPPSRP	SOCS-1	B*07	LL4922N/T						
158	APSLFHLNtL	DLC1	B*07	LL4857T						
159	APSSARAsPLL	DOCK4	B*07	LL4857T						
160	FPLDsPKTLVL	ZNF318	B*07	LL5721T						
161	FPRRHsVTL	ZFP36L1	B*07	LL4922N/T, LL4857T						

#	Sequence	Source Protein	HLA-Type	Liver Samples	Leukemia	Colorectal	Melanoma	Ovarian	Breast	Esophageal
162	FRGRYR _s PY	RBM39	B*07	LL3081T, LL4922N/T		■				
163	FRK _s MVEHY	RAB33A	B*07	LL4857T			■			
164	GPPYQRRG _s L	ETV5	B*07	LL4857T						
165	GPRPG _s PSAL	RPUSD1	B*07	LL4922N/T, LL4857T			■		■	
166	GPRSA _s LL	GPSM3	B*07	LL4857T	■	■	■			
167	GPRSA _s LLSL	GPSM3	B*07	LL4857T	■	■	■			
168	GPRSA _s LLsL	GPSM3	B*07	LL4857T	■					
169	GPR _s PKAPP	ARHGAP4	B*07	LL3081T, LL4857N/T, LL4922N/T	■	■	■			
170	HPKRSV _s L	BNIP3L	B*07	LL3907T, LL3081T			■			
171	HRY _s TPHAF	RAF1	B*07	LL4922T		■				
172	KASPKRL _s L	MTSS1L	B*07	LL4857T						
173	KLSGL _s F	MARCKSL1	B*07	LL4857T	■					
174	KPA _s PKFIVTL	ZC3H14	B*07	LL4922N/T, LL4857T	■	■	■			
175	KPPYRSH _s L	CEP95	B*07	LL4857T	■					
176	KPRPL _s MDL	KIAA1671	B*07	LL3081T, LL4857N/T, LL4922N/T		■				
177	KPRPPPL _s P	TRIP10	B*07	LL3081T, LL4922N/T, LL4857T		■	■			
178	KPRRF _s RsL	RSRC2	B*07	LL4857N/T, LL4922N/T	■	■	■			
179	KPRRF _s RSL	RSRC2	B*07	LL4857T	■	■	■			
180	KPR _s PFSKI	RAB11FIP5	B*07	LL3081T, LL4857N/T, LL4922N/T		■				
181	KPR _s PPRAL	PEG10	B*07	LL4922N/T	■	■	■		■	
182	KPR _s PPRALVL	PEG10	B*07	LL4922N/T			■		■	
183	KPR _s PVVEL	ADRBK1	B*07	LL3081T, LL4857N/T, LL4922N/T	■	■	■		■	■
184	KPS _s PRGSL	AJUBA	B*07	LL3081T, LL4922N/T, LL4857T						
185	KPS _s PRGSL	AJUBA	B*07	LL3081T						

#	Sequence	Source Protein	HLA-Type	Liver Samples	Leukemia	Colorectal	Melanoma	Ovarian	Breast	Esophageal
186	KPVsPKSGTL	ARHGEF7	B*07	LL3081T, LL4922N/T						
187	KPYsPLASL	NFATC2	B*07	LL4857T						
188	KRAsGQAFEL	STMN1	B*07	LL4857T						
189	LPAsPRARL	MAP7D1	B*07	LL3081T, LL4922N/T						
190	LPIFSRLsI	ZFP36L2	B*07	LL4922N, LL4857T						
191	LPKGLSAsL	LARP1	B*07	LL4857T						
192	LPKGLsASL	LARP1	B*07	LL4857T						
193	LPRGsSPSVL	TGIF2	B*07	LL4857T						
194	LPRPAsPAL	MAP1A	B*07	LL4857T						
195	LPRSSsMAA	BAIAP2	B*07	LL4857T						
196	LPRSSsMAAGL	BAIAP2	B*07	LL4857T						
197	MPRQPsATRL	MZT2B	B*07	LL4857T						
198	QPRtPSPLVL	LSP1	B*07	LL4922N/T						
199	RARGIsPIVF	YTHDC1	B*07	LL4922N/T						
200	RKLsVILIL	SLC39A6	B*07	LL370T						
201	RLLsPQQPAL	MEF2D	B*07	LL4857T						
202	RPAFFsPSL	KIAA0930	B*07	LL4922N, LL4857T						
203	RPAKsMDSL	ARHGAP30	B*07	LL3081T, LL4857N/T, LL4922N/T						
204	RPAsAGAmL	MEF2D	B*07	LL4857T						
205	RPAsAGAML	MEF2D	B*07	LL3081T, LL4857N/T, LL4922N/T						
206	RPAsPAAKL	KANSL3	B*07	LL3081T, LL4857N/T, LL4922N/T						
207	RPAsPEPEL	KIF1A	B*07	LL4857T						
208	RPAsPGPSL	MICALL2	B*07	LL3081T, LL4922N/T, LL4857T						
209	RPAsPQRAQL	NA	B*07	LL3081T, LL4857N/T, LL4922N/T						

#	Sequence	Source Protein	HLA-Type	Liver Samples	Leukemia	Colorectal	Melanoma	Ovarian	Breast	Esophageal
210	RPAsPSLQL	PPP1R13L	B*07	LL4857T						
211	RPAsPSLQLL	PPP1R13L	B*07	LL4857T						
212	RPAsYKKKSML	PDGFRA	B*07	LL4857T						
213	RPDsPTRPTL	MICAL3	B*07	LL3081T, LL4857N, LL4922N/T						
214	RPDsRLGKTEL	SETD2	B*07	LL4922N/T						
215	RPDVAKRLsL	BCAR3	B*07	LL3081T, LL4922N/T, LL4857T						
216	RPFHGISTVsL	DENND4C	B*07	LL4857T						
217	RPFsPREAL	LUZP1	B*07	LL3081T, LL4922N/T, LL4857T						
218	RPGsRQAGL	PDLIM2	B*07	LL3081T						
219	RPIsPGLSY	CCDC6	B*07	HepG2, LL3081T, LL5437N/T, LL4922N/T, LL4857T						
220	RPIsPPHTY	ROBO1	B*07	HepG2, LL3081T						
221	RPIsPRIGAL	EPN1	B*07	LL4922N/T						
222	RPKLSsPAL	EP300	B*07	LL3081T, LL4922N						
223	RPKsNIVLL	MS4A1	B*07	LL4922N, LL4857T						
224	RPKsPLSKM	TANC2	B*07	LL3081T, LL4922N/T, LL4857T						
225	RPKsVDFDSL	CD2AP	B*07	LL4922N/T, LL4857T						
226	RPKtPPVVI	SYAP1	B*07	LL3081T, LL4857N/T, LL4922N/T						
227	RPLsLLLAL	JAG1	B*07	LL5721N/T						
228	RPLsVVYVL	MAP3K6	B*07	LL5721N/T						
229	RPMsESPHM	ZFP36L1	B*07	LL3081T, LL4922N/T						
230	RPNsPSPTAL	TLK1	B*07	LL4922N/T, LL4857T						
231	RPPsPGPVL	SCAP	B*07	LL4922N/T, LL4857T						
232	RPQRAtSNVF	MYL9	B*07	LL4857T						
233	RPRAAtVV	PRKAR1A	B*07	LL3081T, LL4857N						

#	Sequence	Source Protein	HLA-Type	Liver Samples	Leukemia	Colorectal	Melanoma	Ovarian	Breast	Esophageal
234	RPRAAtVVA	PRKAR1A	B*07	LL3081T						
235	RPRANsGGVDL	RREB1	B*07	LL3081T, LL4857N/T, LL4922N/T						
236	RPRARsVDAL	LSR	B*07	LL3081T, LL4922N/T, LL4857T						
237	RPRDtRRISL	PIEZO1	B*07	LL4857T						
238	RPRGsESLL	ERBB3	B*07	LL4857T						
239	RPRGsQSLL	ERBB3	B*07	LL3081T, LL4857N/T, LL4922N/T						
240	RPRIPsPIGF	EIF4ENIF1	B*07	LL4922N, LL4857T						
241	RPRPAsSPAL	NEURL1B	B*07	LL4857T						
242	RPRPHsAPSL	MIP	B*07	LL4922N/T, LL4857T						
243	RPRPSsAHVGL	SHROOM3	B*07	LL4922T						
244	RPRPsSVL	DEPP	B*07	LL4857T						
245	RPRPsSVLRTL	DEPP	B*07	LL4857T						
246	RPRPVsPSSL	SIK1	B*07	LL3081T, LL4857N/T, LL4922N/T						
247	RPRPVsPSSLL	SIK1	B*07	LL4922N/T, LL4857T						
248	RPRsAVEQL	PLEKHA5	B*07	LL3081T, LL4922N/T, LL4857T						
249	RPRsAVLL	AKAP13	B*07	LL3081T, LL4857N/T, LL4922N/T						
250	RPRsISVEEF	SETX	B*07	LL4922N/T, LL4857T						
251	RPRsLEVTI	MEFV	B*07	LL4857N						
252	RPRSLsSPTVTL	NEDD4L	B*07	LL4922N/T, LL4857T						
253	RPRsMTVSA	MTSS1	B*07	LL3081T, LL4857N/T, LL4922N/T						
254	RPRsMVRSF	DOCK1	B*07	LL4857T						
255	RPRsPAARL	ZNF219	B*07	LL4857T						
256	RPRsPNMQDL	RASL11A	B*07	LL3081T, LL4922N/T, LL4857T						
257	RPRsPPGGP	ZBTB46	B*07	LL3081T, LL4922N/T, LL4857T						

#	Sequence	Source Protein	HLA-Type	Liver Samples	Leukemia	Colorectal	Melanoma	Ovarian	Breast	Esophageal
258	RPRsPPRAP	PRICKLE3	B*07	LL4922N/T						
259	RPRsPPSSP	PDE4A	B*07	LL3081T, LL4922N/T						
260	RPRsPRENSI	ATXN2	B*07	LL3081T, LL4922N/T						
261	RPRsPRPPP	NA	B*07	LL4922T						
262	RPRsPRQNSI	ATXN2	B*07	LL3081T, LL4922N/T, LL4857T						
263	RPRSPsPIS	GRM5	B*07	LL3081T, LL4857T						
264	RPRsPTGPSNSF	RBM17	B*07	LL3081T, LL4922N/T, LL4857T						
265	RPRsPTGPSNSFL	RBM17	B*07	LL4922N/T, LL4857T						
266	RPRsPWGKL	SEPT4	B*07	LL4857T						
267	RPRsQYNTKL	SRGAP1	B*07	LL4857T						
268	RPRtPLRSL	NA	B*07	LL4922N/T						
269	RPSsLPDL	ARID1B	B*07	LL3081T, LL4922T, LL4857T						
270	RPSsPALYF	TSC22D4	B*07	LL4857T						
271	RPTsFADEL	FAM21C	B*07	LL3081T, LL5721N/T, LL4922N/T, LL4857T						
272	RPTsRLNRL	NCOA1	B*07	LL4922N/T, LL4857T						
273	RPVsPFQEL	NA	B*07	LL3081T, LL5721N/T, LL4922N/T, LL4857T						
274	RPVsPGKDI	HIVEP2	B*07	LL3081T						
275	RPVSPsSLL	SIK1	B*07	LL4922N						
276	RPVsTDFAQY	ABLIM1	B*07	LL3081T						
277	RPVtPVSDL	KLF10	B*07	LI3081T, LL4922N/T						
278	RPWsNSRGL	CDC42SE1	B*07	LL4857T						
279	RPWsPAVSA	SKI	B*07	LL4857T						
280	RPYsPPFFSL	FAM53C	B*07	LL4922N/T, LL4857T						
281	RPYsQVNVL	UTRN	B*07	LL4857T						

#	Sequence	Source Protein	HLA-Type	Liver Samples	Leukemia	Colorectal	Melanoma	Ovarian	Breast	Esophageal
282	RSR _s PRPAL	NA	B*07	LL4922T, LL4857T						
283	RTR _s PSPTL	PHLDB1	B*07	LL4857T						
284	RVRKLP _s TTL	RPS6KA1	B*07	LL3081T, LL4922N/T						
285	SPAsPKISL	ATXN2L	B*07	LL4922N/T, LL4857T						
286	SPFKRQL _s L	NUMBL	B*07	LL3081T, LL4922N/T, LL4857T						
287	SPFL _s KRSL	CDK12	B*07	LL4857T						
288	SPGLARKR _s L	ZNF106	B*07	LL4857T						
289	SPK _s PGLKA	RCSD1	B*07	LL3081T, LL4857N/T, LL4922N/T						
290	SPRER _s PAL	THRAP3	B*07	LL3081T, LL4922N/T						
291	SPRGEAS _s L	YAF2	B*07	LL4857T						
292	SPRGEAS _s L	YAF2	B*07	LL4857T						
293	SPR _s PGRSL	NA	B*07	LL4922N/T, LL4857T						
294	SPR _s PSGLR	TSC2	B*07	LL3081T						
295	SPRSP _s TTYL	CHAF1A	B*07	LL4857T						
296	SPS _s PSVRRQL	ANKRD17	B*07	LL4922N/T						
297	TPMKKHL _s L	FAM126B	B*07	LL4857T						
298	TPR _s PPLGL	MAP3K11	B*07	LL3081T, LL4857N/T, LL4922N/T						
299	TPR _s PPLGLI	MAP3K11	B*07	LL3081T, LL4922N/T, LL4857T						
300	VAKRL _s L	BCAR3	B*07	LL4857T						
301	VPRPERR _s SL	TMCO3	B*07	LL3081T, LL4922N/T, LL4857T						
302	VPR _s PKHAHSSSL	SVIL	B*07	LL4922T						
303	VPT _s PKSSL	RAPH1	B*07	LL4922T						
304	YDPDPH _s PFAV	ETV3	B*07	LL5721T						
305	YPGGRR _s SL	MRC1	B*07	LL3081T, LL4857N/T						

#	Sequence	Source Protein	HLA-Type	Liver Samples	Leukemia	Colorectal	Melanoma	Ovarian	Breast	Esophageal
306	YPYEFsPVKM	SP5	B*07	HepG2						
307	DLKSSKAsL	AHNAK	B*08	LL370T, LL3907T						
308	SsPIMRKKVSL	PPIP5K2	B*08	LL370T						
309	GQLsPGVQF	CDK18	B*15	LL5437N/T						
310	KIKsFEVVF	TXNIP	B*15	LL5721N/T, LL5437N/T						
311	RAHsEPLAL	DCAF15	B*15	HepG2	■					■
312	FRRsPTKSSL	RBM14	B*27	LL3907T	■	■				
313	FRRsPTKSSLD	RBM14	B*27	LL4922N/T	■	■				
314	FRRsPTKSSLDY	RBM14	B*27	LL4922N/T	■	■				
315	GRKsPPPSF	CRYBG3	B*27	LL981T		■				
316	GRLsPAYSL	PHLDB1	B*27	LL981T		■				
317	GRLsPVPVPR	RALY	B*27	LL981T		■				
318	GRQsPSFKL	PPP4R3A	B*27	LL981T						
319	GRsSPPPGY	MAP3K3	B*27	LL981T						
320	KRA sYILRL	SMG1	B*27	LL4857T						
321	KRFsFKKSF	MARCKS	B*27	LL981N/T		■				
322	KRFsFKKsF	MARCKS	B*27	LL981T		■	■			
323	KRFsGTVRL	RPL10A	B*27	LL981T, LL4922N/T		■	■			
324	KRKsFTSLY	CEP170	B*27	LL4857T						
325	KRLEKsPSF	ANKS1A	B*27	LL981T						
326	KRLsPAPQL	SUN2	B*27	LL981T	■	■	■			
327	KRM sPKPEL	CETN2	B*27	LL981N/T		■	■			
328	KRmsPKPEL	CETN2	B*27	LL981T						
329	KRWQsPVTK	SRRM1	B*27	LL981N/T						

#	Sequence	Source Protein	HLA-Type	Liver Samples	Leukemia	Colorectal	Melanoma	Ovarian	Breast	Esophageal
330	KRYsGNMEY	LATS1	B*27	LL981T, LL370T, LL3081T, LL4922N/T, LL4857T						
331	KRYsGNmEY	LATS1	B*27	LL3907T, LL981T						
332	KRYsRALYL	ANAPC7	B*27	LL370T						
333	QRLsPLSAAY	HLX	B*27	LL981T						
334	RKLRsLEQL	LRRC8E	B*27	LL981T						
335	RRAsIITKY	SLC14A2	B*27	LL981T						
336	RRAsLSEIGF	CDK17	B*27	LL981N/T						
337	RRDsIVAEL	COPE	B*27	LL981N/T						
338	RRDsLQKPGL	LATS2	B*27	LL981T						
339	RRFsGTAVY	ZNF518A	B*27	LL3907T, LL981T, LL370T, LL3081T, LL4922N/T, LL4857T						
340	RRFsIATLR	CYP2A13	B*27	LL981N						
341	RRFsLTTLR	CYP2C8	B*27	LL981N/T						
342	RRFsPPRRM	RNPS1	B*27	LL981N/T						
343	RRFsPPRRm	RNPS1	B*27	LL981T						
344	RRFsRSDEL	EGR1	B*27	LL370T						
345	RRFsRsPIR	SON	B*27	LL981N/T						
346	RRFSRsPIR	SON	B*27	LL981T						
347	RRFsRsPIRR	SON	B*27	LL981T						
348	RRGsFEVTL	SELH	B*27	LL370T, LL3081T, LL4922N/T, LL4857T						
349	RRIDIsPSTF	THRAP3	B*27	LL981T						
350	RRIsDPEVF	FILIP1L	B*27	LL4857T						
351	RRIsDPQVF	FILIP1L	B*27	LL981N/T, LL370T, LL3081T, LL4857N/T, LL4922N/T						
352	RRIsQIQQL	AQR	B*27	LL370T						
353	RRKsQVAEL	NIFK	B*27	LL981T, LL370T, LL3081T						

#	Sequence	Source Protein	HLA-Type	Liver Samples	Leukemia	Colorectal	Melanoma	Ovarian	Breast	Esophageal
354	RRLsADIRL	MAST3	B*27	LL981T						
355	RRLsELLY	HSP90AB1	B*27	LL981N/T, LL370T						
356	RRLsGGSHSY	RAPGEF1	B*27	LL981T						
357	RRLsRKLSL	PHACTR2	B*27	LL981T						
358	RRMsFQKP	OXR1	B*27	LL981T						
359	RRMsLLSVV	RIMKLB	B*27	LL981N/T, LL370T						
360	RRmsLLSVV	RIMKLB	B*27	LL981T, LL5721N/T						
361	RRNsAPVSV	ARHGAP31	B*27	LL981T						
362	RRPsIAPVL	KCNT1	B*27	LL3907T, LL4857N/T, LL4922N/T						
363	RRPsLLSEF	NCOR1	B*27	LL981N/T, LL4922N						
364	RRPsLVHGY	FDPS	B*27	LL3907T, LL981T						
365	RRPsYTLGM	SIPA1L1	B*27	LL4857T						
366	RRRsLERLL	MAGI1	B*27	LL981T						
367	RRSFsLE	AKAP13	B*27	LL370T						
368	RRSsFLQ	SEC23A	B*27	LL370T						
369	RRSsFLQVF	SEC23A	B*27	LL981T, LL370T, LL5721N/T, LL4922N, LL4857T						
370	RRSsIQSTF	NCSTN	B*27	LL981T, LL4922N/T						
371	RRSsQSWSL	FAM21C	B*27	LL4857T						
372	RRVVQRSsL	EIF4G1	B*27	LL981T						
373	RRYsKFFDL	SH3PXD2B	B*27	LL370T						
374	RRYsPPIQR	SRRM1	B*27	LL981N/T						
375	RSRsPLEL	DDB2	B*27	HepG2						
376	SPRRsRSISL	SRSF7	B*27	LL4922N/T, LL4857T						
377	SRFNRRVsV	PRKAR2A	B*27	LL981T						

#	Sequence	Source Protein	HLA-Type	Liver Samples	Leukemia	Colorectal	Melanoma	Ovarian	Breast	Esophageal
378	DAKKsPLAL	ZNF703	B*35	HepG2						
379	SDMPRAHsF	SH3BP2	B*37	LL981N/T						
380	SDmPRAHsF	SH3BP2	B*37	LL981T						
381	AENARSAsF	GAB2	B*44	LL981T, LL4857T						
382	AENsPTRQQF	DDX42	B*44	LL4857T	■	■	■			
383	AENsSSREL	PML	B*44	LL4857T						
384	AtAGPRLGW	PPFIBP1	B*44	LL4857T			■			
385	EELsPTAKF	KLF6	B*44	LL4857T	■	■				
386	FKtQPVTF	C11orf96	B*44	LL4922N		■				
387	GEAsPSHII	PRR12	B*44	LL3907T						
388	GEIsPQREV	LMO7	B*44	LL3907T						
389	GETsPRTKI	ADD3	B*44	LL3907T						
390	HEKKAYsF	RPS6KA1	B*44	LL370T						
391	KEKsPFRET	ICE1	B*44	LL3907T						
392	KELARQIsF	UBE2J1	B*44	LL981T						
393	KEMsPTRQL	FAM229B	B*44	LL3907T, LL981T		■	■			
394	KEmsPTRQL	FAM229B	B*44	LL3907T, LL981T						
395	KESsPLSSRKI	LPIN1	B*44	LL3907T						
396	REAPsPLmI	BRD4	B*44	LL3907T						
397	REAsPAPLA	PHRF1	B*44	LL3907T						
398	REAsPRLRV	TNFRSF10A	B*44	LL3907T						
399	REAsPSRLSV	CLASP2	B*44	LL3907T						
400	REIMGtPEYL	STK17B	B*44	LL5437N						
401	REKsPGRmL	CIT	B*44	LL3907T						

#	Sequence	Source Protein	HLA-Type	Liver Samples	Leukemia	Colorectal	Melanoma	Ovarian	Breast	Esophageal
402	RELARKGsL	FAM219A	B*44	LL981T						
403	RELSPLISL	AFF1	B*44	LL5437N/T						
404	REPsPLPEL	TBX2	B*44	LL5437T						
405	RERsPSPSF	PCYT1A	B*44	LL981T						
406	RESsPTRRL	SRCIN1	B*44	LL3907T						
407	REVsPAPAV	SIPA1L3	B*44	LL3907T						
408	REYGsTSSI	SIPA1L1	B*44	LL3907T						
409	RFKtQPVTF	C11orf96	B*44	LL5721N/T, LL4922N/T						
410	RQKsPLFQF	BBX	B*44	LL5437N/T						
411	SEFKAMDsI	CTNNA1	B*44	LL5437N						
412	SELSPGRSV	FLAD1	B*44	LL3907T						
413	TEAsPESML	BRD8	B*44	LL5437T						
414	YEGsPIKV	NPM1	B*44	LL3907T						
415	ADLsPEREV	RHEBL1	B*49	LL3907T						
416	SFDsGSVRL	IRF6	C*04	LL5437T						
417	AGDsPGSQF	FOXO1	C*05	LL4857T						
418	KVDsPVIF	DENND4A	C*05	LL4857T						
419	NMDsPGPML	ELF1	C*05	LL4857T						
420	RADsPVHM	MED26	C*05	LL4857N/T						
421	RLLDPsSPLAL	SHANK2	C*05	LL4857T						
422	RLLDPSsPLAL	SHANK2	C*05	LL4857T						
423	RSDsYVEL	TP53BP1	C*05	LL4857T						
424	RSEsPPAEL	TRIP12	C*05	LL4857T						
425	RVDsPSHGL	DAXX	C*05	LL4857N/T						

#	Sequence	Source Protein	HLA-Type	Liver Samples	Leukemia	Colorectal	Melanoma	Ovarian	Breast	Esophageal
426	sDDEKMPDLE	PTGES3	C*05	LL4857T						
427	SIDSPQKL	TP53BP1	C*05	LL4857N/T						
428	VVDSPGQEV	GTF3C2	C*05	LL4857T						
429	FRFsGRTEY	EPB41L4B	C*06	LL981T						
430	KRAsFAKSV	WNK4	C*06	LL981T						
431	LSSsVIREL	NGDN	C*06	HepG2						
432	RKPsIVTKY	ATRX	C*06	LL981T						
433	RRHsASNLHAL	ZFP36L2	C*06	LL981T						
434	RRLsFLVSY	QARS	C*06	LL981T, LL370T, LL5721N/T, LL4922N, LL4857T						
435	RRLsYVLFI	GPAM	C*06	LL5721N/T						
436	RRPsYRKIL	CREM	C*06	LL370T						
437	RSAsFSRKV	NPHP4	C*06	LL981T, HepG2						
438	SRSSSVLsL	PLEKHG3	C*06	LL981T						
439	TRKtPESFL	EPN1	C*06	LL981N/T						
440	YRYsPQSFL	KIAA1551	C*06	LL981T						
441	RNLsSPFIF	SLC7A2	C*07	LL370T						
442	RTSsFALNL	APOB	C*07	LL370T						
443	TLMERTVsL	FAM114A1	C*07	LL4857T						
444	KTMSPSQMIM	ZMIZ1	C*16	HepG2						
445	RMYSPIPSL	PEG10	C*16	HepG2						
446	RTPsDVKEL	ANP32A	C*16	HepG2						
447	YARsVHEEF	SDF4	C*16	HepG2						
448	AKLsETIS	ODF2L	----	LL370T						
449	AsLGFVF	SLC16A11	----	LL370T						

#	Sequence	Source Protein	HLA-Type	Liver Samples	Leukemia	Colorectal	Melanoma	Ovarian	Breast	Esophageal
450	GsPHYFSPF	SRSF9	-----	LL5721T						
451	KAVsLFLcY	IFI6	-----	LL5721N/T						
452	RAFsVKFEV	OAS1	-----	LL5721N						
453	RGDGYGtF	A1CF	-----	LL3081T						
454	RKSsIIIRM	PLGLB1	-----	LL3081T						
455	RLSsLRASTSK	RPS6	-----	LL3081T						
456	RTHsLLLLL	RNASE4	-----	LL981N/T, LL370T, LL5721N/T, LL5437N/T, LL4857T, HepG2						
457	RYPsNLQLF	TEP1	-----	LL5721T						
458	sYIEHIFEI	PEA15	-----	LL5721T						
459	sYQKVIELF	PBK	-----	LL5721T						

4.4.2 Analysis of Identified HLA-Associated Phosphopeptides

Of the 459 phosphopeptides identified, 423 were nine to eleven amino acid residues in length, the ideal length for binding to HLA class I molecules. The location of the phosphorylated sites for each of these phosphopeptides was analyzed and the percentages relative to the total are shown in Figure 4.2. Additionally, a depiction of the peptide binding cleft illustrates the residues which serve as anchor positions and the residues available for interaction with the T cell receptor.

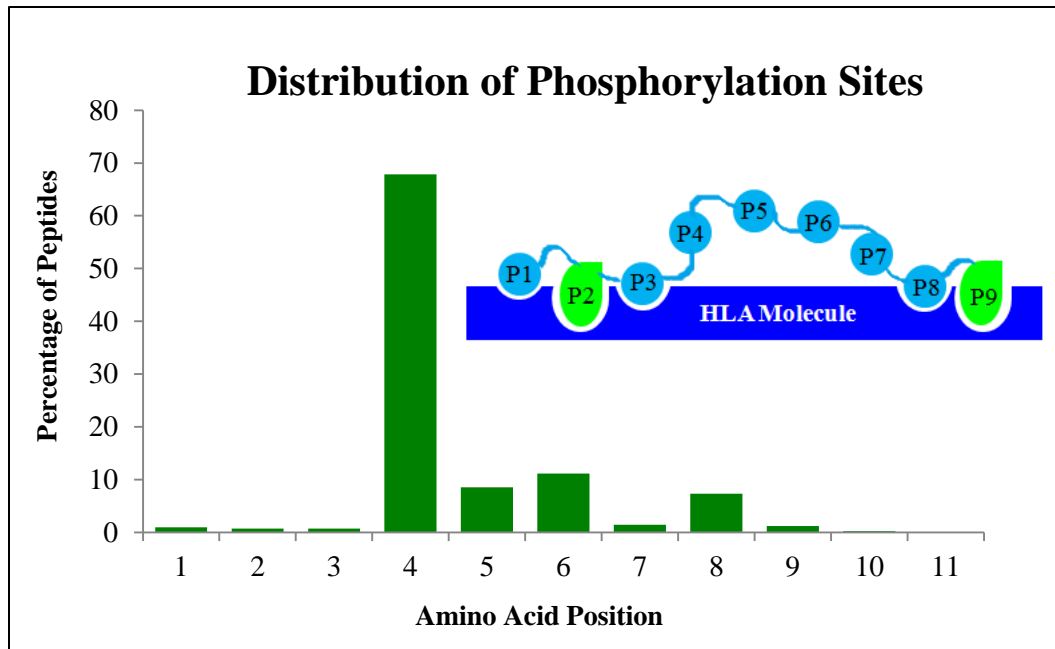


Figure 4.2 Distribution of phosphorylation sites on identified HLA class I-associated phosphopeptides. Phosphorylation sites of peptides 9-11 amino acids in length were analyzed, showing a distinct preference for sites at positions 4-8. Inset shows interaction between a peptide and an HLA molecule within the binding cleft. Positions 2 and 9 serve as anchor residues while positions 3-8 are capable of interacting with T cell receptors.

As depicted in Table 4.2, many of the phosphopeptides identified in liver tissue and the HepG2 cell line overlapped with those seen in previously analyzed samples from varying cancers. The distribution of identified phosphopeptides between the cancer types with the largest amount of overlap is depicted in Figure 4.3. While 459 phosphopeptides were identified in the liver samples analyzed, only 154 were actually unique to this type of cancer. Distinct subsets of 165, 164, and 94 phosphopeptides that were present in liver samples were also observed in colorectal cancer, melanoma, and leukemia, respectively. Furthermore, subsets emerged with an even greater amount of overlap, such as the 48 phosphopeptides that were present in all four cancer types.

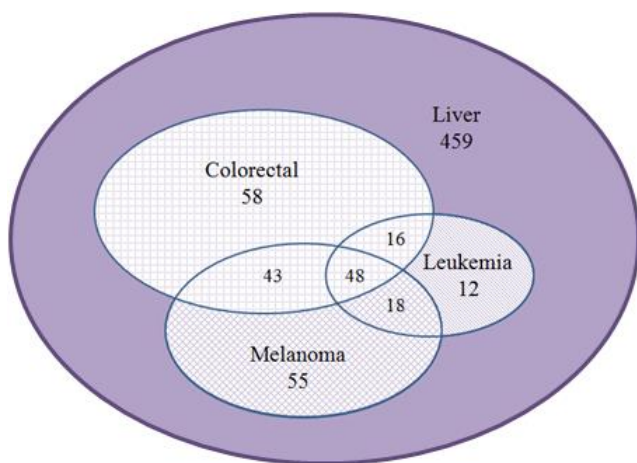
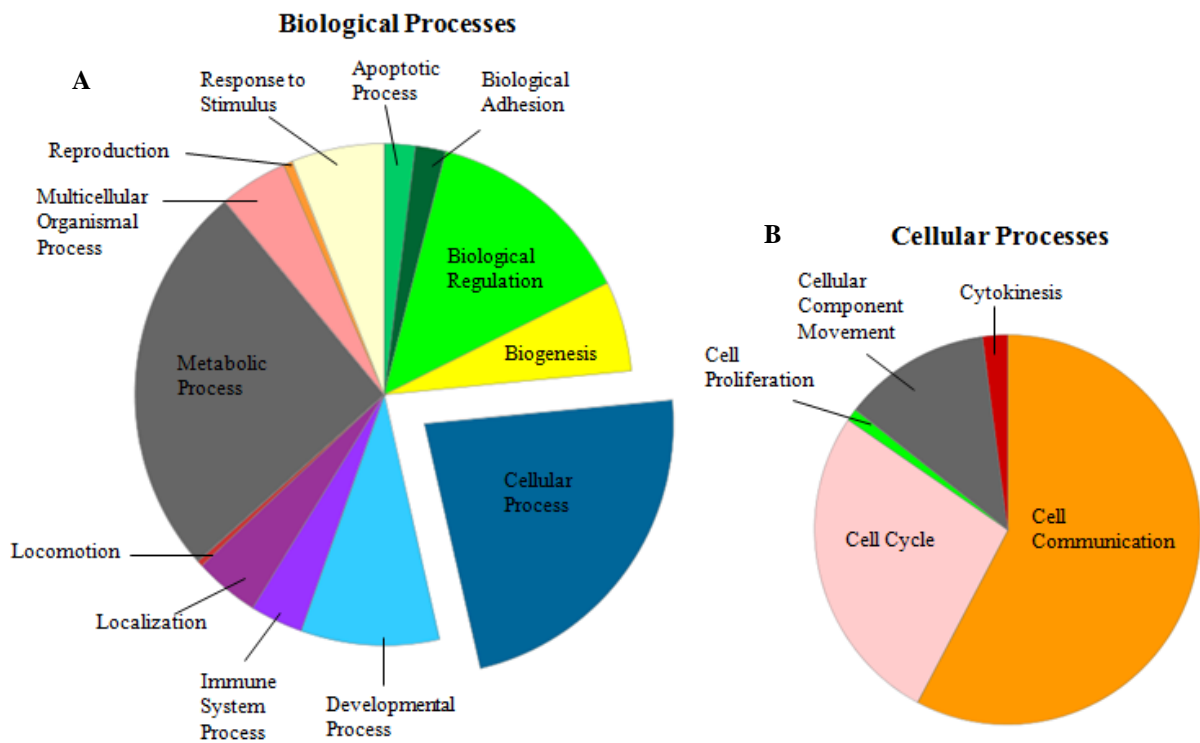


Figure 4.3 Overlap of phosphopeptides identified in various cancer types.

Analysis of the overlap between the phosphopeptides identified in liver samples and those previously seen in colorectal cancer, melanoma, and leukemia samples reveals clear targets for the development of widely-applicable immunotherapeutics.

Further evaluation of the identified phosphopeptides included an analysis of the role of source proteins in association with the development or progression of cancer. The involvement of source proteins in pathways known to be dysregulated or those found to be overexpressed in cancer was determined through extensive literature searches. Source proteins which met these criteria were further analyzed using the comprehensive Protein Analysis THrough Evolutionary Relationships (PANTHER) classification system

(www.pantherdb.org). The PANTHER classification system allows the user to input a large data set of Uniprot gene IDs and view the classification of each in terms of molecular function, biological process, cellular component, protein class, and/or pathway.²² Given that many biological processes have been shown to go awry during the development and progression of cancer, the classification of relevant proteins was analyzed in these terms. Figure 4.4 depicts a pie chart showing the varying biological processes represented by the source proteins from which phosphopeptides were identified in the analyzed liver samples.



Biological processes represented by source proteins included metabolic, multicellular organismal, reproduction, response to stimulus, apoptotic, biological adhesion, biological regulation, biogenesis, cellular, developmental, immune system, localization, and locomotion. While dysregulation of many of these processes are associated with cancer, one of the largest percentages represented was cellular processes. This subset of source proteins was further divided into individual categories including cell cycle, cell proliferation, cellular component movement, cytokinesis, and cell communication.

4.4.3 Immunological Significance of Identified HLA-Associated Phosphopeptides

For selection of phosphopeptides for synthesis and biological testing, we prioritized those primarily observed in tumor tissue or the HepG2 cell line and whose source proteins are involved in pathways shown to be dysregulated in cancer. Additionally we prioritized phosphopeptides that were HLA-A*02-specific, as this allele is present in 50.7% of the US Caucasian population.²³ These criteria resulted in the selection of 21 HLA-A*02-specific phosphopeptides which we believe represented ideal targets for further biological testing. The phosphopeptides were synthesized and the sequences and phosphorylation sites confirmed using mass spectrometry. The synthetic phosphopeptides were then shipped to the University of Birmingham for biological testing conducted by Dr. Nico Büttner.

Peripheral blood mononuclear cells (PBMCs) were collected from HLA-A*02-positive healthy donors and patients with hereditary hemochromatosis (HH), a form of

chronic liver disease. Phosphopeptide-specific CD8⁺ T cell responses were assessed using intracellular cytokine staining (ICS) assays. Cells were stimulated for 7 days with the phosphopeptides of interest in the absence of additional cytokines. After 7 days of stimulation, T cells were stained for two cytokines – interferon gamma (IFN- γ) and tumor necrosis factor alpha (TNF α) – and CD107a, as an indicator of cytotoxic potential, and viewed using flow cytometry. An example of flow cytometric data is depicted in Figure 4.5. Cytokine production and CD107a expression is shown for cells that were unstimulated, stimulated with a positive control, and stimulated with a viral control. These data are compared to cells stimulated with SMTRsPPRV, a phosphopeptide originating from serine-arginine rich splicing factor 8. Summed amounts of reactive T cell populations expressing varying combinations of cytokines and CD107a markers are also illustrated in bar graph form, showing comparable levels of reactivity between the phosphopeptide of interest and the viral control.

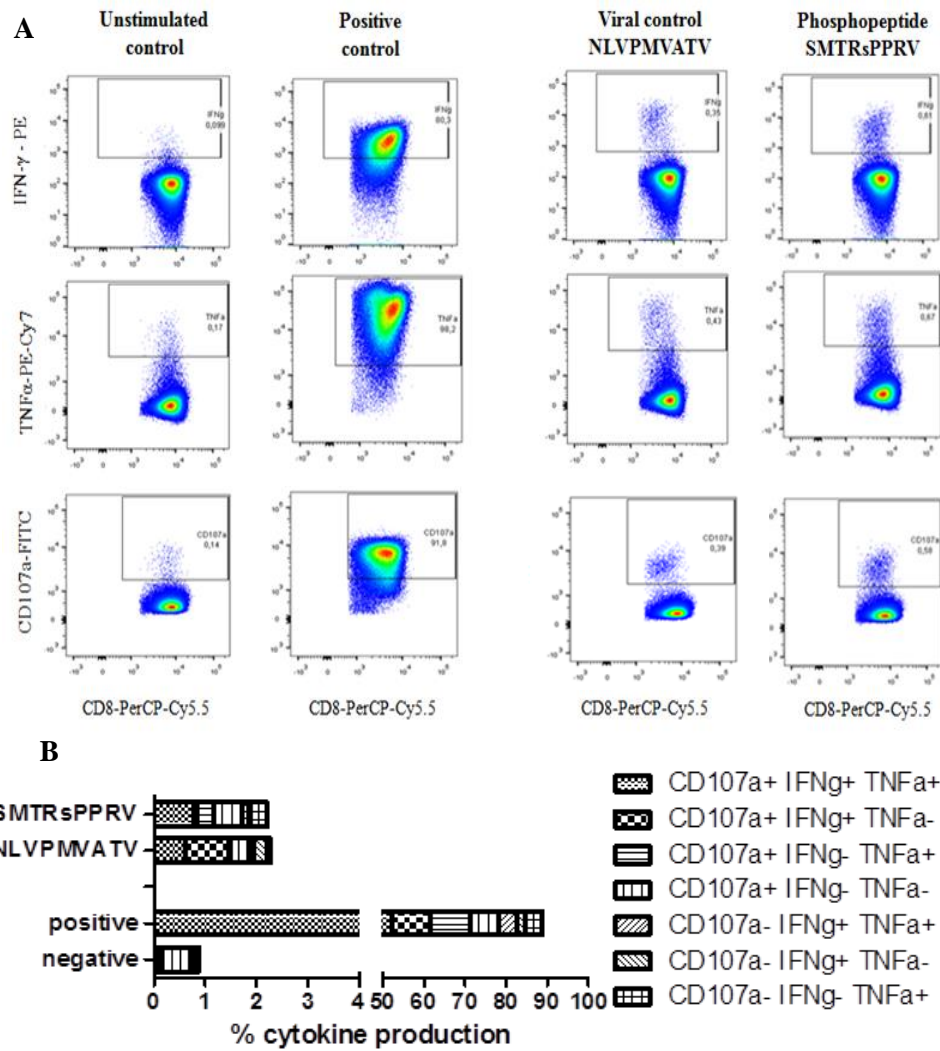


Figure 4.5 Example of intracellular cytokine staining data. Populations of T cells expressing IFN- γ , TNF α , and CD107a were visualized using flow cytometry. A) Populations that are positive for the specific markers are depicted for unstimulated cells and those stimulated with a positive control, a viral control, and SMTRsPPRV, an HLA-A*02-specific phosphopeptide. B) A bar graph showing the summed percentages of reactive T cell populations illustrates the similarity of responses between cells stimulated with the phosphopeptide of interest and the viral control.

The remaining 20 synthetic phosphopeptides were used for stimulation of PBMCs in the same manner as the SMTRsPPRV phosphopeptide. A summary of the percentage of reactive CD8⁺ T cells for each phosphopeptide is shown below in Figure 4.6. Responses to epitopes of two viral controls are illustrated for comparison to responses upon stimulation with phosphopeptides. Overall, the quantity and quality of the observed responses in patients with hereditary hemochromatosis are similar in magnitude to responses produced upon stimulation with viral controls.

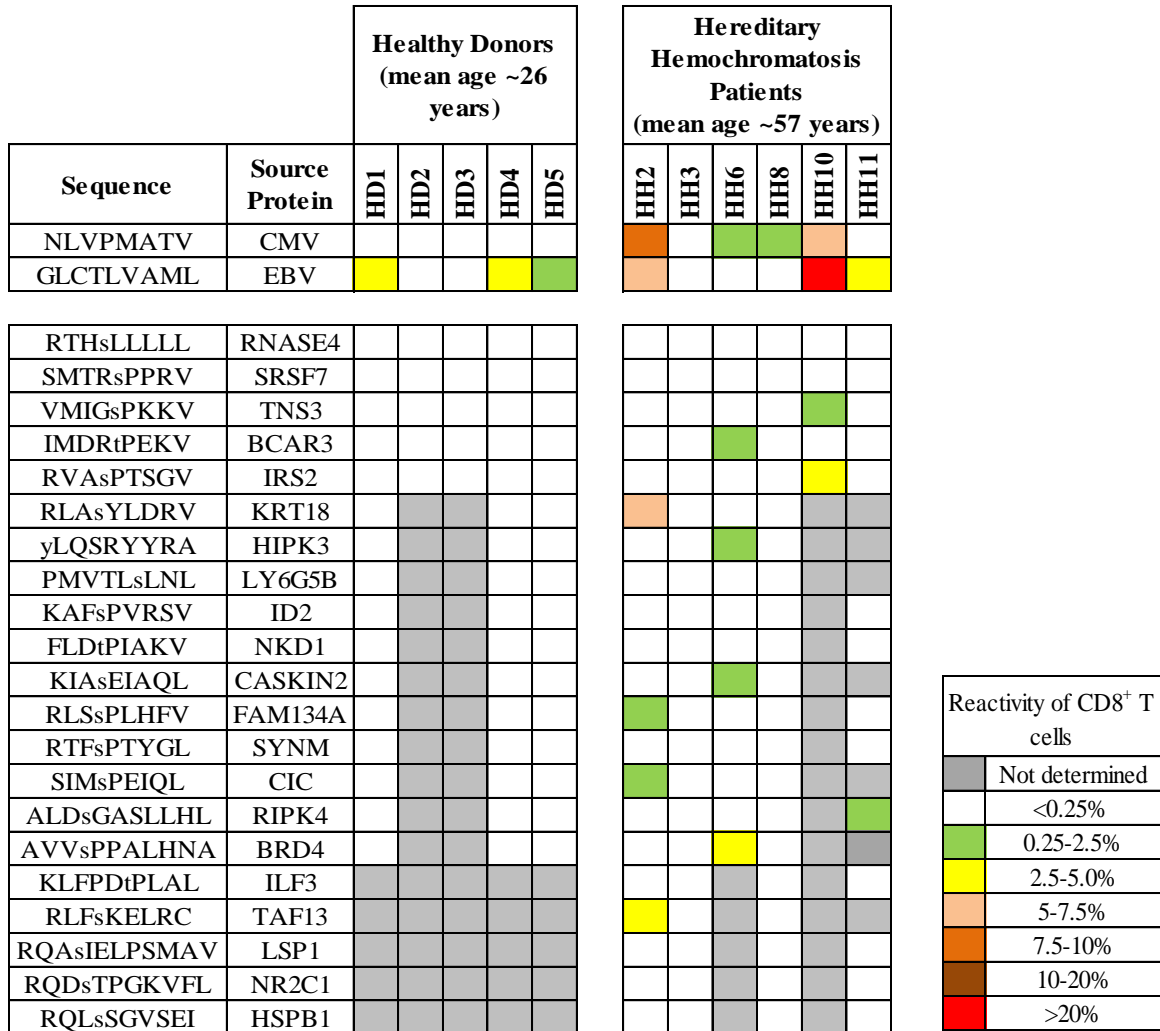


Figure 4.6 Summary of reactive CD8⁺ T cell populations to HLA-A*02-specific phosphopeptides. PBMCs from HLA-A*02-positive healthy donors and patients with hereditary hemochromatosis were stimulated with synthetic phosphopeptides over a 7 day period. Flow cytometry was used to evaluate the reactivity of CD8⁺ T cells following stimulation. A heat map is used to depict the percentages of reactive CD8⁺ T cells specific to viral controls and phosphopeptides of interest.

To ensure that the measured immunological responses to the phosphopeptides we identified were in fact due to the presence of a phosphate group, we had unphosphorylated counterparts synthesized for several of the potential immunotherapeutic candidates. Flow cytometric data from PBMCs stimulated with a peptide of interest with and without the presence of the phosphate moiety illustrated that the observed immunological responses were exclusively phosphate-dependent (Figure 4.7).

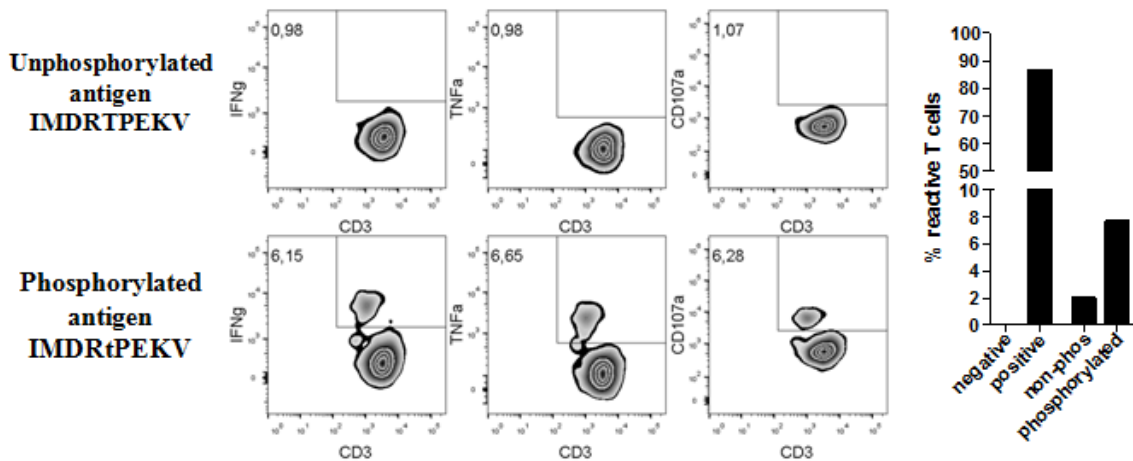


Figure 4.7 Phosphate-dependence of observed immunological responses. PBMCs were stimulated with a peptide originating from breast cancer anti-estrogen resistance protein 3 (BCAR3) with and without the presence of a phosphate moiety. Evaluation of the production of IFN- γ upon stimulation reveals that the observed immunological responses to the phosphopeptides we identified from liver samples are in fact due to the presence of phosphorylation.

4.4.4 Expansion of TIL Cultures for use in Adoptive Cell Transfer Therapies

For evaluation of the use of the identified phosphopeptides in adoptive cell transfer therapies, responses specifically in tumor-infiltrating lymphocytes (TILs) as opposed to PBMCs were analyzed. First, specimens from livers post-transplantation, post-resection, or deceased donors were obtained by Dr. Nico Büttner at the University of Birmingham. Tumor-infiltrating lymphocyte cultures were expanded using a rapid expansion protocol (REP) up to 1×10^9 cells over a period of 14-21 days. Post-expansion, lymphocyte cultures were screened for phosphopeptide reactivity by stimulating the expanded cultures with the HLA-A*02-specific phosphopeptides for 7 days and analyzing responses using ICS in the same manner as for PBMCs. While responses to viral peptides were maintained during the unspecific expansion of lymphocytes, phosphopeptide-specific responses were seemingly lost (Figure 4.8A). To determine if phosphopeptide-reactivity of TILs could be maintained, separate lymphocyte cultures were repeatedly stimulated with a pool of phosphopeptides before and during the expansion process. This phosphopeptide-specific expansion resulted in restoration of the majority of phosphopeptide-specific immunological responses (Figure 4.8B). This data indicates that phosphopeptide-specific expansion of lymphocyte cultures can be performed giving rise to fully functional cells for use in adoptive cell transfer therapies.

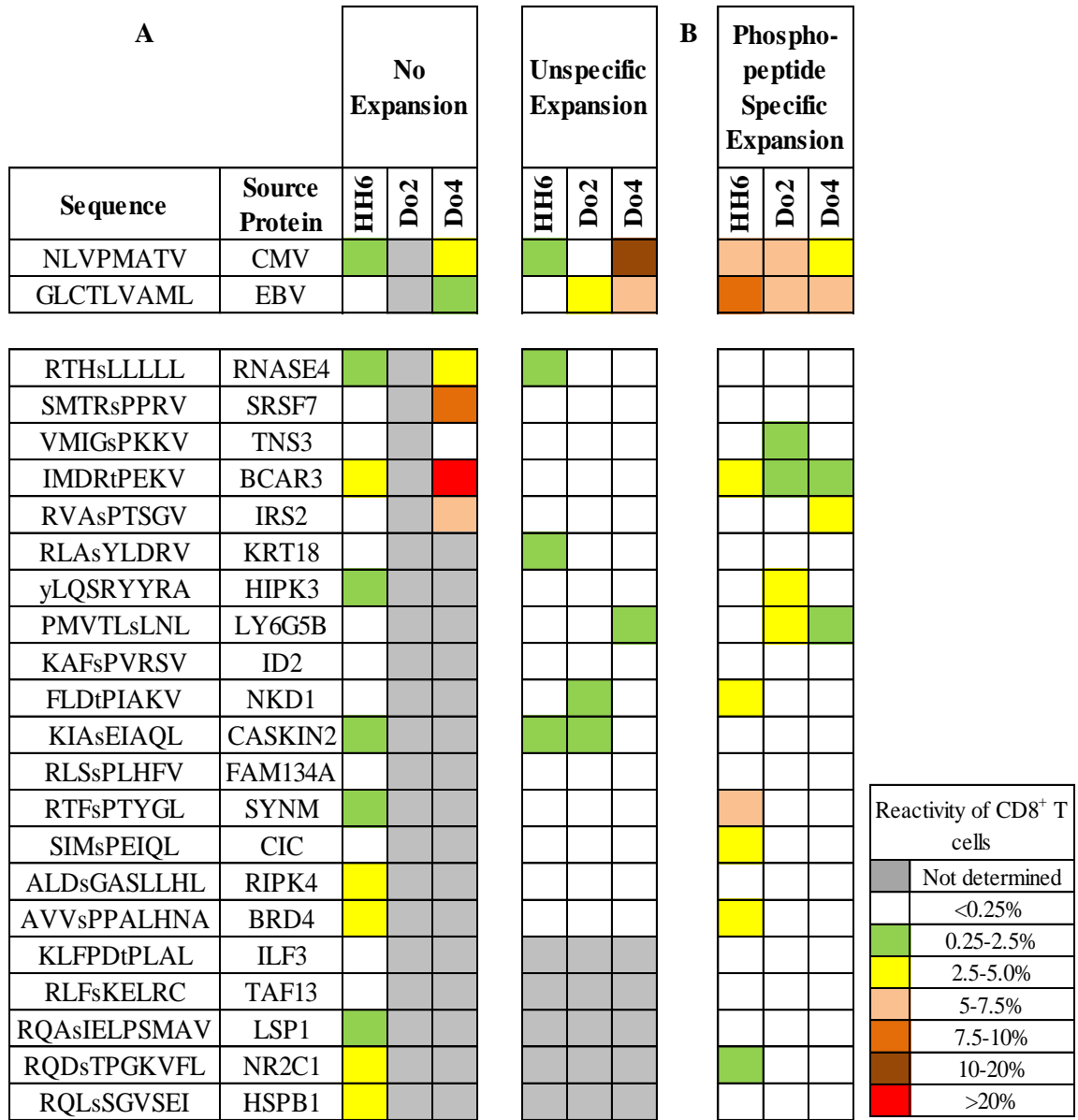


Figure 4.8 Effect of antigen-specific expansion on tumor-infiltrating lymphocyte cultures.

A) TIL cultures which were unspecifically expanded illustrated a loss of reactivity to phosphopeptide antigens. B) Repeated stimulation with phosphopeptides throughout the expansion process of TIL cultures resulted in the restoration of phosphopeptide-specific responses, suggesting positive implications of future use in adoptive cell transfer therapy.

A final experiment was performed to address the presence or loss of phosphopeptide-specific T cell responses throughout the progression of chronic liver disease to hepatocellular carcinoma. Expanded cell cultures from deceased donor livers, livers with end-stage cirrhosis, and livers with the presence of hepatocellular carcinoma nodules were stimulated with the 21 HLA-A*02-specific phosphopeptides and the immune responses measured using intracellular cytokine staining and flow cytometry. The measureable immune responses are depicted below in Figure 4.9.

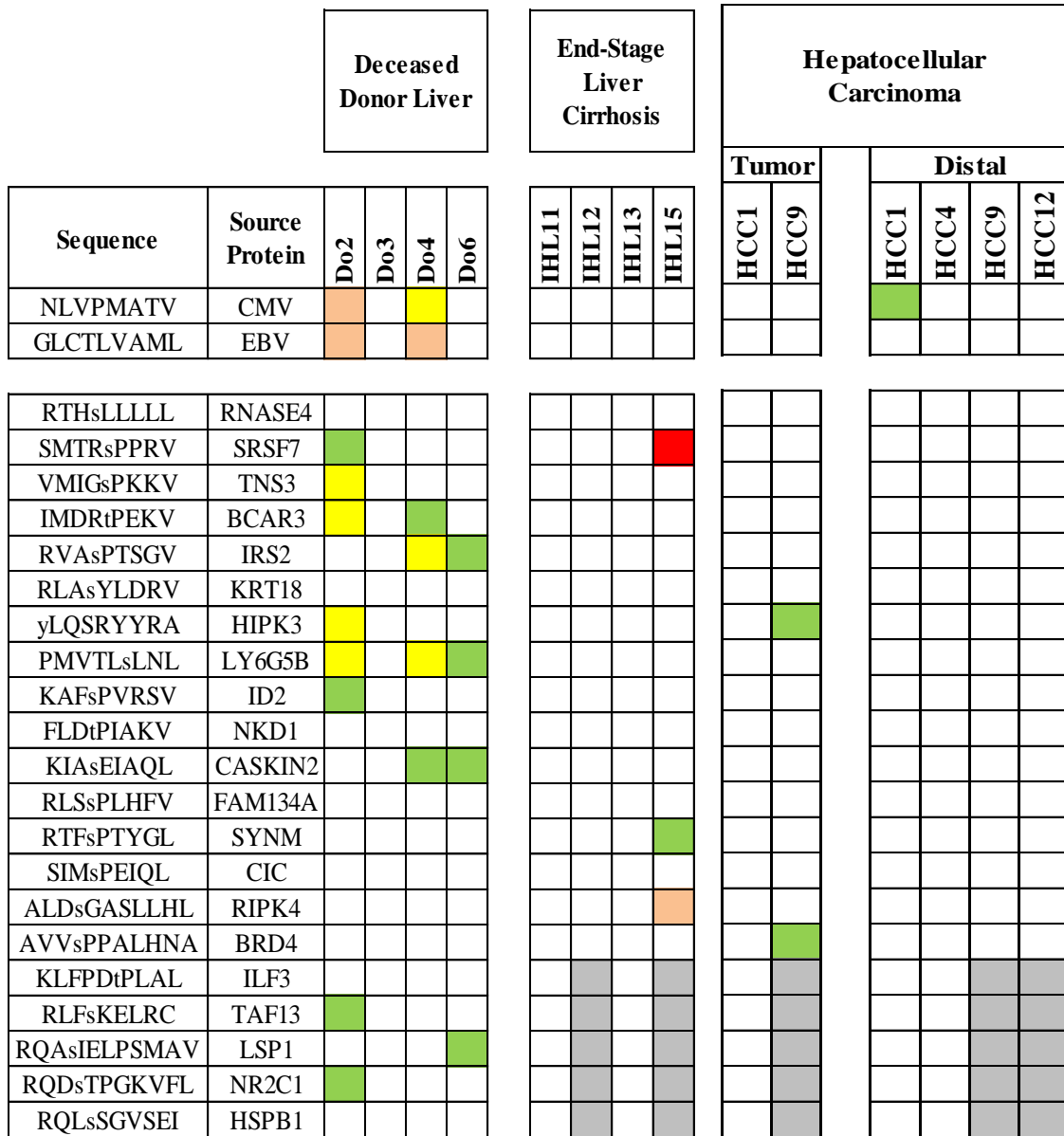


Figure 4.9 Immune responses to phosphopeptide antigens throughout the course of disease progression. Expanded cell cultures from deceased donors, cirrhotic liver tissue, and hepatocellular carcinoma liver tissue were stimulated with the HLA-A*02-specific phosphopeptides and immune responses measured using ICS and flow cytometry. Phosphopeptide-specific immune responses appear to be lost throughout the course of the disease.

Reactivity of CD8 ⁺ T cells	
Not determined	
<0.25%	
0.25-2.5%	
2.5-5.0%	
5-7.5%	
7.5-10%	
10-20%	
>20%	

4.5 Discussion

In this work, we performed a large scale analysis of phosphopeptides presented by HLA class I molecules on the cell surface of liver tissue and a well-characterized hepatoblastoma cell line. Identification of phosphopeptides was achieved through the use of enhanced sample preparatory procedures (desalting via STAGE tips), complementary IMAC enrichment techniques (Fe-IDA and Fe-NTA), and high resolution mass spectrometry. Following identification, the goal of this work was two-fold. First, we sought to analyze the phosphopeptides we identified in terms of tissue expression, presence in varying types of cancer, and relation of source proteins to the development and progression of the disease. Second, we aimed to characterize immunological responses to phosphopeptide antigens in healthy donors, patients with chronic liver disease, and patients with hepatocellular carcinoma in order to elucidate the most ideal targets for the development of novel cancer immunotherapeutics.

Enrichment of a total of five normal tissue samples, seven tumor tissue samples, and one hepatoblastoma cell line resulted in the combined identification of 459 phosphopeptides, 293 of which were tumor-specific (Table 4.2). The majority of the peptides identified were phosphorylated at serine residues (92%) as opposed to threonine (6%) or tyrosine (2%) residues. While serine-threonine kinases are more prevalent than tyrosine kinases, the observation of a lack of peptides with phosphorylated tyrosine residues is further enhanced by the way in which we collect data.²⁴ The use of the triggered instrumentation method in which an ETD scan is only performed if a neutral loss characteristic of a phosphate group is observed in the CAD spectrum, likely

introduces a bias toward identification of peptides with phosphorylated serine and threonine residues. This is due to the fact that CAD fragmentation of peptides with phosphorylated tyrosine residues less commonly results in a highly abundant ion corresponding to the neutral loss of a phosphate group.²⁵ Thus, we are less likely to perform ETD scans of these peptides and the neutral loss program we use to identify spectra containing possible phosphopeptides for analysis is less likely to alert us to the presence of phosphorylated tyrosine residues.

Of the 459 phosphopeptides identified, 423 contained between nine and eleven amino acid residues, the ideal length for favorable binding within the binding cleft of HLA class I molecules.²⁶ Analysis of the sequences of these phosphopeptides revealed that the most common sites for the addition of a phosphate group were positions four through eight in the peptide sequence (Figure 4.2). Specifically, phosphorylation at position four accounted for 67% of all phosphopeptides between nine and eleven amino acid residues in length. These findings are in accordance with Mohammed *et al.* who examined phosphopeptides presented by HLA-A*02 class I molecules. This study revealed that peptides phosphorylated at position 4 showed a notable increase in binding affinity for HLA-A*02 molecules compared to their unphosphorylated counterparts. Additionally, analysis of crystal structures of HLA class I molecules in complex with phosphopeptides illustrated that those phosphorylated at position 4 adopted a conformation in which the phosphate moiety was solvent-exposed and oriented upwards, allowing for direct interaction with T cell receptors of circulating cytotoxic T cells.²⁷

Previous work in our laboratory has involved the analysis of several types of cancer including leukemia, melanoma, colorectal, ovarian, breast, and esophageal, leading to the

identification of a large number of cancer-associated phosphopeptides. Thus, we classified the phosphopeptides we identified in liver cancer based on their presence in previously analyzed cancer samples (Table 4.2). Interestingly, we observed the largest overlap between the phosphopeptides we identified and those observed in colorectal cancer, melanoma, and leukemia (Figure 4.3). Specifically, of the 459 phosphopeptides identified in liver samples, 165, 164, and 94 were previously seen in colorectal cancer, melanoma, and leukemia, respectively. Additionally, 48 of the phosphopeptides we identified were common to all four types of cancer. The presence of certain phosphopeptides in multiple types of cancer further corroborates the notion that dysregulated cell signaling leading to aberrant phosphorylation is a hallmark of cancer in general.²⁸ More importantly, it suggests that immunotherapeutic treatments based on the phosphopeptides we have identified hold the potential to treat hepatocellular carcinoma in addition to many other common types of cancer.

Many of the phosphopeptides we identified originated from source proteins involved in prominent signaling pathways. To further characterize the processes represented by these proteins and their roles in the development and progression of cancer, we utilized the gene analysis tool of the PANTHER classification system.²² This tool enabled us to visualize all of the biological processes in which the source proteins of the phosphopeptides we identified were involved and allowed us to determine which processes were the most represented. As depicted in Figure 4.4, the four most prominent categories observed were metabolic, cellular, biological regulation, and biological adhesion processes, all of which involve signaling pathways that have been shown to go awry in cancer.

Of the 320 source proteins evaluated by PANTHER, 127 were determined to be involved in metabolic processes, an interesting revelation given that in 2011 Hanahan and Weinberg cited reprogramming of cellular energy metabolism as a rapidly emerging hallmark of cancer. Specifically, tumor cells show altered glucose metabolism in that they preferentially utilize glycolysis for ATP production, allowing for satisfaction of their increased energetic and biosynthetic requirements. Alterations in glucose uptake significantly alter downstream signaling pathways. Furthermore, evidence supports that the dysregulation of pathways involved in cellular energy metabolism enables cancer cells to undergo continuous cell growth and proliferation, ultimately contributing to oncogenesis.^{29,30}

The second most prominent category of biological processes represented was cellular processes, including proteins involved in the cell cycle, cell proliferation, cellular component movement, cytokinesis, and cell communication. As discussed in chapters one and three, dysregulation of protein kinase activity in cellular signaling pathways is a key indicator of malignant transformation. Thus, it was not unexpected that many of the source proteins associated with involvement in cellular processes were shown to be protein kinases or proteins associated with kinase-mediated signaling pathways. For example, many proteins involved in the mitogen-activated protein kinase (MAPK) signaling pathway were identified including: death domain-associated protein 6 (DAXX), heat shock protein beta-1 (HSPB1), transcription factor AP-1 (JUN), ribosomal protein S6 kinase alpha-1 (RPS6KA1), RAF proto-oncogene serine/threonine-protein kinase (RAF1), mitogen-activated protein kinase kinase kinase 11 (MAP3K11), and mitogen-activated protein kinase kinase kinase 3 (MAP3K3). MAPK pathways largely control

fundamental cellular processes such as growth, proliferation, differentiation, migration, and apoptosis.³¹ Overexpression or activation of key components in the MAPK pathway has been largely linked to cancer progression in solid tumors as activation of this pathway triggers many downstream phosphorylation events which serve to regulate cellular activity. In hepatocellular carcinoma specifically, MAPK pathways are known to be constitutively activated, leading to aberrant phosphorylation and promoting tumorigenesis.³²

Following the analysis of the phosphopeptides we identified from liver tissue samples and the hepatoblastoma cell line, we aimed to evaluate their significance in terms of the ability to elicit an immunological response. Upon consideration of previous identification in other cancer types, tissue expression, source protein relation to cancer, and HLA allele-specificity, we selected 21 phosphopeptides for further biological testing. These phosphopeptides are HLA-A*02-specific, the most common allele in the US Caucasian population, and are representative of source proteins involved in signaling pathways known to go awry in cancer. Additionally, 20 of these phosphopeptides have been previously detected in other cancer types including leukemia, melanoma, colorectal, ovarian, breast, and esophageal cancers and all were shown to be tumor-specific or tumor-associated.

The ability of the 21 selected phosphopeptides to elicit an immune response in HLA-A*02-positive healthy donors and patients with hereditary hemochromatosis (HH) was assessed using intracellular cytokine staining assays. By measuring the expression of certain cytokines and a marker for degranulation following seven days of stimulation with antigens, we were able to view the cytotoxic potential of each phosphopeptide.

Overall, stimulation of PBMCs from healthy donors and patients with chronic liver disease by these phosphopeptides revealed immunological responses similar in magnitude to those of viral peptide epitopes and identified several candidates for future investigation.

For instance, the phosphopeptide RLAsYLDRV showed the ability to stimulate a large immune response in a patient with hereditary hemochromatosis. This phosphopeptide is derived from the protein keratin-18 (KRT18), a member of the keratin family of proteins which play a large role in filament reorganization. Interestingly, studies have shown that keratin-18 expression levels in the liver increase three-fold in response to injury and that keratin proteins in general become increasingly post-translationally modified in response to cellular stress. Mounting evidence also suggests that keratin proteins play an active role in cancer cell invasion and metastasis. For example, transfection of KRT8 and KRT18 is associated with altered cell shape and increased cell migration in mice and expression increases the invasion and migratory potential of human melanoma and breast cancer cells *in vitro*.³³ Given the association of this protein with cancer and the fact that we identified a representative phosphopeptide in hepatocellular carcinoma tissue and previously analyzed colorectal cancer samples leads us to believe that this phosphopeptide may represent an ideal target for immunotherapeutics.

Another example of a strong immunotherapeutic candidate is the phosphopeptide RVAsPTSGV, originating from the insulin receptor substrate 2 (IRS2) protein. IRS proteins play a major role in regulating cell growth, metabolism, survival, and differentiation as they are adapters that link signaling from growth factors and cytokine

receptors to SH2-containing signaling proteins. Additionally, regulation of IRS proteins is controlled by phosphorylation of serine, threonine, and tyrosine residues. For instance, early events in insulin and insulin-like growth factor (IGF) pathways involve tyrosine phosphorylation of IRS1 and IRS2 which leads to the activation of multiple signaling pathways. In hepatocellular carcinoma specifically, expression levels of IRS2 are largely increased and dysregulation in IGF pathways is linked to the development and progression of the disease. Furthermore, the RVAsPTSGV phosphopeptide is expressed in high levels in mitotically-active tumor cells and has been detected in melanoma, colorectal, and ovarian cancers. These findings in addition to the ability of this phosphopeptide to stimulate an immune response indicate that immunotherapeutic treatments based on this target have the potential to treat a wide variety of cancers.^{34,35}

Of the 21 phosphopeptides tested, 11 showed the ability to stimulate immune responses. Additionally, multiple patients with hereditary hemochromatosis (HH2 and HH6) showed responses to several of the phosphopeptides tested. Interestingly, measureable immune responses in the five healthy donors tested were absent. However, previous work in our laboratory has shown immunological responses to phosphopeptides identified in a wide array of cancers in many healthy donors.³⁶ This finding could be attributed to the difference in age of previously tested healthy donors and those tested in this work. Previously identified immune responses were largely prevalent in middle-aged healthy donors; however, our cohort of healthy donors showed a mean age of approximately 26 years. The absence of an immunological response in these individuals suggests that they may be too young to have been exposed to the phosphopeptide antigens tested whereas patients with underlying chronic liver disease, which predisposes

for the development of HCC, are much older and show measurable immunological responses in 60% of cases. Further investigation of this phenomenon is warranted to fully understand the role that the phosphopeptide antigens identified in hepatocellular carcinoma may play in the development of cancer immunotherapeutics.

In addition to evaluation of immunological significance of the identified phosphopeptide antigens, preliminary steps were taken to show their potential for use in adoptive cell transfer (ACT) therapies aimed at targeting hepatocellular carcinoma. The basic principle of ACT, which will be discussed in more detail in chapter 5, involves the removal of autologous immune cells from patients, *in vitro* expansion, and transfer back into the patient in hopes of inducing cancer-specific killing. The ultimate goal of these experiments was to examine if phosphopeptide-specific immune responses could be found in tumor-infiltrating lymphocytes (TILs), or the liver compartment in general, from patients with HCC, a necessity for ACT treatments centered on tumor-specific phosphopeptide antigens.

Using a rapid expansion protocol (REP)³⁷, our collaborators expanded intrahepatic lymphocyte (IHL) and TIL cultures derived from explanted, resected, or deceased donor liver tissues. Following expansion, the reactivity of the cultures to phosphopeptide antigens was assessed, illustrating a loss of immune responses compared to pre-expansion screens (Figure 4.8). Interestingly, T cell-reactivity to viral epitopes was maintained during the expansion process. These results indicate that large-scale expansion of T cells in a non-directed manner might lead to overgrowth of virus-specific and tumor-nonspecific T cells in comparison to tumor-specific T cells, a possible explanation as to why ACT using autologous T cells fails to result in clinical responses in some cases.³⁸

However, when lymphocyte cultures were repeatedly stimulated with a phosphopeptide pool prior to and during the expansion process, phosphopeptide-specific immune responses were restored. These data provide a basis for ideal conditions for future use of phosphopeptide-mediated ACT treatment of hepatocellular carcinoma.

Finally, we examined the presence of phosphopeptide-specific immune responses in patients tracking with the course of disease progression from chronic liver disease to full-blown hepatocellular carcinoma (Figure 4.9). Large immune responses were seen in many of the deceased donor liver cell cultures, most of which arose from healthy liver tissue. This could be attributed to the age-associated presence of immune responses mentioned previously. The donors from whom these livers originated could have been much older than our previously analyzed control group of healthy donors, of which the mean age was 26 years. Few immune responses were observed in patients with end-stage liver cirrhosis and even less in patients with hepatocellular carcinoma. These data corroborate the basis of the immunoediting theory, in that the ability of the immune system to recognize and trigger specific killing of malignant cells is lost during the progression of healthy cells to a cancerous state.³⁹ In the case of HCC, tumor growth is likely accompanied by immunosuppressive factors within the tumor microenvironment, leading to the disappearance of phosphopeptide-specific immune responses and demonstrating the need to enhance immunity toward these antigens as a future immunotherapeutic strategy.

Future work on this project will involve the analysis of additional liver tissue samples from patients in varying stages of disease to further understand the role that dysregulation of the phosphoproteome plays in the development and progression of hepatocellular

carcinoma. Additionally, further investigations into the immunological significance of the identified phosphopeptides need to be performed. Recently, we selected 21 HLA-B*07-specific phosphopeptides for synthesis based on their tissue specificity and source protein relation to cancer. Studies are currently underway testing immunological responses to these phosphopeptide antigens in PBMCs and TILs from donors in hopes of determining additional candidates for therapeutics which could potentially treat a different portion of the population. Ultimately, we believe that our enrichment and identification process of tumor-associated phosphopeptides and subsequent evaluation of their biological activity results in the identification of strong candidates for the development of novel cancer immunotherapeutics.

4.6 References

1. El-Serag HB, Rudolph KL. Hepatocellular carcinoma: epidemiology and molecular carcinogenesis. *Gastroenterology*. 2007; 132(7): 2557-2576.
2. El-Serag HB. Epidemiology of viral hepatitis and hepatocellular carcinoma. *Gastroenterology*. 2012; 142(6): 1264-1273.
3. El-Serag HB. Hepatocellular carcinoma. *NEJM*. 2011; 365: 1118-1127.
4. De Minicis S, Marzioni M, Benedetti A, Svegliati-Baroni G. New insights in hepatocellular carcinoma: from bench to bedside. *Ann. Transl Med*. 2013; 1(2): 15.
5. American Cancer Society. *Cancer Facts & Figures 2014*. Atlanta: American Cancer Society; 2014.
6. Tsuchiya N, Sawada Y, Endo I, Saito K, Uemura Y, Nakatsura T. Biomarkers for the early diagnosis of hepatocellular carcinoma. *World J Gastroenterol*. 2015; 21(37): 10573-10583.
7. Chih-Yi Sun V, Sama L. Symptom management in hepatocellular carcinoma. *Clin J Oncol Nurs*. 2008; 12(5): 759-766.
8. Sherman M. Hepatocellular carcinoma: epidemiology, risk factors, and screening. *Semin Liver Dis*. 2005; 25(2): 143-154.
9. Sanyal AJ, Yoon SK, Lencioni R. The etiology of hepatocellular carcinoma and consequences for treatment. *Oncologist*. 2010; 15: 14-22.
10. Pellicoro A, Ramachandran P, Iredale JP, Fallowfield JA. Liver fibrosis and repair: immune regulation of wound healing in a solid organ. *Nat Rev Immunol*. 2014; 14(3): 181-194.
11. Farazi PA, DePinho RA. Hepatocellular carcinoma pathogenesis: from genes to environment. *Nat Rev Cancer*. 2006; 6(9): 674-687.
12. Di Bisceglie AM. Hepatitis B and hepatocellular carcinoma. *Hepatology*. 2009; 49(5): 56-60.
13. Goossens N, Hoshida Y. Hepatitis C virus-induced hepatocellular carcinoma. *Clin Mol Hepatol*. 2015; 21(2): 105-114.
14. Forner A, Llovet JM, Bruix J. Hepatocellular carcinoma. *Lancet*. 2012; 379: 1245-1255.
15. Cho YK, Kim JK, Kim MY, Rhim H, Han JK. Systematic review of randomized trials for hepatocellular carcinoma treated with percutaneous ablation therapies. *Hepatology*. 2009; 49(2): 453-459.
16. Yamakado K, Takaki H, Nakatsuka A, Yamaknaka T, Fujimori M, Hasegawa T, Uraki J. Radiofrequency ablation for hepatocellular carcinoma. *Gastrointest Interv*. 2014; 3(1): 35-39.
17. Vogl TJ, Sangos S, Balzer JO, Nabil M, Rao P, Eichler K, Bechstein WO, Zuezem S, Abdelkader A. Transarterial chemoembolization (TACE) in hepatocellular carcinoma: technique, indication, and results. *Rofo*. 2007; 179(11): 1113-1126.
18. Keating GM, Santoro A. Sorafenib: a review of its use in advanced hepatocellular carcinoma. *Drugs*. 2009; 69(2): 223-240.

19. "Nexavar." Web. 10 Apr. 2016.
20. Breous E, Thimme R. Potential of immunotherapy for hepatocellular carcinoma. *J Hepatol.* 2011; 54: 830-834.
21. Pardee AD, Butterfield LH. Immunotherapy of hepatocellular carcinoma. *Oncoimmunol.* 2012; 1(1): 48-55.
22. Mi H, Poudel S, Muruganujan A, Casagrande JT, Thomas PD. PANTHER version 10: expanded protein families and functions, and analysis tools. *Nucl Acids Res.* 2016; 4(44): D336-342.
23. Gonzalez-Galarza FF, Takeshita LY, Santos EJ, Kempson F, Maia MH, Silva AL, Ghattoaraya GS, Alfirevic A, Jones AR, Middleton D. Allele frequency net 2015: update: new features for HLA epitopes, KIR and disease and HLA adverse drug reaction associations. *Nucl Acids Res.* 2015; 28: D784-788.
24. Ubersax JA, Ferrell JE Jr. Mechanisms of specificity in protein phosphorylation. *Nat Rev Mol Cell Biol.* 2007; 8(7): 530-541.
25. Palumbo AM, Smith SA, Kalcic CL, Dantus M, Stemmer PM, Reid GE. Tandem mass spectrometry strategies for phosphoproteome analysis. *Mass Spectrom Rev.* 2011; 30(4): 600-625.
26. Murphy K. (2012) *Janeway's Immunobiology*, 8th edition. New York, NY: Garland Science.
27. Mohammed F, Cobbold M, Zarling AL, Salim M, Barrett-Wilt GA, Shabanowitz J, Hunt DF, Engelhard VH, Willcox BE. Phosphorylation-dependent interaction between antigenic peptides and MHC class I: a molecular basis for the presentation of transformed self. *Nat Immunol.* 2008; 9: 1236-1243.
28. Zarling AL, Ficarro SB, White FM, Shabanowitz J, Hunt DF, Engelhard VH. Phosphorylated peptides are naturally processed and presented by major histocompatibility complex class I molecules in vivo. *J Exp Med.* 2000; 192(12):1755-1762.
29. Hanahan D, Weinberg RA. Hallmarks of cancer: the next generation. *Cell.* 2011; 144(5):646-674.
30. Hirshcey MD, DeBerardinis RJ, Diehl AM, Drew JE, Frezza C, Green MF, Jones LW, Ko YH, Le A, Lea MA, Locasale JW, Longo VD, Lyssiotis CA, McDonnell E, Mehrmohamadi M, Michelottie G, Muralidhar V, Murphy MP, Pedersen PL, Poore B, Raffaghello L, Rathmell JC, Sivanand S, Vander Heiden MG, Wellen KE, Target Validation Team. Dysregulated metabolism contributes to oncogenesis. *Semin Cancer Biol.* 2015; 35: S129-150.
31. Dhillon AS, Hagan S, Rath O, Kolch W. MAP kinase signaling pathways in cancer. *Oncogene.* 2007; 26: 3279-3290.
32. Whittaker S, Marais R, Zhu AX. The role of signaling pathways in the development and treatment of hepatocellular carcinoma. *Oncogene.* 2010; 29: 4989-5005.
33. Karantza V. Keratins in health and cancer: more than mere epithelial cell markers. *Oncogene.* 2011; 30(2): 127-138.
34. Zarling AL, Obeng RC, Desch AN, Pinczewski J, Cummings KL, Deacon DH, Conaway M, Slingluff Jr. CL, Engelhard VH. MHC-restricted phosphopeptides derived from insulin receptor substrate-2 and CDC25b offer broad-based immunotherapeutic agents for cancer. *Cancer Res.* 2014; 74(23): 6784-6795.

35. Boissan M, Beurel E, Wendum D, Rey C, Lecluse Y, Housset C, Lacombe M, Desbois-Mouthon C. Overexpression of insulin receptor substrate-2 in human and murine hepatocellular carcinoma. *Am J Pathol*. 2005; 167(3): 869-877.
36. Cobbold M, De La Pena H, Norris A, Polefrone J, Qian J, English AM, Cummings K, Penny S, Turner JE, Cottine J, Abelin JG, Malaker SA, Zarling AL, Huang H, Goodyear O, Freeman S, Shabanowitz J, Pratt G, Craddock C, Williams ME, Hunt DF, Engelhard VH. MHC class-I associated phosphopeptides are the targets of memory-like immunity in leukemia. *Sci Transl Med*. 2013; 5(203): 203ra125.
37. Dudley ME, Wunderlich JR, Shelton TE, Even J, Rosenberg SA. Generation of tumor-infiltrating lymphocyte cultures for use in adoptive transfer therapy for melanoma patients. *J Immunother*. 2003; 26(4): 332-342.
38. Rosenberg SA, Yang JC, Sherry RM, Kammula US, Hughes MS, Phan GQ, Citrin DE, Restifo NP, Robbins PF, Wunderlich JR, Morton KE, Laurencot CM, Steinberg SM, White DE, Dudley ME. Durable complete responses in heavily pretreated patients with metastatic melanoma using T-cell transfer immunotherapy. *Clin Cancer Res*. 2011; 17(13): 4550-4557.
39. Dunn GP, Bruce AT, Ikeda H, Old LJ, Schreiber RD. Cancer immunoediting: from immunosurveillance to tumor escape. *Nat Immunol*. 2002; 3(11):991-998.

Chapter 5: Conclusions and Future Applications

The research presented in this dissertation focuses on the enrichment and identification of tumor-specific, HLA-associated phosphopeptides using improved sample preparatory techniques and high resolution mass spectrometry. We believe that the phosphopeptides we identify arise from aberrant phosphorylation as a result of dysregulated cellular signaling events linked to the progression and development of cancer. Furthermore, these tumor-specific phosphopeptides have likely not been subjected to central tolerance by the immune system; thus, their presentation by HLA class I molecules to circulating cytotoxic T cells should elicit a significant immune response. Therefore, we believe that our phosphopeptide antigens represent ideal candidates for the development of novel cancer immunotherapeutics which harness an individual's own immune system to target and eliminate cancer.

Prior to identification of tumor-specific phosphopeptides, we sought to improve the current methodology for HLA-associated peptide sample cleanup for subsequent enrichment and mass spectrometric analysis. To do this, we developed a protocol for the use of STop And Go Extraction (STAGE) tips as a robust, sensitive, off-line methodology to replace C18 microcapillary cleanup columns. In doing this, we allowed for the direct elution of peptides bound to HLA class I molecules onto STAGE tips and regularly achieved recoveries of internal peptide standards ranging from 70% to 95%. Additionally, we demonstrated that the implementation of STAGE tips in place of the current method for sample cleanup allowed for 1) decreased sample loss and increased peptide recoveries, 2) a shortened sample cleanup procedure from two days to less than

two hours, and 3) the ability for sample multiplexing in which many samples can be cleaned up in entirety at once.

For improved phosphopeptide enrichment, we compared the use of two immobilized metal affinity chromatography (IMAC) techniques – iron (III) iminodiacetic acid (Fe-IDA) and iron (III) nitrilotriacetic acid (Fe-NTA) IMAC– for enrichment of a human hepatocellular carcinoma tumor tissue sample. This resulted in the identification of a combined total of 262 phosphopeptides from the tumor sample, the largest number of phosphopeptides identified from a single sample in our laboratory to date. Our experiments demonstrated that the tetradentate nature of metal binding to the NTA resin led to decreased nonspecific binding and increased phosphopeptide recovery. Additionally, through sequence analysis of the identified phosphopeptides, we showed that both resins enrich for unique sets of phosphopeptides. Specifically, Fe-IDA was shown to enrich for phosphopeptides with increased numbers of basic amino acid residues, likely a factor of metal dissociation from the resin and the partial transformation to an ion-exchange column. Ultimately, we demonstrated that Fe-IDA and Fe-NTA IMAC techniques are complementary in nature and that their application to tissue samples can provide a more complete representation of the HLA-associated phosphopeptides present.

Finally, we subjected five normal liver tissue samples, seven hepatocellular carcinoma tumor tissue samples, and one hepatoblastoma cell line to the improved sample cleanup procedure, complementary IMAC enrichment techniques, and high resolution mass spectrometry. This led to the identification of 459 HLA-associated phosphopeptides, many of which originate from proteins involved in signaling pathways

known to go awry in cancer. We then selected 21 HLA-A*02-specific phosphopeptides for synthesis and evaluated their ability to elicit an immune response in healthy donors, patients with hereditary hemochromatosis, and patients with hepatocellular carcinoma. Ultimately, we showed that measurable immune responses do exist upon stimulation with our phosphopeptide antigens and that these responses reside in the central memory compartment. These data suggest that the phosphopeptides we have identified may be targets of cancer immune surveillance and therefore represent ideal candidates for use in the development of novel cancer immunotherapeutics.

To fully grasp the impact that our findings have for the potential eradication of cancer, it is necessary to first understand the mechanisms by which these phosphopeptides could be used in a clinical setting. The concept of cancer treatment poses a great challenge to both oncologists and scientific researchers worldwide. While surgery is often an effective treatment option, it is not always viable. Additionally, the two most common methods of treatment, chemotherapy and radiation, are highly non-specific in that they are unable to distinguish between healthy and cancerous tissues. Given the shortcomings of classical cancer treatments and the advancements in immunological research, immunotherapy has become a promising frontier in the search for new, more effective, targeted approaches towards eliminating cancer.¹ These immunotherapies include peptide-based vaccines,² adoptive cell transfer (ACT),³ genetically-engineered T cells,⁴ chimeric antigen receptors (CARs),⁵ and immune-mobilizing monoclonal T cell receptors against cancer (ImmTACs).⁶

Perhaps the most logical extension of this work lies in the incorporation of our tumor-specific phosphopeptides into peptide-based vaccines. Peptide vaccination involves the

injection of tumor-associated antigens (TAAs) into cancer patients in hopes of inducing a systemic immune response. This immune response may then aid in the elimination of cancer growing in tissues throughout the body.² The most obvious advantage of peptide-based vaccines is the ease of synthesis combined with a low manufacturing cost, both of which are rare in comparison to most immunotherapeutic options. Furthermore, peptide-based vaccines are effective at inducing CD8⁺ or CD4⁺ T cell responses in humans, allow for the use of defined antigens as opposed to uncharacterized antigens which may induce autoimmune reactions, and present with little-to-no side effects.⁷

Melanoma is undoubtedly the most commonly studied form of cancer and has shown promising results in the context of peptide-based vaccination. Multiple studies have shown that vaccination with the protein gp100, a melanoma-associated antigen expressed at low levels in melanocytes and high levels in most melanomas, can elicit cytotoxic T cell HLA-A2.1 restricted immune responses.^{8,9,10} Additionally, recent studies have shown that administering a gp100 vaccine combined with doses of Interleukin 2 (IL-2), a cytokine signaling molecule, leads to a reduction in tumor size and prolonged progression-free survival in patients with advanced melanoma.¹¹

Despite promising results in a limited number of cancer types, the use of peptide-based vaccines for cancer treatment has been largely unsuccessful and rarely leads to a significant positive clinical outcome.¹² Moreover, several inherent disadvantages are associated with the use of peptide-based vaccines. These include HLA-restrictions that limit the possibility of a widely applicable vaccine, rapid degradation of injected peptides by peptidases prior to eliciting an immune response, and elicited immune responses too low in magnitude to generate effective tumor clearance.⁷ Significant research is still

underway in increasing the effectiveness of peptide-based vaccines, leading us to believe that our tumor-specific phosphopeptides could still be of great value using this approach; however, alternative treatment options need to be considered.

One of the major obstacles of cancer immunotherapy is the ability to overcome the harsh tumor microenvironment. T cells specific to antigens expressed within a tumor migrate to the tumor site and are known as tumor-infiltrating lymphocytes (TILs). Despite this, tumors still persist. This suggests that TILs are in some way inhibited from tumor eradication. It is likely that TILs are being constantly bombarded with immunosuppressive factors, such as cytotoxic T lymphocyte antigen 4 (CTLA4) and programmed cell death protein 1 (PD1), rendering them ineffective. However, the removal of TILs from this destructive environment, as in adoptive cell transfer (ACT), allows for the *in vitro* expansion to more favorable numbers and increases their effectiveness within the tumor.⁵

Adoptive cell transfer has gained much attention since its debut by Rosenberg and colleagues in the early 1980s.¹³ This immunotherapy involves resection and fragmentation of a tumor, activation of T cells by a growth factor, selection and expansion of T cells displaying the desired T cell receptor (TCR) specificity, and transfer of these T cells back into a cancerous host. Adoptively transferred T cells with TCRs specific to known cancer antigens can then traffic to the tumor site and aid in its destruction. Patients can also undergo lymphodepletion, the temporary ablation of the immune system, by chemotherapy alone or in conjunction with total-body irradiation, prior to the transfer of cells back into the body. This methodology, depicted in Figure 5.1, has been shown to prolong tumor eradication in patients with various cancers.⁵

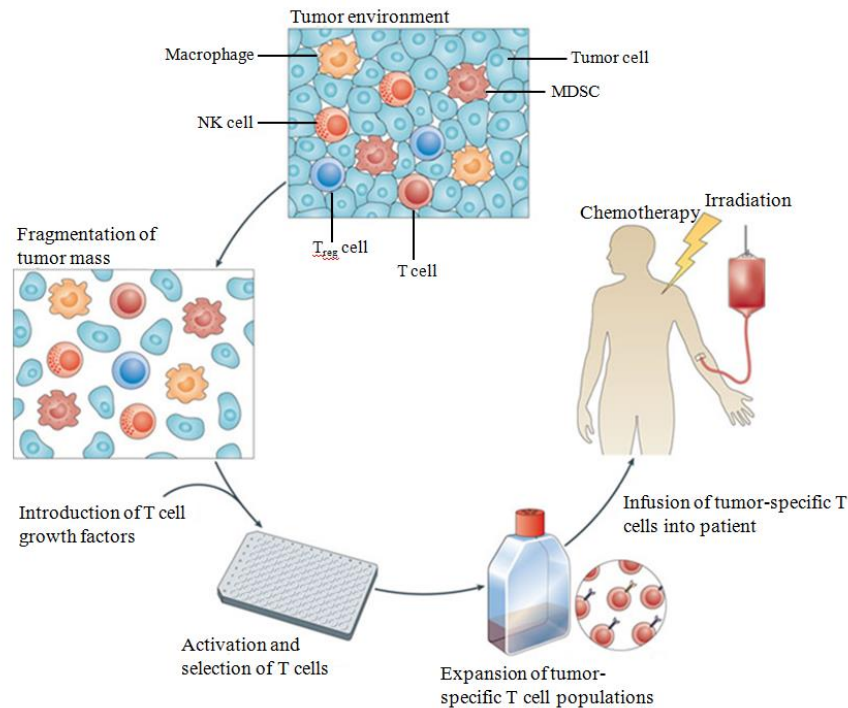


Figure 5.1 Process of adoptive cell transfer (ACT). Tumor masses are surgically removed and fragmented. T cells are incubated with T cell growth factors, such as IL-2. T cell populations with the desired TCR specificity are selected, isolated, and expanded prior to infusion back into the patient to be treated. Prior to this, the patient may undergo a lymphodepleting preparative regimen. Figure adapted from reference 5.

Rosenberg *et al.* treated patients with metastatic melanoma, who had undergone extensive lymphodepletion, with adoptive cell transfer utilizing autologous TILs in conjunction with interleukin-2. Out of the 93 patients treated, 20 (22%) achieved complete tumor regression with 19 patients showing ongoing complete regressions extending to 3 years and effectively demonstrating that TILs can mediate long-lasting complete responses.¹⁴ We believe that the phosphopeptides we have identified represent excellent targets for adoptive cell transfer given that they are 1) solely or overly expressed in tumor tissue, 2) have not been subjected to central tolerance by the immune system,¹⁵ and 3) demonstrate biological activity in healthy individuals. Therefore, T cells

in patients that recognize these phosphopeptides could be isolated using HLA tetramer technology and selectively expanded prior to reintroduction into the body, potentially allowing for phosphopeptide-specific T cell-mediated killing of tumor tissue.¹⁶

An alternative to traditional ACT, involves the incorporation of genetically engineered TCRs or TCR-like biomolecules (Figure 5.2) to enhance T cell-mediated killing of tumor tissues. In this approach, autologous T cells can be removed from a patient presenting with a tumor that expresses an antigen recognized by an available TCR structure. These T cells can then be engineered in a variety of ways. One method begins by removing and cloning T cells from a separate individual who shows positive antitumor responses targeting that specific antigen. Their TCRs can then be cloned and inserted into a viral vector which

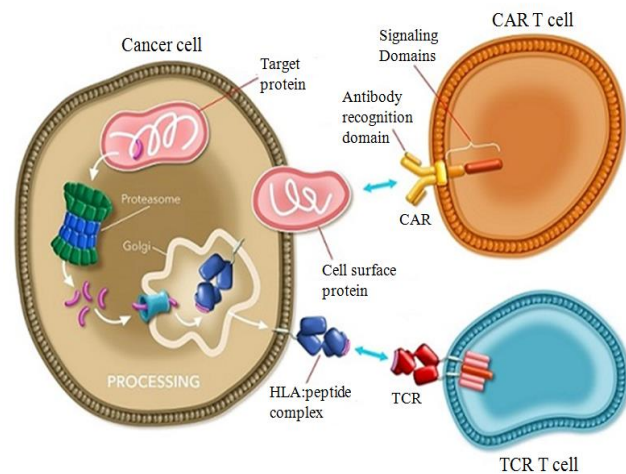


Figure 5.2 Genetically-engineered TCRs and TCR-like biomolecules. T cells can be genetically engineered to express TCRs with specificity to a known tumor antigen in the context of HLA molecules. Alternatively, TCRs can be equipped with chimeric antigen receptors (CARs) which have antibody-like specificities and recognize cell surface proteins in a non-HLA-restricted manner. Figure adapted

can be used to infect the autologous T cells from the patient to be treated.

Alternatively, TCRs can be isolated from mice that have been immunized with the target antigen. T cells specific to this antigen can then be isolated, their TCRs cloned into viral vectors, and used to infect autologous T cells in the same manner as previously described. In both instances, the newly-engineered T cells can then be injected back into the patient for treatment.⁵ These methodologies have been used to target a variety of

malignancies, including leukemia and colorectal cancers.^{17,18,19} However, an inherent disadvantage of using genetically engineered T cells lies in the fact that they can only be used in a subset of patients due to their HLA-restricted nature. In order to combat this, researchers have turned to genetically engineering T cells with chimeric antigen receptors (CARs) which function in a non-HLA-restricted manner.⁴

Chimeric antigen receptors are comprised of an extracellular antigen-specific single-chain antibody variable fragment (scFv) coupled to an intracellular signaling domain via hinge and transmembrane domain regions. The function of CARs is to recognize native antigens, which are generally molecules displayed on the cell surface.⁴ The most commonly targeted antigen by CARs is CD19, a cell-surface marker present on most B cell malignancies. CAR T cell technology targeting CD19 has been shown effective in treating several B-cell malignancies, including acute lymphoblastic leukemia (ALL) and chronic lymphoid leukemia (CLL).^{20,21} However, because CD19 is also expressed on normal B-cells and B-cell precursors, patients who undergo this treatment commonly experience eradication of normal B cells for as long as the treatment persists.²¹ Additionally, using CARs to target cell surface molecules limits the applicability of this technology based on the estimation that only about 20% of available targets are cell surface markers.⁴ Therefore, the use of genetically engineered TCRs, especially in terms of phosphopeptide recognition, offers a distinct advantage over CARs in that it has the potential to target a portion of the remaining 80% of available targets and can truly be tumor-specific. Alternatively, a combinatorial treatment of genetically engineered TCRs targeting HLA-associated phosphopeptides and CARs targeting cell surface markers may be a beneficial approach in order to realize the full curative potential of ACT.

A final application of our tumor-specific phosphopeptides may lie in the development of novel immune-mobilizing monoclonal TCRs against cancer (ImmTACs). ImmTACs are bispecific reagents comprised of a targeting system (soluble, affinity-enhanced TCR) fused to an effector function (anti-CD3 scFv). The mechanism by which ImmTACs work involves four main steps, as depicted in Figure 5.3. First, the TCR region of the ImmTAC recognizes and binds to an HLA:peptide complex displayed on the surface of a cancer cell. This allows for the recruitment of circulating cytotoxic T cells (CTLs) to the tumor site through the interaction with the free end of the ImmTAC molecule via binding to CD3 receptors on the T cell surface. These two events lead to the formation of an optimized immune synapse with the ImmTAC molecule acting as a bridge between the infected cell and the T cell. This redirected T cell is then activated via intracellular signaling and releases the cytotoxic contents of its granules, leading to the destruction of the cancer cell.⁶ Various clinical trials, led by Immunocore (Abingdon, UK), are currently underway using ImmTACs specific to gp100 epitopes in the treatment of melanoma.^{23,24}

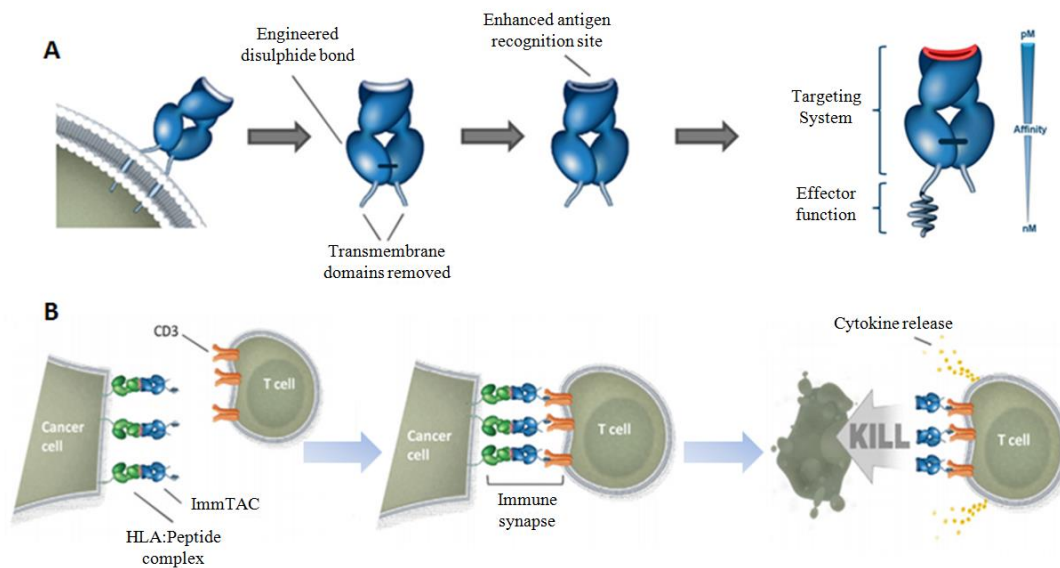


Figure 5.3 ImmTAC generation and mechanism of action. A) Generation of ImmTACs involves incorporation of a disulphide bond and removal of the transmembrane domains of the TCR. Phage display is used to produce an enhanced affinity recognition binding site. The resulting molecule is fused to an effector function resulting in a soluble, bispecific reagent. B) The enhanced affinity TCR portion of ImmTACs specifically binds to a target HLA:peptide complex on the cancer cell surface. T cells are redirected towards the cancer cell, bind to the free end of the ImmTAC via the anti-CD3 scFv portion, and form an optimized immune synapse. Intracellular signaling leads to activation of the T cells and lytic granules are released to kill the cancer cell. Image adapted from reference 6.

ImmTACs are advantageous due to their ability to overcome several barriers of alternative immunotherapies. To begin, ImmTACs contain enhanced, high-affinity antigen recognition sites. These are generated using phage display where mutations are introduced to varying numbers of the complementary determining regions (CDRs) of the TCR. TCRs displaying the highest affinity for the antigen of interest are then selected. This often results in TCRs with picomolar affinities for antigen as opposed to the micromolar affinities of naturally-occurring TCRs. This drastic improvement in affinity

results in enhanced sensitivity, allowing ImmTACs to recognize antigens and trigger activation of T cells at levels as low as 10 copies of antigen per cell. A second advantage of ImmTACs is their ability to render any T cell capable of killing an infected cell regardless of its intrinsic antigen recognition capabilities. This is possible because of the anti-CD3-scFv portion of the ImmTAC which can potentially bind to any T cell in the area and trigger signal-mediated killing of cancer cells.⁶

Despite the promise of ImmTACs as a viable cancer treatment, an obvious downside lies in the fact that targeted antigens must be entirely tumor-specific. Restriction of antigens to tumor tissue is of the utmost importance to avoid sometimes fatal, on-target effects of ImmTAC binding to the target antigen on normal tissue.^{6,25} While the phosphopeptides we have identified in hepatocellular carcinoma could be of great value in the development of ImmTAC-based therapies, it is imperative that their expression in normal tissues be extensively evaluated. Although we did analyze healthy tissue, our samples were not fully representative of normal cells present throughout the entire body. Therefore, exhaustive tissue expression studies need to be completed to definitively label these phosphopeptides as entirely tumor specific prior to their incorporation into ImmTAC-based therapies.

Our analysis of hepatocellular carcinoma tumor tissue and an immortalized hepatoblastoma cell line gave rise to hundreds of potential candidates for the development of novel cancer immunotherapeutics. Furthermore, biological testing of several promising phosphopeptide candidates revealed the ability of these antigens to stimulate significant immune responses in healthy donors and patients with chronic liver disease. Given the advances in immunological research and the new developments in the

field of immunotherapy, we believe that the tumor-specific, HLA-associated phosphopeptides we have identified hold enormous promise for the development of improved cancer treatment options.

5.1 References

1. Schuster M, Nechansky A, Loibner H, Kircheis R. Cancer Immunotherapy. *Biotechnol.* 2006; 1: 138-147.
2. Parmiani G, Castelli C, Dalerba P, Mortarini R, Rivoltini L, Marincola FM, Anichini A. Cancer immunotherapy with peptide-based vaccines: what have we achieved? Where are we going? *J Natl Cancer Inst.* 2002 94(11): 805-818.
3. Gattinoni L, Powell DJ, Rosenberg SA, Restifo NP. Adoptive immunotherapy for cancer: building on success. *Nat Rev Immunol.* 2006; 6(5): 383-393.
4. Kershaw MH, Westwood JA, Darcy PK. Gene-engineered T cells for cancer therapy. *Nat Rev Cancer.* 2013; 13: 525-541.
5. Restifo NP, Dudley ME, Rosenberg SA. Adoptive immunotherapy for cancer: harnessing the T cell response. *Nat Rev Immunol.* 2012; 12: 269-281.
6. Oates J, Hassan NJ, Jakobsen BK. ImmTACs for targeted cancer therapy: Why, what, how, and which. *Mol Immunol.* 2015; 67(2A): 67-74.
7. Slingluff CL. The present and future of peptide vaccines for cancer: single or multiple, long or short, alone or in combination? *Cancer J.* 2011; 17:343-350.
8. Bakker AB, Schreurs MW, Tafazzul G, de Boer AJ, Kawakami Y, Adema GJ, Figdor CG. Identification of a novel peptide derived from the melanocyte-specific gp100 antigen as the dominant epitope recognized by an HLA-A2.1-restricted anti-melanoma CTL line. *Int J Cancer.* 1995; 62(1): 97-102.
9. Rosenberg SA, Yang JC, Schwartzentruber DJ, Hwu P, Marincola FM, Topalian SL, Restifo NP, Dudley ME, Schwarz SL, Spiess PJ, Wunderlich JR, Parkhurst MR, Kawakami Y, Seipp CA, Einhorn JH, White DE. Immunologic and therapeutic evaluation of a synthetic peptide vaccine for the treatment of patients with metastatic melanoma. *Nat Med.* 1998; 4(3): 321-327.
10. Slingluff CL, Yamshchikov G, Neese P, Galavotti H, Eastham S, Engelhard VH, Kittlesen D, Deacon D, Hibbitts S, Grosh WW, Petroni G, Cohen R, Wiernasz C, Patterson JW, Conway BP, Ross WG. Phase I trial of a melanoma vaccine with gp100(280-288) peptide and tetanus helper peptide in adjuvant: immunologic and clinical outcomes. *Clin Cancer Res.* 2001; 7(10):3012-3024.
11. Schwartzentruber DJ, Lawson DH, Richards JM, Conry RM, Miller DM, Treisman J, Gailani F, Riley L, Conlon K, Pockaj B, Kendra KL, White RL, Gonzalez R, Kuzel TM, Curti B, Leming PD, Whitman ED, Balkissoon J, Reintgen DS, Kaufman H, Marincola FM, Merino MJ, Rosenberg SA, Choyke P, Vena D, Hwu P. M.D. gp100 Peptide Vaccine and Interleukin-2 in Patients with Advanced Melanoma. *New Engl J Med.* 2011; 364(22): 2119-2127.
12. Rosenberg, SA. Raising the bar: the curative potential of human cancer immunotherapy. *Sci Transl Med* 2012; 4(127): 1-5.
13. Mathisen DJ, Rosenberg SA. The in vivo distribution of transferred syngeneic, allogeneic, and xenogeneic lymphoid cells: Implication for the adoptive immunotherapy of tumors. *J Immunol.* 1980; 124(5): 2295-2300.
14. Rosenberg SA, Yang JC, Sherry RM, Kammula US, Hughes MS, Phan GQ, Citrin DE, Restifo NP, Robbins PF, Wunderlich JR, Morton KE, Laurencot CM, Steinberg

- SM, White DE, Dudley ME. Durable complete responses in heavily pretreated patients with metastatic melanoma using T-cell transfer immunotherapy. *Clin Cancer Res.* 2011; 17(13): 4550-4557.
15. Cobbold M, La Pena HD, Norris A, Polefrone J, Qian J, English AM, Cummings K, Penny S, Turner JE, Cottine J, Abelin JA, Malaker SA, Zarling AL, Huang H, Goodyear O, Freeman S, Shabanowitz J, Pratt G, Craddock C, Williams ME, Hunt DF, Engelhard VH. MHC class-I associated phosphopeptides are the targets of memory-like immunity in leukemia. *Sci Transl Med.* 2013; 5(203): 1-10.
 16. Cohen CJ, Gartner JJ, Horovitz-Fried M, Shamalov K, Trebska-McGowan K, Bliskovsky VV, Parkhurst MR, Ankri C, Prickett TD, Crystal JS, Li YF, El-Gamil M, Rosenberg SA, Robbins PF. Isolation of neoantigen-specific T cells from tumor and peripheral lymphocytes. *J Clin Invest.* 2015; 125(10): 3981-3991.
 17. June CH. Adoptive T cell therapy for cancer in the clinic. *J Clin Invest.* 2007; 117(6): 1466-1476.
 18. Xue S, Gao L, Hart D, Gillmore R, Qasim W, Thrasher A, Apperley J, Engels B, Uckert W, Morris E, Stauss H. Elimination of human leukemia cells in NOD/SCID mice by WT1-TCR gene-transduced human T cells. *Blood.* 2005; 106(9): 3062-3067.
 19. Parkhurst MR, Yang JC, Langan RC, Dudley ME, Nathan DN, Feldman SA, Davis JL, Morgan RA, Merino MJ, Sherry RM, Hughes MS, Kammula US, Phan GQ, Lim RM, Wank SA, Restifo NP, Robbins PF, Laurencot CM, Rosenberg SA. T cells targeting carcinoembryonic antigen can mediate regression of metastatic colorectal cancer but induce severe transient colitis. *Mol Ther.* 2011; 19(3): 620-626.
 20. Maude SL, Teachey DT, Porter DL, Grupp SA. CD19-targeted chimeric antigen receptor T-cell therapy for acute lymphoblastic leukemia. *Blood.* 2015; 125(26): 4017-4023.
 21. Porter DL, Levine BL, Kalos M, Bagg A, June CH. Chimeric antigen receptor-modified T cells in chronic lymphoid leukemia. *N Engl J Med.* 2011; 365(8): 725-733.
 22. Adaptimmune. "Technology-Adaptimmune." N.p., 2016. Web. 4 Feb. 2016.
 23. Immunocore Ltd. Phase 1b/2 study of the combination of IMCgp100 with durvalumab and/or tremelimumab in cutaneous melanoma. In: ClinicalTrials.gov [Internet]. Bethesda (MD): National Library of Medicine (US). 2000- [cited 2016 Feb 3]. Available from: <http://clinicaltrials.gov/show/NCT02535078> NLM identifier: NCT02535078.
 24. Immunocore Ltd. Study to assess the tolerability of a bispecific targeted biologic IMCgp100 in malignant melanoma. In: ClinicalTrials.gov [Internet]. Bethesda (MD): National Library of Medicine (US). 2000- [cited 2016 Feb 3]. Available from: <http://clinicaltrials.gov/show/NCT01211262> NLM identifier: NCT01211262.
 25. Linette GP, Stadtmauer EA, Maus MV, Rapoport AP, Levine BL, Emery L, Litzky L, Bagg A, Carreno BM, Cimino PJ, Binder-Scholl GK, Smethurst DP, Gerry AB, Pumphrey NJ, Bennett AD, Brewer JE, Dukes J, Harper J, Tayton-Martin HK, Jakobsen BK, Hassan NJ, Kalos M, June CH. Cardiovascular toxicity and titin cross-reactivity of affinity-enhanced T cells in myeloma and melanoma. *Blood.* 2013; 122(6): 863-871.